N 70 30852/876

NASA TECHNICAL TRANSLATION

NASA TT F-587

NASA TT F-587

CASE FILE COPY

PROBLEMS OF ATMOSPHERIC PHYSICS COLLECTION 5

Edited by K. Ya. Kondrat'yev

Leningrad State University Press, Leningrad, 1967

NATIONAL AERONAUTICS AND SPACE ADMINISTRATION • WASHINGTON, D. C. • JUNE 1970

NASA TT F-587

PROBLEMS OF ATMOSPHERIC PHYSICS

COLLECTION 5

Edited by K. Ya. Kondrat'yev

Translation of "Problemy Fiziki Atmosfery. Sbornik 5."
Leningrad State University Press, Leningrad, 1967

NATIONAL AERONAUTICS AND SPACE ADMINISTRATION

For sale by the Clearinghouse for Federal Scientific and Technical Information
Springfield, Virginia 22151 – CFSTI price $3.00

This collection treats the studies of the faculty of atmospheric physics of Leningrad State University on the thermal regime of the troposphere, stratosphere and mesosphere, the problems of atmospheric optics and spectroscopy, and the microphysics of clouds.

The collection is intended for specialists working on the problems of the atmosphere and meteorology, and for undergraduate and graduate students of physics departments and universities and hydrometeorological institutes.

TABLE OF CONTENTS

S.V. Ashcheulov, K.Ya. Kondrat'yev and D.B. Styro. AN ANALYSIS OF THE COUNTERRADIATION SPECTRA OF THE ATMOSPHERE..... 1

S.V. Ashcheulov, K.Ya. Kondrat'yev and D.B. Styro. A DETERMINATION OF THE ABSORPTION COEFFICIENTS FOR CERTAIN ATMOSPHERIC WINDOWS AND ABSORPTION BANDS ACCORDING TO EMISSION SPECTRA..... 8

S.V. Ashcheulov, K.Ya. Kondrat'yev and D.B. Styro. EXPERIMENTAL STUDIES OF THE COUNTERRADIATION OF THE CLOUDED SKY..... 13

S.V. Ashcheulov. CALIBRATION OF INFRARED SPECTROPHOTOMETERS... 18

G.M. Shved. THE THERMAL EFFECT OF RADIATION AND THE FACTORS DETERMINING IT IN THE ATMOSPHERIC LAYER FROM 30 TO 100 KM (REVIEW)..... 23

Yu.M. Timofeyev. TRANSMISSION FUNCTIONS OF THE REAL ATMOSPHERE..... 62

K.Ya. Kondrat'yev and Yu.M. Timoveyev. SOME PROBLEMS IN TEMPERATURE SOUNDING OF THE ATMOSPHERE..... 69

A.G. Pokrovskiy. A METHOD OF CALCULATING THE SPECTRAL ABSORPTION OF INFRARED RADIATION IN THE ATMOSPHERE..... 85

A.P. Gal'tsev. INVESTIGATION OF THE 9.6 μm ABSORPTION BAND OF OZONE IN THE ARTIFICIAL ATMOSPHERE..... 110

A.P. Gal'tsev, V.P. Kozlov and M.M. Rivin. APPLYING STATISTICAL METHODS TO SOME PROBLEMS IN SPECTROSCOPY..... 127

L.V. Popova and I.Ya. Babinov. SOME RESULTS OF MEASUREMENTS OF THE SPECTRAL TRANSMISSION OF THE ATMOSPHERE UNDER THE CONDITIONS OF UPPER-LEVEL CLOUDS..... 145

V.V. Mikhaylov and V.P. Voytov. SPECTROPHOTOMETER WITH A NORMAL EMISSION SPECTRUM AT THE OUTPUT OF THE RECORDER..... 153

K.Ya. Kondrat'yev, N.M. Yevdokimova and G.A. Nikol'skiy. RADIATION BALANCE AND ITS COMPONENTS IN THE TROPOSPHERE AND STRATOSPHERE ACCORDING TO ASCENTS OF AIRSHIPS IN THE AUTUMN IN 1964-1965..... 159

G.A. Nikol'skiy and S.G. Shugayeva. SOME PROBLEMS IN THE METHOD OF ANALYZING THE RESULTS OF OBSERVATIONS OF RADIATION BALANCE COMPONENTS..... 168

G.N. Gayevskaya. EFFECT OF CLOUDS ON RADIATION FLUXES AND RADIATIVE HEAT TRANSFER IN THE FREE ATMOSPHERE..... 179

L.G. Bol'shakova. AN OZONE SONDE FOR MEASURING THE VERTICAL DISTRIBUTION OF ATMOSPHERIC OZONE..... 189

V.N. Konashenok. HYDROGEN COMPOUNDS IN THE MESOSPHERE..... 200

A.M. Bunakova and L.S. Ivlev. ON THE VERTICAL AEROSOL DISTRIBUTION AND AEROSOL LAYERS IN THE ATMOSPHERE..... 207

K.Ya. Kondrat'yev and A.M. Bunakova. THE EFFECT OF THE VERTICAL AEROSOL DISTRIBUTION ON THE RADIATION REGIME OF THE ATMOSPHERE..... 216

A.L. Osherovich and A.K. Suslov. THE SELECTIVITY OF AEROSOL ATTENUATION IN OZONOMETRIC OBSERVATIONS OVER ZAILIYSKIY ALA-TAU..... 225

L.S. Ivlev. THE PROBLEM OF THE ROLE OF THE MECHANISMS FOR THE DISTRIBUTION AND SOURCES OF ATMOSPHERIC AEROSOLS..... 242

L.S. Ivlev. THE EFFECTIVENESS OF DEPOSITING AEROSOL PARTICLES ON A PLANE BACKING..... 248

B.M. Shinyayev. THE EFFECT OF SOME SUBSTANCES ON THE COEFFICIENT OF CONDENSATION OF WATER DROPS..... 257

M.M. Kokhanovich and V.G. Morachevskiy. THE POSSIBILITY OF INTERPRETING THE DATA OF A SEDIMENTATION ANALYSIS..... 262

NASA TT F-587

AN ANALYSIS OF THE COUNTERRADIATION SPECTRA OF THE ATMOSPHERE

S.V. Ashcheulov, K.Ya. Kondrat'yev and D.B. Styro

ABSTRACT: The authors analyze the counterradiation spectra of the atmosphere according to the data of their experiments at Kaunas in the summer of 1965 under the most diversified meteorological conditions and according to the data of other recent studies. A comparison is made of these data and those of theoretical calculations.

Many authors have measured the spectral distribution of the intensity of thermal radiation of the atmosphere [1-6]. However, a comparison between the measured and calculated spectra for the counterradiation of the atmosphere is found only in a small number of recently-published works for specific meteorological situations [4-6]. It follows from these studies that the agreement between the experimental and theoretical spectra can be considered satisfactory in the atmospheric window of 8-13 μm and good in the bands of strong absorption. We should mention that the comparisons between measured and calculated spectra in the cited works [4-6] were made for a small number of meteorological situations, and, therefore, the results are somewhat arbitrary. Naturally, reliable statistical conclusions concerning the qualitative and quantitative relationships between calculations and measurements can be drawn only on the basis of numerous observations. /3*

In this regard, measurements of the intensity of back radiation of the atmosphere were carried out at Kaunas in the summer of 1965 under clear and cloudy skies, at various angles over the horizon, both during the night and day, with the purpose of obtaining statistical materials for different meteorological situations. The measurements of the back radiation of the atmosphere were accompanied by radiosonde observations. The spectra were recorded in three spectral regions: 5-14.5; 9-11.5; 14-25 μm. The average spectral resolution was 0.1; 0.05 and 0.15 μm, respectively. The time for recording one spectrum was roughly equal to 20 minutes. Continuous absolute calibration allowed us to consider the changes in sensitivity of the apparatus in time. At the end, more than 200 spectra were obtained under the most diversified conditions.

---

* Numbers in the margin indicate pagination in the foreign text.

Using an approximative equation for the transfer of infrared radiation (see [7]), we took the calculated values for the intensities of counterradiation of the atmosphere for specific synoptic situations corresponding to the time of the measurements. For the atmospheric window of transparency, the absorption functions were expressed by an exponent, in the calculations of which we used the coefficients of water vapor absorption k_0 (Fig. 1) presented in [8-13]. In the bands of strong absorption, the absorption functions were expressed by the square-root law in terms of an integral for probability of errors [5]. The generalized absorption coefficients for water vapor, ozone and carbon dioxide were taken from [14-16], respectively. /4

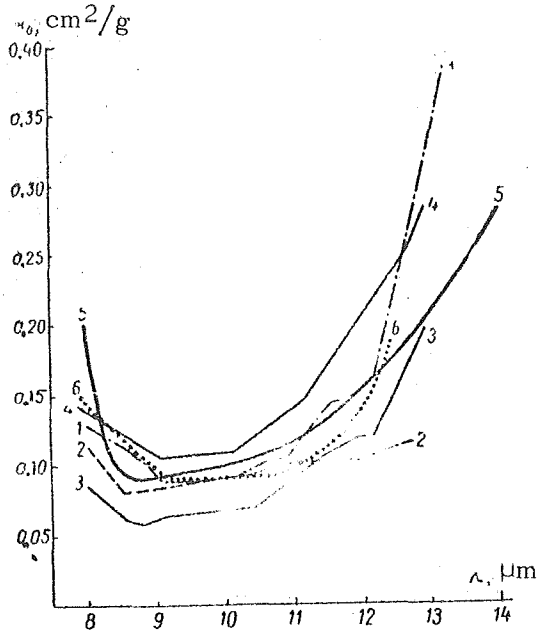

Fig. 1. Values for Coefficients of Absorption According to the Data of Various Authors: (1) A. Adele [10]; (2) W.T. Roach and R.M. Goody [8]; (3) K. Bignell et al. [12]; (4) K.Ya. Kondrat'yev et al. [9]; (5) J.J. Bolle [11]; (6) P.A. Davis and W. Viezee [13].

The best coincidence between measurements and calculations can be expected in those parts of the atmospheric windows (λ = 9.9, 11.1, 12.2, 20.1 μm, etc.) where there are no absorption bands, since the latter have still not been studied sufficiently, and they cannot be taken into account in carrying out quantitative computations. This circumstance results in the case where the experimental curves for the intensity of counterradiation of the atmosphere are above the theoretical ones.

Figures 2 and 3 show characteristic examples of a comparison between measured and calculated curves of thermal radiation of the atmosphere for clear skies, for a spectral range of 5-14.5 μm at the zenith and at an angle of 30° to the horizon. A good coincidence is observed here between the theoretical and experimental values in the bands of strong absorption by water vapor (6.3 μm) and carbon dioxide (14.8 μm). However, there is a discrepancy in the ozone absorption band (9.6 μm); it can be explained in that the ozone stratification in the atmosphere was taken in the calculations from the standard ARDC-1959 model in [17]. /5

In the atmospheric window, the discrepancy between measured

/6

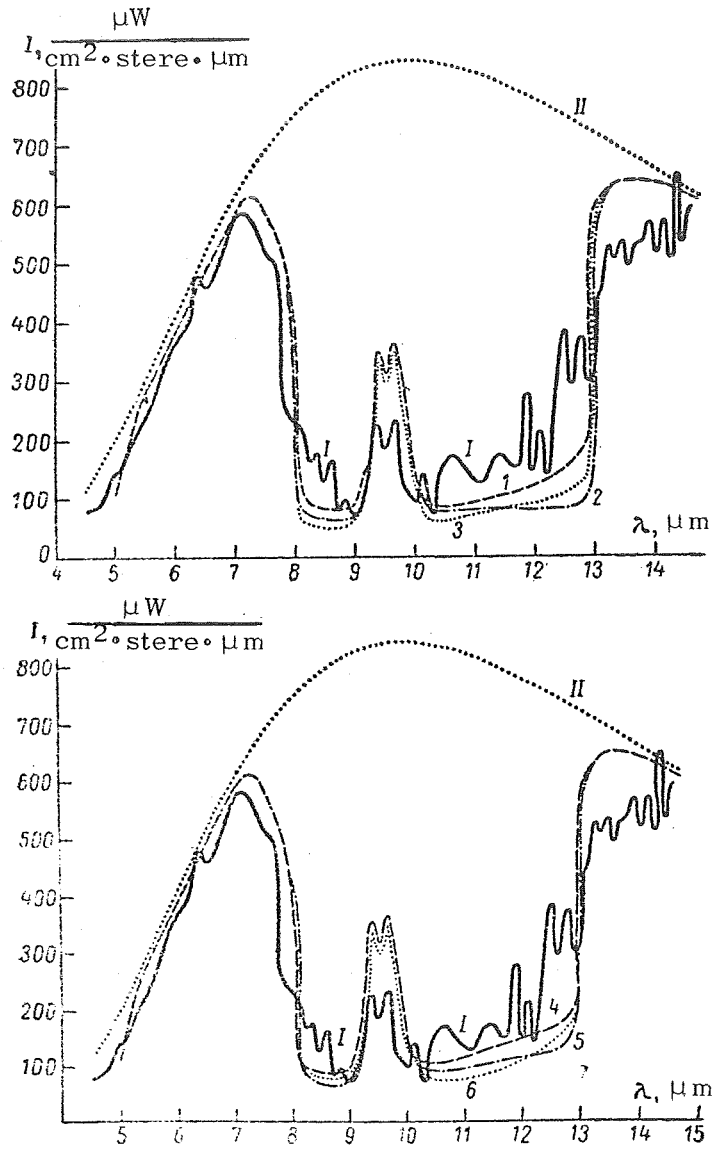

Fig. 2. Spectrum of the Sky. Zenith. Cloudless. August 3, 1965,19:40hrs.Calculations According to the Data of A. Adele (1), W.T. Roach and R.M. Goody (2), K. Bignell et al. (3) K.Ya. Kondrat'yev et al. (4) H.J. Bolle (5), and P.A. Davis and W. Viezee (6). (I) Experimental Curve; (II) Planck Function for Ambient Air Temperature of 16°C.

/7

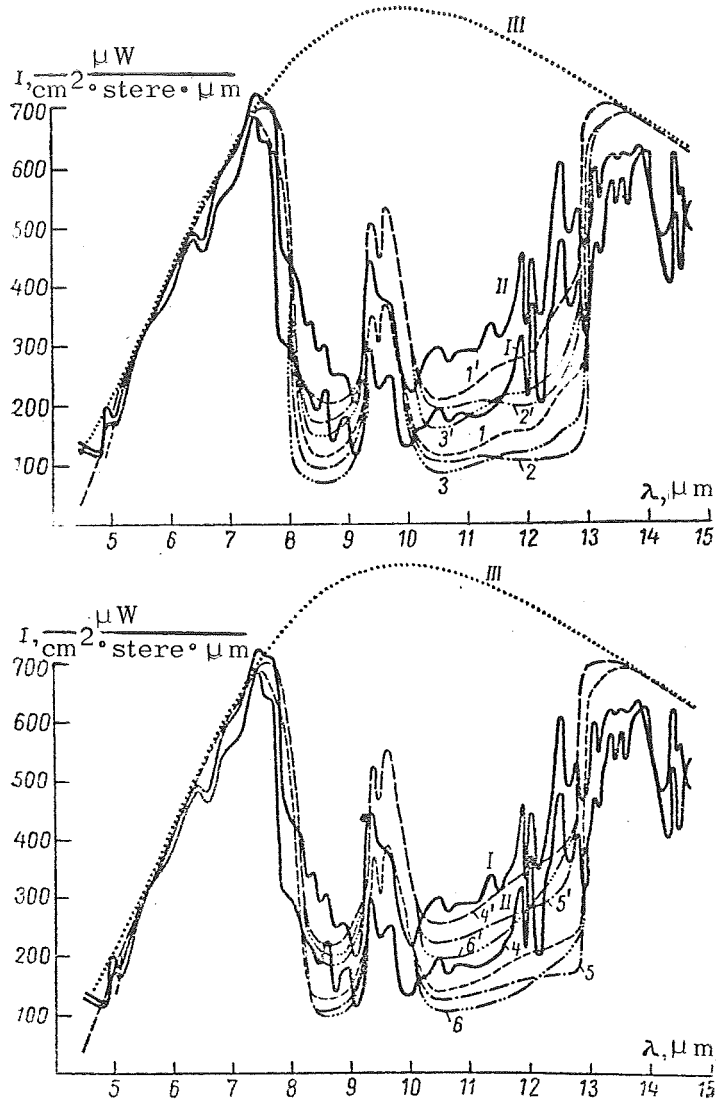

Fig. 3. Spectra of the Sky. Cloudless. July 22, 1965, 01:45. Calculations According to the Data of A. Adele (1 and 1′), W.T. Roach and R.M. Goody (2 and 2′), K. Bignell et al. (3 and 3′), K.Ya. Kondrat'yev et al. (4 and 4′), H.J. Bolle (5 and 5′), P.A. Davis and W. Viezee (6 and 6′) for the Zenith (Curves 1,2,3,4,5,6) and 30° over the Horizon (Curves 1′, 2′, 3′, 4′, 5′, 6′). (I) Experimental Curve, Zenith; (II) Experimental Curve, 30° Over the Horizon; (III) Planck Function for Ambient Air Temperature of 18° C.

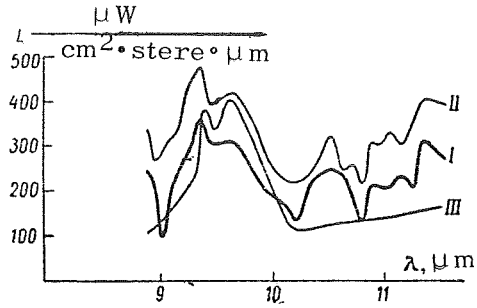

Fig. 4. Spectra of the Sky. Cloudless. July 19, 1965, 23:10. (I, II) Same as in Figure 3; (III) Calculation According to the Data of K.Ya. Kondrat'yev et al. for the Zenith. /8

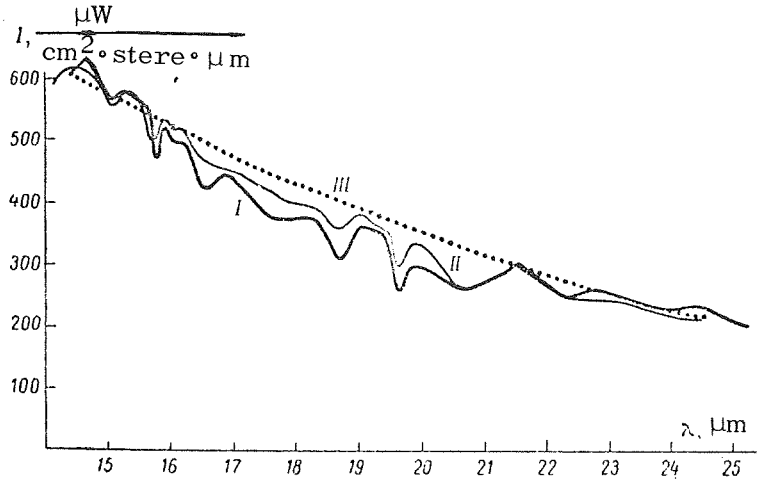

Fig. 5. Spectra of the Sky. Cloudless. August 16, 1965, 19:25. (I, II) Same as in Figure 3; (III) Planck Function for Ambient Air Temperature of 23°C.

and calculated spectra depends on the absorption coefficients used. In the range of 10-13 μm, the greatest difference is found in calculations of the transmission functions according to the data from the work of W.T. Roach and R.M. Goody [8]; the least difference is found in using the results obtained by K.Ya. Kondrat'yev et al. [9]. In the wavelength interval of 8-9 μm, it is difficult to single out the optimal values of the absorption coefficients, since their absolute values differ little from one another (see Fig. 1). In single measurements the best coincidence is obtained by using the absorption coefficients of A. Adele [10], H.J. Bolle [11], etc.

Figure 4 gives values for the intensities of the counterradiation of the atmosphere in the spectral range of 9-11.5 μm measured at the zenith and at an angle of 30° to the horizon, for average spectral resolution of 0.05 μm. It follows from a comparison with Figures 2 and 3 that an increase in the spectral resolution by a factor of two has little effect on the separation of supplementary absorption bands or the amount of new information. The agreement with calculated curves can be called satisfactory.

In the spectral range of 14-25 μm, a number of atmospheric windows stand out clearly (Fig. 5). However, the absolute values for the intensities of counterradiation are high, which can be explained by the greater concentration of water vapor and the high temperature in the layers of air near the ground. The values for generalized coefficients of water vapor absorption presented in the study of D.Q. Wark et al. [14] correspond to spectral intervals which greatly exceed the spectral width of the slit of the measuring device; therefore, a rough average is obtained in calculations using all the values. The theoretical curves here almost do not differ from the curves for radiation of an absolutely black body at a temperature of the layer of air near the ground. It should be added that the present information on the coefficients of absorption in this part of the spectrum is rather meager and, naturally, requires further study.

The following article treats an attempt at decreasing the divergence between calculated and experimental data.

REFERENCES /9

1. Sloan, R.M., J.H. Shaw, and D. Williams: Thermal Radiation from the Atmosphere. J. Opt. Soc. Amer., Vol. 46, p. 543, 1956.
2. Bell, E., L. Eisner, J. Joung and R.A. Oetjen: Spectral Radiance of Sky and Terrain at Wave-Lengths Between 1 and 20 Microns. II. Sky Measurements. J. Opt. Soc. Amer. Vol. 50, p. 1313, 1960.
3. Kondrat'yev, K.Ya., M.P. Burgova and S.V. Ashcheulov: The Problem of the Energy Distribution in the Spectrum of Thermal Radiation of the Atmosphere. Vestnik LGU, No. 22, 1963.

4. Kondrat'yev, K.Ya., S.V. Ashcheulov and M.P. Burgova: Study of the Spectral Composition of the Thermal Radiation of the Atmosphere. Tr. V. Mezhvedomstvennogo soveshchaniya po aktinometrii i optike atmosfery (Procedures of the Fifth Interdepartmental Conference on Actinometry and Optics of the Atmosphere). Moscow, 1964.
5. Kondrat'yev, K.Ya., S.V. Ashcheulov and D.B. Styro: Comparison of Measured and Calculated Spectra of the Self-Radiation of the Atmosphere. Vestnik LGU, No. 22, 1965.
6. Ascheulov, S., and D.B. Styro: Comparison of Measured and Calculated Spectra of the Atmosphere Infra-Red Radiation. Symposium on Radiation Processes in the Atmosphere. Leningrad, 5-12 August 1964. Paris, 1965.
7. Kondrat'yev, K.Ya.: Aktinometriya (Actinometry). "Gidrometeoizdat", 1965.
8. Roach, W.T., and R.M. Goody: Absorption and Emission in the Atmospheric Window from 770 to 1250 cm^{-1}. Quart J. Roy. Meteorol. Soc., Vol. 84, No. 362, 1958.
9. Kondrat'yev, K.Ya., I.Ya. Badinov, S.V. Ashcheulov and S.D. Andreyev: Some Results of Ground Observations of the Infrared Absorption Spectrum and Thermal Radiation of the Atmosphere. Izvest. Akad. Nauk S.S.S.R., ser. fiziki atmosfery i okeana, Vol. 1, No. 4, 1965.
10. Kondrat'yev, K.Ya.: Luchisty teploobmen v atmosfere (Radiant Heat Exchange in the Atmosphere). "Gidrometeoizdat", 1956.
11. Bolle, H.J.: Atmospheric Emission in Single Water Vapor Lines and its Calculation by Means of Radiation Diagrams. Memoires de la société royale des sciences de Liège, Vol. 26, 1964.
12. Bignell, K., F. Saiedy, and P.A. Sheppard: On the Atmospheric Infra-Red Continuum. J. Opt. Soc. Amer., Vol. 53, No. 4, 1963.
13. Davis, P.A. and W. Viezee: A Model for Computing Infra-Red Transmission Through Atmospheric Water Vapor and Carbon Dioxide. J. Geophys. Res., Vol. 69, no. 18, 1964.
14. Wark, D.Q., G. Yamamoto and T.H. Lienesch: Methods of Estimating Infra-Red Flux and Surface Temperature from Meteorological Satellites. J. Atmosph. Sci., Vol. 19, No. 5, 1962.
15. Elsasser, W.M. and M.T. Culbertson: Atmospheric Radiation Tables. Meteorological Monographs, Vol. 4, No. 23, 1960.
16. Möller, F., and E. Raschke: Final Report. Evaluation of TIROS Radiation Data. Ludwid-Maximillians-Universität Meteorologisches Institut. München, 1964.
17. Hanel, R.A., W.R. Bandeen and B.J. Conrath: The Infra-Red Horizon of the Planet Earth. Goddard Space Flight Center. Greenbelt, Md., 1962.

*Translator's Note: Translation of entire book is available as NASA TT F-9712.

A DETERMINATION OF THE ABSORPTION COEFFICIENTS FOR CERTAIN ATMOSPHERIC WINDOWS AND ABSORPTION BANDS ACCORDING TO EMISSION SPECTRA

S.V. Ashcheulov, K.Ya. Kondrat'yev and D.B. Styro

ABSTRACT: Absorption coefficients are determined for certain atmospheric windows and absorption bands according to emission spectra obtained at Kaunas in the summer of 1965 and according to data from other studies. The absorption coefficients in some secondary bands are described well by an exponential function.

The water vapor absorption coefficients have been determined /10
under natural conditions for the continuum either according to the absorption of solar radiation in the atmosphere [1-5] or according to the self-radiation of the atmosphere [6]. The data presented differ somewhat from one another both in absolute values and in the rate of their increase with an increase in wavelength (Fig. 1). In this regard, the absorption coefficients in the cited works were determined on the basis of a small number of measurements, which could involve certain errors in their calculations. The absorption coefficients for the secondary absorption bands in the range of the atmospheric window of 8-13 μm have almost not been determined experimentally, and it is natural that this problem has been little studied, while the data presented in [1] are only provisionally applicable to atmospheric conditions. Apparently, similar calculations on the self-radiation of the atmosphere in the window of 8-13 μm have not been carried out at all. Therefore, it is of great interest to compare the absorption coefficients for the continuum obtained on the basis of a great deal of statistical materials with the data of [1-6], and well as to study the absorption bands in the atmospheric window of 8-13 μm.

Using the formulas given in [7], we analyzed a large number of spectra for the counterradiation of the atmosphere (over 100) obtained at Kaunas in the summer of 1965. The calculated values of the absorption coefficients for the continuum in the most transmissive range of the spectrum are given in Table 1.

The width of the miscalculated intervals exceeded the spectral width of the slit of the measuring device. The control-spectrum tie-in and the band identification were carried out according to the atlas of M. Migeotte et al. [8]. The calculations were carried out mainly on the electronic computer "Ural-4" according to the formulas obtained in [7], or sometimes by the dispersion method. The accuracy of the values obtained for the water vapor absorption

coefficients for the continuum was 15% (see [7]). It can be seen from Figure 1 that these values (Curve 7) agree best of all with the results of K.Ya. Kondrat'yev et al. [4]. /11

TABLE 1

λ, μm	8,35	8,72	9,08	10,29	11,14	11,70	11,96	12,19	17,8	18,8	20,1	20,5
k, cm^2/g	0,145	0,133	0,112	0,097	0,125	0,158	0,190	0,220	1,24	1,68	2,74	3,05

The values of the absorption coefficients for the windows of transparency over the entire spectral range of 8-25 μm are given only by H.J. Bolle [6] (on the assumption that they increase monotonously toward the long waves). The results we obtained were compared to the data of this author. As in the preceding case, the average values for the absorption coefficients differ somewhat from the data of H.J. Bolle. It also can be seen from Figure 2 that the values of the root-mean-square errors in percentages are roughly identical for all wavelengths.

The absorption coefficients in the secondary bands(atmospheric windows of 8-13 μm) were calculated according to the following method. This portion of the continuum was isolated from the total radiation. The absorption coefficients were calculated for the principal emitter (N_2O, CO_2, H_2O) at the wavelength under investigation in intervals corresponding to the spectral width of the slit of the measuring apparatus (0.1 μm). The effect of the absorption lines of the remaining gases in the cited spectral intervals was not considered. The principal absorber was selected according to [8].

The absorption functions for the secondary bands were approximated by an exponent, which was valid under the following conditions estimation only of the vertices of the bands, where the absorption depends little on the wavelength and, consequently, the laws for transfer of monochromatic radiation are applicable; (b) the content of absorbing substance changes insignificantly.

The water vapor content in the atmosphere was determined by radiosonde observations, while the ratios between the concentrations of CO_2 and N_2O and the volume of air were considered to be constant and equal to $3.0 \cdot 10^{-4}$ and $2.7 \cdot 10^{-7}$, respectively [9].

The values calculated for the absorption coefficients in the bands for the spectral range of 8-13 μm are given in Table 2.

The values of the absorption coefficients for a number of atmospheric windows in the wavelength range of 17-25 μm which were calculated in this study on the basis of numerous measurements can

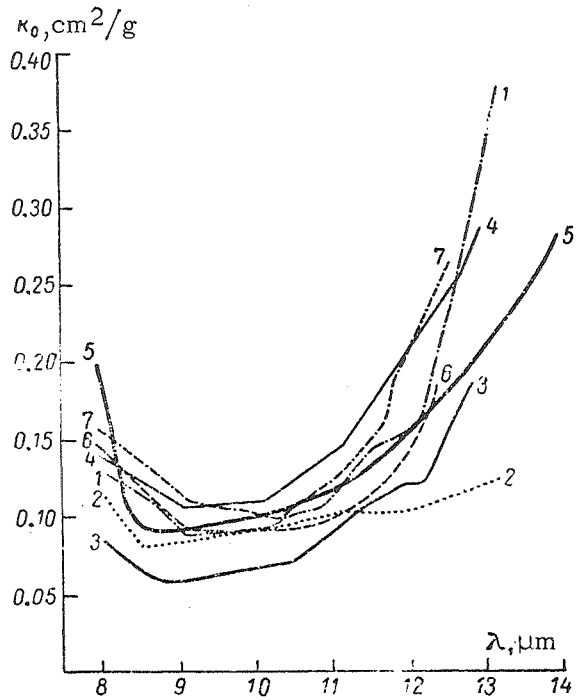

Fig. 1. Values of Absorption Coefficients According to the Data of Various Authors. (1) A. Adele [1]; (2) W.T. Roach and R.M. Goody [2]; (3) K. Bignell et al. [3]; (4) K.Ya. Kondrat'yev et al. [4]; (5) H.J. Bolle [6]; (6) P.A. Davis and W. Viezee [5]; (7) this study (see Table 1)

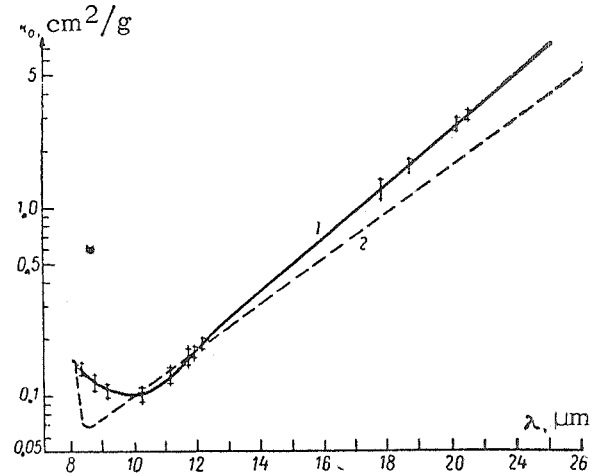

Fig. 2. Values of the Absorption Coefficients for the Continuum. (1) Results of this Study with a Consideration of the Root-Mean-Square Error; (2) Data of H.J. Bolle.

/12

be used in calculations of the thermal radiation of the atmosphere with spectral resolution on the order of 0.1 μm, due to which more precise quantitative results are obtained than those derived from the wide-spread methods of calculations.

TABLE 2

λ, μm	Principal absorber	k, cm^2/g	k, $см^{-1}$
8,45	H_2O	0,068	—
8,59	N_2O	—	1,88
8,82	H_2O	0,04	—
10,49	CO_2	—	0,0018
10,65	CO_2	—	0,0012
10,81	CO_2	—	0,0016
11,34	H_2O	0,074	—
11,50	H_2O	0,063	—
11,87	H_2O	0,207	—
12,02	H_2O	0,099	—
12,12	H_2O	0,096	—
12,41	H_2O	0,282	—
12,53	H_2O	0,503	—
12,63	H_2O	0,218	—
12,70	CO_2	—	0,00457
12,81	CO_2	—	0,00850
12,89	CO_2	—	0,00460
12,97	CO_2	—	0,00440

/13

Finally, let us discuss the physical meaning of the results obtained.

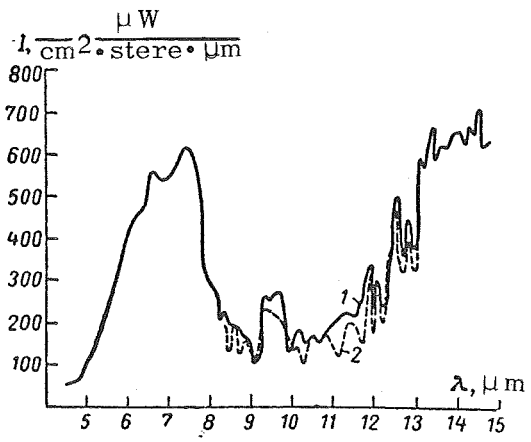

Fig. 3. Comparison of the Measured and Calculated Counterradiation Spectra of the Atmosphere. (1) Measured Spectrum, 7/22/65, 0115, Kaunas; (20 Spectrum Calculated on the Basis of the Data of this Study.

As is well known, the absorption due to the continuum (i.e., limbs of the far bands) in the range of 8-20 μm is described well by an exponential function. Therefore, the data of Table 1 reflect the real picture for the absorption, distorted, perhaps, only by the nonselective effect of aerosols, which were impossible to consider.

As for the secondary absorption bands, the exponential function here is not applicable, strictly speaking. However, considering the finite spectral resolution of the apparatus used, from the point of view of which the absorption in the vertices of the lines was little selective, and noting that the limits to deviations in absolute content and partial pressure of the absorb- /14

ing substance in the real atmosphere from the values used in this study are small, we can also use the exponential approximation. The coefficients calculated on this assumption (Table 2) do not contain any physical information on the absorption mechanism, but are applicable for phenomenological calculations of the counter-radiation of the atmosphere (with corresponding spectral resolution).

The effectiveness of this approach is illustrated in Figure 3, which demonstrates a substantial convergence in the experimental and calculated spectra.

REFERENCES

1. Kondrat'yev, K.Ya.: Luchistyy teploobmen v atmosfere (Radiative Heat Exchange in the Atmosphere). "Gidrometeoizdat", 1956.
2. Roach, W.T. and R.M. Goody: Absorption and Emission in the Atmospheric Window from 770 to 1250 cm^{-1}. Quart. J. Roy. Meteorol. Soc., Vol. 84, No. 362, 1958.
3. Bignell, K., F. Saiedy and P.A. Sheppard: On the Atmospheric Infrared Continuum. J. Opt. Soc. Amer., Vol. 53, No. 4, 1963.
4. Kondrat'yev, K.Ya., I.Ya. Badinov, S.V. Ashcheulov and S.D. Andreyev: Some Results of Ground Studies of the Infrared Absorption Spectrum and the Thermal Radiation of the Atmosphere. Izvest. Akad. Nauk S.S.S.R., ser. fiziki atmosfery i okeana, Vol. 1, No. 4, 1965.
5. Davis, P.A. and W. Viezee: A Model for Computing Infrared Transmission through Atmospheric Water Vapor and Carbon Dioxide. J. Geophys. Res., Vol. 69, No. 18, 1964.
6. Bolle, H.J.: Atmospheric Emission in Single Water Vapor Lines and its Calculation by Means of Radiation Diagrams. Memories de la Societe Royale des Sciences de Liege, Vol. 26, 1964.
7. Kondrat'yev, K.Ya., D.B. Styro, and S.V. Ashcheulov: The Question of the Possibility of Determining the Absorption Coefficients of Water Vapor and Other Components According to the Self-Radiation of the Atmosphere. In the Collection: Problemy fiziki atmosfery (Problems of Atmospheric Physics), No. 4, Leningrad State University, 1966.
8. Migeotte, M., L. Neven and J. Swenson: The Solar Spectrum from 2.8 to 23.7 Microns. Part I. Photometric Atlas. Part II. Measures and Identification. Memories de la Societe Royale des Sciences de Liege, Special, Vol. 1, 1956.
9. Howard, J.N. and J.S. Garing: The Transmission of the Atmosphere in the Infrared. Review. Infra-red Physics, Vol. 2, pp. 155-173, 1962.
10. Hanel, R.A., W.R. Bandeen and B.J. Conrath: The Infrared Horizon of the Planet Earth. Goddard Space Flight Center. Greenbel, Md., 1962.

EXPERIMENTAL STUDIES OF THE COUNTERRADIATION OF THE CLOUDED SKY

S.V. Ashcheulov, K.Ya. Kondrat'yev and D.B. Styro

ABSTRACT: The laws noted in the spectra for the counterradiation of the clouded sky are discussed. Two types of clouds were studied: nimbostratus and stratocumulus. The measured values for the intensities of counterradiation of the sky agreed well with the calculated ones for the nimbostratus, i.e., they almost did not differ from the radiation of an absolutely black body at the temperature of the lower boundary of the cloud, while those for the stratocumulus, in the atmospheric window of 8-12 μm, were found to be much lower than the calculated ones.

The studies of the radiation regime of clouds which have been published mainly treat the scattering, absorption and reflection of solar radiation of their "upper boundary" [1]. Only a few works [2-3] have touched on spectral investigations of the counterradiation of the clouded sky, but they do not contain quantitative evaluations. /15

We measured the counterradiation spectra of cloudy skies at Kaunas in the summer of 1965. The broad viewing angle (15 x 15°) of the measuring apparatus enabled us to some extent to average the spatial discontinuities of the clouds, the distance to the lower boundary of which was determined by radiosonde observations. The method used in calculating the counterradiation spectra of the clouded sky was similar to that applied in [4], and the initial data on the percentage of absorbers and the absorption coefficients were taken from [5]. The calculations were carried out for the zenith, on the assumption that the clouds were absolutely black radiators.

The following obvious laws were noted in the spectra for the counterradiation of the clouded sky. In the atmospheric window of 8-13 μm, the values recorded were characterized by complimentary radiation in respect to a clear sky, while the clouds did not make any extra contribution to the radiation (Fig. 1-3) in the absorption bands of water vapor (6.3 μm) and carbon dioxide (14.8 μm).

We studied clouds of two forms: nimbostratus and stratocumulus. The measured values of the intensities of counterradiation of the sky agreed well with the calculated ones for the nimbostratus, i.e., they almost did not differ from the radiation of an absolutely black body at the temperature of the lower boundary of the cloud (Fig. 1).

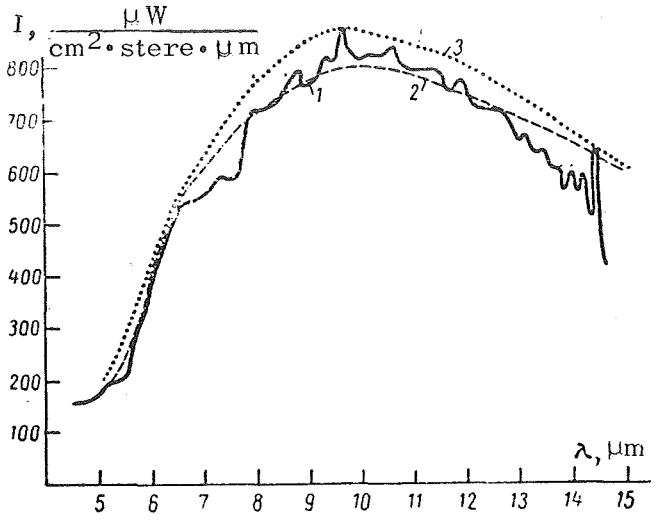

Fig. 1. Counterradiation Spectra of the Sky. Solid Clouds at an Altitude of 750 m, 7/23/65, 13:05. (1) Experiment, Zenith; (2) Calculation, Zenith; (3) Planck Function for Ambient Air Temperature of 19.0° C.

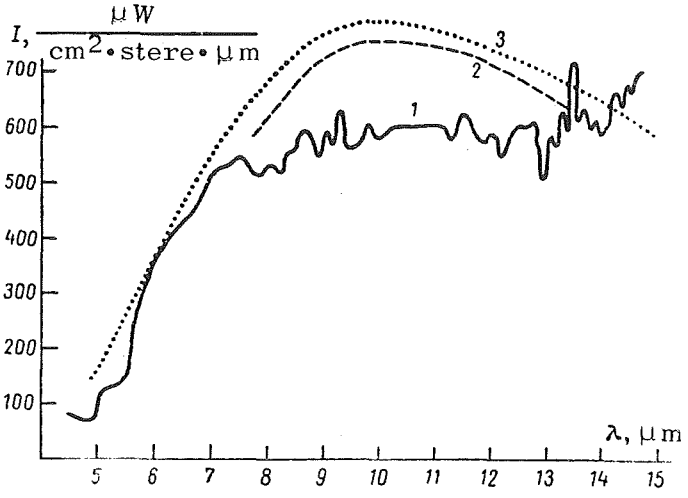

Fig. 2. Counterradiation Spectra of the Sky. Solid Clouds at an Altitude of 500 m, 7/27/65, 20:40. (1-2) Same as in Fig. 1; (3) Planck Function for a Temperature of 13.5° C. for the Layer of Air Near the Ground.

For the stratocumulus, the measured values of the intensities of counterradiation of the atmosphere in the atmospheric window of 8-13 μm were found to be much lower than the calculated ones (Fig. 2,3), although the temperatures of the lower cloud boundary and /17 the layers of air surrounding the measuring apparatus differed by 3-5° in all. The latter results can be explained by the following two causes.

1. Systematic errors in measurements. However, an analysis of the course of the experiment (particularly the multiple repitition of similar results) makes this explanation hardly probable.

2. Partial transmissivity of the clouds. In this case, the radiation arrives at the instrument from higher and, consequently, colder layers of the atmosphere, and the intensity of radiation of the clouded sky decreases correspondingly.

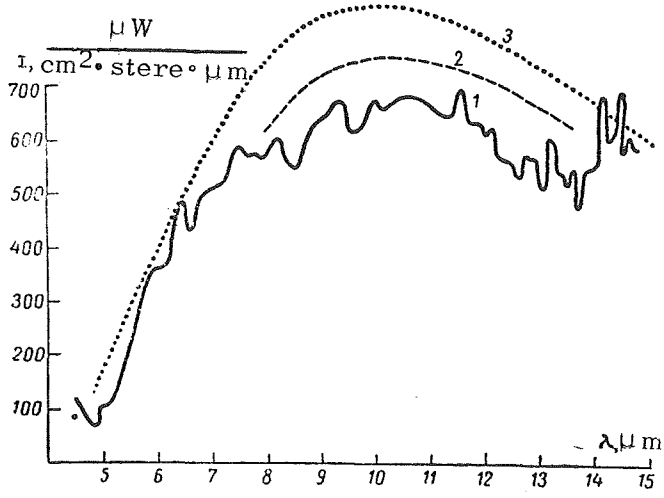

Fig. 3. Counterradiation Spectra of the Sky. Solid Clouds at an Altitude of 1100 m, 7/29/65, 18:00. (1-2) Same as in Fig. 1; (3) Planck Function for Temperature of 16.7° C. for the Layer of Air Near the Ground..

In order to illustrate the partial transmissivity of clouds, Figure 4 shows the altitudes, at which the real temperature is equal to the brightness temperature of the measured counterradiation. It can be seen from this that the radiation reaches the underlying surface from altitudes of 2-3 km, despite the fact that the lower boundary of the clouds is only at an altitude of 500 m.

The difference in absolute values for the intensities of counterradiation of the atmosphere in a cloudless sky, haze and solid clouds (Fig. 5) can be explained primarily by the different

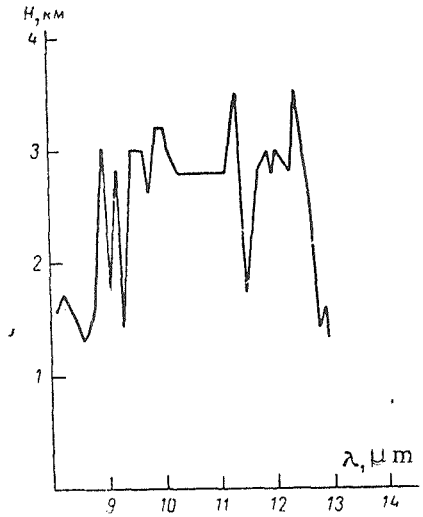

Fig. 4. Values of the Altitudes at which the Temperature Corresponds to the Brightness Temperature of the Radiation for Curve 1 on Figure 2. Altitude of Clouds, 500 m, 7/27/65,20:40; t = 13.5°C.

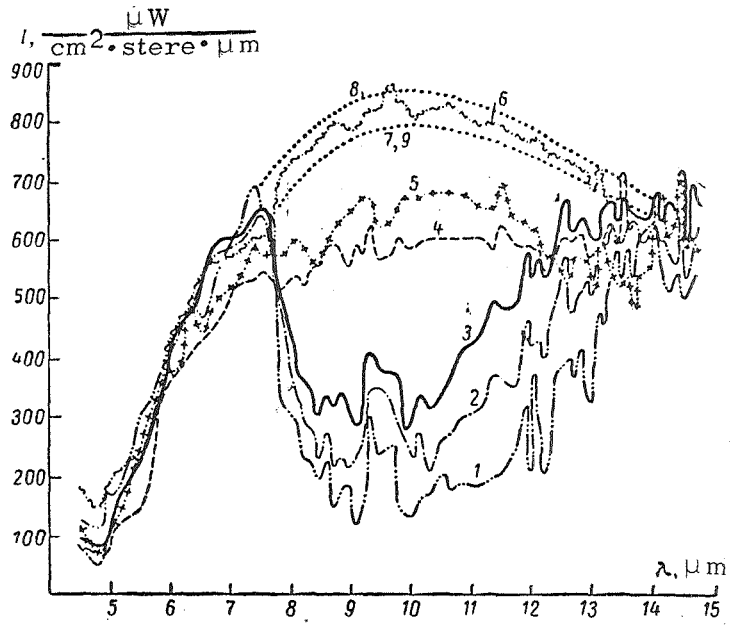

Fig. 5. Counterradiation Spectra of the Atmosphere. Zenith. (1) Cloudless, 7/22/65,05:00, t = 15.5° C; (2) Haze, 7/17/65,02:25, t = 17.5° C; (3) Haze, 7/17/65, 01:00, t = 17.5° C; (4) Solid Clouds at an Altitude of 500 m, 7/27/65,20:40, t = 13.5° C; (5) Solid Clouds at an Altitude of 1100 m, 7/29/65,18:00, t = 16.5°C; (6) Solid Clouds at an Altitude of 750 m, 7/23/65, 13:00, t = 18° C; (7) Planck Function at t = 13.5° C; (8) Planck Function at t = 18° C; (9) Calculated Values of the Counterradiation of the Atmosphere for 7/23/65,13:00 (Coincides with Curve 7).

/18

stratification of temperature and humidity in the atmosphere. All the curves presented here describe some transmissivity of clouds and haze, except for Curve 6, which was recorded the day before a rainfall and which is close to the radiation of an absolutely black /19 body at the temperature of the lower cloud boundary. Curves 2 and 3, which refer to nontransparent haze in the visible spectral range, are unique. The haze generates a certain complimentary (compared to the clear sky, see Curve 1) radiation, but does not completely shield off the 9.6 μm ozone emission from higher altitudes.

The partial transmissivity of the clouds here can be explained by the combined effect of absorption and scattering on particles commensurate with the wavelength, since a consideration of the absorption alone limits the transmissivity of clouds only by several meters. Unfortunately, we could not carry out a detailed quantitative analysis of the process of transfer of infrared radiation, because of the lack of data on the microstructure and vertical capacity of the clouds.

In the case when the partial transmissivity of clouds is substantiated during further studies, this can be used, for example, to distinguish clouds from a snow cover in satellite measurements of the values for the intensities of outgoing radiation. Actually, the radiation of the clouds in two spectral intervals of different transmissivities (for example, the windows of 2.7-4.3 and 8-13 μm) relate to different effective temperatures, while the results obtained in sighting on a snow cover relate to the same temperature of the radiator. It is easy to record this type of difference.

For a final solution to the problem of the transmissivity of clouds, there must be further measurements of the descending and ascending radiation at different levels in a cloudy atmosphere, as well as simultaneous recording of the structural parameters of the medium.

REFERENCES

1. Kondrat'yev, K.Ya.: Aktinometriya (Actinometry). "Gidrometeoizdat", 1965.
2. Bell, E., L. Eisner, J. Joung and R.A. Oetjen: Spectral Radiance of Sky and Terrain at Wave-lengths Between 1 and 20 Microns. II. Sky Measurements. J. Opt. Soc. Amer., Vol. 50, p. 1313, 1960.
3. Jamieson, J.A., R.H. McFee, G.N. Plass, R.H. Grube and R.G. Richards: Infrared Physics and Engineering. N.Y.-Toronto-London, McGraw-Hill Book Company, Inc., 1964.
4. Kondrat'yev, K.Ya., S.V. Ashcheulov and D.B. Styro: Comparison of the Measured and Calculated Spectra of Self-Radiation of the Atmosphere. Vestnik LGU, No. 22, 1965.
5. Ashcheulov, S.V., K.Ya. Kondrat'yev and D.B. Styro: A Determination of the Absorption Coefficients for Certain Atmospheric Windows and Absorption Bands According to Emission Spectra. This Collection, p. 10.

CALIBRATION OF INFRARED SPECTROPHOTOMETERS

S.V. Ashcheulov

ABSTRACT: The author discusses the problems encountered in calibration of infrared spectrophotometers. It is shown that a design with automatic regulation of black body temperature, with cooling, which involves the use of semiconducting condenser batteries, is very compact and reliable.

The studies of the energy distribution in the emission spectra /20
of weakly-heated sources (atmosphere, Earth's surface, clouds), which have greatly expanded during recent years, are making the problems of the method and technique of absolute calibration of spectrophotometers very urgent. By absolute calibration, I mean operations which allow us to convert the indices of an output recording device into values of brightness or radiation flux from the studied source expressed in absolute units. In this regard, a requisite condition is the stabilization (or consideration) of the self-radiation of the modulator which is comparable to the radiation under investigation or exceeds this radiation; this is accomplished either by measuring the temperature of the blades of the modulator, or by a special optical diagram in which the blade is constantly within the field of vision of the device, or finally, by using a mirror modulator inclined on the optical axis. In the last case, which is most wide-spread and is sometimes called differential modulation, the emission of the modulator is replaced by the emission of a stabilized reference source, which gives better accuracy compared to the other methods.

The most complicated process is strictly absolute calibration, which is usually accomplished by supplying standardized radiation to the input of the device; this aids in finding the ratio between the indices of the device and the input flux. Here, there can be a number of typical errors permitted by different authors which make the final results of their measurements doubtful. They include the following: calibration is accomplished either long before the measurements and not in the operational regime of the apparatus, or according to one standardized emission, or without a consideration of the self-radiation of the mirror modulator, or considering it theoretically, or according to an emitter which is not located at the output of the device [2], etc. [1,2].

The measurements we carried out under laboratory and field /21
conditions, as well as the evaluations of possible errors, showed that the following basic recommendations should be obeyed.

(1) Calibration must be accomplished during the measurements in the operational regime of the device.

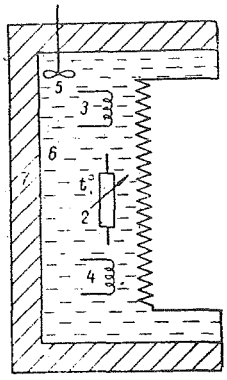

Fig. 1. Black Body with Heating. (1) Emitting Surface (2) Thermistor; (3) Controllable Heater R_{H_1}; (4) Heater for Forced Warm-Up R_{H_2}; (5) Stirrer (6) Oil; (7) Thermal Insulation.

(2) The calibration should be carried out according to no less than two standardized fluxes [3]. The intensity of one of them should be comparable to that of the emission under investigation.

(3) It is advisable that the emission intensity of the reference emitter (added to the emission intensity of the mirror modulator) be kept either lower or higher than the intensity of all the standardized fluxes and those under investigation. The temperature of the modulator and optical elements located in front of it must be stabilized.

We can suggest the following variations for the temperatures of the emitters in correspondence with the second recommendation: (1) reference emitter (liquid nitrogen), 196° C, standardized emitters (dry ice), 79° C and any positive temperature. However, the technical difficulties connected with the use of liquid nitrogen and dry ice under field conditions force us to use a basically different selection of temperatures: (2) reference emitter, +40° C, standardized emitters, +20 and -79° C or (3) reference emitter, ΔT = +10° C (relative to the surrounding temperature), standardized emitters, ΔT = +5 and -20° C. The use of semiconducting coolers makes this variation very easy, and it is very satisfactory, methodologically speaking.

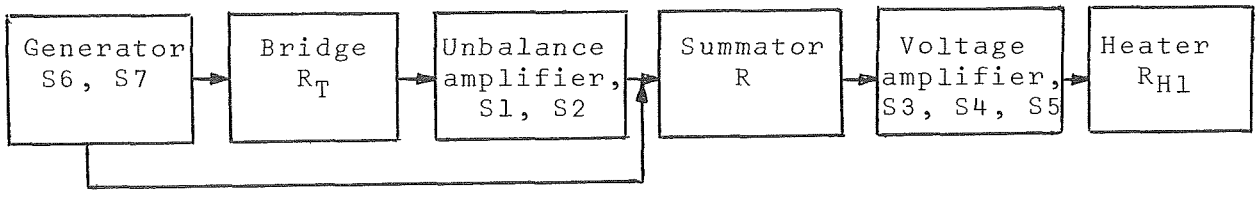

Fig. 2. Block-Diagram of the Automatic Regulation of the Temperature of a Black Body with Heating.

Specific diagrams for variations (2) and (3) are described below; they were developed in respect to aircraft and aerostat spectrophotometers. A black body controlled thermostatically on positive temperatures (Fig. 1) was realized in the form of a shallow tank with a crimped bottom. The blackness coefficient was /22
0.95-0.97. The block-diagram of the electronic regulator was arranged in the following way (Fig. 2). Rectilinear pulses from

the master oscillator enter on the Wheatstone bridge with the thermistor. The amplified signal of the unbalance is summed up over the resistance with the reference signal of the master oscillator. The phase of the reference signal is selected in such a way that the signal of the unbalance is supplied to the summator in opposition to the reference signal during heating. This decreases the voltage at the input of the terminal amplifier and ultimately results in a decrease in power supplied to the heater. A specific diagram (Fig. 3) aids in maintaining the temperature with accuracy up to 0.5° C for separable yielded power up to 30 W.

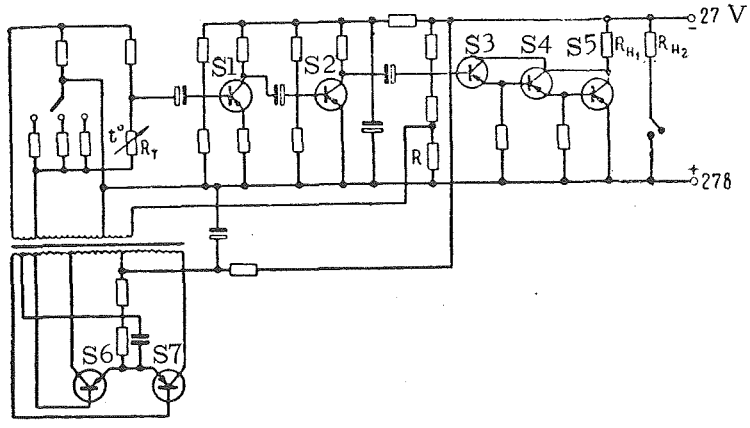

Fig. 3. Total Diagram for Automatic Regulation of the Black Body Temperature with Heating.

The principal disadvantage of this design is that the thermostatic control is accomplished by the regulated heater and, consequently, only temperatures exceeding that of the surrounding medium can be maintained.

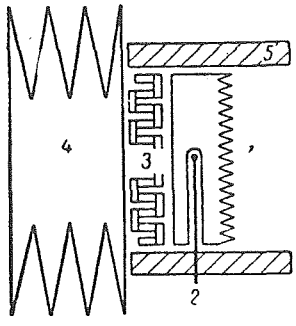

Fig. 4. Black Body with Cooling. (1) Emitting Surface; (2) Thermistor; (3) Semiconducting Thermopile; (4) Radiator (5) Thermal Insulation.

The variation of the design using [4] semiconducting condenser batteries was found to be much more compact and attractive (Fig. 4). The latter aid in cooling the emitting surface by 20-25°C relative to the surrounding temperature, are reliable in operation, and require less energy. The design of the automatic regulator (Fig. 5 and 6) is different here. The power amplifier and the two rectifiers guarantee the supply to the thermopile (8a at 1.5-3 V). The unbalance amplifier is connected to a phase detector, which connects one of the two relays, depending on the phase of the unbalance, thus changing the polarity of

the thermopile supply, in dependence on which the latter operates either as a cooler or as a heater. When a given temperature is reached, the supply is turned off completely. /23

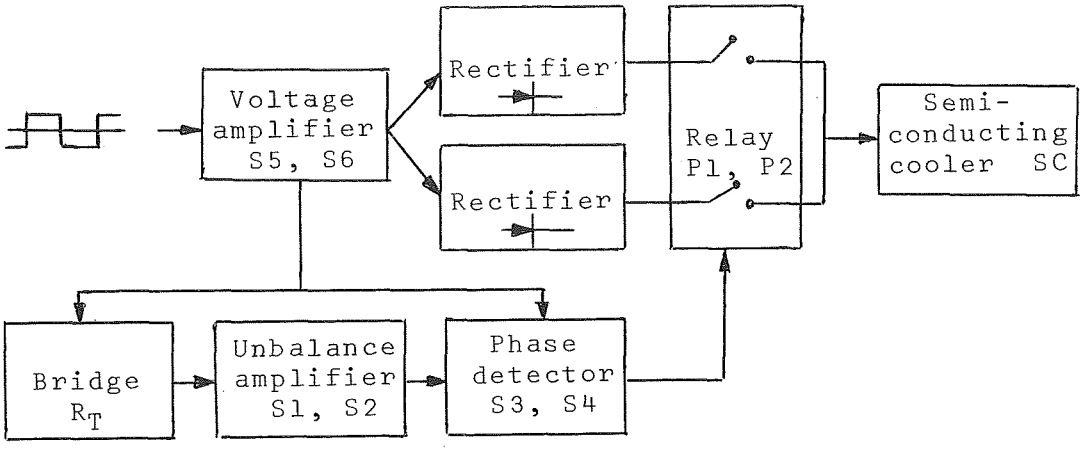

Fig. 5. Block Diagram of Automatic Regulation of Black Body Temperature with Cooling.

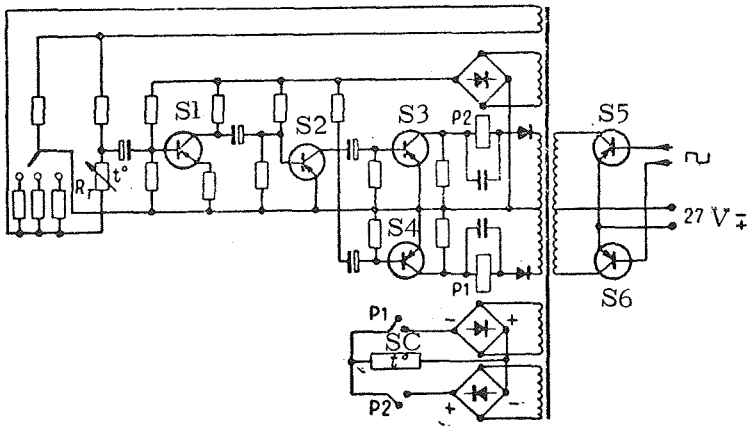

Fig. 6. Complete Diagram of Automatic Regulation of Black Body Temperature with Cooling.

The low time constant of the battery allows the standardized source to be connected only for the time of the calibration. All this yields a substantial economy of energy which is significant, for example, under the conditions of aerostatic measurements. The accuracy in maintaining the temperature is on the order to 0.5° C. In this regard, a temperature of the reference emitter which is close to that of the surrounding medium makes the measurement regime similar to the compensation one. A technical realization /24 of the last variation yields a relatively small infrared spectrophotometer which is suitable for operation on board an aircraft or aerostat.

In conclusion, we must mention one more circumstance which is very important from the point of view of absolute calibration. A monochromator in the composition of the instrument is not equivalent in terms of penetration of the emission components polarized in two mutually perpendicular planes. However, the addition of mirrors arranged at an angle to the optical axis to the illuminator (for example, coelostat ones) brings about partial polarization of the emission under investigation and the calibrated emission. Therefore, in order to eliminate systematic errors due to this, which are difficult to consider, two conditions must be fulfilled: (a) the calibration emission should not be polarized; (b) in transition from measurements to calibration (and the inverse), the mirrors either should not change position at all or should change to a symmetrical position relative to the optical axis of the instrument.

REFERENCES

1. Lebedinskiy, A.I., D.N. Glovatskiy, V.I. Tulupov, B.V. Khlopov, A.A. Fomichev and G.I. Shuster: Infrared Spectrophotometry of the Thermal Radiation of the Earth. Space Research. Tr. Vsesoyuznoy konferentsii po fizike kosmicheskogo prostranstva (Procedures of an All-Union Conference on Space Physics). "Nauka", 1965.
2. Popov, I.O. and Ye.O. Fedorova: Measurement of the Emission Spectra of the Atmosphere and the Earth's Surface in the Range of 2-6 μm from Altitudes up to 4 km. Optika i Spektroskopiya, Vol. 18, No. 3, 1965.
3. Kondrat'yev, K.Ya., S.A. Ashcheulov, and M.P. Burgova: Study of the Spectral Composition of the Thermal Radiation of the Atmosphere. Actinometry and Atmospheric Optics. Tr. 5-go mezhduvedomstvennogo soveshchaniya (Procedures of the 5-th Inter-Departmental Conference). "Nauka", 1964.
4. Kolenko, Ye.A.: Termoelektricheskiye okhlazhdayushchiye pribory (Thermoelectric Cooling Devices). Akad. Nauk S.S.S.R., 1963.

THE THERMAL EFFECT OF RADIATION AND THE FACTORS DETERMINING IT IN THE ATMOSPHERIC LAYER FROM 30 TO 100 KM (REVIEW)

G.M. Shved

ABSTRACT: This article is a review which sums up the basic points of information on the role of radiation in the thermal regime of the layer of 300-100 km. The basic difficulties encountered in solving the problem are also noted. The relationship of this problem to the intensity of solar radiation, the composition of the atmosphere, the temperature and its variations, the absorption functions and the fluorescence processes is discussed.

Introduction

The layer under investigation includes the upper stratosphere, /25
the mesosphere and the lowest layers of the thermosphere. The vertical temperature distribution from 30 to 100 km has two interesting peculiarities: a temperature maximum around 50 km (stratopause) and a minimum around 85 km (mesopause). It has long been established that most of the basic rules for the altitudinal and longitudinal temperature distributions in the stratosphere and mesosphere and their seasonal changes can be explained well by the characteristics of the absorption of short-wave solar radiation. Therefore, radiation can be considered to be the most important factor in the thermal regime of the atmospheric layer in question. Nevertheless, an explanation for certain characteristics of the temperature distribution and its variation cannot be found without considering the dynamic and photochemical processes.

This article is a review in which I attempted to sum up the basic points of information on the role of radiation in the thermal regime of the layer of 300-100 km. The basic difficulties encountered in solving the problem are also noted. Earlier reviews on this theme can be found in monographs [1, 2]. The article also gives some results I obtained rather recently; a separate article will investigate the method for the calculations.

1. Formulation of the Problem

A direct measurement of radiant fluxes at different altitudes within the limits of the layer in question is a very complicated experimental task, and such measurements have as yet not been carried out. Therefore, all the existing information on the role of radiation in the thermal regime have been obtained by theoretical calculations. The studies have been carried out in two directions. First of all, the radiative heat fluxes have been calculated for a /26

specified distribution of absorbing gases, temperature and spectral composition of the extraterrestrial solar radiation. Secondly (a smaller number of studies), the altitudinal equilibrium temperature distribution has been computed from the viewpoint of the theory of radiation equilibrium. The difficulty in calculations by such an approach is atoned for by the graphic clarity of the results. In particular, it can be seen immediately when there is a sharp need for considering factors other than radiation in the theory of the thermal regime.

The radiation factors of the thermal regime of the atmosphere can be divided into two types: absorption of short-wave solar radiation and transfer of natural long-wave radiation. For the thermal regime of the 30-100 km layer, the factor of the first type is the absorption of radiation by molecular oxygen (Schumann-Runge continuum, 1300-1750 Å; Schumann-Runge bands, 1750-2000 Å) and ozone (Hartley bands, 1800-3400 Å) in the ultraviolet spectral region. In the infrared and visible spectral regions, there are many bands which absorb solar radiation. Let us write out a list of these bands, although it is doubtless that their relative contribution to the heating varies: O_3 - Chappuis bands (4400-7500 Å); CO_2 bands of 1.4, 1.6, 2.0, 2.7 and 4.3 μm (strongest); H_2O - bands of 0.72, 0.81, 0.94, 1.1, 1.38, 1.87, 2.7, 3.2 and 6.3 μm; O_2 - bands of 0.69, 0.76 and 1.25 μm; CH_4 - 3.3 μm band; N_2O - 4.5 μm band. It is not impossible that the absorption of solar radiation by an aerosol could play a determinental role in the thermal regime. In the transfer of the self-radiation of the atmosphere, the 15 μm CO_2 and 9.6 μm O_3 bands and the rotational 6.3 μm H_2O band (the last to a lesser degree), as well as the O lines near 63 μm, yield the thermal effect. Moreover, the emissive OH radiation, which occupies a broad spectral range from 0.5 to 4.5 μm, can be an important factor of the thermal regime in the region of the mesopause.

The radiant influx of energy per unit volume, H, which is due to the absorption of solar radiation, is usually calculated according to a simple and physically clear formula, i.e.,

$$H_{\Delta\nu}(z) = \int_{\Delta\nu} d\nu \varkappa_\nu(z) k_\nu(z) n(z) I_{\infty,\nu} e^{-m\tau_\nu(z)}, \qquad (1)$$

where z is the altitude; ν is the frequency; Δν is the spectral interval in which the radiation is absorbed; n is the concentration of the absorbing gas; k_ν is the absorption coefficient of this gas; κ_ν is the percentage of absorption energy used in heating; $I_{\infty,\nu}$ is the spectral intensity of the extraterrestrial solar radiation; m is the mass of the atmosphere in the direction toward the Sun; $\tau_\nu(z)$ is the optical thickness of the air, reading along the vertical from the upper boundary of the atmosphere to the level z. Formula (1) does not take into account the scattering of radiation. Calculations [3] show that the thermal contribution of radiation scattered on molecules and particles can be disregarded in the ultraviolet spectral region in frequency intervals where the absorption is strongest. /27

In these spectral intervals, the incident radiation is completely depleted in the upper atmosphere, where the density of the air and the concentration of the aerosol are still so low that the intensity of the scattered radiation is insignificant. For example, the albedo at the center of the Hartley bands around 2500 Å is less than 1%. In the limbs of this band, the albedo is also small, and does not exceed 10%. This shows that we can consider the molecular and aerosol scattering in approximation simply by increasing the value of $I_{\infty,\nu}$ in (1) by the value of the corresponding ascending radiation. The fluorescent scatter can be substantial in certain parts of the ultraviolet spectrum. However, at least for the Hartley band, rocket and satellite measurements of the albedo [3] give values for the outgoing radiation which are two and more orders less than the incident radiation. The smaller the value of κ_ν, the greater the effectiveness of the reradiation processes. However, we should mention at once that there are no calculations where this effect could be considered. In addition, there have been no computations of the heating due to absorption of the solar radiation in the infrared spectrum, where the scattering of light and the albedo would be taken into account. They can be considered in first approximation by a simple increase in the intensity of solar radiation by the value for the ascending flux of radiation at the level under investigation.

Calculations of the radiant heat flux due to the transfer of the long-wave self-radiation of the Earth and the atmosphere in a certain spectral interval of $\Delta\nu$ generally require a calculation of the following expression:

$$H_{\Delta\nu}(z) = -\frac{4}{\Delta\nu} S_{\Delta\nu}(z) B_{\Delta\nu}(z) + \int_{z_0}^{z} \frac{\partial^2 A_F(z', z)}{\partial z \partial z'} B_{\Delta\nu}(z')\, dz' + \int_{z}^{z_\infty} \frac{\partial^2 A_F(z, z')}{\partial z \partial z'} B_{\Delta\nu}(z')\, dz' + \frac{\partial A_F(z_0, z)}{\partial z} F_{0,\nu}^{\uparrow}, \qquad (2)$$

where $B_{\Delta\nu}$ is the radiant flux of an absolutely black body in the spectral range of $\Delta\nu$; $F_0^{\uparrow}$ is the flux of radiation ascending from the initial level z_0; $S_{\Delta\nu}$ is the total intensity of the lines of the given absorbing gas over the interval $\Delta\nu$ per unit volume; $A_F(z_1, z_2)$ is the absorption function of the atmosphere for the radiation flux between the z_1 and z_2 levels ($z_2 > z_1$); z_∞ is the altitude of the upper boundary of the atmosphere. Single terms in the right-hand part of (2) have a clear physical meaning. The first term characterizes the self-radiation at the level in question, and the second and third terms characterize the heating contribution of the atmosphere between the z_0 and z levels and the atmosphere above the z /28 level, respectively. The fourth term considers the contribution to heating of the Earth's surface and the atmosphere below the z_0 level. Expression (2) was written for the conditions when there is local thermodynamic equilibrium (l.t.e.). The l.t.e. is upset in the

mesosphere. This results, first of all, in a situation where the Planck function B_ν for the radiation of an absolutely black body should be replaced by some other value, and, secondly, it results in a change in the absorption coefficient, on which A_F depends.

As follows from the above, radiant fluxes of heat depend on the spectral distribution of solar radiation, the concentration of gases absorbing the radiation, the vertical course of the temperature, the coefficient or functions of absorption, the intensity of the fluorescence processes and the degree of l.t.e. disruption. Therefore, before going into the results of studies on the thermal regime, we must briefly discuss the presently available information on the cited factors.

2. Intensity of Solar Radiation

As for the spectral composition of the solar radiation beyond the boundaries of the atmosphere, we will limit ourselves here to discussions of the latest investigations and summaries of the results of [4, 5, 6, 7, 8]. The measurements of the solar radiation in the ultraviolet region of interest to us were carried out on rockets. Obviously, the relative error in measurements in this spectral region can reach several tens of a percent. This can be seen by comparing the results presented in [5] with recent aerostat measurements of [9] in the atmospheric window around 2100 Å. The intensity in the infrared spectral region was obtained both with high-altitude aerostat measurements (up to 30 km) and with extrapolation of ground data. The errors in measurements of the brightness temperature of the Sun reach 100-150°K in some studies, while the discrepancy in the results obtained by different authors can even be greater - up to 300°K. A more specific value for the spectral intensity of solar radiation depends on an improvement of the methods for absolute measurements on rockets and satellites for the ultraviolet spectrum and on aerostats for the infrared.

3. Composition of the Atmosphere

Molecular Oxygen. The absorption of ultraviolet solar radiation by molecular oxygen results in dissociation of O_2 and its gradual replacement (with the altitude) by atomic oxygen. The "dissociation level" occurs at an altitude of 85 km and higher [10, 11] and apparently has yearly and latitudinal variations. At present, there are only a few sporadic rocket measurements of the O_2 /29 concentration in the lower thermosphere [12, 13, 14]; they were obtained either in recording the solar ultraviolet radiation or with mass spectrometers. The absolute values for the O_2 concentration according to different studies for the same altitudes can differ even by an order of magnitude. The rate in increase of the concentration with the height varies to the same extent. The average value for the height of the uniform atmosphere for O_2 in the 100-120 km layer can be taken as 7 km. At present, it is impossible to say whether or not the differences in the O_2 distributions can be explained

by the conditions in the atmosphere or the errors in measurements, which reach 50% and more in many studies.

Atomic Oxygen. There have been very few observations of the O concentration in the lower layers of the thermosphere [13,15], since the results were obtained here solely with mass-spectrometers. Photochemical analyses [11] show that the maximum O concentration should be found around an altitude of 100 km. Observations of the chemiluminescence of atomic oxygen in a cloud of nitric oxide gave a maximum concentration at altitudes of 103-107 km [15]. However, it is not impossible that the maximum O concentration can be much lower than 100 km under certain conditions. This can be expected, first of all, by considering the observations in [10] of the strong yearly variation in the level for the beginning of O_2 dissociation (decrease roughly by 10 km around the summer) and, secondly, by considering the calculations for the displacement of the maximum O concentration, if we take the descending air currents [16] and turbulent diffusion [17] into account.

Ozone. Due to the numerous ground measurements, the O_3 distribution up to an altitude of 50 km and its oscillations are fairly well known [18]. However, there have been only a few rocket and satellite measurements for the mesosphere, and many of them were also described in [18]. All of the rare measurements of the daily O_3 concentration above 50 km were close to the distributions which are given in Figure 1 and which were obtained from optical measurements from a rocket on July 14, 1949 in New Mexico (32°N) and froma satellite on a polar orbit (32° and 13° N) [19]. In the first case, the sounding was carried out up to a level of 70 km. In the second case, the concentration was obtained up to 80 km, but the results can be approximated only roughly by an exponential curve because of the great discrepancy in the experimental points. (Above these levels, the O_3 distributions in Figure 1 were extrapolated by the exponential function.)

Many authors have calculated the O_3 concentration on the basis of the photochemical theory. The calculations were carried out both for a pure oxygen atmosphere, e.g. [20,21,22], and for an oxygen-hydrogen atmosphere, e.g. [11]. According to the observations of [18], the photochemical theory is untenable below 40 km. However, in higher layers the calculations are only of a qualitative or, in the best case, semi-quantitative nature. The reason for this is the indefiniteness of our knowledge on the velocities of the reactions, the spectral intensity of the solar ultraviolet radiation, the absorption coefficients of the gases, the quantum effectiveness of their photodissociation, the concentration of the water vapor in the upper stratosphere and the mesosphere. Moreover, the photochemistry must be examined in combination with dynamic processes. /30

Let us consider the characteristic aspects of the seasonal and

latitudinal variations in the daily concentrations of O_3 obtained from photochemical analyses in a pure oxygen atmosphere in steady-state approximation. All the way to broad average daily zenith angles of the Sun (about 75°), the O_3 concentration either decreases slightly with an increase in the zenith angle roughly above 55 km, or it practically does not depend on it in the 40-45 km layer. Therefore, the vertical temperature profile appearing in the velocities of the chemical reactions acquires great significance in the seasonal and latitudinal variation of the O_3 concentration. An increase in the temperature results in a decrease in the concentration. Because of the characteristics of the temperature distribution (Sect. 4) and the different heights of the Sun over the horizon, the least concentrations of O_3 are obtained in the winter in the high-latitude upper mesosphere, and the greatest concentrations are found in the summer. A self-regulation mechanism is effective in the layer of 40-50 km. A decrease in the /31 concentration due to an increase in the temperature results in a deeper penetration of the ozone-generating radiation (2000-2400 Å) and, consequently, causes an increase of O_3. The photochemical theory gives practically identical concentrations for this layer during different seasons and at different latitudes, while the latter conclusion is confirmed by ground observations [18].

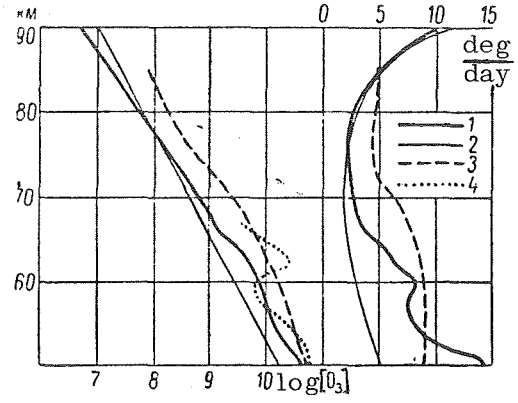

Fig. 1. Distribution of O_3 Concentration (on the left) and the Corresponding Rates of Heating (on the right) Due to Absorption of Solar Ultraviolet Radiation During a Solstice at the Equator. (1) Rocket Measurements on July 14, 1949 in New Mexico [18]; (2) Satellite Measurements [19]; (3) Photochemical Calculations for Noon at the Equator during a Solstice [20]; (4) Nocturnal Measurements According to the Ultraviolet Emission of the Atmosphere [25].

In considering the daily oscillations of the O_3 [20] in general outline, the O_3 distribution by altitude is of the same nature as in the steady-state approximation, while both methods give virtually identical values for the concentrations in the layer of 30-60 km. Above 60 km, a nonstationary examination yields lower O_3 concentrations, all the way to a factor of 3 at an altitude of 85 km. This is caused by the fact that O, which is the raw material for obtaining O_3, is not reduced to its equilibrium concentrations during the lighted part of the day.

Figure 1 gives a typical calculated profile for O_3 [20]; it was calculated during a solstice at the equator for noon. A comparison of the calculated distributions and the observations shows that the photochemistry in the pure oxygen atmosphere possibly could give increased O_3 concentrations in the upper mesophere. A consideration of the reactions with hydrogen-containing compounds [11] brings about a decrease in the O_3 concentration in the 55-95 km layer. However, the accuracy of such calculations is still less than in a pure oxygen atmosphere, both because of the great indefiniteness of the velocities of the reactions and because of the insufficiency of information on the H_2O content in the upper atmosphere. The decrease in O_3 concentration is all the greater when the H_2O concentration increases. For a mixing ratio of water vapor on the order of 10^{-4} g/g, the decrease in O_3 concentration can even reach two orders.

In order to calculate the rate of infrared cooling of the atmosphere, it is also important to know the nocturnal O_3 concentrations. According to the photochemical theory, the O_3 concentration should increase during the night for a pure oxygen atmosphere, because of the decrease in O content. In a layer above 60 km, there could be an increase in the concentration by a large factor, sometimes even by more than an order, as the Sun rises. The amplitude of the daily oscillation depends on the altitude, the temperature, and the relative length of the night. As for the daily variation in the O_3 concentration for an oxygen-hydrogen atmosphere, calculations in dependence on the latitude and season show both an increase and a decrease in the O_3 concentration. However, we must remember that these calculations are not completely accurate.

The observations which were carried out during twilight from the "Echo" satellite [23], the rocket measurements before and during a solar eclipse [24] and nocturnal rocket soundings [25,26] seem to confirm the conclusion of the photochemical theory, that the O_3 /32 increases after sunset. While measurements of the nocturnal ultraviolet emission of the atmosphere [25] give a relatively small secondary maximum in the O_3 concentration at altitudes of about 63 km (Fig. 1), a record of the light reflected from the Moon [26] indicates that the O_3 increases by three orders at an altitude of 85 km, compared to the diurnal concentrations obtained from photochemical calculations.

We should note the positive correlation between the O_3 concentrations above 35 km and the eleven-year cycle in solar activity [27]. This shows the possible variations in the spectral distribution of the intensity of ozone-generating and ozone-decomposing radiation in dependence on the processes on the Sun and, thus, the essential role of the latter in the O_3 distribution.

Carbon Dioxide. At present, the average volume concentration of CO_2 over the planet according to the data of measurements in the lower layers of the troposphere is considered to be close to $3.15 \cdot 10^{-4}$

[28]. Most of the recent studies on the ratio between the Ar and N_2 concentrations in the upper atmosphere (see [14], for example) indicate that the diffusive distribution of gases begins at altitudes of 105-110 km. The photodissociation of CO_2 also becomes substantial in the lower thermosphere [29]. Therefore, it can be assumed that the volume concentration of CO_2 all the way up to the mesopause is close to that of the troposphere. A volume concentration c_v equal to $3.1 \cdot 10^{-4}$ was obtained during sounding observations carried out in 1954 and 1956 for altitudes from 15 to 33 km [30]. Measurements at a level of 36 km in May of 1962 [31] gave a value of $3.0 \cdot 10^{-4}$. The values obtained practically coincide with the values of c_v in the troposphere.

Water Vapor. Altitudes of 25-35 km are the ceiling for measurements of the humidity with hygrometers and spectrometers. Different measurements indicate that there is a wide range of possible values for the mixing ratio: $\sim 10^{-6}$ - 10^{-4} g/g [32]. However, a critical analysis of the high-altitude measurements of H_2O tends to indicate that the high-humidity value was obtained in error [33,34] and that the mixing ratio obviously does not exceed 10^{-5} g/g in order of magnitude. Calculations of radiant heat fluxes (Sect. 10) also speak in favor of a "dry" upper stratosphere. Moreover, the discovery of such low temperatures as 130° K in a zone of noctilucent clouds can also be explained by the arisal of such clouds in the case of a "dry" mesosphere. Because of the photodissociation of H_2O above 65-75 km, the humidity, according to the photochemical theory, should decrease rapidly with an increase in the altitude [11,29,35]. It should be expected that turbulent diffusion actually would have a strong retarding effect on this decrease [36]. The vertical air movements could displace the "dissociation boundary" [35].

4. Temperature and Its Variations /33

Recently, because of the development of methods for direct rocket sounding of the upper atmosphere, rather reliable data have been obtained on the structural parameters of the atmosphere up to altitudes of about 80 km. An example of this development is the studies whose results were published in the collections [37,38]. Up to 30-35 km, the data on the temperature have also been obtained by radiosondes. However, there is still very little information on the layers above 80 km. It can be said that there has recently been a transition from sporadic soundings to previously-planned series of observations carried out with the purpose of studying definite processes or phenomena. Here, we will discuss mainly the principal results of direct soundings of the upper atmosphere carried out by the rocket-shell (acoustic) method, the falling sphere methods, and manometric measurements [1].

Vertical Profile. Figures 2 and 3 illustrate the characteristics of the temperature field graphically. The principal characteristic of the vertical profiles is the existence of a temperature

maximum (of the stratopause) at altitudes of 45-60 km and a temperature minimum (of the mesopause) at altitudes of 70-100 km. This type of altitudinal variation in the temperature occurs during all the seasons of the year and at all latitudes, except perhaps the highest latitudes, in the winter (see below).

Observations of the shadow of the Earth during lunar eclipses, on the assumption that the edge of the shadow is due to the absorption of solar radiation by an aerosol layer in the lower thermosphere, indicate that the altitude of the latter is greater at the equator than the pole, while the difference in altitudes is about 25 km. Assuming that there is a dependence between the height of the aerosol layer and the position of the mesopause, at least for lower latitudes, we can use the model of the two-layered mesopause [40]. The upper minimum occurs at an altitude of about 100 km, while the lower one (regular) is roughly 80 km. It is interesting that measurements by the method of falling spheres over Kwajalein (9°N) substantiate this hypothesis (see [41]. A two-layered mesopause with a local temperature maximum around 80 km was detected in many descents (Fig. 4).

Yearly and Latitudinal Variation. It can be easily seen from Figure 2 that the mesopause is much warmer at high latitudes in the winter than in the summer. At an altitude of about 65 km, there are practically no seasonal and latitudinal variations in the temperature (range of variations of 230-240°K) [33]. Below this altitude, the direction of the yearly oscillations is "normal", i.e., it corresponds to the yearly course of insolation. We should mention that the temperature maximum in the upper stratosphere, at least at middle and high latitudes, tends toward the spring, while the minimum tends somewhat toward the autumn at high latitudes [42].

The averaged temperature gradients of the mesosphere over the planet are close to 2-3 deg/km on the average. Obviously, /35
there is an inverse correlation between the temperature of the stratopause and the mesopause [33]. The lowest gradients are typical of high latitudes in the winter. According to the preliminary data of one of the highest-altitude stations (Alaska, 71°N) carrying out observations in January of 1965, there was almost isothermy with temperature of about 240°K in the layer of 40-80 km [33]. The highest average gradients all the way to 5 deg/km are typical of high latitudes in the summer. The lowest temperatures for high latitudes, equal to 130-135°K, were recorded in the summer over northern Sweden at an altitude of 80 km in a zone of noctilucent clouds. However, we must mention that an extremely low temperature, 126°K, was also recorded at low latitudes (Kwajalein, 9°N) [41] in June of 1963 at an altitude of 94 km. Some spectroscopic observations of air glow [2] also indicate that there can be very low temperatures in the mesopause. The greatest temperatures observed in the stratopause were close to 300°K.

/34

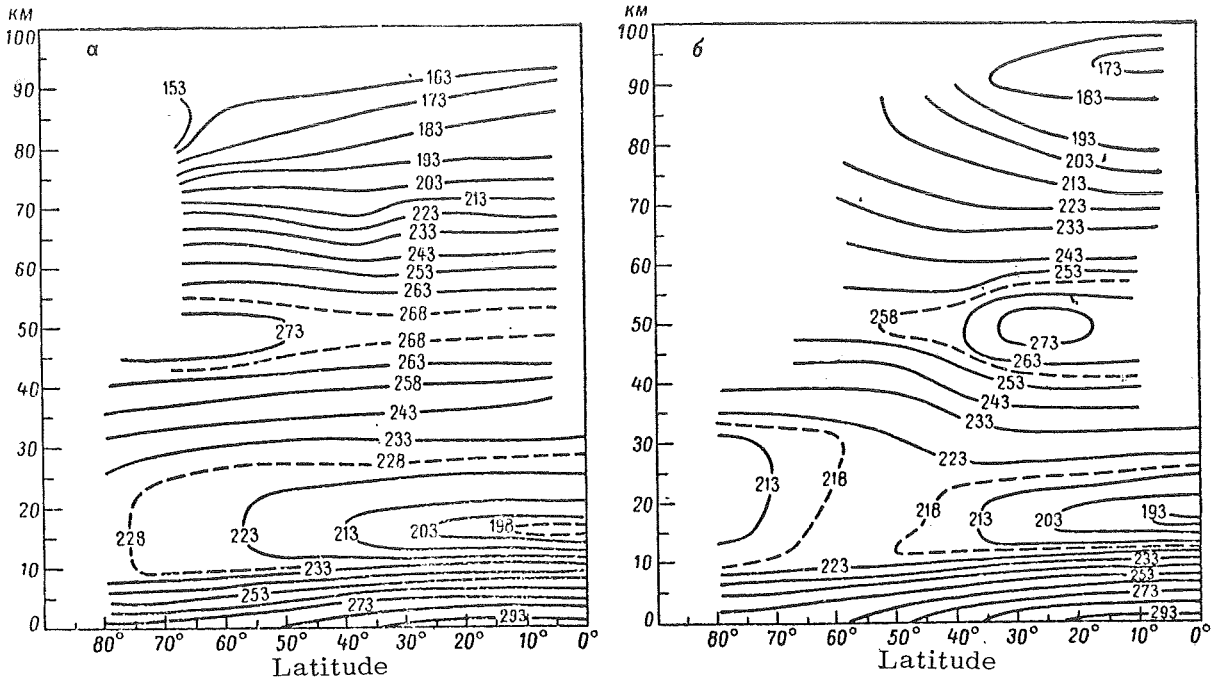

Fig. 2. Meridional Altitudinal Section of the Temperature Field (°K) of the Northern Hemisphere in the Summer (a) and Winter (b) according to American Rocket Data [39].

/35

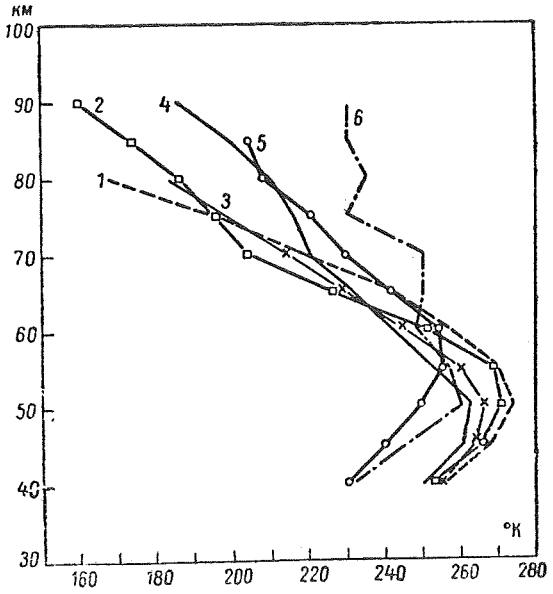

Fig. 3. Average Vertical Temperature Profiles Obtained by the Acoustic Method (according to NASA Data).
(1) High Latitudes, Summer (Churchill, 1957; Sweden, 1963); (2) Wollops Island, Summer, 1960-1963; (3) Guam, Winter, 1958; (4) Wollops Island, Winter, 1960-1963; (5) Churchill, Winter, 1962-1963; (6) Churchill, Winter, 1956-1958.

Diurnal Variation. A direct observation of the diurnal variation in the temperature of the upper atmosphere is made difficult by the stronger irregular temperature changes due to dynamic processes. Moreover, the diurnal variation in the layer under investigation has been very little studied. A number of launchings with intervals of 2 hours up to an altitude of 60 km was carried out over White Sands (32°N) in February of 1964 [43]. Diurnal temperature changes on the order of 15-20°K were obtained in the range of the stratopause; the minimal temperatures were recorded at 0400 and 0600, and the maximum was recorded at 1400. According to soundings at Fort Churchill (59°N) in the summer (see [37], it might be expected that the temperature increases from the first half of the day to the second by 5-10°K at an altitude of 50 km. There have also been indirect determinations of the temperature up to altitudes of 25-30 km according to the wind variations [44]. /36

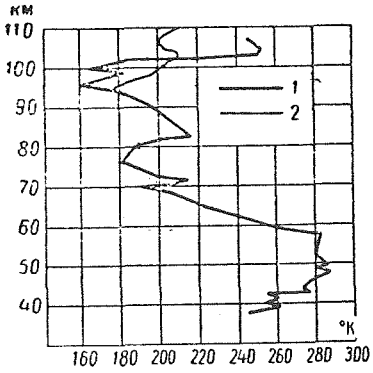

Fig. 4. Vertical Temperature Distribution Obtained on May 12, 1964 over Kwajalein [41] according to an Analysis of the Trajectories of a Balloon Flying Down (1) and Up (2).

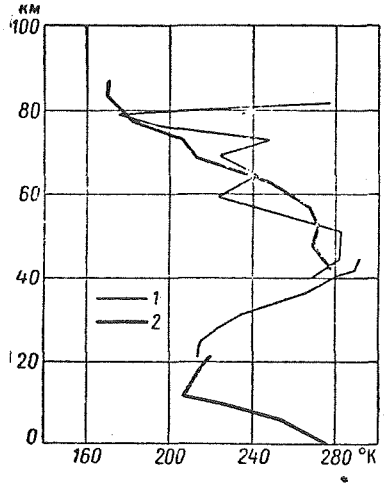

Fig. 5. Change in the Vertical Temperature Profile in 6 Hours on May 5, 1961, over Wollops Island according to the Data of Two Soundings (Curve 1, at 16:00; Curve 2, at 23:54). Up to 20 km, the temperature was measured by radiosonde, and practically did not change in the 6 hours. From 20 to 40 km, the temperature was measured at 16:00 from a small meteorological rocket. The acoustic method was used over 40 km.

Irregular Space and Time Variations. The results of specific soundings actually do not give such smooth temperature distributions as the averaged distributions on Figures 2 and 3, as a rule. This fact is illustrated well in Figures 4 and 5. Moreover, it can be said that the nature of the altitudinal temperature variation can change radically in a short period of time, often less than one day [45]. For example, Figure 5 shows such a change in the profile for middle latitudes (Wollops Island, 38°N) in 6 hours in all. We can speak of typical temperature profiles for a certain season /37 of the year and latitude only in the statistical sense. The rapid space and time irregularities in the temperature distribution can be connected solely with the dynamic processes in the atmosphere.

The presence of one or more secondary temperature maxima which are displaced along the vertical and change in magnitude during a rough twenty-four hour period is characteristic of the winter mesosphere of high latitudes [37,38,45]. The highest temperature recorded for a secondary maximum was 290°K (altitude of 73 km). As can be seen from Figures 4 and 5, profiles of such a type also occur at middle and low latitudes.

The second half of January and February have a climatological peculiarity at high altitudes - sudden heating of the stratosphere (see [37,46,47,48], for example). This phenomenon sometimes encompasses more than half of the northern hemisphere. Slight warm-ups of the stratosphere were also observed in the summer [49]. Beginning at higher levels, the heating process gradually extends downwards. The heating can "originate" in the mesosphere, but it appears particularly markedly in the upper stratosphere, where the temperature can increase by 50° in a few days (time-independent process). Sometimes the heating does not extend below 30 km. It can be assumed that the sudden warm-ups of the stratosphere also occur in the southern hemisphere [50].

According to the data of rocket soundings [51], the seasonal effect of mainlands and oceans on the yearly temperature variation is maintained up to a level of about 45 km. It seems that the difference in the temperature fields of the stratosphere over the Arctic Circle and Antarctica can be explained by the characteristics of the underlying surface.

Effect of Solar Activity. Apparently, we can speak of an effect of the solar activity on the temperature of the upper atmosphere. Yearly temperature changes of about 70°K were recorded over Fort Churchill (59°N) at the level of the mesopause during the years of maximum solar activity, as opposed to 45°K during quiet sun years [33].

5. Absorption Functions

Ultraviolet Radiation

We know of a large number of experimental studies on the absorption of ozone and molecular oxygen in the ultraviolet region of the spectrum. Experimental data are given in [4,52,53,54,55, 56] in the form of absorption coefficients or graphs. The dependence of absorption on the temperature was studied in the Hartley ozone bands, and was found to be insignificant. Measurements show /38 that the absorption coefficient at the absorption maxima in the Schumann-Runge oxygen bands exceeds the absorption coefficient at the minima by one order of magnitude. However, in order to carry out strict calculations of the radiant heating, we must know the dependence of the absorption coefficient on the frequency in more detail than can be given by the present observations. It is not impossible that a modeling of this, and perhaps other, absorption bands in the short-wave spectral region will be required for more precise calculations.

Infrared Radiation

A great deal of experimental and theoretical studies has treated the radiation-absorption functions in the infrared. All this attention to the problem is due to the importance of the infrared radiant transfer in the thermal regime of the lower alyers of the atmosphere, as well as in the solution to the inverse problems leading to a determination of the temperature, composition of the atmosphere, etc., according to the emission field.

Experimental Data. Measurements of the absorption functions have been carried out by many researchers under laboratorial conditions [52]. The absorption functions have been obtained for the intensity of radiation in a broad range of changes of the pressure and quantity of absorbing gases. In a number of studies [52,57,58,59], the laboratorial data are presented in the form of empirical formulas, which are valid in certain intervals for the pressure p and value of the masses of the absorbing gas u, while the absorption is modeled by functions which depend on the variable up^n in the most recent studies. Here n is the exponent, which is determined by the method of fitting. It can be concluded that, regarding the range of values for p and u, the laboratorial data satisfy the tropospheric conditions well; however, most of the measurements are limited to room temperatures.

It would be very good if the experimental absorption functions and, in particular, the cited empirical formulas could be used in calculations of the radiant heat fluxes in the upper layers of the atmosphere. However, because of the great experimental difficulties, the existing data are limited from the viewpoint of the very low values of p and u characteristic of the upper stratosphere and, all the more, the mesosphere. In [59], empirical

formulas were constructed for a large set of H_2O, CO_2, CH_4 and N_2O rotation-vibration absorption bands, as well as for O_2 bands, according to laboratory measurements for the lowest p and u and according to high-altitude observations of the absorption of solar radiation. These formulas should now be considered as the most appropriate for the conditions of the stratosphere. We should mention that the formulas were obtained in approximation of the strong line, i.e., the exponent n = 1. According to the experiment in [57], approximation of the strong line is realized at high values for the absorption which are close to saturation conditions. Since the absorption for all the bands is far from saturation under stratospheric conditions, there is danger in great errors in calculating the radiant heat fluxes by the formulas obtained in [59]. The well-known formula of Walshaw [52] for the 9.6 μm O_3 band is valid, apparently, up to altitudes of about 30 km. As for measurements of the absorption functions in the rotational H_2O band [60], they were carried out for particularly tropospheric conditions.

The absorption functions obtained by extrapolation in the range of low p and u from higher values should always be treated with great care. First of all, the extrapolation is poor in that, in calculating radiant heat fluxes, great requirements are imposed on the accuracy for the absorption functions - in fact, the derivatives of this function are necessary. Secondly, certain characteristic dependences of the absorption on p and u are valid only in a certain range for changes in p and u. Moreover, there is one more circumstance under the conditions of the stratosphere which makes extrapolation difficult: the Lorentz and Doppler linewidths become values of one order at stratospheric altitudes [52]. In contrast to the troposphere, the absorption coefficient in the line in the upper stratosphere cannot be described by the Lorentzian contour

$$k_\nu = \frac{S}{\pi} \frac{\alpha_L}{(\nu - \nu_0)^2 + \alpha_L^2}, \tag{3}$$

but has a more complex, Lorentz-Doppler form, i.e.,

$$\begin{gathered} k_\nu = k_0 H(a, \omega), \\ H(a, \omega) = \frac{a}{\pi} \int_{-\infty}^{\infty} dx \frac{e^{-x^2}}{a^2 + (\omega - x)^2}, \\ k_0 = \sqrt{\frac{\ln 2}{\pi}} \frac{S}{\alpha_D}, \quad a = \sqrt{\ln 2} \frac{\alpha_L}{\alpha_D}, \quad \omega = \sqrt{\ln 2} \frac{\nu - \nu_0}{\alpha_D}. \end{gathered} \tag{4}$$

When a <<1 (mesosphere), the contour in (4) converts into a Doppler contour, i.e.,

$$k_\nu = \sqrt{\frac{\ln 2}{\pi}}\,\frac{S}{\alpha_D}\,e^{-\frac{(\nu-\nu_0)^2}{\alpha_D^2}\ln 2}. \qquad (5)$$

The following symbols were used in (3), (4) and (5): ν_0 is the frequency at the center of the line, S is the line intensity, α_L and α_D are the Lorentz and Doppler half-widths of the lines, respectively. We will not examine at all those difficulties [52] which arise in applying laboratorial data obtained for uniform optical paths (constancy of pressure and temperature) to the real optical paths in the atmosphere.

Many important studies of the effect of radiant transfer on /40 the thermal regime of the upper stratosphere and even the mesosphere have nevertheless been carried out on the basis of laboratorial absorption functions extrapolated for low p and u (see [58,59, 61-66], for example). For the above-mentioned reasons, numerical estimates obtained in such studies must be used very carefully, and these results become extremely indefinite for the mesosphere. The calculated distributions of radiant heat fluxes and radiation temperatures primarily reflect the nature of the altitudinal variations in the temperature and the concentrations of absorbing gases (Sect. 1). Even in using absorption functions which are far from the real ones, we can obtain qualitatively intelligible distributions of the radiant heat fluxes and the radiation temperatures. Thus, absorption functions obtained with great accuracy are necessary in order to obtain rather precise numerical estimates.

Theoretical Calculation. The following method of obtaining the absorption functions is a calculation method based on information concerning the structure of the absorption band (line distribution in the spectral interval and by intensities), as well as knowledge on the shape of the contour and width of the lines. The absorption functions can be calculated precisely only in that case when the above-mentioned characteristics are rather well known. However, a measurement of the latter depends primarily on the development of the methods of high-resolution spectroscopy. There is no precise information for a number of bands, for example for the 0.6 μm O_3 band.

The problem amounts to a calculation of expressions of the following type:

$$A_F(z_1, z_2) = \frac{1}{\Delta\nu}\int_{\Delta\nu} d\nu\left(1-2\int_1^\infty dm\, m^{-3} e^{-m\int_{z_1}^{z_2} k_\nu(z)\,dz}\right). \qquad (6)$$

In a comparison with the experimental functions, the basic advantages of theoretical calculations consist, first of all, in the possibility of calculating the derivatives of the absorption functions immediately, with a great deal of accuracy and, secondly, in a more correct consideration of the nonuniformity in the real optical paths. The latter means that we can take rather good account of the change in the shape of the contour with the pressure and temperature, as well as the dependence of the line intensity on the temperature. However, in contrast to using empirical data, the calculation methods are distinguished by a great deal of time-consuming computations, and can be realized only with an electronic digital computer.

Let us examine the basic difficulties in theoretical calculations and the ways of overcoming them in relation to a layer of the atmosphere above 30 km.

1. Integration by the frequency ν takes the frequency dependence of the absorption coefficient in the interval of $\Delta\nu$ into /41 account. Calculations using the real structure of the band are so laborious that even the modern high-speed computers are incapable. An example of such an approach is [67]. A model of the band in dependence on the nature of the line distribution in the frequency interval and over the intensities is used erroneously in [52,68]. Since $\alpha_L \propto p$, while $\alpha_D \sim 10^{-3}$-10^{-4} cm^{-1}, it is natural to expect that, starting with certain altitudes, a model of nonintersecting lines can be used in each spectral interval of the infrared spectrum. More accurate information on the suitability of this model for calculating radiant heat fluxes in definite frequency intervals can be obtained on the basis of a number of lines realized in the radiant transfer, and their intensity in the interval under investigation. The most definite evaluations can be obtained for the 15 μm CO_2 band [69], for which calculations of the radiant heat flux in the mesosphere in approximation of an isolated line should have satisfactory accuracy. An approximation of nonintersecting lines in the upper stratosphere is not valid in intervals occupied by lines of the Q-branches (we should mention that about half the intensity of the entire 15 μm band is concentrated in the Q-branches). In evaluations of the validity of approximating an isolated line, it is also important to know whether the radiant heat fluxes are caused by absorption of solar radiation or by transfer of the self-radiation of the atmosphere. In the first case, the radiant heat fluxes depend on the transfer of radiation in frequency intervals further removed from the center of the line than in the second case. The studies [69,70] can be found useful in evaluating the validity of the model of nonintersecting lines in various spectral intervals. Of the other models for calculating radiant heat fluxes, only the quasi-random model of [68] has been tested, and this is again for the 15 μm CO_2 band. According to [71], it results in very great errors.

2. Integration by m takes account of the diffusivity of the radiation, which is important in the transfer of the self-radiation of the atmosphere. As a rule, because of a simplification of calculations, the transmission for diffuse radiation is replaced by the regular transmission for directed radiation

$$\exp\left(-m\int_{z_1}^{z_2} k_\nu(z)\,dz\right),$$

having selected a certain value of m. The value m = 1.66 is used most frequently; many researchers maintain that this value is correct [52,71]. However, it is still unclear to what extent this value is valid in calculations of the radiant heat fluxes for a line contour which differs greatly from the Lorentz one.

3. Integration by z takes account of the change in concentration of absorbing gas and the line intensity with the altitude, as well as the variation in the shape of the line contour. The calculations can be simplified substantially by the widely-used /42
Curtis-Godson method [52]. This method can reduce the absorption for the nonuniform atmosphere to the case of absorption in a uniform atmosphere, selecting the effective pressure and mass of the absorbing gas in the following way:

$$\left.\begin{aligned} \tilde{p} &= \frac{\sum_i \int_{(1)}^{(2)} S_i p\,du}{\sum_i \int_{(1)}^{(2)} S_i\,du}, \\ \tilde{u} &= \frac{\sum_i \int_{(1)}^{(2)} S_i\,du}{\sum_i \tilde{S}_i}. \end{aligned}\right\} \qquad (7)$$

Here summation is carried out over all the lines in the frequency interval under investigation; (1) and (2) are indices of the levels between which the transmission is calculated; $\tilde{S}$ is the line intensity for some definite temperature. The Curtis-Godson approximation is completely valid only in extreme cases of a weak and strong isolated Lorentz line. Use of this method results in great erros when one part of the optical path corresponds to the conditions for approximation of the strong line while another part corresponds to that of the weak line, and each region makes a substantial contribution to the absorption. Such a situation arises when the mixing ratio for the absorbing gas (for example, O_3) increases with the altitude. For an isolated line (approximation frequently used in the upper atmosphere), a generalization of the Curtis-Godson method is given in [72] for a Lorentz-Doppler contour and practically any nature of the dependences of the line intensity and concentration of absorbing gas on the altitude.

4. One more difficulty is encountered in a precise numerical calculation of the Lorentz-Doppler contour of the line in (4). We

will limit ourselves so that we will only discuss the most recent studies [73,74,75] treating the development of methods for calculating the function $H(a,\omega)$ over the entire region for change in the variables a and ω. The function $H(a,\omega)$ has been tabulated many times, and the most detailed tables were obtained recently in [76,77]. Great simplifications can be made in approximation of nonintersecting lines in calculations of the radiant heat fluxes if we establish the limits to use of different approximating expressions for the line contour and the absorption functions [78,79,80]. It is always helpful to separate the regions where the line can be represented as purely Lorentzian or a Doppler one, and also if we define the limits to application of the approximations for the strong and weak lines in each of them.

Studies of the thermal effect of radiation in the atmosphere above 30 km which were carried out on the basis of theoretically /43 calculated absorption functions are very rare ([20,71,81,82], as well as the results we obtained and presented in this study).

6. Fluorescence Processes

The fluorescence must be considered in calculations of a radiant heat flux in those cases when the radiation lifetime of an atom or molecule in the excited state is of the same order as or less than the effective time necessary for deactivation by collisions [52,83]. The fluorescence effects in the atmosphere amount either to a disruption of the l.t.e. (deviation from the Kirchoff law for radiation) during the transfer of natural radiation, or to a decrease in the value of κ in comparison with unity and the necessity for considering the field of scattered radiation during the transfer of solar radiation.

If a transfer occurs between two levels of an atom or molecule, then the transfer equation has the following form when the molecular and aerosol scattering is disregarded:

$$\left.\begin{aligned} \frac{dI_\nu}{ds} &= -k_a(\nu) I_\nu + J_\nu, \\ k_a(\nu) &= \frac{\frac{n_1}{\bar{n}_1} e^{\frac{h\nu}{kT}} - \frac{n_2}{\bar{n}_2}}{e^{\frac{h\nu}{kT}} - 1} k_\nu, \\ J_\nu &= k_\nu \frac{n_2}{\bar{n}_2} B_\nu(T(s)). \end{aligned}\right\} \qquad (8)$$

Here I_ν is the intensity of radiation at a frequency of ν; J_ν is the source function; B_ν is the intensity of radiation of an absolutely black body at a temperature T equal to the kinetic temperature of the gas; s is the coordinate along the ray; h is the Planck constant; k is the Boltzmann constant; n_1 and n_2 are the concentration of atoms or molecules in the lower and upper

states, respectively; $\bar{n}_1$ and $\bar{n}_2$ are the same under the conditions of thermodynamic equilibrium at the same temperature T; $k_a(\nu)$ is the real absorption coefficient; $k\nu$ is the regular absorption coefficient under the conditions of thermodynamic equilibrium. It follows from (8) that radiant heat fluxes should depend on the population of the levels.

The speed of the change in population of some state is determined, on the one hand, by the optical transitions and, on the other hand, by collisions accompanied by excitation and de-excitation. Under steady-state conditions, the populations of the levels are connected by way of a system of kinetic equations: (a) with each other; (b) with the radiant heat fluxes due to transitions /44 between various combinations of states of the atoms or molecules under investigation; (c) with the population of levels of other components of the gaseous mixture, if the energy of the states of atoms or molecules of another type are sufficiently close to the energies of the states of the particles in question. Thus, a calculation of the radiant heat fluxes and a determination of the distribution of atoms or molecules by states is essentially the same problem in the general case. This problem is very difficult, but simplifications are possible in many cases, e.g., sometimes an ordinary relaxation equation can be used instead of a system of kinetic equations.

Two limit cases are well known. The first consists in a situation where, if we can disregard the role of optical processes in the establishment of the level population, we can consider that the distribution by states satisfies the Boltzmann law ($n_i = \bar{n}_i$). This is the case of l.t.e., and then the Kirchoff law is valid for the transfer of self-radiation, while the source function can be considered as equal to zero in the transfer of short-wave radiation. Thus, the fluorescence processes can be disregarded entirely under l.t.e. conditions. In the other extreme case, when the role of collisions in the establishment of the population by levels is insignificant, the radiant fluxes are practically equal to zero. However, these limiting approximations cannot always be used in the layer of the atmosphere under investigation.

Violation of the Kirchoff Law. The criterion for the beginning of deviation from this law can be considered as an approximate fulfillment of the relationship $\theta_r/\tau \simeq 1$, where θ_r is the radiation lifetime of the excited state, while τ is the relaxation time for collisions ($\tau \propto p^{-1}$). The values of θ_r of the first excitation levels are given in Table 1 for some of the most important vibrational transitions of atmospheric gases. The values of θ_r were calculated according to the intensities of the fundamental rotation-vibration bands obtained from experiments. At room temperatures and p = 1 atm, and the vibrational relaxation times obtained experimentally for most of the diatomic and triatomic molecules were equal in order of magnitude to 10^{-3}-10^{-6} sec [88,89].

However, the relaxation times of importance to us for CO_2, O_3 and H_2O were actually not measured in the collision of these molecules with N_2 and O_2 molecules. Moreover, we must know τ for low, mesospheric temperatures. The theory gives very rough estimates, primarily because of the indifiniteness of the repulsive forces between the particles. In many cases, different experiments and theoretical calculations live values of τ which differ by one order (for example, in the case of deformation vibrations in CO_2-CO_2 collisions [90]). We can expect that τ is in an interval of $2\cdot10^{-5}$-$2\cdot10^{-6}$ sec for $T \simeq 200°K$ for vibrational relaxation in CO_2-N_2 and CO_2-O_2 collisions [83]. There is an indirect indication that $\tau \sim 10^{-6}$ sec (Sect. 10). /45

TABLE 1. INTENSITIES OF THE FUNDAMENTAL ROTATION-VIBRATION BANDS AND RADIATION LIFETIMES OF THE CORRESPONDING STATES FOR SOME VIBRATIONAL FREQUENCIES OF ABSORBING ATMOSPHERIC GASES.

Absorption Band	Vibrational Quantum Frequency, cm^{-1}	Intensity of Fundamental Transition under Normal Conditions, $cm^{-1}(cm\cdot atm)^{-1}$	θ_r, sec
15 μm CO_2	667	208 [84]	$7.7\cdot10^{-1}$*
9.6 μm O_3	1043	514 [85]	$6.4\cdot10^{-2}$
6.3 μm H_2O	1595	225 [86]	$6.2\cdot10^{-2}$
4.3 μm CO_2	2349	2706 [87]	$2.4\cdot10^{-3}$

* A value decreased roughly by a factor of two θ_r is often found (for example, in [33, 52]). This is due to the fact that the degeneration of the state 01^10 is not considered.

We should point out two circumstances which must be considered in determining τ. First of all, in some cases τ can depend mainly on collisions with molecules of small impurities in a gas. This holds when the chemical forces have effect during collisions [89]. For example, CO_2-H_2O collisions are roughly 10^2-10^3 times more effective for CO_2 vibrational relaxation than CO_2 collisions with N_2 and O_2 molecules [83].[1] However, since the mesosphere should apparently be "dry" (Sect. 3), this effect of H_2O can be disregarded. Secondly, if the energies of the vibrational levels are close to

[1] It was recently shown in [91] that the high effectiveness of H_2O observed in the CO_2 vibrational relaxation can be explained without disregarding the model of strong, chemical, interaction.

those of molecules of $N_2(\nu = 2331\ cm^{-1})$ and $O_2(\nu = 1555\ cm^{-1})$, then τ will probably be determined not so much by the exchange of energy between vibrational and translational degree of freedom as by the exchange of energy between the vibrations of molecules of different types [89]. The fact that such a situation can occur in the atmosphere can be easily seen in Table 1. The probability of this exchange is particularly high when the energy of the excited level is high (for example, for asynmetric vibration of CO_2).

Considering the high chemical activity of O_3 and H_2O, as well as the high probability of an exchange of vibrational energy between H_2O and O_2, we can assume that the vibrational relaxation times for O_3 and H_2O are no greater than orders of magnitude of 10^{-5} sec. However, according to the known values of θ_r, a substantial violation of the Boltzmann distribution by vibrational levels can be ex-/46 pected only above altitude of ~ 60 km.

As for the rotational relaxation, experimental and theoretical studies give values of $\tau \sim 10^{-10}-10^{-9}$ sec [88, 89]. The exception is H_2 with high energy of rotational quanta, for which $\tau \sim 10^{-8}$ sec. Thus, in the problems of radiant fransfer all the way to the altitudes of photochemcial dissociation of H_2O, CO_2 and O_3, it can be considered that the rotational levels are populated according to the Boltzmann law.

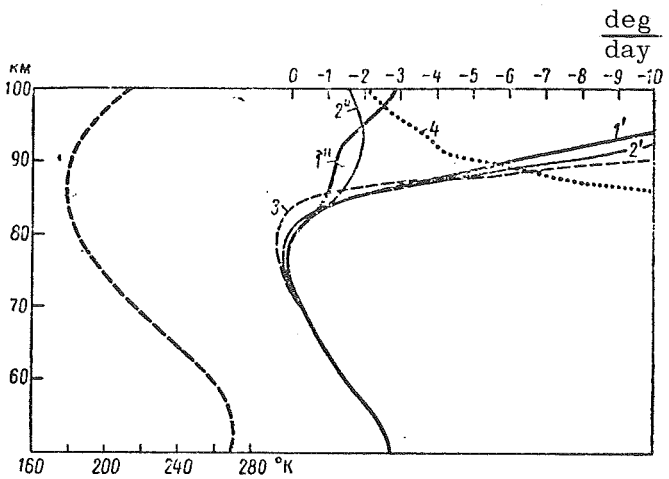

Fig. 6. Radiant Heat Fluxes Caused by Transfer of Radiation in the Lines of the Fundamental Transition of the 15 μm $C^{12}O_2^{16}$ Band. (1') Curve considering the dependence of τ on the temperature at $\tau = 2\cdot10^{-6}$ sec; (1'') Same, at $\tau = 2\cdot10^{-5}$ sec; (2') Curve obtained in approximation of the dependence of τ on the temperature at $\tau = 2\cdot10^{-6}$ sec; (2'') Same, at $\tau = 2\cdot10^{-5}$ sec; (3) Results of calculations on the sssumption that the Kirchoff law is valid; (4) Curve illustrating the results of the calculations in [71] for the transfer of radiation over the entire 15 μm band for $\tau = 10^{-5}$ sec. A standard model of the atmosphere, CIRA-1961, is given on the left. All the calculations were carried out for $c_V = 3\cdot10^{-4}$.

Calculations of the radiant heat fluxes which consider the deviation from the Kirchoff law have been carried out only for the 15 μm CO_2 band (see [52, 71, 81] and also the results we have obtained and given in this study). The great indefiniteness in the value for the vibrational relaxation time results, first of all, in the impossibility of determining the altitude of the level for the beginning of the l.t.e. violation precisely and, secondly, in great variations in the values for the radiant heat fluxes. Profiles of a radiant heat flux during the transfer of radiation in lines belonging to the transition $00^00 \rightarrow 01^10$ of the $C^{12}O_2^{16}$ molecule are given in Figure 6 according to my calculations, for the CIRA-1961 model of the atmosphere. The calculations were carried out on the assumption that l.t.e. is also valid for two τ which are equal to $2 \cdot 10^{-6}$ and /47
$2 \cdot 10^{-5}$ sec. It can be seen from Figure 6 that the beginning of the deviation from the Kirchoff law occurs at an altitude where $\theta_r/\tau \approx 1$.

According to theoretical and experimental studies [89, 92, 93], $\tau \propto e^{-T^{-1/3}}$ at temperatures which are not very low. The effect of the dependence of τ on T on radiant heat fluxes during the transfer of radiation in the 15 μm CO_2 band is also illustrated in Figure 6.

Fluorescence in Absorption of Solar Radiation. This effect has not been investigated to a great extent; therefore, we will limit ourselves to an indication of where it apparently must be considered.

It can be expected that the effect of vibrational relaxation is found in the absorption of solar radiation in the rotation-vibration bands of CO_2, O_3, H_2O, CO and N_2O. We should point out the 4.3 μm CO_2 band in particular, the possible role of which in the heating of the layer near the mesopause was mentioned recently in [33, 94]. However, if we consider the vibrational relaxation, then, apparently, this effect is very small (κ is close to 0). The precise value of τ is not known. However, if we limit ourselves even to the decreased value of $\tau = 10^{-6}$ sec, which is proable, and consider that $\theta_r = 2.4 \cdot 10^{-3}$ sec, then almost all the energy absorbed in the 4.3 μm band is re-radiated in the range of the mesopause. This also allows us to make an interesting conclusion, that scattered solar radiation can be found beginning with some level, for each of the CO_2, H_2O, CO and N_2O bands lying in the infrared. The altitude of this level depends on the values of τ and θ_r. At the same time, the vibrational relaxation times can virtually be determined by measurements of this altitude.

In the case of a forbidden transition, the excited electron state has a lifetime of $\sim 10^{-8}$ sec. For the gas densities of the interval under investigation, this results in a situation where $\kappa \approx 0$ during absorption in the electron bands. However, $\kappa \neq 0$ when there is predissociation. This situation occurs in the absorption in the Schumann-Runge band. Calculations of the radiant heat fluxes according to values of κ_ν taken for this band in [20] were carried

out in our studies (Sect. 7), where the field of the scattered radiation was not considered.

7. Absorption of Solar Radiation

Ultraviolet Radiation. The molecular oxygen in the lower layers of the thermosphere absorbs ultraviolet radiation shorter than 2000 Å intensively. According to my calculations (Fig. 7), in that case when all the energy absorbed at some level converts into thermal energy at the same level, a rate of heating of about 50 deg/day/48 at an altitude of about 100 km should be considered as erroneous. Such high values for radiant energy fluxes agree with the results of calculations in [95]; they exceed the values obtained earlier for the lower thermosphere in [81, 96] by a large factor. Obviously, this discrepancy can be explained by the incompleteness of initial data used in the calculation in [81, 96].

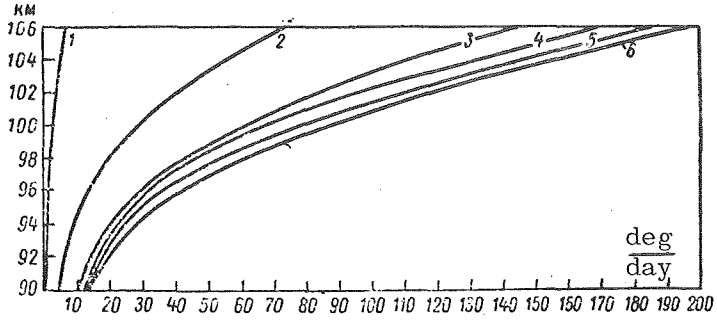

Fig. 7. Absorption of Ultraviolet Solar Radiation by Molecular Oxygen in Units of Daily Heating (the calculations were carried out for days of a solstice). (1) 60° latitude, winter; (2) 30° latitude, winter; (3) 0° latitude, winter; (4) 80° latitude, summer; (5) 60° latitude, summer; (6) 30° latitude, summer.

As the altitude decreases, the radiation shorter than 2000 Å is depleted, and from altitudes of 75-85 km (depending on the zenith angle of the Sun), the predominant role in absorption transfers to O_3. As all studies show, the absorption of ultraviolet radiation has a minimum roughly in this range of altitudes (see Fig. 1). This allows us to understand the origin of the mesopause. All the calculations (see [81,96], for example) also show an absorption maximum at an altitude of 45-50 km. The appearance of the maximum is the result of an increase in the volume concentration of O_3 with a decrease in altitude, on the one hand, and a weakening of the solar radiation in the Hartley band, on the other hand. Its existence explains the origination of the stratopause. However, the reasons for the ordinary inversion variation in the temperature in the upper stratosphere of polar latitudes remain unexplained. The meriodional gradient for the speed of the warm-up due to the absorption of solar radiation is directed from the winter pole to

the summer at all altitudes. The meriodional temperature gradient has the same direction in the upper stratosphere, but its direction changes to the opposite in the mesosphere.

In the absorption of solar ultraviolet radiation by molecular oxygen in the lower thermosphere, most of the energy goes to O_2 dissociation and converts into thermal energy only in recombination of oxygen atoms. Depending on the altitude of the level and concentration of O, the lifetime of an atom in the 85-100 km layer can change from several days to several months [29]. Due to eddy /49 diffusion or descending air currents, the recombination of O atoms can take place substantially below the level of their formation [16,95]. Thus, a consideration of the turbulence and vertical motions can greatly change the profiles of radiant heat fluxes obtained from the very simple calculations illustrated in Figures 1 and 7. It was suggested in [16] that descending air currents can, in principle, explain the local temperature maxima in the upper high-latitude mesosphere in the winter. It is not impossible that a decrease of the level of maximum liberation of chemical energy in O recombination on account of an eddy diffusion is somehow connected with the two-layered mesopause observed at low latitudes (Fig. 4).

The absorption of solar ultraviolet radiation and the chemical reactions caused by it lead to the arisal of excited particles of $O(^1D)$, $O_2(^1\Sigma_g^+)$ and $O_2(^1\Delta_g)$ in the atmospheric layer under examination [16,22,52]. If the rate of deactivation due to radiation transfers is greater than, or of the same order as, the rate of deactivation by collisions at certain levels of the atmosphere, then it may be found that the corresponding emissions should be considered in the theory of the thermal regime of the upper atmosphere.

Atomic oxygen is formed in the metastable ^1D state during the dissociation of O_2 and O_3 by radiation with wavelengths shorter than 1750 and 3100 Å, respectively. Observations of airglow and low-level aurorae indicate that $O(^1D)$ is effectively deactivated by collisions [97]. Consequently, the emissions of atomic oxygen of $^1D \rightarrow {}^3P$ in the thermal regime in the atmospheric layer in question can be disregarded.

Many processes result in the arisal of O_2 in the metastable electron states $^1\Delta_g$ and $^1\Sigma_g^+$:

$$O_3 + h\nu \rightarrow O(^1D, {}^1S) + O_2(^1\Delta_g, {}^1\Sigma_g^+) \text{(Wave length less than 3100Å)}$$
$$O(^3P) + O_3 \rightarrow O_2 + O_2(^1\Delta_g),$$
$$O(^1D) + O_3 \rightarrow O_2 + O_2(^1\Sigma_g^+),$$
$$O(^1D) + O_2 \rightarrow O(^3P) + O_2(^1\Sigma_g^+),$$
$$O + O + M \rightarrow O_2(^1\Delta_g, {}^1\Sigma_g^+) + M.$$

Evaluations of the thermal effect of excited O_2 states were carried out in [16]. It was assumed that the source of the excited states was the last of the enumerated reactions, while the deactivation due to collisions was represented by the following process:

$$O(^3P) + O_2(\alpha) \rightarrow O(^3P) + O_2(\beta),$$

where α is a higher state than β. According to [16], most of the /50 energy of excited O_2 converts into thermal energy in the atmospheric layer under investigation. In this case, the process of deactivation by collisions takes place more rapidly in the range of the maximum O concentration, and the re-emission of energy here is least probable. On the other hand, if we use the results of photochemical calculations in [22], then, ia approximation of the optically thin atmosphere at altitudes of about 50 km, where the calculated O_3 concentration is close to that observed, the rate of cooling during emission $^1\sum_g^+ \rightarrow {}^3\sum_g^-$ is found to be on the order of several degrees per day. Consequently, the thermal effects of O_2 emissions require further investigation. A theoretical analysis is made difficult because of the scarcity of knowledge on the speeds of the photochemical reactions determining the concentrations of excited O_2 states. All the calculations of the absorption of solar energy which have been completed have disregarded this effect.

The basic indefiniteness in calculations of the ozone absorption of solar ultraviolet radiation in the mesosphere is due to the lack of information on O_3 concentrations. In the studies in which concentrations obtained by the photochemical calculations were used, the rates of heating in the upper mesosphere are much greater than when the observed profile of the O_3 concentration is used (see Fig. 1). Sometimes [21,98] even a secondary warm-up maximum which is comparable to or exceeds the maximum in the region of the stratopause is obtained at altitudes of about 70 km. Since the O_3 concentrations calculated on the basis of the photochemical theory are very unreliable, we must question the reality of such a great warm-up of the upper mesosphere.

We can assume [99] that an automatic-regulation mechanism occurs in the layer around the stratopause. According to the photochemical theory, an increase in the temperature has such an effect on the speed of the reactions that the O_3 concentration decreases. However, the heating due to ozone absorption of solar radiation then decreases. This effect, together with the increase in infrared cooling during a temperature increase, tends to bring the layer back to the initial temperature.

Visible Radiation. The absorption of ozone in the visible region of the spectrum (Chappuis band) becomes substantial below 30 km [18], where the ultraviolet radiation is greatly weakened

by absorption in the overlying layers of the atmosphere. At the altitudes of the stratopause, the contribution of this band to the heating is 1-2 orders less than that of the Hartley bands. The rate of heating due to absorption of solar radiation by an aerosol has been evaluated only up to an altitude of 50 km [100]. It is found to be negligibly low: about 0.03 deg/day for this altitude. However, because this problem has been little studied, an aerosol /51 remains a fundamentally possible factor of the radiant heating of the upper atmosphere. For example, if in the region of the maximum aerosol concentration at altitudes of 80-100 km the concentration of particles is of the same order as on the 50 km level, then, based on the results of [100], we can expect that the rate of heating at these altitudes is equal to several degrees per day because of the decrease in density of the air.

Infrared Radiation. As a rule, the absorption in this spectral range (bands presented in Sect. 1) has not been calculated for layers about 30-40 km [58,59,94,100,101]. The contribution of infrared radiation to heating above 30 km is negligibly small compared to the contribution of ozone, except possibly for the layer near the mesopause [33,94], where the warm-up due to ultraviolet radiation has a minimum. It has been suggested that the heating near the mesopause is due to absorption in the 4.3 μm CO_2 band. However, this seems doubtful, in view of Section 6.

The most reliable data [59] show that the heating of the atmosphere at the 40 km level due to absorption of infrared radiation does not exceed 0.4 deg/day in the case of the "dry" stratosphere, when the basic contribution is due to CO_2. In the "humid" stratosphere, there could be increases in the total heating compared to the "dry" one roughly by a factor of two [58,59]. The contribution of the absorption of molecular oxygen is about 10% that of CO_2.

Daily Temperature Variation. The simplest radiation theory for the daily temperature variations is that a heat flux obtained by absorption of solar radiation during the day is compensated by a constant (in speed) outflow during the entire twenty-four hour period. In this case, the temperature minimum should be observed somewhat after sunrise, while the maximum should be found somewhat before sunset. According to this model, the daily temperature change is equal to the solar heating multiplied by the percentage of the duration of the darkness period in the day. Figure 8 shows a meriodional section of daily temperature oscillations obtained in [20]. The most detailed theoretical variation in the daily temperature was followed in [102]. Those rare measurements of the daily variation which were mentioned in Section 4 both affirm the radiation theory [37,44] and contradict it [43].

8. Transfer of the Self-Radiation of the Atmosphere

15 μm CO_2 Band. Compared to other bands in the spectrum of the self-radiation of the atmosphere, this band gives the greatest

thermal contribution in the atmospheric layer under investigation. The values of the rates of cooling of the upper stratosphere and the lower mesosphere, which were obtained in [62,81] as well as by the author of this study for the well-known standard model of the /52 atmosphere "Rocket Panel" (Table 2), are close in order of magnitude, although they do differ. They all give a maximum of cooling in the region of the stratopause. Apparently, the calculations in [62] are burdened with the greatest errors; they were based on laboratorial absorption functions. The profile for the radiant heat flux repeats the principal characteristics of the high-altitude temperature distribution. However, the rate of cooling in the lower thermosphere increases only up to a certain level, after which it should gradually decrease to zero. This is connected with the fact that, first of all, the volume concentration of CO_2 should decrease (Sect. 3) and, secondly, θ_r becomes much less than the vibrational relaxation time (Sect. 6).

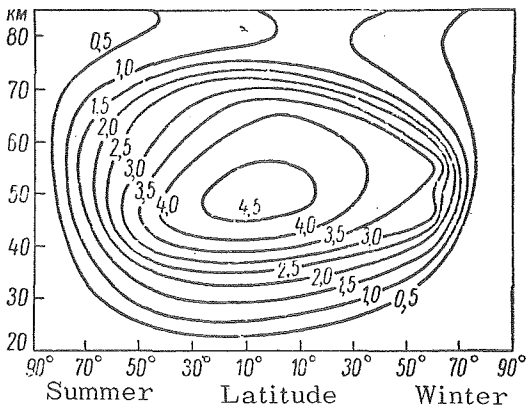

Fig. 8. Daily Temperature Variation (°K) [20].

The cooling in the lower thermosphere depends very greatly on the value of τ. Thus, according to my calculations, at $c_V=3\cdot10^{-4}$, the rate of cooling due to the fundamental transfer of the 15 μm band of the molecule $C^{12}O_2^{16}$ around 100 km, according to the CIRA-1961 atmospheric model, is about 100, 20 and 3 deg/day for τ equal to 0, $2\cdot10^{-6}$ and $2\cdot10^{-5}$ sec, respectively (p = 1 atm, T = 200°K). Above 90 km, it is precisely this transition which makes the principal contribution to the cooling due to transfer of radiation in the 15 μm band; therefore the cited figures are very close to the total rate of cooling due to the entire band. A consideration of the deviation from the Kirchoff law in calculations of the radiant heat fluxes can become necessary only for layers above 70 km.

Figure 6 shows the cooling rate obtained in [71] for $\tau = 10^{-5}$ sec and the standard American atmospheric model of 1962, which is close to the CIRA-1961 model. Around 100 km, the values given in /53 [71] are of the same order as those I obtained for $\tau = 2\cdot10^{-5}$ sec. However, as the altitude decreases, the cooling rates increase all the way to 23 deg/day at a level of 80 km. It is hard to understand why the cooling rates are a large factor higher in the range of the minimum temperatures than in the stratopause. Moreover, this conclusion contradicts the results given in [81] and those we obtained. In our opinion, the results of [71] are erroneous, at

least for the layer below 90 km.

TABLE 2. RATES OF COOLING (deg/day) DUE TO THE TRANSFER OF RADIATION IN THE 15 μm CO_2 BAND AND THE 9.6 μm O_3 BAND FOR THE STANDARD ATMOSPHERIC MODEL "ROCKET PANEL".

Altitude km	CO_2			O_3
	$c_v=3.3\cdot10^{-4}$ [62]	$c_v=2.4\cdot10^{-4}$ [81]	$c_v=3.0\cdot10^{-4}$ (my calculations)	[61]*
30	2.4	2.8	-	0.5
35	3.3	4.1	-	1.3
40	4.5	5.2	-	1.8
45	4.9	6.6	-	2.1
50	4.6	6.8	6.1	1.5
55	4.0	5.0	6.0	0.8
60	2.3	3.8	4.7	0.3
65	1.7	-	3.2	0.1
70	1.3	-	1.6	0.0

* The O_3 distribution obtained during the launching of a rocket on June 14, 1949 in New Mexico was used (see Fig. 1).

In the range of the secondary temperature maxima in the mesophere which are typical for the winter at high latitudes, the rates of cooling can reach 10 deg/day. For the summer high-latitude type of temperature distributions characterized by very low temperatures of the mesopause, the transfer of radiation in the 15 μm CO_2 band should result in the warming of the layer touching the mesopause from below [81,82]. In this case, we can expect warm-ups up to several deg/day. We should mention that the effect of vibrational relaxation decreases the rate of the warm-up (see Fig. 6).

9.6 μm O_3 Band. For the atmospheric layer under investigation, there have still been no calculations of the radiant heat fluxes which use the theoretically calculated absorption functions. Table 2 gives the results of calculations of the cooling rates according to laboratorial absorption functions [61]. The altitude of the cooling maximum is close to that of the stratopause. It was shown in [67] that it should be expected most probably below the stratopause. The thermal effect of the 9.6 μm band becomes negligibly small above 60 km, as can be seen from Table 2. However, indications of a higher concentration of O_3 in the mesosphere /54 during the night than during the day (Sect. 3) can result in a re-investigation of the role of this band in the thermal regime of the mesosphere.

Rotational and 6.3 μm H_2O Bands. There have been no special calculations evaluating the radiant heat fluxes in the upper stratosphere and the mesosphere. It can be concluded from [58,64] that, for a constant mixing ratio above 30 km equal to $2\cdot10^{-5}$g/g,

the rates of cooling in the layer of 30-45 km could be roughly equal to 1-1.5 deg/day. It is not impossible that water vapor plays a substantial role in the cooling at altitudes where its relative concentration decreases abruptly because of photodissociation [103]. This effect is similar to the cooling of the atmosphere near the upper boundary of a cloud. The indefiniteness of the thermal effect of H_2O is due mainly to the lack of experimental data on the concentration of water vapor in the upper stratosphere and the mesosphere.

63 μm O Line. The $^3P_1 \rightarrow {}^3P_2$ transition which gives this line is very important in the thermal regime of the lower thermosphere [29]. For example, according to measurements of the structural parameters and composition of the atmosphere in [14], the rates of cooling at altitudes of 100, 110 and 120 km are 5.5, 9 and 13.5 deg/day, respectively. The cited figures were obtained for an optically thin emitting layer. A consideration of the transfer of radiation should decrease the cooling rates. Atomic oxygen can make a substantial contribution to the thermal regime below 90 km only when the dynamic processes (Sect. 3) result in a great increase in the concentration below this band, as opposed to the values anticipated from the photochemical theory. If the thermal effect of the line near 63 μm is found to be important for the level of the mesopause, then the radiant heat flux for it has a positive sign, in all probability. This is easily understood, since the radiation comes from above and below to the mesopause from warmer layers of the atmosphere, while the optical thickness of the atmosphere above the mesopause is no less than several units.

OH Radiation. The hydroxyl radiation has a non-thermal nature: the excited molecules are the product of chemical reactions. A value of 3.2 erg/cm^2. sec has been obtained for the total OH radiation [97]. If the OH layer is at an altitude of about 80 km, this value for the emitted energy can guarantee cooling rates on the order of 1 deg/day at these altitudes.

9. Total Radiant Heat Fluxes

The total radiation balance for the altitudes within the atmospheric layer under investigation has been calculated only in three studies [63,66,81]. Experimental absorption functions were used for calculations of the radiant heat fluxes in the transfer of infrared radiation in [63,66]. Therefore, the quantitative results of these studies must be treated with carefulness. Figure /55
9 shows a meridional vertical cross section of the field of overall radiant heat fluxes taken from [39], and, for altitudes exceeding 40 km, the results of [81] underlay the construction of this section. It can be seen from the figure that radiant heat fluxes which do not exceed 2 deg/day in absolute value correspond mainly to the upper stratosphere and the mesosphere from 30°

in the winter hemisphere to 60° in the summer hemisphere. A negative radiation balance is characteristic of the 80-90 km layer; this can possibly be explained by an underestimation of the heating due to absorption of solar radiation by molecular oxygen. A consideration of the cooling of the atmosphere due to the transfer of the intrinsic thermal radiation greatly decreases the meriodional /56 gradients of the overall radiant heat fluxes, compared to the gradients in the case of the absorption of solar radiation (Sect. 7), but their direction remains the same. The latitudinal distribution of the radiant heat fluxes indicates that the energy transfers from the summer pole to the winter one.

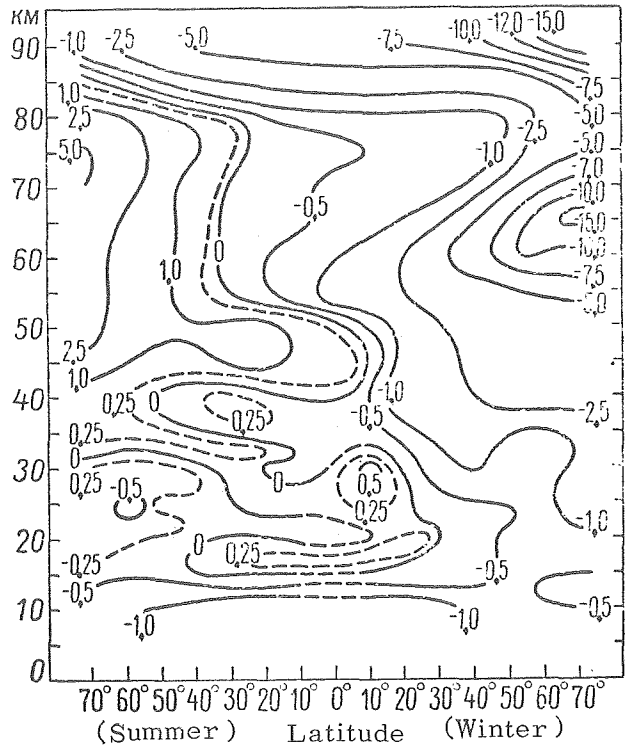

Fig. 9. Meridional Vertical Section of the Field of Overall Radiant Heat Fluxes (deg/day) [39].

10. Approximation of Radiation Equilibrium

The number of studies where the temperature distribution in the upper stratosphere and the mesosphere was obtained in approximation of the radiation equilibrium is extremely limited [20,64, 65]. Such calculations have not been carried out at all for the lower thermosphere. The calculated vertical temperature profiles reflect the principal characteristics of the real distributions, except for the high-altitude temperature variation during the polar night. In correspondence with observations in the upper stratosphere and the region of the stratopause, the temperature decreases monotonously from the summer pole to the winter one. However, the calculated yearly oscillations in the temperature exceed the real values.

The meridional vertical section of the temperature field all the way to 85 km (Fig. 10) was obtained only in [20]. The O_3 concentration in this study was found on the basis on the non-stationary photochemical theory in a pure oxygen atmosphere. A comparison of the calculated temperatures averaged over the entire planet and the average observed temperatures indicates that the calculated temperatures are mainly increased by 10-15°K, while they are

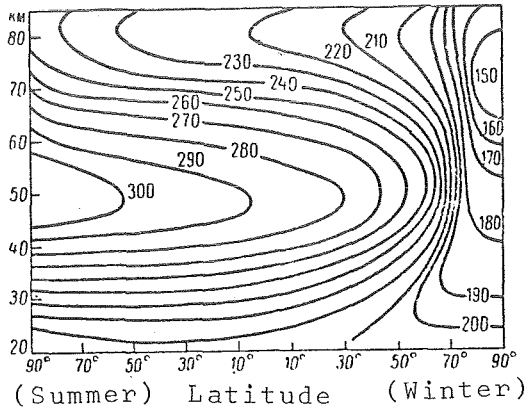

Fig. 10. Meridional Vertical Section of the Temperature Field (°K) Calculated on the Assumption of Radiation Equilibrium [20].

increased by even more than 30°K /57 in the region of the mesopause. For the average observed temperatures, assuming that there is a single cooling factor, the transfer of radiation in the 15 μm CO_2 band for the levels near the mesopause obviously cannot compensate for the warm-up resulting from absorption of solar radiation (see Fig. 6). The precise energy balance can be obtained only for a temperature of the mesopause which is higher than the average observed one; however, the excess of the calculated temperatures obtained in [20] for the region of the mesopause over the observed ones is very great. It is possible that this is partially due to the overexaggerated role of the warm-up by solar radiation because of increased calculated concentrations of O_3. A comparison of Figures 2 and 10 shows that the theoretical yearly temperature variation in the mesosphere is the opposite of that observed.

The calculations of the temperatures in [64] were limited to a pressure of 2.3 mb (about 43 km). An increase in the mixing ratio of water vapor for the upper stratosphere from values on the order of 10^{-6} to values of $\sim 10^{-4}$ g/g should result in a temperature decrease at an altitude of about 45 km roughly by 15°K relative to the averaged observed values. This is one more indication that the stratosphere is "dry" (Sect. 3). However, we must mention that the evaluations in [64] were given on the basis of experimental absorption functions.

We may have an idea of the order of magnitude of the CO_2 vibrational relaxation time by assuming that the radiant heat fluxes due, on the one hand, to the absorption of solar radiation by molecular oxygen and, on the other hand, to the transfer of radiation in the 15 μm CO_2 band and the 63 μm O line largely compensate for each other in the layer of 90-100 km. Despite the possible transfer of a substantial part of the O_2 absorbed energy to lower levels in the form of latent chemical energy (Sect. 7), the warm-up due to the O_2 nevertheless remains great. The probability of obtaining a radiation balance close to zero is greater if $\tau \sim 10^{-6}$ sec.

Conclusion

Our task was not to discuss all the aspects of the thermal regime of the layer from 30 to 100 km. The problem was to show

the role of various radiation factors and of radiation in general in the thermal regime, and to call attention to the difficulties encountered in solving this problem. An analysis of the existing studies shows that there is an urgent need for re-investigating the distributions of the overall radiant heat flux and the equilibrium temperatures in this layer. There are two basic difficulties in this regard. First of all, there is little information on the concentrations of absorbing gases, particularly for O_3 and H_2O. Here we depend completely on improvements in the /58 experimental methods of studying the atmosphere. Secondly, we must have accurate data on the absorption functions, and those which consider the diversity of conditions in the atmosphere. In our opinion, it is a basically practicable problem, although a very laborious one, to obtain these absorption functions for the transfer of infrared radiation.

Many phenomena cannot be explained within the framework of the radiation theory: the warmer mesopause of higher latitudes in the winter, as compared to the summer, the increase in temperature with altitude from 30 to 50 km under the conditions of the polar night, the rapid and substantial changes in the vertical temperature profiles in the mesosphere, the sudden warm-up in the winter stratosphere of high latitudes, the secondary temperature maxima in the mesosphere, etc. These problems can be solved, and reliable quantitative characteristics of the thermal regime can be obtained, only by considering the photochemical and dynamic processes. The latter implies a broad range of atmospheric motions. It involves both systems of ordered horizontal and vertical dislocations of air masses (general circulation of the atmosphere, wave processes, etc.) and turbulences of different scales. The closed theory of the thermal regime must necessarily consider the reciprocal effect of radiation factors, photochemistry and dynamics. Studies of this type have appeared very recently [104-107].

REFERENCES

1. Kondrat'yev, K.Ya. and O.P. Filipovich: Teplovoy rezhim verkhnikh sloyev atmosfery (Thermal Regime of the Upper Layers of the Atmosphere). "Gidrometeoizdat", 1960.
2. Khvostikov, I.A.: Fizika Atmosfery i ionosfery. Ionosfernyye Issledovaniya (Physics of the Atmosphere and Ionosphere. Ionospheric Studies), No. 11. Akad. Nauk S.S.S.R., 1963.
3. Germogenova, T.A. and M.S. Malkevich: Spectral Distribution of the Reflected Radiation of the Earth in the 0.20-0.34 μm Ozone Absorption Band. Fizika Atmosfery i Okeana, Vol. 1, No. 9, 1965.
4. Spravochnik po geofizike (Handbook on Geophysics). "Nauka", 1965.
5. Okolozemnoye kosmicheskoye prostranstvo. Spravochnyye dannyye (The Space Around the Earth. Reference Data), Ed. F.S. Johnson. "Mir", 1966.
6. Makarova, Ye.A.: The Energy Distribution in the Continuous Spectrum of the Sun. Astronom. Zhur., Vol. 41, No. 2, 1964.
7. Sitnik, G.F.: Absolute Measurements of the Solar Spectrum with a Standard Source. In the Collection: Aktinometriya i optika atmosfery (Actinometry and Optics of the Atmosphere). "Nauka", 1964.
8. Kondrat'yev, K.Ya., S.D. Andreyev, I.Ya. Badinov, V.S. Grishechkin and L.V. Popova: Atmospheric optics investigations on mt. Elbrus. Appl. Opt., Vol. 4, No. 9, 1965.
9. Brewer, A.W., and A.W. Wilson: Measurements of solar ultraviolet radiation in the stratosphere. Quart. J. Roy. Meteorol. Soc., Vol. 91, No. 390, 1965.
10. Kupperian, D.E., E.T. Bairam and H. Friedman: Density of Molecular Oxygen in the Mesosphere over Fort Churchill. In the Collection: Issledovaniya verkhney atmosfery s pomoshch'yu raket i sputnikov (Studies of the Upper Atmosphere with Rockets and Satellites). Foreign Literature Publishing House, 1961.
11. Hesstvedt, E.: Some characteristics of the oxygen-hydrogen atmosphere. Geofys. Publikasjoner. Geophys. Norvegica, Vol. 26, No. 1, 1965. /59
12. Jursa, A.S., M. Nakamura, and Y. Tanaka: Molecular oxygen distribution in the upper atmosphere, 2. J. Geophys. Res., Vol. 70, No. 11, 1965.
13. Nier, A.O., J.H. Hoffman, C.Y. Johnson, J.C. Holmes: Neutral composition of the atmosphere in the 100 to 200-kilometer range. J. Geophys. Res., Vol. 69, No. 5, 1964.
14. Pokhunkov, A.A.: Gravitation Division, Composition and Structural Parameters of the Nocturnal Atmosphere at Altitudes from 100 to 210 km. Iskusstv. Sputn. Zemli, No. 13, 1962.
15. Golomb, D., N.W. Rosenberg, C. Aharonian, J.A.F. Hill, and H.L. Alden: Oxygen atom determination in the upper atmosphere by chemiluminescence of nitric oxide. J. Geophys. Res. Vol. 70, No. 5, 1965.

16. Young, C., and E.S. Epstein: Atomic oxygen in the polar winter mesosphere. J. Atmosph. Sci., Vol. 19, No. 6, 1962.
17. Colegrove, F.D., W.B. Hanson, and F.S. Johnson: Eddy diffusion and oxygen transport in the lower thermosphere. J. Geophys. Res., Vol. 70, No. 19, 1965.
18. Gushchin, G.P.: Ozon i aerosinopticheskiye usloviya v atmosfere (Ozone and the Aerosynoptic Conditions in the Atmosphere). "Gidrometeoizdat", 1964.
19. Rawcliffe, R.D., D.E. Meloy, R.M. Friedman and E.H. Rogers: Measurement of the Vertical Distribution of Ozonefrom a Satellite Moving in Polar Orbit. In the Collection: Ozon v zemnoy atmosfere (Ozone in the Earth's Atmosphere). "Gidrometeoizdat", 1966.
20. Leovy, C.: Radiative equilibrium of the mesosphere. J. Atmosph. Sci., Vol. 21, No. 3, 1964.
21. London, Yu. and K. Prabkhakara: Absorption Processes in the Stratosphere and Mesosphere. In the Collection: Ozon v zemnoy atmosfere (Ozone in the Earth's Atmosphere". "Gidrometeoizdat", 1966.
22. Hunt, B.Q.: The need for a modified photochemical theory of the ozonosphere. J. Atmosph. Sci., Vol. 23, No. 1, 1966.
23. Venkateshvaran, S.V., Yu. Mur and A.Yu. Kryuger: Determination of the Vertical Distribution of Ozone by the Photometric Method with the Aid of a Satellite. In the Collection: Ozon v zemnoy atmosfere (Ozone in the Earth's Atmosphere). "Gidrometeoizdat", 1966.
24. L'vova, A.A., A.Ye. Mikirov and S.M. Poloskov: Rocket Measurements of the Ozone Distribution with the Altitude over the Level of Maximum Concentration during the Total Solar Eclipse of February 15, 1961. Geomagnetizm i Aeronomiya, Vol. 4, No. 6, 1964.
25. Brewer, A.W.: The measurement of the vertical distribution of ozone and its meteorological significance. Les problèmes météorologiques de la stratosphère et de la mésosphère. Paris, Press universitaires de France, 1966.
26. Mikirov, A.Ye.: Evaluation of the Ozone Concentration at Altitudes of 44-102 km according to Data Obtained during Nocturnal Launchings of Geophysical Rockets (thesis). In the Collection: Issledovaniye kosmicheskogo prostranstva (Space Research). "Nauka", 1965.
27. Rangarajan, S.: Effect of solar activity on atmospheric ozone. Nature, Vol. 206, No. 4983, 1965.
28. Bolin, B., and C.D. Keeling: Large-scale atmospheric mixing as deduced from the seasonal and meridional variations of carbon dioxide. J. Geophys. Res., Vol. 68, No. 13, 1963.
29. Nicolet, M.: Aeronomiya (Aeronomy). "Mir", 1964.
30. Hagemann, F., J. Cray, L. Machta, and A. Turkevich: Stratospheric carbon-14, carbon-dioxide and tritium. Science, Vol. 130, No. 3375, 1959.
31. Rohrbough, S.F.: Determination of the mixing ratios of water vapour and carbon dioxide in the stratosphere. Science Vol. 137, No. 3530, 1962.

32. Malkevich, M.S., Yu.B. Samsonov and L.I. Koprova: Water Vapor in the Stratosphere. Uspekhi Fiz. Nauk, Vol. 80, No. 1, 1963.
33. Kondrat'yev, K.Ya.: Conference on Meteorology of the Stratosphere and Mesosphere. Izvest. Akad. Nauk S.S.S.R., ser. fiziki atmosfery i okeana, Vol. 1, No. 8, 1965.
34. Badinov, I.Ya., S.D. Andreyev and V.B. Lipatov: Measurements of the Humidity in the Upper Layers of the Atmosphere. Meteorologicheskiye issledovaniya (Meteorological Studies), No. 12. "Nauka", 1966.
35. Hesstvedt, E.: On the spatial distribution of some hydrogen components in the mesosphere and lower thermosphere. Tellus, Vol. 17, No. 3, 1965. /60
36. Konashenok, V.N.: Hydrogen Compounds in the Mesosphere. This Collection, p. 200.
37. Rakety i iskusstvennyye sputniki v meteorologii (Rockets and Artificial Satellites in Meteorology), Ed. M.S. Malkevich. Foreign Literature Publishing House, 1963.
38. Rocket and Satellite Meteorology. Trudy pervogo mezhdunarodnogo simpoziuma po raketnoy i sputnikovoy meteorologii (Procedures of the First International Symposium on Rocket and Satellite Meteorology). "Gidrometeoizdat", 1964.
39. Newell, R.E.: A Review of Studies of Eddy Fluxes in the Stratosphere and Mesosphere. Les problemes meteorologiques de la stratosphere et de la mesosphere (Meteorological Problems of the Stratosphere and Mesosphere). Paris, Presses Universitaires de France, 1966.
40. Schilling, C.F.: Latitudinal variation of mesopause height inferred from eclipse observations. J. Atmosph. Sci., Vol. 22, No. 2, 1965.
41. Petersen, J.W., W.H. Hansen, K.D. McWatters and G. Bonfanti: Falling sphere measurements over Kwajalein. J. Geophys. Res. Vol. 70, No. 18, 1965.
42. Ryazanova, L.A.: Characteristics of the Temperature Regime of the 25-50 km-Layer. Trudy Tsentral'noy Aerologicheskoy Observatorii, No. 52, 1964.
43. Beyers, N.J., B.T. Miers: Diurnal temperature change in the atmosphere between 30 and 60 km over White Sands Missile Range. J. Atmosph. Sci., Vol. 22, No. 3, 1965.
44. Harris, M.F., F.G. Finger, and S. Teweles: Diurnal variation of wind pressure and temperature in the troposhere and stratosphere over the Azores. J. Atmosph. Sci., Vol. 19, No. 2, 1962.
45. Smith, W., L. Katchen, P. Sacher, P. Swartz and J. Theon: Temperature, pressure, density, and wind measurements with the rocket grenade experiment, 1960-1963. Goddard Space Flight Center. Greenbelt, Md., NASA technical-report R-211, October 1964.
46. Petrov, A.A. and L.A. Ryazanova: Three Cases of a Sudden Warm-up of the Arctic Stratosphere. Trudy Tsentral'noy Aerologicheskoy Observatorii, No. 52, 1964.
47. Jones, L.M., J.W. Peterson, E.J. Schaefer and H.F. Schulte:

Upper-air density and temperature: some variations and an abrupt warming in the mesesphere. J. Geophys. Res., Vol. 64, No. 12, 1959.
48. Morris, J.E., and B.T. Miers: Circulation disturbances between 25 and 70 kilometers associated with the sudden warming of 1963. J. Geophys.. Res., Vol. 69, No. 2, 1964.
49. Scherhag, R.: Stratospheric temperature changes and the associate changes in pressure distribution. J. Meteorol., Vol. 17, No. 6, 1960.
50. Rotolante, R.A. and A.M. Parra: Meteorological rocket data profile on the stratosphere, McMurdo, Antarctica. J. Geophys. Res., Vol. 70, No. 4, 1965.
51. Khvostikov, I.A., M.N. Izakov, G.A. Kokin, Yu.V. Kurilova and N.S. Lifshits: Studies of the Stratosphere from Meteorological Rockets in the USSR. Meteorologiya i Gidrologiya, No. 1, 1963.
52. Goody, R.M.: Atmosfernaya radiatsiya. Osnovy teorii (Atmospheric Radiation. Theory Principles). "Mir", 1966.
53. Gushchin, G.P.: Issledovaniye atmosfernogo ozona (Investigation of the Atmospheric Ozone). "Gidrometeoizdat", 1963.
54. Watanabe, K.: Processes of Ultraviolet Radiation Absorption in the Upper Atmosphere. In the Collection: Issledovaniya verkhney atmosfery s pomoshch'yu raket i sputnikov (Studies of the Upper Atmosphere with Rockets and Satellites). Foreign Literature Publishing House, 1961.
55. Thompson, B.A., P. Harteck and R.R. Reeves: Ultra-violet absorption coefficients of CO_2, CO, O_2, H_2O, N_2O, NH_3, NO, SO_2 and CH_4 between 1850 and 4000 A.J. Geophys. Res., Vol. 68, No. 24, 1963.
56. Metzger, P.H. and G.R. Cook: A reinvestigation of the absorption cross-sections of molecular oxygen in the 1050-1800 Å region. J. Quant. Spectr. Rad. Transf., Vol. 4, No. 1, 1964.
57. Burch, D.E. and D. Williams: Test of theoritecal absorption band model approximations. Appl. Opt., Vol. 3, No. 1, 1964.
58. Manabe, S. and F. Möller: On the radiative equilibrium and heat balance of the atmosphere. Monthly Weather Rev., Vol. 89, No. 12, 1961.
59. Houghton, J.T.: The absorption of solar infra-red radiation by the lower stratosphere. Quart. J. Roy. Meteorol. Soc., Vol. 89, No. 381, 1963. /61
60. Palmer, C.H.: Experimental transmission functions for the pure rotation band of water vapour. J. Opt. Soc. Amer., Vol. 50, No. 12, 1960.
61. Plass, G.N.: The influence of the 9.6 μ ozone band on the atmospheric infra-red cooling rate. Quart. J. Roy. Meteorol. Soc., Vol. 82, No. 351, 1956.
62. Plass, G.N.: The influence of the 15 μ carbon-dioxide band on the atmospheric infra-red cooling rate. Quart. J. Roy. Meteorol. Soc., Vol. 82, No. 353, 1956.
63. Ohring, G.: The radiation budget of the stratosphere. J. Meteorol., Vol. 15, No. 5, 1958.

64. Manabe, S. and R.F. Strickter: Thermal equilibrium of the atmosphere with a convective adjustment. J. Atmosph. Sci., Vol. 21, No. 4, 1964.
65. Moller, F. and S. Manabe: On the Radiation Equilibrium of the Atmosphere. Za. fur Meteorol., Vol. 15, No. 1-6, 1961.
66. Borisenkov, Ye.P. and B.A. Osipov: Evaluation of the Seasonal Characteristics of the Energy Balance of the Upper Atmosphere of the Northern Hemsiphere. Trudy Arkticheskogo i Antarkticheskogo Nauchno-Issledovatel'skogo Instituta, Vol. 271, 1964.
67. Hitschfeld, W. and J.T. Houghton: Radiative transfer in the lower stratosphere due to the 9.6 micron band of ozone. Quart. J. Roy. Meteorol. Soc., Vol. 87, No. 374, 1961.
68. Wyatt, P.J., V.R. Stull and G.N. Plass: Quasi-random model of band absorption. J. Opt. Soc. Amer., Vol. 52, No. 11, 1962.
69. Shved, G.M.: Approimation of an Isolated Line in the Transfer of Radiant Energy in the Upper Atmosphere. Vestnik Leningrad. Gosudarstv. Univ., ser. fiziki i khimii, No. 1, 1964.
70. Timofeyev, Yu.M.: Applicability of the Model of the Isolated Spectral Line. Izvest. Akad. Nauk S.S.S.R., ser. fiziki atmosfery i okeana, Vol. 1, No. 12, 1965.
71. Young, C.: A study of the influence of carbon dioxide on infra-red radiative transfer in the stratosphere and mesosphere. Technical report. The University ff Michigan, ORA project 04682, March 1964.
72. Goody, R.: The transmission of radiation through an inhomogeneous atmosphere. J. Atmosph. Sci., Vol. 21, No. 6, 1964.
73. Young, C.: Calculation of the absorption coefficient for lines with combined Doppler and Lorentz broadering. J. Quant. Spectr. Rad. Transf., Vol. 5, No. 3, 1965.
74. Chiarella, C. and A. Reichel: On the evaluation of Voigt spectral line functions. Monthly Not. Roy. Astronom. Soc., Vol. 134, No. 1, 1966.
75. Pokrovskiy, A.G.: Method of Calculating the spectral Absorption of the Infra-red Radiation in the Atmosphere. This Collection, p. 85.
76. Young, C.: Tables for calculating the Voigt profile. Technical report. University of Michigan, Contr. No NASr-54(03), July 1965.
77. Finn, G.D. and D. Mugglestone: Tables of the line broadering function H (a, v). Monthly Not. Roy. Astronom. Soc., Vol. 129, No. 2, 1965.
78. Plass, G.N. and D.J. Fivel: Influence of Doppler effect and damping on line-absorption coefficient and atmospheric radiation transfer. Astrophys. J., Vol. 117, No. 1, 1953.
79. Plass, G.N. and D.J. Fivel: A method for the integration of the radiative-transfer equation. J. Meteorol., Vol. 12, No. 3, 1955.
80. Shved, G.M. and I.V. Tsaritsina: The Absorption Functions of Infra-red Radiation in the Mesosphere and Upper Stratosphere. In the Collection: Problemy fiziki atmosfery (Problems of Atmospheric Physics), No. 1. Leningrad State University Press, 1963.

81. Murgatroyd, R.J. and R.M. Goody: Sources and sinks of radiative energy from 30 to 90 km. Quart. J. Roy. Meteorol. Soc., Vol. 84, No. 361, 1958.
82. Shved, G.M.: The Thermal Effect of the 15 m CO_2 Band in the Upper Atmosphere. In the Collection: Problemy fiziki atmosfery (Problems of Atmospheric Physics), No. 3. Leningrad State University Press, 1965.
83. Shved, G.M.: Method of Considering the Deviation form the Kirchoff Law in the Mesosphere in the Transfer of Radiation /62 in the 15 m Carbon Dioxide Band. Vestnik L.G.U., No. 1, 1965.
84. Madden, R.P.: A High-Resolution Study of CO_2 Absorption Spectra between 15 and 18 Microns. J. Chem. Phys., Vol. 35, No. 6, 1961.
85. Kaplan, L.D.: A method for Calculation of Infra-red Flux for use in Numerical Models Atmospheric Motions. "The Atmosphere and Sea in Motion". Ed. by B. Bolim. N.Y., 1959.
86. Goldstein, R.: Measurements of Infra-red Absorption by Water Vapor at Temperatures to 1000°K. J. Quant. Spectr. Rad. Transf., Vol. 4, No. 2, 1964.
87. Penner, S.S.: (Kolichestvennaya molekulyarnaya spektroskopiya i izluchatel'naya sposobnost' gazov (Quantiative Molecular Spectroscopy and the Emissivity of Gases). Foreign Literature Publishing House, 1963.
88. Leskov, L.V. and F.A. Savin: The Relaxation of Non-Equilibrium Gas Systems. Uspekhi Fiz. Nauk, Vol. 72, No. 4, 1960.
89. Lambert, J.: Relaxation Processes in Gases. In the Collection: Atomnyye i molekulyarnyye protsessy (Atomic and Molecular Processes), Ed. D. Bates. "Mir", 1964.
90. Marriott, R.: Molecular Collision Cross Section and Vibrational relaxation in Carbon Dioxide. Proc. Phys. Soc., Vol. 84, No. 542, 1964.
91. Marriott, R.: Molecular Collision Cross Section and Vibrational relaxation in Carbon Dioxide. Proc. Phys. Soc., Vol. 88, No. 559, 1966.
92. Vanderslice, J.T. and S. Weissman: On the Theory of Vibrational Energy Exchange. J. Chem. Phys., Vol. 37, No. 10, 1962.
93. Millikan, R.C. and D.R. White: Systematics of Vibrational Relaxation. J. Chem. Phys., Vol. 39, No. 12, 1963.
94. Yamamoto, G.: Direct Absorption of Solar Radiation by Atmospheric Water Vapor, Carbon Dioxide and Molecular Oxygen. J. Atmosph. Sci., Vol. 19, No. 2, 1962.
95. Johnson, F.S. and E.M. Wilkins: Thermal Upper Limit on Eddy Diffusion in the Mesosphere and Lower Thermosphere. J. Geophys. Res., Vol. 70, No. 6, 1965.
96. Murgatroyd, R.J.: Meteorological Office Discussion: Winds in the Outer Atmosphere. Meteorol. Mag., Vol. 85, No. 1004, 1956.
97. Chamberlain, D.: Fizika polyarnykh siyaniy i izlucheniya atmosfery (Physics of Aurorae and Atmospheric Radiation). Foreign Literature Publishing House, 1963.
98. Horiuchi, G.: Odd Oxygen in the Mesosphere and some Meteorological Considerations. Geophys. Mag., Vol. 30, No. 3, 1961.

99. Craig, R.A. and G. Ohring: The Temperature Dependence of Ozone Radiational Heating Rates in the Vicinity of the Mesopeak. J. Meteorol., Vol. 15, No. 1, 1958.
100. Kastrov, V.G. and L.A. Biryukova: The Diurnal Temperature Variation in the Lower and Middle Stratosphere. Trudy Tsentral'noy Aerologicheskoy Observatorii, No. 45, 1962.
101. Roach, W.T.: The Absorption of Solar Radiation by Water Vapour and Carbon Dioxide in a Cloudless Atmosphere. Quart. J. Roy. Meteorol. Soc., Vol. 87, No. 373, 1961.
102. London, J.: A Study of the Atmospheric Heat Balance. Final Report. Contract No AF 19(122)-165. Research Division College of Engineering New York University, July 1957.
103. Khvostikov, I.A.: Thermal Regime of the Atmosphere in the Zone of Noctilucent Clouds. Procedures of a Conference on Noctilucent Clouds, No. 1. Tartu, 1959.
104. Leovy, C.: Simple Models of Thermally Driven Mesospheric Circulation. J. Atmosph. Sci., Vol. 21, No. 4, 1964.
105. Lindsen, R. and R. Goody: Radiative and Photochemical Processes in Mesospheric Dynamics. Part I. Models for Radiative and Photochemical Processes. J. Atmosph. Sci., Vol. 22, No. 4, 1965.
106. Lindsen, R.S.: Radiative-Photochemical Response of the Mesosphere to Fluctuations in radiation. J. Atmosph. Sci., Vol. 22. No. 5, 1965.
107. Smagorinsky, J., S. Manabe, and .L. Holloway: Numerical Results from a Nine-Level General Circulaiton Model of the Atmosphere. Monthly Weather Rev., Vol. 93, No. 12, 1965.

TRANSMISSION FUNCTIONS OF THE REAL ATMOSPHERE

Yu.M. Timofeyev

ABSTRACT: After discussing the various methods of calculating the transmission functions of the real atmosphere, it is concluded that the method of considering the nonuniformity of the atmosphere in approximation gives the greatest errors for the atmospheric stratifications where an increase in the mixing ratio of the absorbing gas is observed with a decrease in the pressure. The Curtis-Godson method is found to be unsuitable for certain types of equations and conditions, as is the effective-mass method.

A large number of computations must be carried out in order to calculate various quantitative characteristics of the field of thermal radiation of the earth-atmosphere system. This is due to the fact that, for example, in order to calculate a flux of thermal radiation at some level there must be a number of integrations: by spatial coordinates, by angles and by frequency. If we consider that all these operations must be carried out each time for each specific state of the atmosphere, then the need for applying different approximation methods in the calculations becomes obvious. As examples of such approximation methods, we could mention that of considering the diffusivity of the radiation, and those of considering the nonuniformity of the atmosphere [1, 2]. Let us discuss the approximation methods for calculating the transmission functions of the real atmosphere in more detail.

As is well known, transmission functions P (or absorption functions A = 1 - P) obtained by an experimental of theoretical method for so-called uniform media, i.e., for media with constant pressure and temperature, are often used in theoretical calculations of certain characteristics of the thermal radiation. Although methods have been developed recently for obtaining the transmission functions of media with pressure and temperature changing along the path of the rays, they nevertheless require either expensive experiments or laborious machine calculations. We are speaking here of a study of the absorption of thermal radiation in a successive series of gas cuvettes in which the pressure, temperature and percentage of absorbent can be changed independently [3, 4] (such an experiment models a nonuniform medium to some extent), as well as precise calculations of the transmission functions on the basis of quantum-mechanic data on the position, half-width and intensities of the spectral lines of various absorption bands [5]. It is scarcely probably that such methods will be widely used in calculations encompassing large spectral intervals and a wide range of

atmospheric conditions: however, they can play an important role in testing different approximation methods. /64

In using the transmission functions for uniform media for calculations of the real atmosphere, the following approximation methods for considering the nonuniformity of the atmosphere are used most frequently.

1. Effective Mass Method. In this case, it is assumed that a layer with changing pressure p and temperature T can be replaced by a layer with constant pressure p_0 and temperature T_0 containing an effective quantity of absorbent which is determined by the following relationship:

$$u_{\text{eff}} = \frac{1}{g} \int \left(\frac{p}{p_0}\right)^n \left(\frac{T}{T_0}\right)^m q(p)\, dp. \tag{1}$$

Here g is the acceleration of free fall; $q = \frac{\rho_W}{\rho}$ is the mixing ratio; ρ_W is the density of the absorbing gas; ρ is the density of the air.

2. Curtis-Godson Method [2]. By this method, it is considered possible to substitute a layer with variable pressure and temperature by a layer with reduced pressure $\tilde{p}$ and mass $\tilde{u}$ which are found from the following formulas:

$$\tilde{p} = \frac{\int \sum_i S_i(T)\, p q(p)\, dp}{\int \sum_i S_i(T_0)\, q(p)\, dp}, \tag{2}$$

$$\tilde{u} = \frac{1}{g} \int \frac{\sum_i S_i(T)}{\sum_i S_i(T_0)} q(p)\, dp, \tag{3}$$

Where S_i are the intensities of the lines which affect the absorption in the spectral interval under investigation.

The effect of the temperature on absorption is disregarded quite frequently in calculations, and then (1), (2) and (3) are simplified:

$$u_{\text{eff}} = \frac{1}{g} \int \left(\frac{p}{p_0}\right)^n q(p)\, dp, \tag{1a}$$

$$\tilde{p} = \frac{\int p q(p)\, dp}{\int q(p)\, dp}, \tag{2a}$$

$$\tilde{u} = \frac{1}{g} \int q(p)\, dp. \tag{3a}$$

The effect of the temperature on the transmission functions will be considered subsequently.

Considering the approximative nature of these calculation methods, we must test the accuracy of these computations for various spectral intervals and atmospheric conditions. The authors of [5, 6, 7] tested the accuracy of the Curtis-Godson method and /65 yields good results for many absorption bands of atmospheric gases. The unfavorable exception is the ozone absorption band in the 9.6 μm region, for which the Curtis-Godson method results in substantial errors. Considerable errors are also observed for the rotational water vapor band in certain cases. R.M. Goody [7] suggested a new method of considering the nonuniformity of the atmosphere, which he called a three-parametric method. It follows from [7] that this method yields much better results in all cases, and, what is particularly important, in calculations for the ozone band. The disadvantage of this method is its great complexity. Therefore, the problem of testing and clarifying the effective mass method and the Curtis-Godson method, which are vary convenient because of their simplicity, remains open. Using numerous laboratory studies, D. Burch and D. Williams [8] concluded that the absorption by many bands of atmospheric gases in uniform media can be calculated with the aid of the following expressions:

$$A = C\,[u\,(p_l)^n]^b,\ x_1 < u\,(p_l)^n < x_2,$$
$$A = D \log\,[u\,(p_l)^n] + E,\ x_2 < u\,(p_l)^n < x_3. \qquad (4)$$

Here C, D, E, n and b are empirical constants (most frequently $0.5 < n < 1$; $b \sim 0.5$); x_i are the limits oo applicability of the formulas; $p_l = p_0 + (B-1)\,p$ is the effective pressure; p_0 is the total pressure of the absorbing and broadening gases; p is the partial pressure of the absorbing gas; B is the automatic broadening factor which takes account of the high effectiveness of reciprocal collisions of molecules of the absorbing gas; u is the percentage of absorbent. For atmospheric conditions, $p_l \approx p_0$ most frequently.

Having generalized the experimental data relating to the same absorption bands as (4) for the transmission of infrared radiation in two cuvettes modeling a nonuniform medium, J. Shaw [9] concluded that the absorption function in the nonuniform medium can be written thus;

$$A = C\left[\int p_l^n du\right]^b,$$
$$A = D \log\left[\int p_l^n du\right] + E. \qquad (5)$$

The formulas of (5) are valid for the same values of the constants and in the same ranges of x_i as the relationships in (4).

They were obtained on the basis of a study of the absorption in the N_2O and CO bands. Therefore, the application of such relationships to other bands can be considered as an extrapolation, which requires a check. However, considering the experimental nature of the relationships in (5), they can be used for testing and clarifying the approximation methods for considering the nonuniformity of a medium.

The following expressions for the effective absorbing mass and reduced pressure are easily obtained from (4) and (5): /66

$$u_{\text{eff}} = \int \left(\frac{p}{p_0}\right)^n du, \tag{6}$$

$$\tilde{p}' = \left[\frac{\int p^n du}{\int du}\right]^{\frac{1}{n}} \tag{7}$$

Naturally, the use of (6) and (7) in calculating the absorption gives identical results, since they were obtained on the basis of identical data. However, these formulas show that, while the effective mass method is confirmed by Shaw's data, the effective pressure must be calculated according to (7), which coincides with the Curtis-Godson formula only at n = 1. Moreover, (6) points out the well-known fact that the index in (1a) should be selected on the basis of measurements of the dependence of the absorption on the pressure for uniform media.

Shaw's data indicate that the effective mass method is applicable when the absorption functions can be represented as certain functions of the product up^n, while it is completely unnecessary that the form of these functions be identical for all the absorption bands and the entire range of changes in the pressure and percentage of absorbents. As regards the approximating nature of these representations of the absorption functions, the index n, generally speaking, is not a constant value, but depends on the spectral interval, the pressure, the percentage of absorbents and, in the general case, the temperature. The possibility of an effective application of this method is connected with the low variability of n in the range of this spectral interval and in the range of the changes in u, p and T corresponding to the atmospheric conditions. It is the great variability of the index n for the 9.6 μm ozone band [10] which is one of the reasons for the difficulty in using this approximation method.

Let us study the effect of the index n in (6) on the results of calculations of the effective quantity of absorbents. For this, we will evaluate the ratio $k = \frac{u_{eff}(n_1)}{u_{eff}(n_2)}$ for different n_1 and n_2 and different layers of the atmosphere. In calculations of k in (6), we can convert to integration by the pressure with the aid of the relationship $du = \frac{-q(p)}{g} dp = -Ap^l dp$. Here $\underline{l}$ acquires both positive

and negative values (and $\underline{l} = 0$ corresponds to a distribution of the CO_2 type, $\underline{l} = \underline{l}$ corresponds to the water vapor distribution, $\underline{l} = -\underline{l}$ can characterize the ozone distribution). The following conclusions can be formulated on the basis of the calculations.

1. The ratio k depends largely on the distribution of the absorbent with the altitude. The maximum values of the coefficient /67 for given n_1 and n_2 (n_2 greater than n_1) are observed at $l < 0$, i.e. when the mixing ratio increases with a pressure decrease (for example, for ozone in the stratosphere). The value for the coefficient is much less at $\underline{l} = 0$ and $\underline{l} > 0$, i.e., the effect of inaccuracy in n is much less considerable for distributions of the carbon dioxide and water vapor type. For example, at $n_1 = 0.5$, $n_2 = 1.0$ and $\underline{l} = 1$, max $k \to 1.2$; at $\underline{l} = 0$, max $k \to 1.3$; at $\underline{l} = -1$, max $k \to 2$.

2. The coefficient increases with an increase in the thickness of the absorbing layer, i.e., the maximum errors connected with inaccuracy in the assignment of n can arise during calculations for extended layers. Let us examine (7) further. As was found, it coincides with (2) at n = 1. However, the parameter n changes within a rather broad range in dependence on the absorption band under investigation (thus, $n \approx 0.9 - 1.0$ for the rotational water vapor band, while $n \approx 0.3$ for the ozone band). A comparison of the results of calculations for the pressure according to (7) and (2a) for various distributions of the absorbing gas and for different values of the parameter n allows us to draw the following conclusions. 1. For the distributions of absorbing gases where the mixing ratio is constant or decreases with a decrease in pressure (as in the case with CO_2 and H_2O vapors), the differences in the values for the pressure obtained by (2a) and (7) are not great. Thus, at $n \approx 0.5$ and $\underline{l} = 0$ (worst case) the maximal difference between $\tilde{p}$ and $\tilde{p}'$ do not reach 15%. This indicates that (2a) and (7) are practically equivalent. 2. For the distribution of absorbing gases with which an increase in the mixing ratio is observed with a decrease in the pressure, the differences between the results of calculation by (2a) and (7) are great. For example, at n = 0.5 and $\underline{l} = -1$, the difference is 30%. It is essential that the pressure calculated according to (7) always be less than the pressure obtained by (2a). The authors of [11] and [12] established that, for the type of distribution of the absorbent (ozone) under investigation, an application of the Curtis-Godson method always results in an overevaluation of the absorption, i.e., the spectroscopic pressure is always less than the pressure obtained by (2a). Considering this, we can assume that (7) gives better results in using it in order to calculate the absorption functions of the real atmosphere. An additional basis for this assumption can be seen in the better coincidence of the spectroscopic pressure and the pressure given by (7), for certain examples from [11].

Studies [6, 13] showed two possible reasons for the inapplicability of the Curtis-Godson method to the 9.6 μm ozone band.

First of all, there is the structure of the ozone band and, secondly, there is the unique type of distribution of the ozone with the altitude, for which great absorbing masses are found under low pressures. We can hope that the second reason will be eliminated by a generalization of the Curtis-Godson method in the form of (7). However, the improvements given by this generalization for the ozone band will have to be evaluated quantitatively. /68

Conclusions

(1) For the atmospheric stratifications where an increase in the mixing ratio of the absorbing gas is observed with a decrease in the pressure, the method of considering the nonuniformity of the atmosphere in approximation gives the greatest errors.

(2) In using the effective mass method, we must know the average value of n for different ranges of u and p from measurements for uniform media. The value of n must be particularly accurate for distributions of the ozone type.

(3) The use of (7) for determining the reduced pressure can give better results in calculating the absorption of the real atmosphere than the Curtis-Godson method.

REFERENCES

1. Kondrat'yev, K.Ya.: Luchistyy teploobmen v atmosfere (Radiative Heat Transfer in the Atmosphere). "Gidrometeoizdat", 1956.
2. Goody, R.M.: Atmospheric Radiation, Vol. 1. Theoretical Basis. London, Clarendon Press, 1964.
3. Gryvnak, D.A. and J. H. Shaw: Study of the Total Absorption Near [Sic] by Two Samples of CO as Their Total Pressures and CO Concentrations Were Independently Varied. J. Opt. Soc. Amer., Vol. 52, 1962.
4. Abels,L.L. and J. H. Shaw: Study of Total Absorptance Near 4.5 μ by Two Samples of N_2O As Their Total Pressures and N_2O Concentrations Were Independently Varied. J. Opt. Soc. Amer., Vol. 53, No. 7, 1963.
5. Kondrat'yev, .Ya. and Yu. M. Timofeyev: The Applicability of Approximating Methods For Considering the Nonuniformity of the Atmosphere in Calculating the Transmission Functions of the Rotational Water Vapor Band. Izvest. Akad. Nauk S.S.S.R., ser. fiziki atmosfery i okeana (Unpublished).
6. Walshaw, C.D. and C. D. Rodgers: The Effect of the Curtis-Godson Approximation on the Accuracy Radiative Heating-Rate Calculations. Quart. J. Roy. Meteorol. Soc., Vol. 89, 1963.
7. Goody, R.M.: The Transmission of Radiation Through an Inhomogeneous Atmosphere. J. Atmosph. Sci., Vol. 21, No. 6, 1964.
8. Burch, D.E. and D. Williams: Total Absorptance by N_2O by Infra-red Appl. Opt., Vol. 1, No. 4, 1964.
9. Shaw, J.H.: Empirical Methods for Computing the Integrated Absorptances of Infra-red Bands of Atmospheric Gases and

Nonuniform Pressures. Appl. Opt., Vol. 6, 1963.
10. Kondrat'yev, K. Ya. and Kh. Yu. Niylisk: The Thermal Radiation of the 9.6 μm Ozone Absorption Band in the Atmosphere. In the Collection: Problemy fiziki atmosfery (Problems of Atmospheric Physics), No. 2, Leningrad State University Press, 1964.
11. Ooyama, K.: Accuracy of the Determination of the Vertical Distribution of Atmospheric Ozone by the Infra-red Method Mesospheric Dynamics. Final Report Cont. No. AF 19(604)-5492, 1962.
12. Mayot, M.: and E. Vigroux: On the Application of Curtis-Godson's Approximation to the 9.6 μ Band of Atmospheric Ozone. Technical note, No. 1, AF 61(052)-685 TN-1, 31 January 1965.
13. Curtis, A.R.: Discussion of Goody's a Statistical Model for Water-vapor Apsorption. Quart. J. Roy. Meteorol. Soc., Vol. 78, 1952.

SOME PROBLEMS IN TEMPERATURE SOUNDING OF THE ATMOSPHERE

K. Ya. Kondrat'yev and Yu. M. Timoveyev

ABSTRACT: A brief review is given of the results obtained in studies of the problems of temperature sounding in the atmosphere, and the basic unsolved aspects of the problem are discussed. It is shown that, in selecting the spectral intervals, possible random deviations in the transmission functions must be considered. The effect of variability in the concentration of carbon dioxide and water vapor and the temperature on outgoing radiation is also evaluated.

The problem of the temperature sounding of the atmosphere /69
according to data on the spectral or angular distribution of outgoing thermal radiation has recently caught the attention of scientists of many countries, and this is no coincidence. On the one hand, it is of immense value to obtain global data on the thermal stratification of the atmosphere for weather predictions and solutions to other applied problems; on the other hand, although the solution to this problem may be complex, it is nevertheless completely feasible for the near future. The latter is connected both with the intensive conquest of the space around the Earth and with the successful solution to many important problems concerning the methods for measuring and interpreting the data. The purpose of this article is to make a brief review of the results on the problem of temperature sounding and to discuss those unsolved aspects of the problem which seem to us to be most essential.

The problem of temperature sounding of the atmosphere was first formulated by J. King [1,2] in regard to an interpretation of the angular dependence of outgoing radiation, and by L. Kaplan [3] in regard to an analysis of the spectral distribution. In the latter case, it was considered that the use of data from spectral measurements of the outgoing radiation in the 15 μm carbon dioxide band was most advantageous for the solution to the problem, although the use of the emission bands in the near infrared and microwave spectral regions was not excluded.

G. I. Marchuk [4] formulated the general approach to the solution of the inverse problems of atmospheric optics. Let us review the results of this study in brief. We will consider the equation for transfer of radiation in the operational form:

$$L\phi = f. \tag{1}$$

Here L is the integro-differential operator for transfer of /70
radiation; ϕ is the emission intensity; f is the source of emission

(belongs to the classes of functions for which the equations of (1) have significance).

The indices of the instruments are functionals of the field of emission, which can be represented in the following form:

$$I_p(\varphi)=(p,\ \varphi). \tag{2}$$

Let us now write out the following conjugate equation in relation to the arbitrary linear functional:

$$L^*\varphi_p^*=p. \tag{3}$$

The parentheses in (2) signify the scalar product, i.e., integration of these functions over the entire range of variables of the problem, and conjugation is used in the Lagrangian sense. It is easy to show that this functional can be calculated both with the aid of (2) and according to the following formula:

$$I_p(\varphi)=(f,\ \varphi_p^*), \tag{4}$$

In other words, the functional I_p can be calculated either with the aid of the solution to the principal problem of (1) or on the basis of the solution to the conjugate problem of (3).

In his investigation, G. I. Marchuk used the standard atmosphere, which is characterized by the assignment of the distributions of meteorological elements: temperature, humidity, aerosols, etc. This atmosphere and the corresponding inverse problem can be called "undisturbed". Satellite measurements of the functionals generally related to the real, i.e., the "disturbed" problem. The principal problem is that the variation in characteristics of the atmosphere should be determined according to given variations of the functionals. For this, the corresponding formulas of the theory of disturbances are constructed for the functionals.

Let us write out the following for the problem concerning disturbances:

$$L'\varphi'=f', \tag{5}$$

$$L'=L+\delta L,\ f'=f+\delta f. \tag{6}$$

We can then find the following expression, which links the variations in the functional with the variations in the characteristics of the atmosphere:

$$(\varphi_p^*,\ \delta L\varphi'-\delta f)=-\delta I_p. \tag{7}$$

The function ϕ_p^* is a statistical weight in (7) and characterizes the range where the disturbance $\delta L\phi'-\delta$ has effect over the entire phase space. Considering this, the function ϕ_p^* can be called the importance of information in relation to the functional I_p.

Since the instrument carries out measurements in different parts of the spectrum, we actually have a set of variations of the functionals I_{p_n}, n = 1,2...N and the corresponding functions $\phi_{p_n}^*$. Obviously, the information in different functionals should be independent, i.e., /71

$$\varphi_{p_n}^* \neq \varphi_{p_m}^*. \tag{8}$$

A study of the functions for importance of information aids in planning a satellite-based experiment in the most meaningful way. G. I. Marchuk also applied this general formulation of the problems of atmospheric optics to that of temperature sounding.

Methods of Solving the Problem of Temperature Soundings

The problem of temperature sounding is often formulated as an integral Fredholm equation of the first kind. This equation can be written out, for example, in the following form:

$$I(\nu)=\int B[T(p)]\frac{\partial P(p,\nu)}{\partial p}dp+B[T(p_0)]P(p_0,\nu).$$

Here B[T(p)] is the Planck function of absolutely black radiation; P(pν) is the function of atmospheric transmission from its upper boundary to a level with pressure p. However, this representation (and is not always considered) is approximative. It is connected, for example, with the dependence of the Planck function on the frequency, or which is more important, with the nonlinearity of the cited equation, since, generally speaking, the unknown temperature distribution has a certain effect on the kernel of the integral equation (transmission function). Moreover, other simplifying assumptions used in formulating the problem cannot be fulfilled in the real atmosphere.

As is well known, integral Fredholm equations of the first kind are incorrect in the classical sense. Thus, in particular, one of the conditions for correctness, or continuous dependence of the solution on the data of the problem, is not fulfilled for them. Infinitely small changes in the term outside the integral I(ν) can correspond to non-infinitely small deviations in the values of the unknown function. This results in a situation where the regular methods for the approximative solution to the equation are unreliable in relation to small errors in the function I(ν). The first methods for solving this equation were incomplete, since they did

not consider an important characteristic of the problem--its incorrectness. The result was, in particular, that attempts at applying such methods to complex temperature distributions, or at obtaining highly accurate results, were unsuccessful.

The first interpretation methods, proposed by J. King, L. Kaplan and D. Wark [5], consisted in a representation of the integral in the form of a finite sum and a reduction of the problem for /72 solving the integral equation to the solution of an algebraic system. However, this system was poorly established, which often made its effective solution impossible. G. Jamamoto [6] suggested that the unknown function be represented in the form of an expansion into power series or series of orthogonal polynomials, and that the unknown coefficients of the expansions again be found from algebraic equations. However, in such a case it was necessary to use such a large number of terms in order to obtain sufficient accuracy that incorrectness of the problem again arose. Instead of an improvement, the solution to the problem was worsened with the large number of terms of the expansion. M. S. Malkevich and V. I. Tatarskiy [7] found a way to overcome this difficulty; they used statistical methods in solving the problem of temperature sounding. They suggested that the unknown function be approximated in the optimal fashion relative to a small number of terms. Systems of statistical-orthogonal functions guarantee such an approximation; the strict theory for these systems was developed by A. M. Obukhov [8]. If we represent T(p) in the form of

$$T(p)=\overline{T}(p)+T'(p), \tag{9}$$

where T'(p) are random deviations from the norm $\bar{T}(p)$, $T' \ll \bar{T}$, it is easy to obtain the equation to find T'(p). A. M. Obukhov showed that the optimal approximation of the random function, for example T'(p), is achieved with a system of orthogonal functions $\{\phi k\}$ which are eigen-functions of the corresponding correlation functions (in this case, of the correlation function of the temperature K_{tt}). The unknown random function T'(p) is thus found in the form of the following expansion,

$$T'(p)=\sum_{k=1}^{n} t_k \psi_k(p). \tag{10}$$

Use of the optimal systems does not eliminate unsteadiness of the solution connected with the incorrectness of the inverse problem, but, since these systems guarantee the best approximation with a small number of terms in (10), satisfactory accuracy can nevertheless be obtained in the solution.

The effect of systematic and random errors on the accuracy of

the solution to the problem of temperature sounding was first studied by L. Kaplan [9]. He showed that, even with the simplest method where great accuracy is not required, the effect of errors, primarily random ones, is very substantial: they can completely exclude the possibility of a correct interpretation of the results. A further investigation of the effect of random errors in measurements of outgoing radiation on the unknown temperature distribution was carried out by M.S. Malkevich and V.I. Tatarskiy [7]. For the characteristic of this effect, they introduced the gain coefficient of the error, i.e., /73

$$k_T(p) = \frac{\delta T}{\delta f},$$

where δT is the root-mean-square error in determining T'; δf is the root-mean-square error in measuring the radiation, expressed in degrees of the effective temperature. The gain coefficient of the error varies greatly and can reach values on the order of 20 and more, and it increases with an increase in the number of terms in the expansion. In this increase of the coefficient, there is again incorrectness of the problem and unsteadiness of the solution. The authors of [7] suggested that a greater number of measurements of N than of the unknown coefficients of the expansion n be used in order to decrease the gain coefficient. In this case, k_T decreases roughly by a factor of $\sqrt{\frac{N}{n}}$. However, this requires a substantial complication of the apparatus and increase in the volume of information obtained.

The method of optimal approximation was further developed in a study by V.P. Kozlov. [10]. He analyzed the measurement possibilities of the method of temperature sounding while taking account of the statistical properties of random errors. In order to single out the steady part of the solution obtained in a numerical solution to the integral equation (algebraic system), the range for the change in measured values was compared to the errors in their measurement on the basis of a use of the quadratic information metrics, which was correlated to an extent with the measurement method. Using this comparison, V.P. Kozlov developed an optimal method for analyzing experimental data which stabilized the unsteady inverse problem. A practical application of this method was the development of a method of evaluating the effectiveness of measurements of the temperature distribution with its aid.

The number of temperature distributions which can be distinguished with the aid of this measurement method is taken as a quantitative characteristic of the effectiveness. For example, the effectiveness of a series of measurements in three spectral intervals which were used in the study of M.S. Malkevich and V.I. Tatarskiy was not great - on the order of 100 (for rather high accuracy

in measurements, the root-mean-square error is 0.4° K). The method proposed by V.P. Kozlov not only aids in evaluating the effectiveness of a given series of measurements but also helps in selecting the optimal measurement conditions.

As is clear from the above, the method of optimal approximation requires a knowledge of the average vertical profiles of the temperature, as well as the correlation functions obtained by analyzing the data of measurements of a large number of temperature profiles. In principle, this information should be known for any season of the year and any point on the globe. As M.S. Malkevich and V.I. Tatarskiy showed, there is some simplification in the fact that "extraneous" correlation functions can be used for solving the problem. /74

Interesting prospects in solving the inverse problem, particularly in solving the problem of temperature sounding, are being found in connection with the development by A.N. Tikhonov [11] of mathematical methods for solving incorrect problems. According to this method, the so-called regularization method, the approximate solutions $\{z^{\alpha}(s)\}$ of the equation

$$A[x, z(s)] = \int_{-1}^{1} K(x, s)\bar{z}(s)\,ds = \bar{u}(x) \tag{11}$$

are determined as functions realizing the minimum of the following functional:

$$M^{\alpha}[z, \bar{u}(x)] \equiv \int_{-l}^{l} \{A[x, z(x)] - \bar{u}(x)\}^2\,dx + \alpha\Omega[z(x)],$$

$$z'(-1) = z'(1) = 0, \quad \Omega[z] = \int_{-1}^{1} [z'^2 + qz^2]\,ds. \tag{12}$$

In the USA, methods of stabilizing the unsteady solution to integral Fredholm equations of the first kind were developed by D.L. Phillips [12] and S. Twomey [13]. These methods were used later by D.Q. Wark and H.E. Fleming [29] both for model computations and for analyzing the first experimental data for launchings of a model of the instrument on airships. The instrument was a spectrometer of the Ebert-Fasti design with a five-inch grid. It had 6 channels for measuring the radiation in the 15 μm CO_2 band and one channel for measuring the radiation in the atmospheric window in the region of 11.1 μm. The tests of the device, which were carried in September 1964, showed that it operated well and that a temperature profile close to the real one could be obtained. The need for measuring the radiation with high accuracy (1%) was noted. Random errors of 3-5% could entirely exclude the possibility of solving the problem of temperature sounding. Preparations are being made in the USA to use instruments similar to that described on meteorological satellites for measurements of the tem-

perature distributions in the atmosphere.

Finally, we should point out that prospects of using the radiation in the oxygen band in the millimeter range for the purposes of temperature sounding have recently been considered. Measurements in this region have at least two essential advantages:

1. The millimeter radiation can pass through most clouds and, /75 consequently, there are prospects of a deeper sounding of the atmosphere.

2. A much higher spectral resolution can be obtained in the millimeter range; in particular, the profile of the emission line can be observed, which simplifies the problem of interpreting the measurement results.

Determination of the Carbon Dioxide Transmission Functions

One of the important problems of temperature sounding is a precise representation of the kernel of the integral equation (of the transmission function or their derivatives) for those spectral regions in which the measurements of outgoing radiation are being carried out.

As is well known, the transmission functions of atmospheric gases are determined most frequently with the aid of laboratorial experiments or theoretical calculations based on the use of different spectroscopic models of the absorption bands. Neither of these methods completely satisfies the requirements imposed on the transmission function in the problem of temperature sounding. A laboratorial experiment cannot give the transmission functions for all the conditions existing in the real atmosphere with the requisite accuracy. This holds primarily for the transmission functions for low pressures and low percentages of the substance absorbing the radiation. An extrapolation of the existing transmission functions for all the necessary conditions does not always lead to desirable results. Substantial difficulties arise in considering the apparatus distortions during measurements in narrow frequency intervals.

The use of models of the absorption bands in calculations is often invalid for those narrow spectral intervals which are used in temperature sounding, because it must be assumed that the spectrum has a fine structure, which does not correspond to reality. Even such detailed models as the quasi-static one, calculations according to which are rather complex, do not always give satisfactory results [14]. Both methods, experimental and theoretical, most often give transmission functions for uniform media, i.e., media with constant pressure and temperature along the path of the ray, which cannot be applied directly to the real atmosphere. The use of approximation methods for considering the nonuniformity

of the atmosphere results in new errors in the transmission functions.

The method of a direct calculation of the transmission functions based on data on the parameters of the fine structure of the absorption bands--position, intensity, half-widths and shape of the contours of spectral lines--have recently become of more and more widespread usage. This is connected with certain achievements in calculations of these parameters, as well as with the further developments of computer technology. This method yields transmission functions for practically any physical conditions, for arbitrary spectral intervals and for the real atmosphere. The disadvantages of this method include the great amount of computations, as well as the fact that it is practically impossible to introduce any corrections into the values obtained for the transmission functions--there must be new calculations with new and more precise data. /76

All the advantages of the direct method of calculating the absorption are real only when the initial data on the parameters of the fine structure of the spectrum are determined with great accuracy. The use of transmissions functions obtained with the aid of the direct calculation method without a careful experimental comparison and clarification of the parameters can result in large errors. In this regard, we could mention, for example, that a number of experiments studying the rotational water vapor band and atmospheric windows [15, 16, 17] indicate that the theoretical data of W. Benedict and L. Kaplan [18] are apparently inaccurate. Experiments give values for the absorption which are 1.5-2 times greater than that which theory predicts. There are reasons to assume that the greatest errors are found in the values for the half-width of the spectral lines.

In the calculations of S. Dreyson [14] for the 15 μm carbon dioxide band, it was assumed that the half-widths of all the spectral lines were constant. The existing data in [18] show a notable variability in this characteristic from line to line; therefore, Dreyson's data could contain substantial errors.

Together with the planning of economical programs for a direct calculation of the absorption, particularly in the case of complex line contours, a comparison of the theoretical and experimental results and a specification of the parameters of the fine structure of the absorption bands are quite important. However, even in the case when the transmission functions in the spectral intervals selected for solving the problem of temperature sounding are known with the requisite accuracy for a definite model of the atmosphere, the real transmission functions can differ from those obtained for standard conditions. The fact is that, first of all, the assumption on the constancy of the volume concentration of carbon dioxide in the atmosphere, on which all the methods of interpreting measure-

ment results are based, may not be fulfilled in specific cases. Secondly, the transmission functions of the spectral intervals under investigations depend on the unknown temperature distribution and the unknown distribution of water vapor in the atmosphere. The effect of these factors can be greatly decreased by using the average profiles for the temperature, humidity and content of carbon dioxide for a given season and site and a temperature distribution obtained in first approximation. The water vapor distribution can be clarified according to the data from measurements of the out- /77 going radiation in various segments of the water vapor absorption bands. However, in using average profiles, which are hardly known for all the conditions, there can be random deviations in the temperature, humidity, and percentage of carbon dioxide at different altitudes, which results in random deviations in the transmission functions.

Random errors in the kernel are somewhat equivalent to random errors in the measured values for the radiation in terms of their effect on the results obtained. Actually, let us have n measurements (we will consider them precise) of outgoing radiation, i.e.,

$$I_i = \int B(p) K_i(p) dp, \quad i = 1, 2 \ldots n,$$

where K_i (p) are the transmission functions of their derivatives; B(p) is the unknown dependence of the Planck function on the atmospheric pressure p. In this case, we will consider that, either there is no contribution to the outgoing radiation from the Earth's surface (clouds), or that the contribution is known precisely, which merely decreases the possible effect of an error in the transmission functions.

Considering that the transmission functions are not known precisely, we will assume that the results are interpreted by using the new kernel $\overline{K}_{ip}$:

$$K_i(p) = \overline{K}_i(p) + \delta K_i(p),$$

where $\delta K_i(p)$ are random deviations of the transmission function from its average values due to the factors enumerated above. We now have the following:

$$I_i - \int B(p) \delta K_i(p) dp = \int B(p) \overline{K}_i(p) dp.$$

Here the second term in the left-hand part of the equation (we will call it γ_i) characterizes random deviations introduced into the measured radiation because of deviations in the transmission func-

tions. Because the latter are of a random nature, γ_i are also random values. Although they are of a specific physical nature, we can consider, disregarding this nature, that these random deviations are due to random errors in the measurements. As was already shown, M.S. Malkevich and V.I. Tatarskiy [7] studied the effect of these errors. They drew the conclusion that even small random errors in the measured values can result in great distortions of the unknown temperature profile. That is why a study of the values of $\gamma_i = \int B(p)\delta K_i(p)dp$ is of definite interest.

For convenience in analysis, it would be very desirable to evaluate the dispersion of radiation. Let us write out the solutions to the transfer equation in the following form:

$$I(\nu) = B(0) - \int \frac{\partial B}{\partial p} P(p, \nu)\, dp = B(0) - \frac{\partial \bar{B}}{\partial p} \int P(p, \nu)\, dp, \qquad /78$$

where $\overline{\frac{\partial B}{\partial p}}$ is the average gradient of the Planck function in the atmosphere characterizing its thermal nonuniformity. We then find the following expression for the dispersion $I(\nu)$:

$$D[I(\nu)] = \left(\frac{\partial \bar{B}}{\partial p}\right)^2 \iint \tilde{K}_{pp}(p_1 p_2)\, dp_1 dp_2, \qquad (13)$$

where $\tilde{K}_{pp}(p_1 p_2)$ is the auto-correlation function of the transmission function. In the particular case of $\overline{\frac{\partial B}{\partial p}} = 0$, i.e., for the isothermal atmosphere, the dispersion of radiation due to random discrepancies in the transmission function is equal to zero, as can be seen from (13) and as follows from the physical nature of the transformation of radiation.

At present, there are no data on the auto-correlation function. Therefore, we can use analytical correlation functions of uniform statistical processes, for example, in the form of

$$\tilde{K}_{pp}(|p_1 - p_2|) = \sigma_p^2 \exp\left[-\frac{|p_1 - p_2'|}{p'}\right], \qquad (14)$$

where σ_p^2 is the dispersion of the transmission function; p' is the correlation radius. In this case, we have the following:

$$D[I(\nu)] = 2\left(\frac{\partial \bar{B}}{\partial p}\right)^2 \sigma_p^2 \left[p'\left(p_0 + p' e^{-\frac{p_0}{p'}} - p'\right)\right]. \qquad (15)$$

Here P_0 is the limit to integration by pressure, characterizing the thickness of the effective emitting layer.

The representation of the auto-correlation function in the form of (14) is rather unreliable. Considering the integral nature of the transmission function, we can expect that its dispersion is not constant, as in (14).

Let us represent $\widetilde{K}_{pp}$ in the following way:

$$\widetilde{K}_{pp}(p_1 p_2) = \sigma_p^2 \frac{p_0 - p_1}{p_0} \exp\left[-\frac{|p_1 - p_2|}{p'}\right] \tag{16}$$

We then have

$$D[I(\nu)] = \left(\frac{\partial \bar{B}}{\partial p}\right)^2 \sigma_p^2 \left[p'\left(2p'^2 + p_0^2 - p'p_0 + p'p_0 e^{\frac{p_0}{p'}}\right)\right]. \tag{17}$$

Quantitative evaluations of $D[I(\nu)]$ with the aid of (15) and (17) are complicated because of the indefiniteness of σ_p^2 and p'; however, even qualitative conclusions from (15) and (17) are of definite interest.

1. The dispersion of radiation due to random deviations in the transmission function depend primarily on the thermal nonuniformity of the atmosphere. Particularly substantial errors can arise for the atmosphere with great temperature nonuniformities.

2. The dispersion in radiation increases with an increase of the correlation radius, and the errors accumulate.

3. Relationships (15) and (17) characterize the dependence of the the dispersion on p_0, i.e., the boundary of the effective emitting layer. The greater the value of p_0, the greater the dispersion of radiation, i.e., the greatest errors can be expected for relatively transmissive channels. The dependence on p_0 implicitly characterizes the dependence of the dispersion of radiation on the frequency. Since random errors have a particularly negative effect on an interpretation of the measurement results, and they should not exceed 3-5%, according to the data of a number of authors, the relationships in (15) or (17) (for known σ_p^2 and p') can be used in selecting the channels for temperature sounding for which the dispersion does not exceed a permissible value. However, we must not forget that there is also a random error connected with the measurement process itself in the measurements.

It would be very desirable to determine the auto-correlation function of the transmission function on the basis of statistical characteristics of the distributions affecting its value. There is no difficulty in expressing $\widetilde{K}_{pp}$ in terms of auto-correlation and reciprocal-correlation functions of the distributions of carbon

dioxide, water vapor and the temperature, as well as in terms of the derivatives of the transmission function which characterize its dependences on these distributions. However, the incompleteness of information on the statistical characteristics of these distributions (this relates particularly to carbon dioxide) complicates a use of this approach. In the future, as experimental materials are accumulated and analyzed, this approach would be fruitful. An evaluation of certain average values of γ_i based on the use of average values for deviations in the initial distributions is a well-known but but very limited solution to the problem.

Approximative Evaluation of the Effect of Variability In the Concentration of Carbon Dioxide and Water Vapor and the Temperature on the Outgoing Radiation

Effect of Carbon Dioxide. At present, there is a relatively large amount of data on the CO_2 content on the Earth's surface. The effect of natural and artificial sources and sinks of CO_2 has been studied. The essential variability of the values for the concentration at various sites has been noted. For average values /80 of the volume concentration of about 0.031-0.033%, substantial fluctuations can be observed even during the course of one day (reaching 0.01% [19,20]). A daily, monthly, and yearly concentration has been found. However, these variations are usually small and they reach 0.001% on the average. Attempts have been made at studying the spatial distribution of the CO_2 content. Thus, measurements of the CO_2 content over the Pacific and Indian Oceans were carried out on the Soviet craft "Vityaz'" [22]. A substantial increase in the CO_2 content at low latitudes was noted in a comparison with middle and high latitudes. The CO_2 content depends on the type of air masses and fronts and the direction of the wind. Measurements along the coast of the Black Sea showed a substantial variability in the CO_2 (0.0240-0.0380%). Obviously, the deviations in the concentration from average values by 10-30% and more can be considered completely realistic, particularly for large masses of vegetation, and near industrial objects and city complexes. The altitudinal distribution of CO_2 has been studied insufficiently. In a number of studies [23], there was noted a small decrease in the CO_2 content with an increase in distance from the Earth's surface, as well as a decrease in the range of possible deviations from the average values. It was found in [21,20] that the effect of vegetation on the CO_2 content is significant up to altitudes on the order of 1 km. Nevertheless, it can certainly be held that the greatest effect of a fluctuation in the CO_2 content is found in the outgoing radiation in the most transmissive spectral regions, since these fluctuations reach the greatest values in the lower layers of the atmosphere.

In order to evaluate the effect of possible deviations in the distributions of CO_2 concentration on the outgoing radiation, we carried out the following calculations. We examined two atmospheric stratifications: in one of them, the concentration of CO_2 was

constant over the entire atmosphere, while, in the other, there was a maximum at the Earth's surface and a decrease according to the law $q(p) = \bar{q}(1 + e^{-\frac{A}{p}})$. The calculations were carried out for a number of spectral intervals of the 15 μm CO_2 band, and the effective-mass method and the data of [24] were used for obtaining the transmission functions of the real atmosphere. The table below shows values for the intensity of radiation, expressed in $erg/cm^2 \cdot sec \cdot stere \cdot cm^{-1}$ for the spectral intervals under investigation. Two thermal models of the atmosphere were used in the calculations; they can be characterized in the following way:

Distribution I T(1000 mb) = 308°K, T(100) = 212°K, T(10) = 235°K.
Distribution II T(1000 mb) = 257°K, T(100) = 213°K, T(10) = 233°K.

(The level with pressure of 10 mb was taken as the upper boundary of the atmosphere.)

TABLE

Temperature Stratification I								Temperature Stratification II						
1	2	3	4	5	6	7	8	9	10	11	12	13	14	15
697,5	52,9	—	—	52,4	51,9	51,6	48,1	45,7	—	—	—	45,0	44,8	43,4
702,5	59,3	—	58,9	58,5	58,3	58,1	53,7	47,4	—	—	—	47,1	46,6	45,5
710,0	75,9	74,3	73,9	72,7	70,9	70,3	64,8	53,0	52,5	51,3	51,8	51,2	51,0	49,2
720,0	57,6	56,5	56,2	56,0	55,2	54,9	51,2	46,8	—	—	—	46,0	45,8	45,0

-- Difference from column 2 or 9 in the range of calculation errors.
1- Centers of spectral intervals, cm^{-1}
2.9- Standard CO_2 distribution
3.10-Non-standard CO_2 distribution
4.11-Standard CO_2 distribution + consideration of H_2O (theoretical transmission functions)
5.12-Non-standard CO_2 distribution + consideration of H_2O (theoretical transmission functions)
6.13-Standard CO_2 distribution + consideration of H_2O (experimental transmission functions)
7.14-Non-standard CO_2 distribution + consideration of H_2O (experimental transmission functions)
8.15-Calculations with the aid of transmission functions for T = 300°K (all the preceding calculations were with transmission functions for T = 250°K)

Effect of Absorption by Water Vapor. As is well known, the weak lines of water vapor bands and the branches of strong remote lines of the rotational and ν_2 water vapor bands has a definite effect on the processes of transformation of radiation in a number of the intervals used for the purposes of temperature sounding.

Calculations were carried out with a consideration of the radiation and absorption by water vapor wnd without a consideration of the effect of water vapor. It was assumed in the calculations that the transmission function of the gas mixture could be represented in the form of the product of transmission functions for single gases. Since the water vapor absorption in the spectral region under investigation was due largely to the branches of the remote spectral lines, this assumption should be fulfilled for narrow spectral intervals with sufficient accuracy, for a broad range of pressures and content of absorbent. This conclusion was confirmed by direct calculations of the transmission functions of a number of spectral regions on the basis of data concerning the parameters of the fine structure of the spectrum [25]. There are many experimental studies [26,27,28] in which the water vapor absorption was studied for frequencies close to the range of interest to us. Moreover, as was found, the water vapor functions can be obtained by direct calculations on the basis of the data in [18]. However, the calculations which were carried out showed a substantial difference between the theoretical transmission functions and the transmission functions obtained by extrapolation of experimental data [26,27,28].

The effect of water vapor was evaluated both with theoretical /82
and with experimental transmission functions. A model of the atmosphere with relatively high humidity (q(1000 mb) = 0.018 g/g) was used in the calculations, as were the temperature distributions I and II examined previously. As is easy to see, the effect of the water vapor is substantial for relatively transmissive spectral intervals, and it cannot be disregarded if substantial errors are to be avoided. In order to decrease these errors, we can use the average humidity distributions in the atmosphere in the calculations; however, because of the great variability of the water vapor content, random deviations from these average distributions could complicate an interpretation of the radiation measurements. These random errors can be considered in carrying out simultaneous satellite measurements of the radiation in the water vapor absorption bands.

Effect of Temperature Dependence of Transmission Functions

The transmissions functions of atmospheric gases depend to some extent on the temperature. This is connected primarily with the dependence of the intensities of the spectral lines on the temperature. In order to illustrate the effect of the temperature dependence of the transmission functions on the value of the outgoing radiation, the latter were calculated with the aid of transmission functions corresponding to temperatures of T = 250° and T = 300° K. As can be seen from the table, the temperature can have a significant effect on the magnitude of radiation and the transmission functions; therefore, it may be necessary to use the method of successive approximations in interpreting the radiation data.

Conclusion

It is not only the factors examined above which affect the accuracy in interpretation of the data of radiation measurements for a solution to the problem of temperature sounding. Obviously, in a number of cases, particularly for the combined effect of different factors, we can expect noticeable distortions of the real picture for the temperature stratification of the atmosphere if we disregard this effect. Therefore, in selecting the spectral intervals, we must consider the possible random deviations in the transmission functions. It is necessary, in particular, that the method of V. P. Kozlov, evaluating the informativeness of the spectral regions in temperature sounding, also be generalized for this case. The development of independent methods of determining the distributions of the concentration of water vapor and carbon dioxide in the atmosphere is also an important problem.

REFERENCES /83

1. King, J. J. F.: The Earth Satellite Vehicle as a Stratospheric Temperature Probe. Proc. of the VII Intern. Astron. Congr. Rome, 1956.
2. King, J. J. F.: Deduction of Vertical Thermal Structure of a Planetary Atmosphere from a Satellite. Planet. Space. Sci., Vol. 7, July 1961.
3. Kaplan, L.D.: Inference of Atmospheric Structure from Remote Radiation Measurements. J. Opt. Soc. Amer., Vol. 49, 1959.
4. Marchuk, G.I.: Equation for the Importance of Information from Meteorological Satellites and Formulation of the Inverse Problems. Kosmich. Issled., Vol. II, No. 3, 1964.
5. Wark, D.Q.: On Indirect Temperature Sounding of the Stratosphere From Satellites. J. Geophys. Res., Vol. 66, 1961.
6. Jamamoto, G.: Numerical Method for Estimating the Stratospheric Temperature Distribution from Satellite Measurements in the CO_2 Band. J. Meteorol., Vol. 18, 1961.
7. Malkevich, M.S. and V.I. Tatarskiy: Determination of the Vertical Distribution of the Temperature of the Atmosphere According to the Outgoing Radiation in the CO_2 Absorption Band. In the Collection: Kosmicheskiye issledovaniya (Space Research), Vol. III, No. 3, Akad. Nauk S.S.S.R., 1964.
8. Obukhov, A.M.: Statistically Orthogonal Expansions of Empirical Functions. Izvest. Akad. Nauk S.S.S.R., ser. geofiziki, No. 3, 1960.
9. Kaplan, L.D.: The Spectroscope as a Tool for Atmospheric Sounding by Satellites. Fall. Instrum. Autom. Conf. Instr. Soc. Amer. N.Y., September 26-30, 1960.
10. Kozlov, V.P.: On a Reproduction of the Altitudinal Temperature Profile According to the Spectrum of Outgoing Radiation. Izvest. Akad. Nauk S.S.S.R., ser. fiziki atmosfery i okeana, Vol. 2, No. 2, 1966.
11. Tikhonov, A.N.: A Solution to Incorrectly Formulated Problems and a Regularization Method. Doklady Akad. Nauk S.S.S.R., Vol. 151, No. 3, 1963.

12. Phillips, D.L.: A Technique for the Numerical Solutions of Certain Integral Equations of the First Kind. J. Assoc. Computing Mach., Vol. 9, 1962.
13. Twomey, S.: On the Numerical Solution of Fredholm Integral Equations of the First Kind by the Inversion of the Linear System Produced by Quadrature. J. Assoc. Computing Mach. Vol. 10, 1963.
14. Dreyson, S.R.: Atmospheric Slant Path Transmission in the 15 CO_2 Band. Technical Report ORA. Project 05863. The University of Michigan, 1964.
15. Bignell, K., F. Saiedy and P. A. Sheppard: On the Atmospheric Infrared Continuum. J. Opt. Soc. Amer., Vol. 53, No. 4, 1963.
16. Zhevakin, S.A. and A. N. Naumov: Absorption Electron Microscopy of the Radiation by H_2O Vapors at Waves of 10 μm-2 cm in the Upper Layers of the Atmosphere. Geomagnetizm i Aeronomiya, Vol. III. No. 3, 1963.
17. Furashev, N.I.: Study of the Absorption of Long-Wave Infrared Radiation by Atmospheric Water Vapors. Optika i Spektroskopiya, Vol. XX, No. 3, 1966.
18. Benedict, W.S. and L.D. Kaplan: Atlas Rotational Water Vapor Data. J.P.L., 1963.
19. Madden, R.P.: A High Resolution Study of CO_2 Absorption Spectra Between 15 and 18 microns. J. Chem Phys., Vol. 35, 2083, 1961.
20. Lieth, H.: The Role of Vegetation in the Carbon Dioxide Content of the Atmosphere. J. Geophys. Res., Vol. 68, No. 13, 1963.
21. Bischof, W.B.: Periodical Variations of the Atmospheric CO_2 Content in Scandinavia. Tellus. Vol. XII, No. 2, 1960.
22. Bruyevich, S.V. and S. V. Lyutsarev: The CO_2 Content in the Atmosphere Over the Pacific and Indian Oceans and in the Region of the Black Sea. Doklady Akad. Nauk S.S.S.R., Vol. 136, No. 2, 1961.
23. Bischof, W.: Variations in Concentration of Carbon Dioxide in the Free Atmosphere. Tellus. Vol. XIV, No. 1, 1962.
24. Stull, V.R., P. J. Wyaft, and G. N. Plass: The Infrared Absorption of Carbon Dioxide. Infrared Transmission Studies. Final Report, Vol. 111, 1963.
25. Kondrat'yev, K.Ya. and Yu. M. Timofeyev: Numerical Experiment /84 on the Study of the Transmission Functions of Atmospheric Gases. Materials of the VIth Inter-Departmental Conference on Actinometry and Atmospheric Optics. Tartu, 1966.
26. Bolle, H.J.: Atmospheric Emission in Single Water Vapor Lines and its Calculation by Means of Radiation Diagrams. Mem. Soc. Roy. Sci. Liege, Vol. 26, 1964.
27. Stauffer, F.R. and T. E. Walsh: Transmittance of Water Vapor - 14 to 20 Microns. J. Opt. Soc. Amer., Vol. 56, No. 3, 1966.
28. Ashcheulov, S.V., K. Ya. Kondrat'yev and D.B. Styro: Determination of the Absorption Coefficients for Some Atmospheric Windows and Absorption Bands According to the Emission Spectra. This Collection, p. 8.
29. Wark, D.Q. and H. E. Fleming: Monthly Weather Rev., Vol. 94, pp. 351-362, 1966.

A METHOD OF CALCULATING THE SPECTRAL ABSORPTION OF INFRARED RADIATION IN THE ATMOSPHERE

A. G. Pokrovskiy

ABSTRACT: The author develops a method of calculating atmospheric spectra of water vapor absorption for arbitrary distributions of concentration, temperature and atmospheric pressure, with a consideration of the line broadening due to the Doppler effect. It is shown how this method will be useful in solving many atmospheric problems in which a precise value must be given for the absorption function.

Introduction

A method of calculating the transmission spectra of the solar radiation in the atmosphere is discussed in this study for the infrared water vapor absorption bands. Interest in this problem has recently increased to a great extent in connection with studies of the Earth's atmosphere. To present, two basic tendencies have been noted in the theoretical calculations of the atmospheric transmission. The first is the tendency to calculate certain models [1-6] and the second is to carry out direct calculations on the basis of a computation of the principal molecular parameters of the absorbing medium, such as the intensity, position and half-width of the spectral lines. The most significant study on direct calculations is the monograph by D. Gates, R. Calfee, D. Hansen and W. Benedict [7]. However, this monograph discusses a calculation of the absorption only for the spectral line contours whose shape is determined by the Lorentz formula [8]. Moreover, all the calculations were carried out only for a small number of values of the concentrations of water vapor and atmospheric pressures. The method of calculating atmospheric spectra of water vapor absorption is developed in this study for arbitrary distributions of concentration, temperature and atmospheric pressure, with a consideration of the line broadening due to the Doppler effect. The amount of computations is determined mainly by the quantity of spectral lines selected for the calculations and by the profiles for the distributions of the atmospheric parameters. /85

1. Formulation of the Problem

The magnitude of integral absorption in a spectral region of $\Delta\nu = \nu_2' - \nu_1'$ containing n single lines is determined by the following formula:

$$W(\nu_1';\ \nu_2') = \int_{\nu_1'}^{\nu_2'} \left\{ 1 - \exp\left[-\int_0^{z^*} \sum_{i=1}^{n} K_i(z,\ \nu)\, \rho_{H_2O}^{(i)}(z) \operatorname{cosec}\theta\, dz \right] \right\} d\nu, \qquad (1)$$ /86

where $K_i(z,\nu)$ is the mass absorption coefficient of the i-th spectral line; ν_1' and ν_2' are the boundaries of the selected spectral region; z^* is the thickness of the vertical atmospheric layer, cm; θ is the height of the Sun; ν is the wave number; $\rho_{H_2O}^{(i)}$ is the partial density of the water vapor isotope corresponding to the absorption of the i-th spectral line.

For the subsequent calculations, it is convenient to write out $K_i(z,\nu)$ in the form of

$$K_i(z,\nu) = \frac{K_i(z,\nu)}{K_{0i}(z)} K_{0i}(z), \tag{2}$$

$$K_{0i}(z) = \frac{S_i(z)}{\gamma_{Di}(z)} \sqrt{\frac{\ln 2}{\pi}}, \tag{3}$$

$$S_i(z) = \int_{-\infty}^{\infty} K_i(z,\nu)\, d\nu, \tag{4}$$

$$\frac{K_i(z,\nu)}{K_{0i}(z)} = H(a_i(z);\ \omega_i(z)) = \frac{a_i(z)}{\pi} \int_{-\infty}^{\infty} \frac{e^{-x^2} dx}{a_i^2(z) + [\omega_i(z) - x]^2}, \tag{5}$$

$$a_i(z) \frac{\gamma_{Li}(z)}{\gamma_{Di}(z)} \sqrt{\ln 2};\ \omega_i(z) = \frac{\nu - \nu_i}{\gamma_{Di}(z)} \sqrt{\ln 2}. \tag{6}$$

Here $K_{0i}(z)$ is the absorption coefficient at the center of the i-th spectral line, the broadening of which is due solely to the Doppler effect [8]; $S_i(z)$ is the integral intensity of the i-th spectral line; $\gamma_{Di}(z)$ is the Doppler half-width of the i-th spectral line; $\gamma_{Li}(z)$ is the Lorentz half-width of the i-th line; ν_i is the wave number corresponding to the center of the i-th line.

The dependence on the altitude of the values $S_i(z)$, $\gamma_{Li}(z)$ and $\gamma_{Di}(z)$ is determined by the following well-known [9] relationships:

$$S_i(z) = S_{i0} \left[\frac{T_0}{T(z)}\right]^{3/2} \exp\left[-\frac{(T_0 - T(z))}{T_0 T(z)} \frac{E_i''}{k/hc}\right], \tag{7}$$

where S_{i0} is the integral intensity of the i-th line, determined at a temperature of T_0 = 288°K; T(z) is the temperature of the atmosphere at an altitude of z(km); E_i'' is the energy of the ground state of the i-th molecular transition; k is the Boltzmann constant; h is the Planck constant; c is the speed of light in the medium.

$$\gamma_{Li}(z) = \gamma_{Li}(0) \frac{P(z)}{P(0)} \left[\frac{T_0}{T(z)}\right]^{0.62}, \tag{8}$$

$$\gamma_{Di}(z) = \frac{\nu_i}{c} \sqrt{2R \ln 2} \left[\frac{T(z)}{M_{H_2O}^{(i)}}\right]^{1/2}, \tag{8a}$$

where R is the universal gas constant; $M^{(i)}_{H_2O}$ is the molecular weight of the H_2O isotope causing the absorption of the i-th spectral line; γ_{Li} (0) is the Lorentz half-width, determined at a temperature of T_0 and pressure of $P(0) = 1.01325 \cdot 10^6$ dyn·cm^{-2}; P(z) is the atmospheric air pressure at an altitude of z.

For the principal parameter characterizing the water vapor content in the atmosphere, we took the mixing ratio w(z). Then

$$\rho^{(i)}_{H_2O} = \frac{w(z)P(z)M_a(z)f_i}{RT(z)}, \tag{9}$$

where $M_a(z)$ is the molecular weight of air; f_i is the relative percentage in the total mass of water vapor of the H_2O isotope causing the absorption of the i-th spectral line. Because the parameters of the atmosphere T(z), w(z) and P(z) depend largely on the specific state of the atmosphere at the moment of the observation, it is obviously unnecessary to represent them in the form of certain functional dependences on the altitude. Moreover, this would be a very complicated task, not to speak of the time-consuming computations. In this regard, we applied a method usually used [10] in solving atmospheric problems of such a type. The entire width of the atmosphere was divided into single, rather thin layers, and it was assumed that the values P(z), w(z) and T(z) remained constant within the limits of a layer. In this case, (1) acquired the following form:

$$W'(\nu_1'; \nu_2') = \int_{\nu_1'}^{\nu_2'} A(\nu)\, d\nu, \tag{10}$$

$$A(\nu) = 1 - \exp\left[-\sum_{j=1}^{m}\sum_{i=1}^{n} K_{ij}(\nu)\,\rho^{(ij)}_{H_2O}\cdot\Delta z_j \operatorname{cosec}\theta\right]. \tag{10a}$$

Thus, the problem can be solved, in principle, if T_j, P_j, w_j and the spectral parameters ν_i, $\gamma_{Li}(0)$ and S_{i0} are known.

2. Method of Calculating the Integral Absorption $W(\nu_1'; \nu_2')$

A calculation of $W(\nu_1'; \nu_2')$ amounts to a solution for two basic problems: (1) finding the optimal method for calculating the integrand $A(\nu)$ [see (10a)], and (2) finding the optimal approximation method for integrating the function $A(\nu)$ in the given spectral interval of $\Delta\nu = \nu_2' - \nu_1'$.

Let us first consider the method of calculating the integrand /88
$A(\nu)$. The main difficulty in the calculations is that the value of $Q_{ij}(\nu - \nu_i)$ must be calculated repeatedly. This value is determined by the following formulas:

$$Q_{ij}(\nu-\nu_i)=K_{0ij}H(a_{ij};\ \omega_{ij})\,\rho_{H_2O}^{(ij)}\Delta z_j \operatorname{cosec}\theta, \tag{11}$$

$$H(a_{ij};\ \omega_{ij})=\frac{a_{ij}}{\pi}\int\limits_{-\infty}^{\infty}\frac{e^{-x^2}dx}{a_{ij}^2+(\omega_{ij}-x^2)}. \tag{11a}$$

The method of calculating $H(a_{ij};\ \omega_{ij})$ will be discussed in Section 3.

For a definite value of the wave number ν, the number of elements of the matrix $||Q_{ij}(\nu - \nu_i)||$ is equal to the product $n \cdot m$ [see 10a)], i.e., is determined by the number n of spectral lines selected for calculating the absorption at the point ν and the number m of layers on which the absorbing medium was divided from the upper boundary of the atmosphere up to the altitude at which the spectrum is calculated. The optimal conditions for the calculation (minimum of the product $n \cdot m$) are determined by the requisite accuracy for calculations of the function $A(\nu)$. For given accuracy in $A(\nu)$, the value of m depends on the nature of the distribution of temperature, pressure and humidity with the altitude; therefore, it is not quite specific. The problem of optimization of the selection of atmospheric layers and their number is not considered in this study.

On the other hand, the optimal selection of the value n virtually amounts to the problem of a correct consideration at each point ν of the branches of only those lines which affect the value for the absorption in it with a given degree of accuracy. In this regard, we must keep in mind that the nature of the dependence of the spectral absorption of $A(\nu)$ changes greatly with the altitude.

Consideration of the Effect of the Branches of Spectral Lines Located Outside the Interval $\Delta\nu = \nu_2^1 - \nu_1^1$

First of all, we must define which of the spectral lines located beyond the limits of the selected spectral region $\Delta\nu$ affect the absorption inside it. The following algorithm is suggested.

1. All the lines inside the given absorption band, which are outside the interval $\Delta\nu$, with integral intensities [see (4)] greater than some value S_0 given previously (for example, $S_0 = 10\ g^{-1} \cdot cm$) are considered. If this band intersects with neighboring ones, we must also consider all the lines with intensities greater than S_0 in them.

2. Of the wave numbers corresponding to the centers of these lines, two increasing sequences are constructed $\{\nu_i\}$ $(i = 1,2,3,..,n_0)$ and $\{\nu_{n_0+r}\}$ $(r = 1,2,3,...,r_0)$ so that

$$\begin{gathered}\nu_1<\nu_2<\ldots<\nu_{n_0}<\nu_1',\\ \nu_2'<\nu_{n_0+1}<\nu_{n_0+2}<\ldots<\nu_{n_0+r_0}.\end{gathered} \tag{12}$$ /89

Here $n_0 + r_0$ is the total number of spectral lines considered ($s_i \geq s_0$) outside the interval $\Delta\nu = \nu_2' - \nu_1'$.

3. The values of R_i and R_{n_0+r} corresponding to terms in the sequences of $\{\nu_i\}$ and $\{\nu_{n_0+r}\}$ at the boundary points of ν_1' and ν_2' are calculated according to the following formulas:

$$R_i = \sum_{j=1}^{m} Q_{ji}(\nu_1' - \nu_i); \quad i = 1, 2, 3, \ldots, n_0; \tag{13}$$

$$R_{n_0+r} = \sum_{j=1}^{m} Q_{jn_0+r}(\nu_2' - \nu_{n_0+r}), \quad r = 1, 2, 3, \ldots, r_0. \tag{13a}$$

The program is constructed so that each of the computed values of R_i and R_{n_0+r} is stored.

4. Of the values obtained for R_i and R_{n_0+r}, two increasing sequences are constructed $\{R^{(N)}\}$ ($N = 1,2,3,\ldots,n_0$) and $\{R^{(M)}\}$ ($M = n_0+1, n_0+2,\ldots,n_0+r_0$) so that

$$R^{(1)} < R^{(2)} < \ldots < R^{(n_0)} \tag{14}$$

and

$$R^{(n_0+1)} < R^{(n_0+2)} < \ldots < R^{(n_0+r_0)}. \tag{14a}$$

5. Of the sequences $\{R^{(N)}\}$ and $\{R^{(M)}\}$, we take those parts $\{R^{(N)}\}^*$ ($N = N_0, N_0 + 1, N_0 + 2,\ldots,n_0$) and $\{R^{(M)}\}^*$ ($M = M_0, M_0+1, M_0 + 2,\ldots,n_0 + r_0$) whose terms are determined by the following conditions:

$$\sum_{N=1}^{N_0} R^{(N)} \geqslant \frac{\varepsilon}{n_0}, \quad \sum_{N=1}^{N_0-1} R^{(N)} < \frac{\varepsilon}{n_0} \tag{15}$$

and

$$\sum_{M=n_0+1}^{M_0} R^{(M)} \geqslant \frac{\varepsilon}{m_0}, \quad \sum_{M=n_0+1}^{M_0-1} R^{(M)} < \frac{\varepsilon}{m_0}. \tag{16}$$

Here ε is a small parameter determined by the formula

$$\varepsilon = -\ln[1 - \Delta A(\nu)]; \tag{17}$$

$\Delta A(\nu)$ is the absolute precision in calculating the value of the spectral absorption $A(\nu)$; n_0 and m_0 are fitting parameters whose significance will be discussed below.

The wave numbers corresponding to the terms of the sequences

$\{R^{(N)}\}^*$ and $\{R^{(M)}\}^*$ determine the spectral ranges B_1 and B_2 which affect the absorption inside the interval $\Delta\nu$ with a given degree of accuracy. $\Delta\nu = \nu_2' - \nu_1'$; B_1 and B_2 are then determined by the conditions

$$\begin{aligned} &\text{if } \nu \in B_1, \text{ then } \nu_i^{\min} \leqslant \nu < \nu_1', \\ &\text{if } \nu \in B_2, \text{ then } \nu_2' < \nu \leqslant \nu_i^{\max}. \end{aligned} \tag{18}$$

/90

(18a)

Here $\nu_i^{\min}$ is the minimum value from the set of wave numbers corresponding to the terms of the sequence $\{R^{(N)}\}^*$, while $\nu_i^{\max}$ is the maximum value from the set of wave numbers corresponding to the terms of the sequence $\{R^{(M)}\}^*$. The weaker lines ($S_1 \leq S_i < S_0$) whose centers belong to regions B_1 and B_2 are then selected in a similar way. Here S_1 and S_0 are fitting parameters determined by numerical experiments on a digital computer. For example, $S_1 = 1\ g^{-1}\cdot cm$. This preliminary analysis greatly shortens further computations and aids in throwing out a substantial number of weak lines outside the interval $\Delta\nu$ whose contribution to the absorption in it is negligible.

It is easy to obtain the condition which permits a selection of the fitting parameters S_1, S_0, m_0 and n_0 in such a way that the absolute error in determining the spectral absorption at any point $\nu \in [\nu_1', \nu_2']$ which is connected with the specific characteristics of the method does not exceed the preset value of $\Delta A(\nu)$.

Let $\Delta\tau(\nu_1')$ be the absolute error in calculating the value $\tau(\nu_1')$ determined by the formula

$$\tau(\nu_1') = -\ln[1 - A(\nu_1')],$$

where $A(\nu_1')$ is determined by (10a). It is then easy to show that

$$\Delta\tau(\nu_1') = \Delta\tau_1(\nu_1') + \Delta\tau_2(\nu_1') + \frac{2\varepsilon(n_0 + m_0)}{n_0 m_0},$$

where ε is determined by (17); $2\varepsilon(n_0 + m_0)/n_0 m_0$ is the error arising in taking out lines, according to the criteria of (15) and (16), which are applicable both to the lines with intensities of $S_1 \leq S_i < S_0$ and to the lines with $S_i \geq S_0$; $\Delta\tau_1(\nu_1')$ is the error connected with a disregard for the lines with centers ν_i lying outside the interval $[\nu_i^{\min}, \nu_i^{\max}]$; $\Delta\tau_2(\nu_1')$ is the error connected with a disregard for the lines with intensities less than S_1 and with centers of $\nu_i \in [\nu_i^{\min}, \nu_i^{\max}]$. If we impose the condition below on $\Delta\tau(\nu_1')$

$$\Delta\tau(\nu_1') \leqslant \varepsilon,$$

then $\Delta\tau_\Sigma(\nu_1') = \Delta\tau_1(\nu_1') + \Delta\tau_2(\nu_1')$ will satisfy the condition

$$0 < \Delta\tau_\Sigma(\nu_1') \leqslant \varepsilon\left[1 - \frac{2\varepsilon(n_0 + m_0)}{n_0 m_0}\right], \tag{16a}$$

from which $2(m_0 + n_0)/n_0 m_0 < 1$. The parameters S_0 and S_1 should be selected as a result of numerical experiments on the digital computer in such a way that the condition of (16a) is fulfilled.

Consideration of the Isolation of Spectral Lines /91

We must consider the fact that some lines inside the spectral region $\Delta\nu$ can be isolated. The following algorithm is suggested.

1. Of the wave numbers corresponding to the centers of the spectral lines selected for calculating the absorption inside the interval $\Delta\nu$, the sequence $\{\nu_i\}^*$ $(i = 1, 2, 3, \ldots, S)$ is constructed. The sequence $\{\nu_i\}^*$ includes lines belonging to the regions B_1 and B_2 and lines determined from a preliminary analysis, as well as all the spectral lines inside the interval $\Delta\nu$ with integral intensities greater than S_1. The terms of the sequence $\{\nu_i\}^*$ are arranged in increasing order:

$$\nu_i^{\min} \leqslant \nu_1 < \nu_2 < \nu_3 < \ldots < \nu_{S-1} < \nu_S \leqslant \nu_i^{\max}. \tag{19}$$

Here $\nu_i^{\min}$ and $\nu_i^{\max}$ are determined by (18) and (18a).

2. Of the sequence $\{\nu_i\}$, we select that part $\{\nu_{l+r}\}^*$ which is inside the interval $\Delta\nu$: the terms of the sequence $\{\nu_{l+r}\}^*$ are determined by the following inequalities:

$$\nu_1' \leqslant \nu_l < \nu_{l+1} < \ldots < \nu_{l+n} \leqslant \nu_2'. \tag{20}$$

Let us now construct the increasing sequence $\{\nu_k^*\}$ whose terms are calculated by the following formulas:

$$\nu_0^* = \nu_i^{\min}, \tag{21}$$

$$\nu_1^* = \nu_l - \frac{\nu_l - \nu_1'}{2}, \tag{22}$$

$$\nu_k^* = \nu_{l+k-1} - \frac{\nu_{l+k-1} - \nu_{l+k-2}}{2},$$

$$k = 2, 3, 4, \ldots, n+1, \tag{23}$$

$$\nu_{n+2}^* = \nu_2' - \frac{\nu_2' - \nu_{l+n}}{2},$$

$$\nu_{n+3}^* = \nu_i^{\max}, \tag{24}$$

where ν_{l+k-1}, ν_{l+k-2}, ν_{l+n} are terms of the sequence $\{\nu_{l+r}\}^*$ (r = 0, 1, 2,..., n).

3. Let us now take from the sequence $\{\nu_k^*\}$ (k = 0, 1, 2,..., n + 3) the increasing subsequence $\{\nu_N^{**}\}$ (N = 1, 2, 3,...) so that its first and last terms are equal to ν_0^* and ν_{n+3}, respectively, while the remaining terms satisfy the following criterion:

$$A(\nu_N^{**}) < \Delta A(\nu);\ A(\nu_N^{**}) = 1 - \exp\left[-\sum_{j=1}^{m}\sum_{i=1}^{s} Q_{ij}(\nu_N^{**} - \nu_i)\right] \qquad (25)$$
$$N = 2, 3, 4, 5, \ldots$$

Here $\Delta A(\nu)$ is the given absolute accuracy in calculating the spectral absorption $A(\nu)$. If the criterion of (25) is not fulfilled at any point of the sequence $\{\nu_N^{**}\}$ N = 1, 2,...), then it is composed of the two terms ν_0^* and ν_{n+3}^* alone. /92

4. After the sequence $\{\nu_N^{**}\}$ is found, the absorption at any point ν inside the interval $\Delta\nu = \nu_2' - \nu_1'$ is calculated by the following formula:

$$A(\nu) = 1 - \exp\left[-\sum_{j=1}^{m}\sum_{i=k}^{k+q} Q_{ij}(\nu - \nu_i)\right], \qquad (26)$$

where k and q are determined by the inequalities

$$\nu_N^{**} \leqslant \nu \leqslant \nu_{N+1}^{**};\ \nu_N^{**} < \nu_k < \nu_{k+1} < \ldots < \nu_{k+q} < \nu_{N+1}^{**}. \qquad (27)$$

Here ν_k is the wave number corresponding to the center of the k-th spectral line belonging to the sequence $\{\nu_i\}^*$ [see (19)]. As a result, only the branches of those lines which affect the absorption in it with given accuracy are considered at each point $\nu \in \Delta\nu$.

Method of Integrating the Function a(ν)

The selection of a method for calculating the integral absorption [see (10)] is based on the fact that any approximating integration methods are satisfactory (in the sense of use of machine time) only for functions which do not change abruptly. The function $A(\nu)$ [see (10a)] changes greatly either near the center of the i-th spectral line or near the point ν_i^A satisfying the condition

$$A(\nu_i^A) = 1 - \Delta A(\nu). \qquad (28)$$

Therefore, a calculation of the integral $W(\nu_1', \nu_2')$ [see (10)] over the entire interval $\Delta\nu$ with a fixed step is irrational. An attempt was made in [7] to reduce the amount of computations with the aid

of a selection of two fixed steps h_1 and h_2, while the step h_1 = 0.005 cm^{-1} was used in the neighborhood $\Delta\nu_{i0}$ of the center of the i-th spectral line, and the step h_2 = 0.01 cm^{-1} outside this neighborhood. The interval $\Delta\nu_{i0}$ is determined by the following condition:

$$\text{if } \nu \in \Delta\nu_{i0}, \text{ then } \nu_i - 0{,}05\ cm^{-1} \leqslant \nu \leqslant \nu_i + 0{,}05\ cm^{-1}. \quad (29)$$

With such a calling sequence h_1 completely disregards the different dependence of the absorption $A(\nu)$ on the wave number in the neighborhood of various lines located inside the interval $\Delta\nu$, the change in absorption in single lines with the altitude, and the presence in the most intensive lines of wide ranges of total absorption $\Delta\nu_i^A$, which are determined by the following condition:

$$\text{if } \nu \in \Delta\nu_i^A, \text{ then } A(\nu) \geqslant 1 - \Delta A(\nu). \quad (30)$$

Thus, for most of the strong lines in the troposphere and the layer /93
near the ground, the width of this range varies within the limits from 0.02 to 1 cm^{-1}. Consequently, in this case almost all the values of the wave numbers taken inside $\Delta\nu_{i0}$ are incident in the range of total absorption $\Delta\nu_i^A$. On the other hand, for spectral lines in the upper atmosphere (above 30 km), the half-width of the contour for penetration of which is equal to (0.001-0.005) cm^{-1}, the neighborhood of $\Delta\nu_{i0}$ is found to be too great, while the step h_1, on the one hand, is insufficient for a precise reconstruction of the line contour (near $\nu = \nu_i$), and, on the other hand, is too small (near $\nu = \nu \pm \Delta\nu_{i0}$). The same should be said of the value of the step h_2. It is unjustifiably small for narrow lines and lines far from one another, and too great for lines near each other. Consequently, the step by wave numbers, selected either for constructing a graph of the function $A(\nu)$ or for integrating it over a given interval, should be variable and should depend both on the nature of the absorption on single lines and on their relative position. For this, the entire interval for integration $[\nu_1', \nu_2']$ is divided into single parts containing the center of only one line. the integral $W(\nu_1', \nu_2')$ then can be calculated according to the following formulas:

$$W(\nu_1', \nu_2') = \int_{\nu_1'}^{\nu_2'} A(\nu)\,d\nu = \sum_{i=0}^{l} (I_i' + I_i''),$$
$$I_i' = \int_{\nu_i}^{\nu_i + \frac{\nu_{i+1} - \nu_i}{2}} A(\nu)\,d\nu, \quad (31)$$
$$I_i'' = \int_{\nu_i + \frac{\nu_{i+1} - \nu_i}{2}}^{\nu_{i+1}} A(\nu)\,d\nu,$$

where $\nu_0 \equiv \nu_1'$; $\nu_{l+1} \equiv \nu_2'$; l is the number of the spectral lines investigated in the interval $[\nu_1', \nu_2']$; ν_i are the wave numbers corresponding to the centers of these lines.

The method of integrating the function $A(\nu)$ inside $\left[\nu_i, \nu_i + \frac{\nu_{i+1}-\nu_i}{2}\right]$ amounts to the following. The entire rnage for change in $A(\nu)$ is divided into N zones of B_n ($n = 1, 2, 3, \ldots, N$) so that

$$\begin{aligned}
&\text{if } A(\nu) \in B_1, \text{ then } \lambda_0 \leqslant \frac{A(\nu)}{A_{\max i}} < \lambda_1, \\
&\text{if } A(\nu) \in B_2, \text{ then } \lambda_1 \leqslant \frac{A(\nu)}{A_{\max i}} < \lambda_2, \\
&\ldots\ldots\ldots\ldots\ldots\ldots \\
&\text{if } A(\nu) \in B_n, \text{ then } \lambda_{n-1} \leqslant \frac{A(\nu)}{A_{\max i}} < \lambda_n, \\
&\ldots\ldots\ldots \qquad \ldots\ldots\ldots \\
&\text{if } A(\nu) \in B_N, \text{ then } \lambda_{N-1} \leqslant \frac{A(\nu)}{A_{\max i}} < \lambda_N,
\end{aligned} \tag{32}$$

/94

while $\lambda_0 \equiv 0$ and $\lambda_N \equiv 1$ always.

The values of $\lambda_0, \lambda_1, \lambda_2, \ldots, \lambda_N$ form an increasing sequence $\{\lambda_n\}$ ($n = 0, 1, 2, \ldots, N$). Each term λ_n of the sequence $\{\lambda_n\}$ is put in correspondence with a term q_n belonging to the sequence $\{q_n\}$ ($n = 1, 2, \ldots, N$).

The integral I_i' is found as the sum of

$$I_i' = \sum_{k=1}^{M} I_{ik}' + \left(-\int_{\nu_{iM+1}}^{\nu_i} A(\nu)\, d\nu\right),$$

where

$$\begin{aligned}
I_{ik}' &= \sum_{r=1}^{m_{ik}} I_{ikr}', \\
I_{ikr}' &= \int_{\nu_{ik}^* + \frac{\nu_{ik+1}^* - \nu_{ik}^*}{m_{ik}} \times (r-1)}^{\nu_{ik}^* + \frac{\nu_{ik+1}^* - \nu_{ik}^*}{m_{ik}} \times r} A(\nu)\, d\nu.
\end{aligned} \tag{33}$$

The significance of dividing the total interval for integration of $\left[\nu_i, \nu_i + \frac{\nu_{i+1} - \nu_i}{2}\right]$ into single parts is to reduce the calculation of the integrals I_i' ($i = 0, 1, 2, 3, \ldots, l$) by regions where

the integrand $A(\nu)$ changes abruptly (which greatly complications numerical integration) to a calculation of the integrals I'_{ikr} ($i = 0, 1, 2, \ldots, l$; $k = 1, 2, 3, \ldots, M$; $r = 1, 2, \ldots, m_{ik}$) by single parts in which the integrand changes to a much lesser degree. The latter circumstance aids in approximating the function $A(\nu)$ satisfactorily in the intervals obtained by second-order curves, which greatly simplifies numerical integration.

The parameters m_{ik} and the values ν^*_{ik} and ν^*_{ik+1}, which define the limits to integration of the summable integrals I'_{ikr}, are found with the aid of the division parameters λ_n and q_n introduced earlier in the following way.

1. We calculate

$$\nu^*_{i1} = \nu_i + \frac{\nu_{i+1} - \nu_i}{2},$$

$$A(\nu^*_{i1}),\ A(\nu_i) \text{ and } A(\nu_{i+1}).$$

2. We find $A_{\max i}$ as the greater of the two values $A(\nu_i)$ and $A(\nu_{i+1})$. /95

3. From the sequence $\{\lambda_n\}$ ($n = 0, 1, 2, \ldots, N$) we find the values λ_s and λ_{s+1} which satisfy the following condition:

$$\lambda_s \leqslant \frac{A(\nu^*_{i1})}{A_{\max i}} < \lambda_{s+1}. \tag{34}$$

The value q_{s+1} corresponding to λ_{s+1} is determined at the same time.

4. Using the division parameter q_{s+1} found, we calculate the following point ν^*_{i2} according to the formula

$$\nu^*_{i2} = \nu^*_{i1} + \frac{\nu_i - \nu^*_{i1}}{q_{s+1}}.$$

5. We find the value $A(\nu^*_{i2})$ corresponding to ν^*_{i2}.

6. We determine $\lambda_{s'}$ and $\lambda_{s'+1}$ which satisfy the condition

$$\lambda_{s'} \leqslant \frac{A(\nu^*_{i2})}{A_{\max i}} < \lambda_{s'+1}.$$

The value $q_{s'+1}$ corresponding to $\lambda_{s'+1}$ is found at the same time.

7. We calculate the parameter m_{i1} equal to the number of zones B_n located between the levels of $\lambda_{s'}$ and λ_{s+1} by the formula

$$m_{i1} = |s - s'| + 1.$$

The following point ν^*_{i3} is then selected by analogy with Operation 4, and the entire cycle is repeated.

The problem of an optimal selection of the upper limit to the sum M in (33) is very important, since the value M is essentially a singular parameter limiting the cycle by k.

The value M could be defined on the basis of the condition

$$\frac{A(\nu_{iM+1})}{A(\nu_i)} \geqslant \eta, \tag{35}$$

where η is a value which is close to unity but always less than it.

However, this is found to be insufficient, since, in an unsuccessful selection of the division parameters λ_n and q_n, there could be a case when the condition in (35) is fulfilled even in the first step by k and, consequently, the range for an abrupt change in the function $A(\nu)$ in the neighborhood of the center of the i-th line ν_i is not subjected to division. Therefore, together with (35), we impose the condition $M > k_0$, where k_0 is a certain preset number. In our calculations, we selected $k_0 = 3$ and $\eta = 0.9$.

In view of the fact that the integration interval $\left[\nu_i, \nu_i + \frac{\nu_{i+1} - \nu_i}{2}\right]$ is divided into parts in which the function $A(\nu)$ changes rather smoothly with this method, a special program of integrating smooth functions constructed by V.Ya. Galin and Ts. Kh. Mil'ner was used for calculating the integrals I'_{ikr}. Therefore, the number of square units p necessary for calculating I'_{ikr} with given relative accuracy δI was limited before by the condition /96

$$3 \leqslant p \leqslant p_{max}.$$

The assignment of p_{max} aids in avoiding lengthy computations when the initial assumption of smoothness of $A(\nu)$ inside the selected interval $\left[\nu^*_{ik} + \frac{\nu^*_{ik+1} - \nu^*_{ik}}{m_{ik}}(r - 1), \nu^*_{ik} + \frac{\nu^*_{ik+1} - \nu^*_{ik}}{m_{ik}} r\right]$ is not fulfilled, i.e., with an unsuccessful selection of the division parameters q_n and λ_n. A description of the program for calculating the integral $I(a,b) = \int_a^b f(x)dx$ from the smooth function $f(x)$ with

given relative accuracy δI is given below.

I(a,b) is calculated according to the formula

$$\int_a^b f(x)\,dx \cong \frac{h}{3}\left\{f(a) + 4\sum_{k=1}^{N/2}[f(a+(2k-1)h)] + \right.$$
$$\left. + 2\sum_{k=1}^{(N/2)-1}[f(a+2kh)] + f(b)\right\},$$

where $N = \frac{b-a}{h}$; h is the integration step. The value of h is determined by the following formulas:

$$\left|\frac{I(h_{p+1}) - I(h_p)}{I(h_{p+1})}\right| < \delta I,$$
$$h_{p+1} = \frac{h_p}{2}, \quad h_0 = b - a,$$

for p = 0, 1, 2, 3,..., Pmax.

The following value is taken as zero approximation of the value I(a,b):

$$I(h_0) = \frac{f(a) + f(b)}{2} \cdot h_0.$$

In integration with the step h_{p+1}, all the preceding square units on the axis of integration become even (the value $x = a$ is taken as the zero unit), while all the new units become odd, and there are no other odd units except for those in [a,b]. Therefore, in order to calculate the value $I(h_{p+1})$, it is sufficient to have the sum

$$F_p = f(a) + 2\sum_{i=1}^{p}\sum_{k=1}^{N_i/2}[f(a+2kh_i)] + f(b),$$

where $N_i = \frac{b-a}{n_i}$, and to calculate the sum /97

$$\Phi_{p+1} = \sum_{k=1}^{N_{p+1}/2} f(a+(2k-1)h_{p+1})$$

Then

$$I(h_{p+1}) = \frac{(h_{p+1})}{3}[F_p + 4\Phi_{p+1}],$$

while, in order to calculate the following approximation $I(h_{p+2})$, we must have the value

$$F_{p+1} = F_p + 2\Phi_{p+1}.$$

The effectiveness of the proposed program was tested in a calculation of the integrals $\int_0^5 e^{-x^2}\,dx$ and $\int_1^5 x^4 dx$. In order to reach $\delta I = 10^{-5}$ by this program, it was sufficient to calculate the values of the integrals onle in 32 square units (in both cases), while a calculation of these integrals with the same initial step and the same relative accuracy by the generally-accepted method (see the standard program of integral computation by the Simpson method with automatic calling sequence developed at Leningrad State University), there must be calculations of the integrands in 320 and 300 units, correspondingly.

For the calculations, we selected the following division parameters:

$$\lambda_0 = 0,\ \lambda_1 = 0{,}01,\ \lambda_2 = 0{,}1,$$
$$\lambda_3 = 0{,}3,\ \lambda_4 = 0{,}5,\ \lambda_5 = 0{,}7,\ \lambda_6 = 1{,}0,$$
$$q_1 = q_2 = q_3 = q_4 = q_5 = q_6 = 2.$$

With such parameters, the average number of values of the arguments in which the integrands $A(\nu)$ had to be found in order to compute the integrals I_i' and I_i'' with relative accuracy of $\varepsilon = 0.01$ was equal to 50, while it could be no less than 200 in Gates' calculations [7].

3. Calculation of the Voigt Integral

In view of the fact that, in calculations of the integral absorption [see (10) and (10a)], we must find a very large amount of elements $Q_{ij}(\nu - \nu_i)$ [see (11)], it becomes clear that an application of the most economical method of calculating the integral $H(a, \omega)$ greatly reduces the amount of calculations.

A significant number of studies treating a tabulation of the function $H(a, \omega)$ (see [11-20]) has been published to the present. /98
However, we must keep in mind that not every method which is convenient in tabulation is satisfactory for use in specific calculations. Let us discuss the methods proposed for tabulation of $H(a, \omega)$ in [17,19] from this point of view. According to these methods, $H(a, \omega)\sqrt{\pi}$ is found as one of the solutions to the system of corresponding differential equations (see [17]) under specific initial conditions. A set of integral curves $H(a_k, \omega)\sqrt{\pi}$ was constructed in [17] as solutions to this system of differential equations. Here ω is a variable value. The values of ω are determined by the

step of integration of the system of equations to be solved by the Runge-Kutta method [21], i.e., by the accuracy in calculating the function $H(a_k, \omega)\sqrt{\pi}$, where $a_k = a_1, a_2, a_3, \ldots, a_n$ are constant values of the parameter a which distinguish the given curve for $H(a_k, \omega)$ from the other curves of the set.

An analogous system of differential equations is solved in [19], but a set of integral curves for $\sqrt{\pi}H(\omega_k, a)$ is constructed. This numerical method of determining the function $H(a, \omega)$ is very fruitful in tabulations, since each calculated point $H(a_s, \omega_k)\sqrt{\pi}$ of the integral curve $H(a, \omega_k)\sqrt{\pi}$, where $a_s = a_0 + s\Delta a$ $(s = 1, 2\ldots)$ is a value determined by the step of integration Δa, occurs in the limits of the table constructed for the integral $H(a, \omega)$. An analogous discussion is also applicable for the integral curve $H(\omega, a_k)\sqrt{\pi}$. However, this method is not optimal when $H(a, \omega)$ must be calculated for the specific values of the parameters $a = a_0$ and $\omega = \omega_0$, since all the intermediate points of the computed integral curves $H(a_k, \omega)\sqrt{\pi}$ or $H(\omega_k, a)\sqrt{\pi}$ in this case, except for the latter $\omega = \omega_0$ or $a = a_0$, are essentially not used for the calculation. It is most expedient, apparently, to calculate $H(a, \omega)$ with the aid of interpolation by the corresponding table. However, the basic hindrance here is the insufficient volume of the operative storage used for calculations on a digital computer. Based on these ideas, the following algorithm for finding the function $H(a, \omega)$ was developed in our study.

Algorithm for Calculating the Integral $H(a, \omega)$

For low values of the parameter a $(a < 0.1)$, the integral can be calculated by the expansion presented in the study by Plass and Fivel [24]:

$$H(a, \omega) = \sum_{n=0}^{\infty} A_n,$$

$$A_n = \frac{(-1)^n 2^{n+1}}{\sqrt{\pi}\, n!} a^n \int_0^{\infty} x^n \exp(-x^2) \cos 2\omega x \, dx. \qquad (36)$$ /99

In calculating $H(a, \omega)$ on the digital computer, a recurrence relationship is obtained for the expansion coefficients of (36), i.e.,

$$A_{n+2} = \frac{2a^2}{(n+1)(n+2)} [(2n - 2\omega^2 + 1) A_n - 2a^2 A_{n-2}],$$

$$A_0 = e^{-\omega^2},$$

$$A_1 = -\frac{2a}{\sqrt{\pi}} [1 - 2\omega F(\omega)]; \quad F(\omega) = \int_0^{\omega} e^{-\omega^2 + x^2} dx,$$

$$A_2 = a^2 [1 - 2\omega^2] e^{-\omega^2},$$

$$A_3 = -\frac{2a^3}{\sqrt{\pi}} \left[\frac{2}{3}(1 - \omega^2) - 2\omega \left(1 - \frac{2}{3}\omega^2\right) F(\omega) \right].$$

The coefficients A_0, A_1, A_2 and A_3 coincide with the coefficients $H_0(\omega)$, $H_1(\omega)$, $H_2(\omega)$ and $H_3(\omega)$ obtained in a study by Harris [11].

The integral $F(\omega)$ was calculated with the aid of the expansions used in the studies of W. Miller and A. Gordon [22] and D. Hummer [27, 28]. Because the function $F(\omega)$ is used in almost all the methods for tabulating the integral $H(a, \omega)$, the corresponding formulas are given below:

$$|\omega| < 1,$$
$$F(\omega) = \sum_{n=0}^{\infty} \frac{(-2\omega^2)^n}{(2n+1)!!}, \tag{37}$$
$$(2n+1)!! = 1 \cdot 3 \cdot 5 \times \ldots \times (2n+1).$$

$$1 \leqslant |\omega| < 5,$$
$$F(\omega) = \sum_{n=0}^{\infty} a_n T_{2n+1}(x), \tag{38}$$

where $x = \frac{\omega}{5}$; a_n are the coefficients given in [27]; $T_{2n+1}(x)$ are Chebyshev polynomials determined by the formula

$$T_{2n+1}(x) = \cos((2n+1) \arccos x).$$
$$|\omega| \geqslant 5,$$
$$F(\omega) = \frac{1}{2\omega}\left\{1 + \sum_{n=1}^{\infty}\left(\frac{1}{2\omega^2}\right)^n (2n+1)!!\right\}. \tag{39}$$

It is important to note that a calculation of $F(\omega)$ with the expansions of (37-39) takes much less time than the approximative integration of $F(\omega)$ by the method of Simpson or Gauss-Jacobi [21]. The same can be said of numerical integration of $H(a,\omega)$. The /100
latter is connected with the fact that, for low a ($a < 0.1$), the integrand

$$f(a, \omega) = \frac{a}{\pi} \frac{\exp[-x^2]}{a^2 + (\omega - x)^2}$$

has a sharply-pronounced peaked nature and not one but two maxima. In the range of values for $0.1 \leq a < 1.2$ and $0 \leq |\omega| < 4$, the method of Gronwoll [14] gave excellent results. In this case, the function $H(a,\omega)$ was calculated according to the following formulas:

$$H(a,\ \omega)=\sum_{n=0}^{\infty} I'_n(a)\,(n!)^{-1}\omega^{2n}\exp(-x^2),$$

$$I_n(a)=\frac{a}{2n-1}\left[\frac{2}{\sqrt{\pi}}-2aI_{n-1}(a)\right],$$

$$I_0(a)=\exp(a^2)\left[1-\frac{2}{\sqrt{\pi}}\int_0^a e^{-x^2}dx\right].$$

The quadratic Gauss-Hermite formula was used for values of $a \geq 1.2$, i.e.,

$$H(a,\ \omega)=\sum_{k=1}^{n} H_k f(c_k),\ n=20,$$

$$H_k=H_{n-k+1};\ c_k=-c_{n-k+1};\ f(c_k)=\frac{a}{\pi}\frac{1}{[a^2+(\omega-c_k)^2]}.$$

Here H_k are the coefficients computed by Kopal [25]; c_k are the roots of the Hermite polynomials presented in [25]. The range of values of ω, a where the Gauss-Hermite formula gives good accuracy was evaluated according to the data of D. Posener [13].

Calculation of $H(a,\omega)$ in the Branches of the Spectral Lines

Due to the fact that, in calculating the value of $A(\nu)$, the greatest number of elements of the matrix $||Q_{ij}(\nu-\nu_i)||$ occurs in the range of the branches of the spectral lines ($\omega_{ij}>>1$), a selection of good asymptotic representations of $H(a,\omega)$ decreases the machine time spent. The quadratic formula of Gauss-Hermite and the asymptotics of Krylov and Baryshev [15] were used in the range of $|\omega_{ij}|\geq 4$ in our study. In the range of $|\omega_{ij}|\geq 4$; $0.1 \leq a < 1.2$, the quadratic Hermite formula guaranteed relative accuracy no worse than $0.5\cdot 10^{-4}$. The asymptotics of Krylov and Baryshev were used successfully in the same range:

$$H(a,\ \omega)=\sum_{n=0}^{\infty} A_n,$$

$$A_n=\frac{2n-1}{2(a^2+\omega^2)^2}\left[(\omega^2-a^2)A_{n-1}-2B_{n-1}a\omega\right],$$

$$B_n=\frac{2n-1}{2(a^2+\omega^2)^2}\left[(\omega^2-a^2)B_{n-1}+2A_{n-1}\omega a\right],$$ /101

$$A_0=\frac{a}{\sqrt{\pi}}\frac{1}{(a^2+\omega^2)},\quad B_0=-\frac{\omega}{\sqrt{\pi}}\frac{1}{(a^2+\omega^2)}.$$

As a result, the calculations of the integral $H(a,\omega)$ were carried out in the following way:

$a<0,1;\ |\omega|\geq 0\}$ - expansion of (36)
$0,1\leq a<1,2;\ |\omega|<4\}$ - Gronwoll method
$a\geq 1,2,\ |\omega|\geq 0\}$ - quadratic Gauss-Hermite formula
$0,1\leq a<1,2;\ |\omega|\geq 4\}$
$|\omega|\geq 4;\ a\geq 0\}$ - asymptotics of Krylov and Baryshev

Results of Calculations on the Digital Computer BESM-2

To illustrate the method described, and to model the program constructed, we carried out a preliminary specific calculation of the absorption spectra $A(\nu)$. The following distributions of atmospheric parameters were selected for the calculations. The concentration of water vapor in the atmosphere was determined by the profile of Houghton with a constant mixing ratio of $w = 2.2\cdot 10^{-6}$(g/g) for altitudes higher than 13.716 km [10]. This distribution is depicted in Figure 1. The changes in temperature and air pressure with the altitude were selected according to the standard atmosphere ARDC-1959 [26]. The layer of the atmosphere from 100 to 11 km was divided into 21 layers in the following way (in kilometers):

$$
\begin{array}{lll}
74 \leqslant z \leqslant 100 & \Delta z_j = 26 \\
50 \leqslant z \leqslant 74 & \Delta z_j = 8 \\
34 \leqslant z \leqslant 50 & \Delta z_j = 4 \\
16 \leqslant z \leqslant 34 & \Delta z_j = 2 \\
13{,}716 \leqslant z \leqslant 16 & \Delta z_j = 2{,}284 \\
13 \leqslant z \leqslant 13{,}716 & \Delta z_j = 0{,}716 \\
11 \leqslant z \leqslant 13 & \Delta z_j = 1
\end{array}
$$

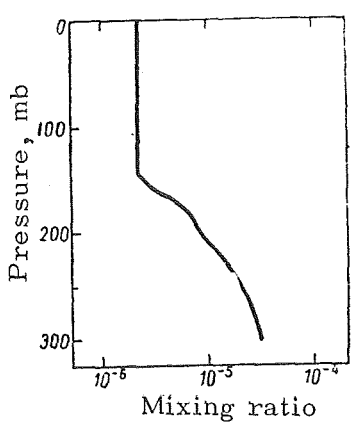

Fig. 1

Here z is the height over the ground of the point at which the absorption spectrum under investigation is being observed, km; Δz_j is the thickness of a single layer, km. The spectral parameters γ_i, $s_{i0}\gamma_{1i}(0)$ were taken from [7]. The range of (3795-3836)cm^{-1} was taken as the spectral region of $\Delta\nu = \nu_2'-\nu_1'$. In order to simplify the calculations, we selected only the spectral lines with intensities higher than 100 $g^{-1}cm$. It was assumed in the computations that the absorption line broadening was determined by the Voigt formula [see (5)]. The results of the calculations are shown in Figures 2-5. Moreover, Figures 6-9 show the results of a calculation of the absorption at different altitudes in the atmosphere for the isolated line ν_0 = 1677.95 cm^{-1}. The requisite parameters of this line were taken from [10]. The shape of the contour of the line under examination was determined by the Voigt formula [see (5) again].

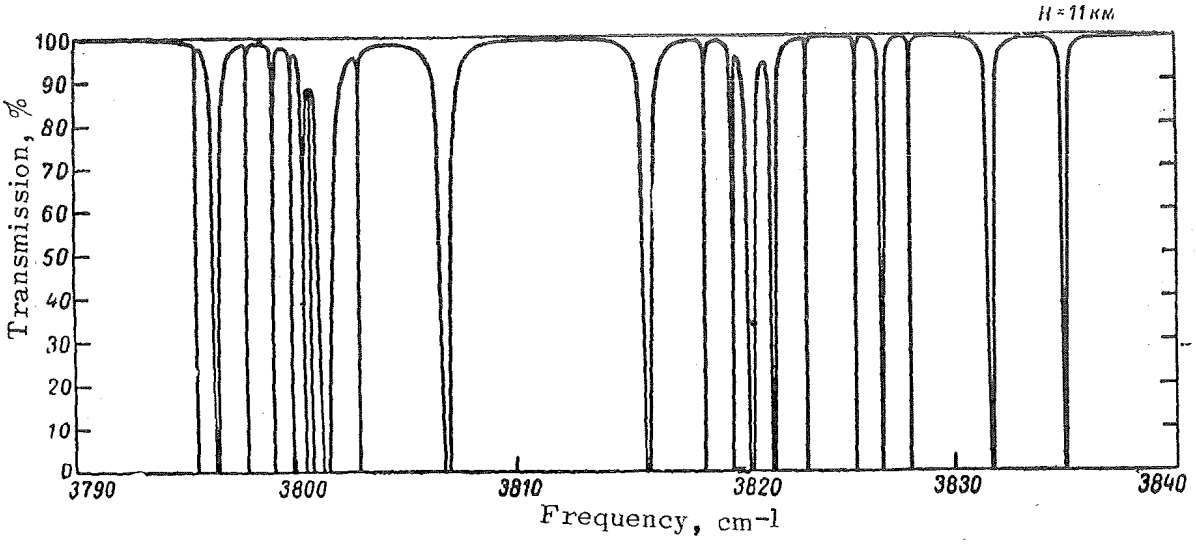

Fig. 2

/102

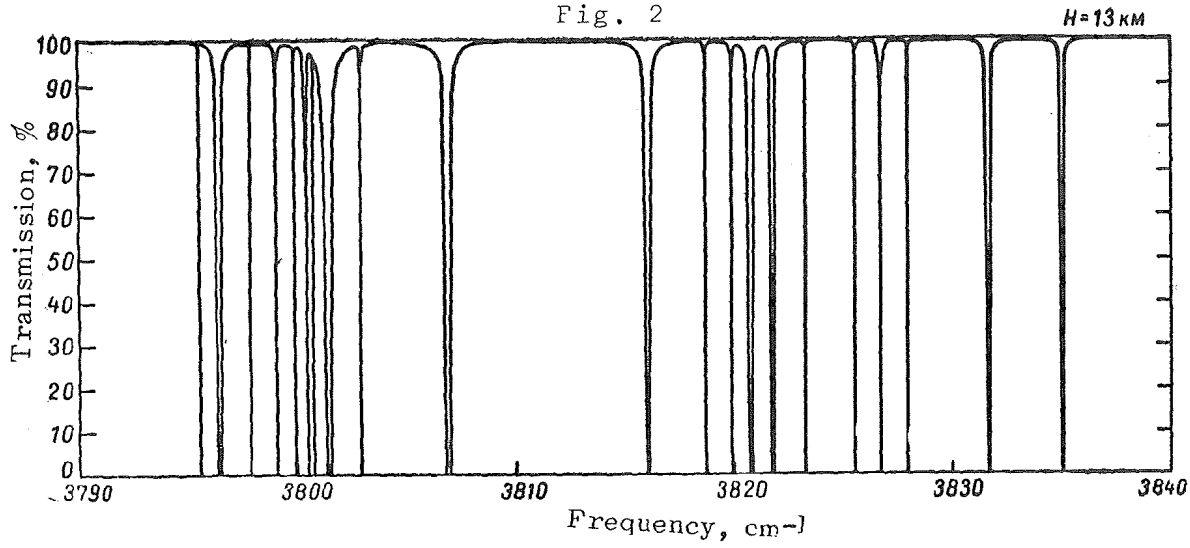

Fig. 3

/103

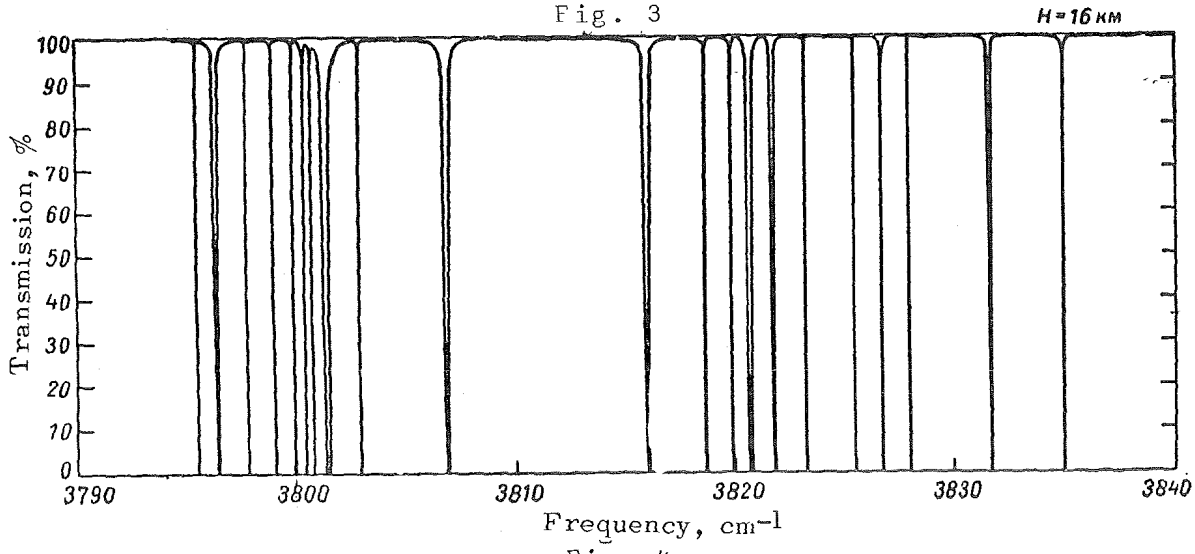

Fig. 4

/104

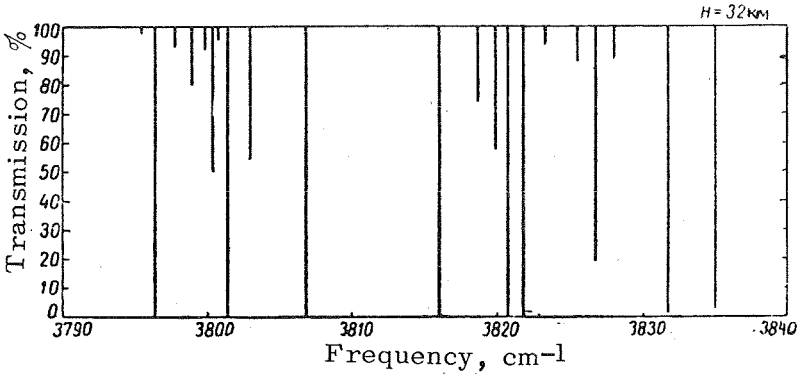

Fig. 5

/105

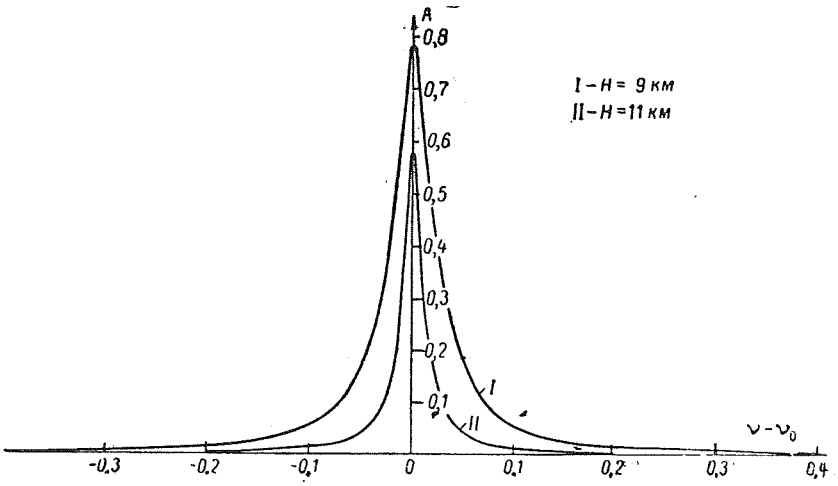

Fig. 6

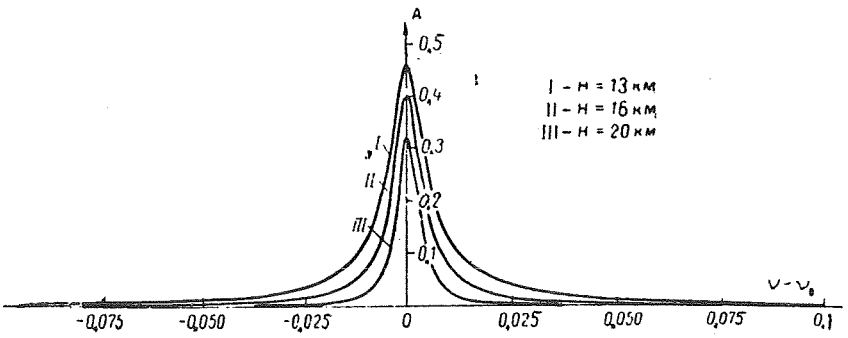

Fig. 7

/106

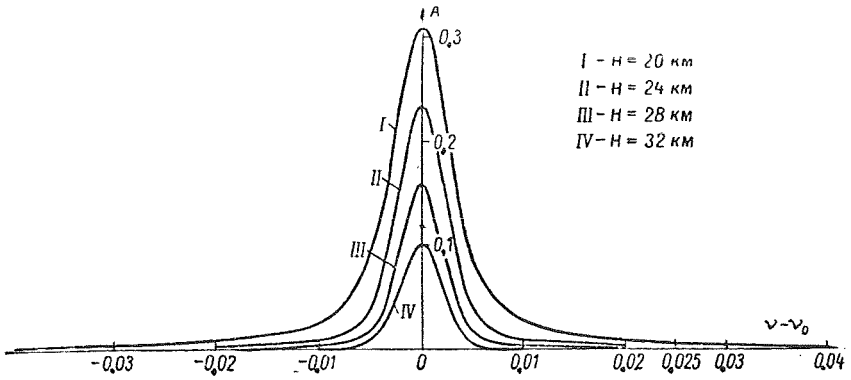

Fig. 8

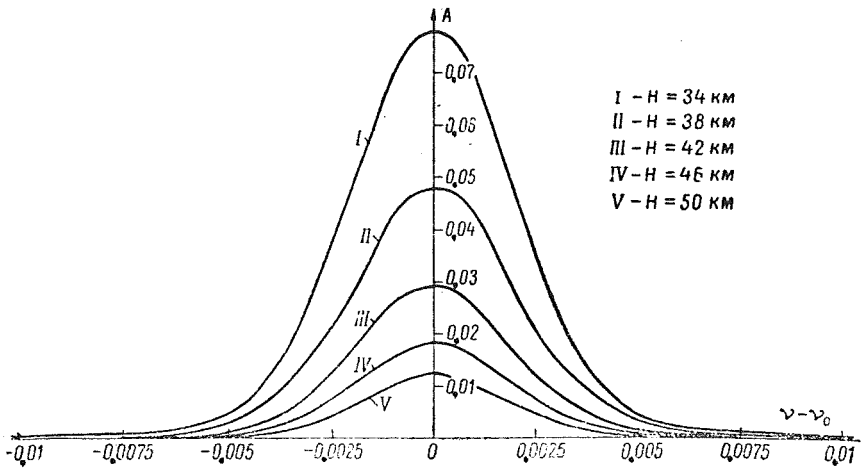

Fig. 9

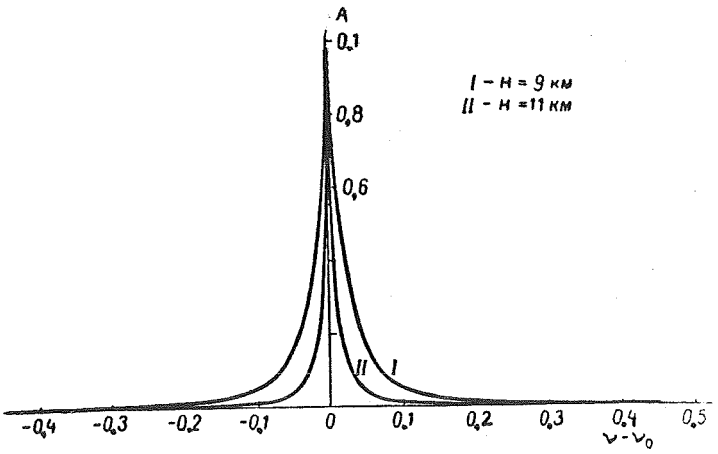

Fig. 10

/107

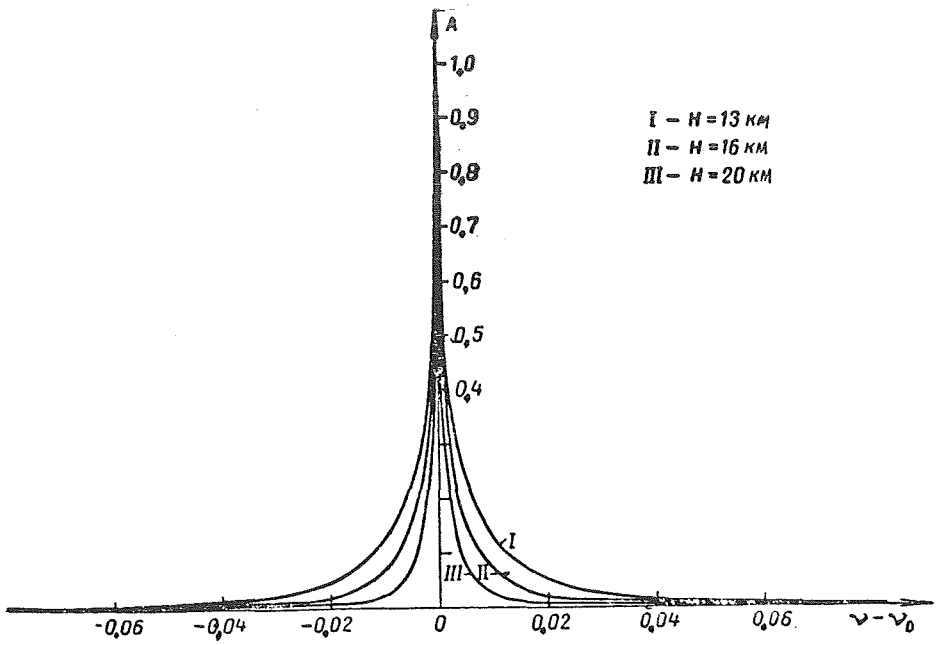

Fig. 11

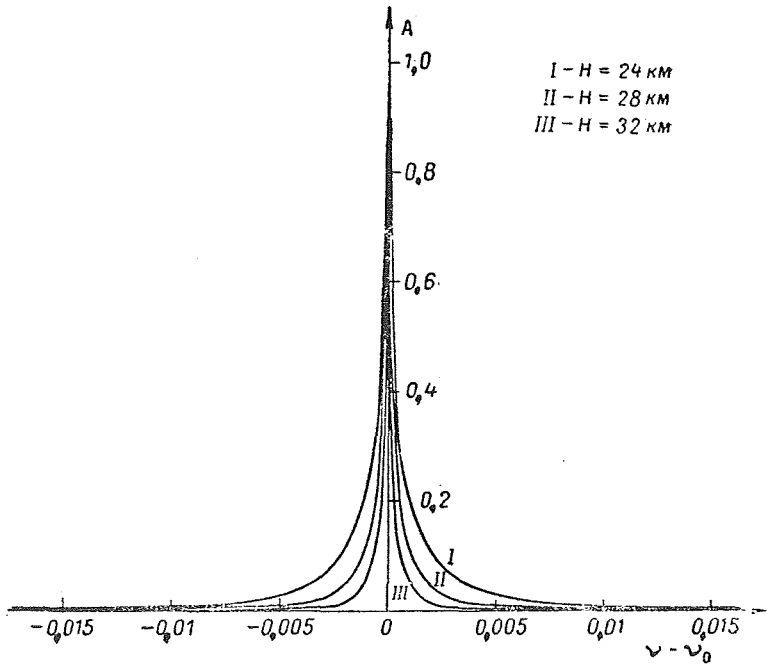

Fig. 12

/108

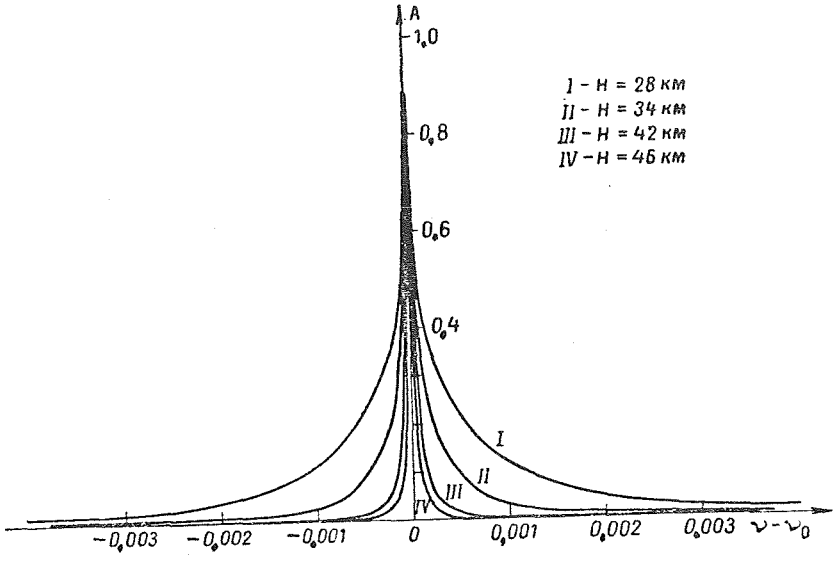

Fig. 13

In order to show the influence of the Doppler effect on the broadening of the spectral Lorentz line, Figures 10-13 give the data from calculations of the value A(ν) at different altitudes for the same line ν_0 = 1677.95 cm^{-1} in the case when the shape of its contour is determined by the following Lorentz formula: /109

$$K_i(\nu, z) = K_{0i}(z) H_L(a_i(z), \omega_i(z)),$$

$$H_L(a, \omega) = \frac{a}{\sqrt{\pi}(a^2+\omega^2)}; \quad K_{0i}(z) = \frac{S_i(z)}{\gamma_{Di}(z)}\sqrt{\frac{\ln 2}{\pi}}.$$

Conclusions

Obviously, the method we have described will be useful in solving a large number of atmospheric problems in which a precise value must be given for the absorption function. Moreover, this method should be used in order to solve the problem of the real distribution of atmospheric water vapor with the altitude, since the integral absorption can be found by this method in any spectral region for any requisite altitude and for any assumed water vapor distribution.

In conclusion, I would like to express my deep gratitude to B.S. Neporent and K.Ya. Kondrat'yev for directing this study, and also to a colleague at Leningrad State University, Ts. Mil'ner and a colleague at the Computation Center of the Siberian Department of the Academy of Sciences of the U.S.S.R., V. Ya. Galin, for constructing the computation program.

REFERENCES

1. Godson, W.L.: Spectral Models and Properties of Transmission Functions. Proc. Toronto Meteorol. Conf., 1953, 1954.
2. Goody, R.M.: Atmospheric Radiation. 1. Theoretical Basis. Oxford, Clarendon Press, 1964.
3. Plass, G.N.: Model for Spectral Band Absorption. J. Opt. Soc. Amer., Vol. 48, No. 10, 1958.
4. Kaplan, L.D.: A Quasi-statistical Approach to the Calculation of Atmospheric Transmission. Proc. Toronto Meteorol. Conf., 1953, 1954.
5. Elsasser, W.W.: Heat Transfer in the Atmosphere. Harvard Meteorol. Studies, No. 6 Milton (Mass), 1942.
6. Gal'tsev, A.P.: Methods of Calculating the Magnitude of Absorption Due to Vibration-Rotation Bands. In the Collection: Problemy fiziki atmosfery (Problems of Atmospheric Physics), No. 3. Leningrad State University Press, 1965.
7. Gates, D.M., R. F. Calfee, D. W. Hansen and W. S. Benedict: Line Parameters and Computed Spectra for Water Vapor Bands at 2.7 μ. National Bureau Stand., No. 71, 1964.
8. Mitchell, A. and M. Zemanskiy: Resonansnoye izlucheniye i vozbuzhdennyye atomy (Resonance Radiation and Excited Atoms). Association of Scientific and Technical Publishing Houses, 1937.
9. Benedict, W.S., and L. D. Kaplan: Calculation of Line Widths in H_2O-N_2 Collisions. J. Chem. Phys., Vol. 30, No. 2, 1959.
10. Houghton, J.T.: Absorption in the Stratosphere by some Water-Vapor Lines in the ν_2 Band. Quart. J. Roy. Meteorol. Soc., Vol. 89, No. 381, 1963.
11. Harris, D.L.: III. On the Line-Absorption Coefficient Due to Doppler Effect and Damping. Astrophys. J., Vol. 108, No. 1, 1948.
12. Hjerting, F.: Tables Facilitating the Calculation of Line Absorption Coefficients. Astrophys. J., Vol. 88, No. 4, 1938.
13. Posener, D.W.: The Shape of Spectral Lines Tables of the Voight /110 Profile. Austr. J. Phys., Vol. 12, No. 2, 1959.
14. Penner, S.S.: Kolichestvennaya molekulyarnaya spektroskopiya i izluchatel'naya sposobnost' gazov (Quantitative Molecular Spectroscopy and the Emissivity of Gases). Foreign Literature Publishing House, 1963.
15. Baryshev, V.A. and G.N. Krylov: On a Calculation of Certain Integrals in the Absorption Theory. In the Collection: Problemy fiziki atmosfery (Problems of Atmospheric Physics), No. 3, Leningrad State University Press, 1965.
16. Faddeyeva, V.N. and N.M. Terent'yev: Tablitsy integralov veroyatnosti ot kompleksnogo argumenta (Tables of Probability Integrals from a Complex Argument). Computation Center of the Academy of Sciences of the U.S.S.R. Press, 1961.
17. Fried, B.D. and S.D. Conte: The Plasma Dispersion Function. N.Y. Academic Press, 1961.
18. Finn, G.D. and D. Mugglestone: Tables of the Line Broadening Functions $H(a,\omega)$. Monthly Not. Roy. Astron. Soc., Vol. 129, no. 2, 1965.

19. Young, C.: Calculation of the Absorption Coefficient for Lines With Combined Doppler and Lorentz Broadening. J. Quant. Spectrosc. Radiat. Transfer, Vol. 5, No. 3, 1965.
20. Young, C.: Tables for Calculating the Voight Profile. Technical report, University Michigan, NASA Contract No. NASr-54(03), July 1965.
21. Kantorovich, L.V. and V.I. Krylov: Priblizhennyye metody vysshego analiza (Approximation Methods of Higher Analysis). "Fizmatgiz", 1962.
22. Miller, W.L. and A. R. Gordon. Numerical Evaluation of Infinite Series. J. Phys. Chem., Vol. 35, No. 10, 1931.
23. Dawson, M.G.: The Numerical Value of $\int_0^h e^{x^3} dx$. Math. Soc., Vol. 28, Pt. II, London, 1898.
24. Plass, G.N. and D. I. Fivel: Influence of Doppler Effect and Damping on Line-absorption Coefficient and Atmospheric Radiation Transfer. Astrophys. J., Vol. 117, No. 1, 1953.
25. Kopal, Z.: Numerical Analysis. London, Chapmen and Hall, 1959.
26. Handbook of Geophysics. N.Y., Macmillan Company, 1960.
27. Hummer, D.G.: Expansion of Dauson's Function in a Series of Chebyshev Polynomials. Math. Comp., Vol. 18, No. 86, 1964.
28. Anolik, M.V. and Ts. Kh. Mil'ner: Standartnaya programma vychisleniya integral Foygta (Standard Program for Computing the Voigt Integral) (unpublished).

INVESTIGATION OF THE 9.6 μm ABSORPTION BAND OF OZONE IN THE ARTIFICIAL ATMOSPHERE

A.P. Gal'tsev

ABSTRACT: After studying the 9.6 μm absorption band of ozone in the artificial atmosphere, the author found that the data of C. Walshaw must be made more accurate (his values for the ozone content were roughly 5% lower than those of the author), and he derived an equation to describe experimental results.

The problems which are connected with the transformation of in-/111 fra-red radiation in the atmosphere have recently acquired great significance. It has been particularly important to improve the methods of calculating the flux of infra-red radiation at different levels in the atmosphere. These calculations are necessary for determining the temperature balance of the Earth, the amount of energy expended by the Earth-atmosphere system by radiation into space, in order to solve various applied problems, etc. The present tendency toward numerical methods of weather prediction with the aid of electronic computers, using the equations for transfer of thermal radiation, also requires an improvement in the methods of calculating the radiant heat flux.

The development of satellite meteorology has brought about the need for developing methods of solving the inverse problems, which amount to a determination of the composition and structural characteristics of the atmosphere according to the data from measurements of the outgoing radiation.

A solution to all these problems is impossible without solving the problem of the absorption of infra-red radiation by different optically active gases of the atmosphere, particularly ozone O_3, which means a construction of theoretical methods for calculating the magnitude of absorption for real bands and corresponding laboratory studies.

Ozone has several vibration-rotation absorption bands in the infra-red which are presently ascribed to the following transitions: principal transitions, $\nu_1 = 9.0$, $\nu_2 = 14$, $\nu_3 = 9.6$ μm; overtone, $\nu_1 + \nu_3 = 4.7$ μm [1, 2]. The remaining bands of 2.7, 3.25, 3.57 and 5.75 μm have still not been defined unambiguously.

Only the most intensive 9.6 μm band is observed clearly under atmospheric conditions. The remaining bands are either very weak (9.0 μm) or occur in the drop of the curve for the energy distribution in the spectrum of thermal radiation of the Earth's surface

and the atmosphere, and are overlapped by the more intensive bands /112 of water vapor and carbon dioxide.

The role of the ν_3 band in different processes of the transformation of infrared radiation varies. The absorption and radiation of this band is usually neglected in calculations of the transfer of thermal radiation or the radiative heat exchange in the atmosphere. However, the absorption in the 9.6 μm band absolutely must be considered, for example, in calculating the decrease in intensity of outgoing radiation within the limits of the Earth's atmosphere [3], in constructing the theory for the thermal regime of the stratosphere, etc. It was shown in [4] that the change in the temperature gradient during one day in the lower stratosphere, which is due to absorption in this band, varies from +0.4 to -0.4°C, which is comparable to the magnitude of the gradient due to the absorption of radiation by carbon dioxide. A very interesting idea concerning the effect of ozone and, consequently, the absorption in the 9.6 μm band, on the weather in the troposphere is discussed in [5]. The requisite quantitative characteristics of the absorption of radiation due to this band can be obtained only according to the data of laboratory measurements, since there are no reliable quantum-mechanical calculations of the intensity and half-width of the rotational lines at present.

Laboratory studies have been carried out by J. Strong [6], Summerfield (the work of Summerfield entitled "The Effect of Pressure on the Ozone Absorption of Infrared Radiation" has not been published), C. Walshaw [7,8,9] and myself.

J. Strong carried out measurements of different quantities of ozone and different pressures, from 6 to 722 mm Hg. He described the results he obtained with the aid of the square-root law. Summerfield established a graphic dependence between the magnitude of absorption and the product of the pressure times the amount of ozone. The pressure was equal to 6, 13, 25.8 and 56 mm Hg. However, the incompleteness of the measurement method used by these authors (for example, Summerfield used light filters, and not a spectral device) and the limited range for the change in pressure and quantity of ozone brought about the need for conducting new measurements, which was done by C. Walshaw in 1954. He used an infrared spectrometer with spectral width of the slit of 6.5 cm^{-1}. The optical length of the path remained constant, at 35 cm. The ozone content was varied from $5.58 \cdot 10^{-3}$ to 1.5 cm, reduced to normal conditions, and the pressure was changed from 0.5 mm Hg to atmospheric.

In 1964-1965, we also carried out quantitative measurements of the absorption due to this band, but with the aid of a more perfected apparatus, which allowed us to test the results of C. Walshaw, as well as to expand the interval for the change in ozone content to a large extent.

1. Experimental Apparatus

In order to investigate the 9.6 μm absorption band under laboratorial conditions, we assembled a device consisting of the following basic elements: /113

(a) infrared spectrophotometer IKS-21;

(b) multipass gas cuvette KMP-1;

(c) ultraviolet spectrophotometer SFD-2;

(d) ozonizer.

The infrared spectrophotometer is a somewhat modernized standard instrument which records the ozone absorption band with resolution on the order of 4 cm^{-1} (geometric NaCl prism, slit width of 200 μm). It was mainly the electrical flow sheet of the device which underwent the change. The mechanical synchronous detector was replaced by an electrical one, and the amplifier was supplied separately: the heater-current was taken from a high-voltage direct-current regulator VS-26, and the anode voltage was taken from a general-purpose voltage supply UIP-1. These measures resulted in a significant improvement of the characteristics of the instrument: decrease in noises, increase in recurrence of the indices. The receiving-recording system had linear characteristics. We used LiF for the filter cutting off the long-wave part of the spectrum. Using this, we determined the magnitude of scattered light. It was found that it did not exceed 1-2% even for the maximum length of the path of the ray. The calibration of the IKS-21 was carried out with the aid of the pyridine and ammonia absorption spectra and tested systematically. In order to exclude the absorption due to the atmospheric water vapor and carbon dioxide, the space for the path of the ray was pressurized, and dry argon or oxygen was blown through the entire system. The absorbing mixture (ozone+oxygen) was produced in a multipass gas cuvette KMP-1. By changing the number of reflections, the optical length of the path could be varied from 1.25 to 10 m every 1.25 m. Since ozone is extremely active chemically and, moreover, it explides in the presence of the smallest impurities of organic substances (such as rubber, Ramsay paste) [10], special precautionary measures were taken. The surface of the cuvette was coated with a special black-colored ozone-resistant lac. Instead of rubber for the vacuum sealing, we used teflon, while the Ramsay paste was replaced by a special fluorinated paste which did not react with ozone. The mirrors in the cuvette were gold-plated. These measures resulted in the situation where the ozone content remained practically constant (maximum change of 5-8%) for two hours (time for carrying out the series of measurements). The vacuum attained was equal to 10^{-3} mm Hg, and no leaks were observed during the experiment. The ozone was obtained by the method of electrosynthesis in a quartz ozonizer, through which oxygen was filtered. Before going to the /114

ozonier, the oxygen was carefully purified of CO_2 and dried, since the presence of water vapor molecules decreases the effective yield of ozone [11]. The mixture of ozone with oxygen was sent to a special catcher cooled by liquid nitrogen. The oxygen was then stripped from the mixture by fractional distillation. However, we always worked with a mixture of oxygen and ozone in order to avoid explosion of pure oxone. After distillation, the mixture was evaporated into a special preliminary cylinder connected to the KMP-1, which was detached from the cuvette after the ozone and oxygen were let into it. The pressure of the gas mixture was measured by a glass spiral manometer by the zero method. Its sensitivity was constant over the entire pressure interval, and equal to 5 mb/mm·m. Since the accuracy in reading on the mirror scale was 0.5 mm, the maximum absolute error with which the pressure was determined was equal to 2.5 mb. Consequently, at pressures higher than 100 mb, the relative error was less than 2%. Pressures less than 100 mb were measured by a manometer of the test bureau, MBP-1. In order to prevent the ozone from having any contact with mercury, the mercury surface was covered with a thin film of concentrated sulfuric acid.

2. Determination of the Ozone Content and Amount of Absorption

At present, there are several methods of determining the ozone content in a gas mixture: chemical, by changing the pressure as the ozone decomposes, optical, etc. [12,13]. We could never use the chemical method in our study, despite its rather high accuracy. In determining the amount of ozone according to the change in pressure of the gas mixture, it is necessary to keep the ozone content from decreasing because of oxidizing reactions, and to have its initial partial pressure rather high. (Obviously, a manometer of high sensitivity was also necessary.) Since these conditions were not fulfilled in our study, the quantity of ozone was determined by the optical method, according to the amount of absorption in the ultraviolet. The ozone absorption coefficients in the ultraviolet have now been defined quite accurately, and, as is well known, do not depend on the pressure [10,12]. The magnitude of the absorption in the ultraviolet spectral region was measured with the aid of a diffraction spectrophotometer SFD-2 with linear dispersion of 32 Å/mm operating by the zero method. The error in determining the optical density was 1%. An ultraviolet light beam was transmitted directly through the cuvette. The optical scheme of the device is shown on Figure 1 (where the numbers designate: 1 - output slit; 2,4 - plane mirrors; 3 - quartz lens; 5,6 input and output windows on the cuvette).

In order to increase the accuracy and reliability of measurements of the quantity of ozone, the optical density was determined /115 by two methods.

1. The receiver was turned from Position I to Position II, mirror 2 was extracted from the beam, and the dark current and

sensitivity of the SFD-2 were compensated for that wavelength at which some ozone band was centered. The receiver was then put back in Position I, the mirror was injected into the beam, and the optical density D_0 of the pumped cuvette KMP-1 was measured. If there was ozone in the cuvette, then the optical density was measured in a similar way, and the optical density due to ozone absorption was found as the difference

$$D_{O_3} = D - D_0. \qquad (1)$$

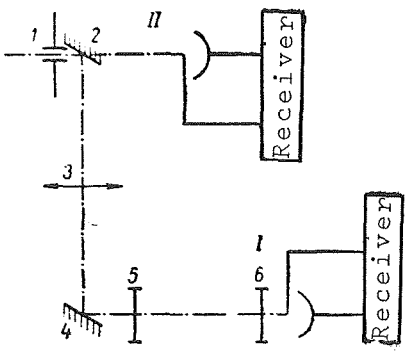

Fig. 1.

2. The receiver was put in Position I, and mirror 2 remained in the beam of light. The compensation for the dark current and sensitivity of the SFD-2 was achieved relative to λ = 360 mμ, where there is no absorption due to ozone and oxygen. When the cuvette was pumped, the optical density D_0' was determined for those wavelengths at which the ozone absorption bands were centered. The optical density D' was then determined in the presence of ozone, and the optical density due to ozone absorption was found as the difference

$$D'_{O_3} = D' - D'_0. \qquad (2)$$

The amount of ozone (in centimeters) was calculated under normal conditions according to the following formula:

$$w = \frac{D_{O_3}}{k_\lambda l} \cdot L_n, \qquad (3)$$

where k_λ is the ozone absorption coefficient in the ultraviolet for different wavelengths, cm^{-1}; L_n is the length of the path for the ultraviolet beam, i.e., the distance between the quartz windows 5-6, which was equal to 15.6±0.1 cm. It can be seen from (3) that the accuracy in measuring the amount of ozone is determined by the accuracy in measuring the optical density. The ozone content was measured during each recording of the 9.6 μm absorption band spectrum by the two methods described above. In this case, it was found that, for high values of the ozone content, the relative error is equal to 1-2%, and with a decrease in the ozone content, the error increases and reaches 4-5%. The results obtained by the /116 two methods coincide within the limits of the error in the measurements. This means that the amount of scattered light in the instrument was small and did not affect the measurements of the ozone content. The ozone absorption coefficients in the ultraviolet were taken from [7,12] and put into Table 1. The 9.6 μm ozone band was recorded on an EPP-09 for all reflections in the cuvette under

constant total pressure and practically constant partial ozone pressure. In this regard, the recording started with the maximum number of reflections (optical path of 10 m), and the series ended with a recording again for the maximum path length, for a control. The absorption was determined by planimetry. The frequency interval occupied by the band was selected from 960 to 1110 cm^{-1} (9.01-10.42 μm). We should mention that the selection of the short-wave boundary was ambiguous, since the neighboring 9.0 μm band was superposed on the 9.6 μm band. The contribution of the absorption due to the 9.0 μm band to the total absorption was taken into account by the graphic method in the analysis. (It was considered that the 9.6 and 9.0 μm bands are symmetrical relative to their central ordinates.) The measurements showed that the absorption in the 9.0 μm band could be disregarded for $w \leq 0.4$ cm.

TABLE 1

λ, mμ	k_λ, cm^{-1}	
	from [7]	from [12]
253.6	115.7	133.9
289.4	16.0	17.2
302.1	3.29	3.34

3. Results of the Measurements

The amount of absorption was measured in a broad range for the change in ozone content, beginning with 0.017 cm. The total pressure was taken as 10, 20, 40, 50, 100, 200, 300 and more than 400 mb. The maximum ozone content for pressures of 100 and 300 mb was roughly equal to 1.2 cm. For the other pressures, it was greater; in particular, it reached a value of 4.744 cm at p = 20 mb. The results obtained are presented in Figures 2 and 3 in the form of the dependence of the absorption A (for the entire band of 990-1110 cm^{-1}) on the ozone content under different pressures.

Figure 2 shows the dependence of the amount of absorption on the ozone content in that case when the absorption coefficients in the ultraviolet in [7] were used for calculating w (Column 1 in Table 1). The results of C. Walshaw are also shown on the figure for the sake of a comparison (in the form of the small triangles). The discrepancy between them does not exceed the deviation of the /117 experimental points.

Careful measurements of the ozone absorption coefficients in the ultraviolet region of the spectrum are described in [12]. The values obtained do not differ from those used by C. Walshaw (see Table 1, Column 2). Therefore, the ozone content was re-calculated

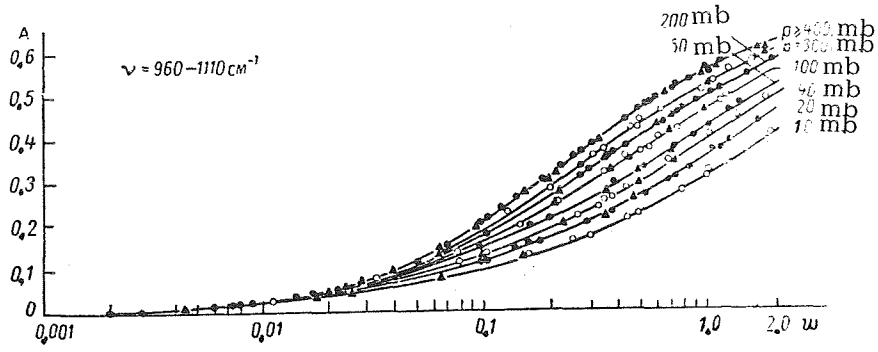

Fig. 2.

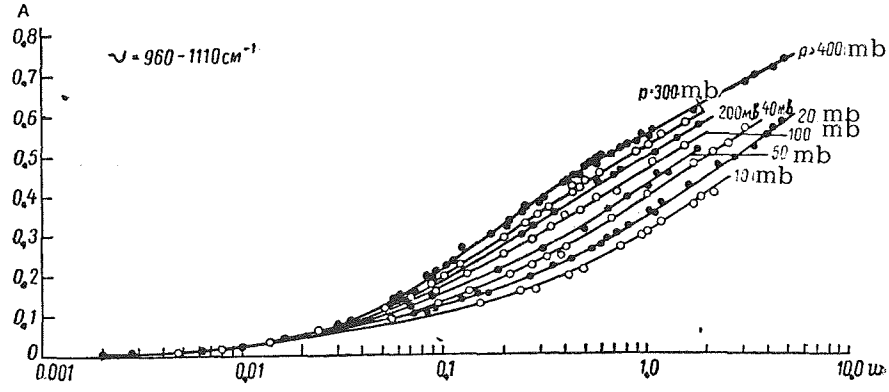

Fig. 3

using these new absorption coefficients. The results obtained are given in Figure 3 (in the form of the dependence of A on w) and in Table 2. A comparison between these data and those of C. Walshaw showed that the deviation between them reaches 5-7%, particularly in the intermediate range for the change in ozone content. In this case, the results of C. Walshaw were decreased. Moreover, the interval for the change in ozone content was much greater in our study than in Walshaw's, in contrast to which we carried out measurements for a constant total pressure. It was impossible to compare our results with the data of J. Strong, since /121 he determined the absorption in another frequency interval (from 1010 to 1063 cm^{-1}) containing only part of the band.

Summerfield's results (interval of 990-1087 cm^{-1}) were decreased in comparison to our data, which were determined for the interval of 990-1080 cm^{-1}. The magnitude of absorption is represented in Figure 4 on a semi-logarithmic scale as a function of the pressure for different values of the ozone content. It can be seen from the figure that, as would be anticipated, the absorption depends greatly on the pressure at first but, starting with pressures on

TABLE 2

w, cm	A			
	$\nu = 960-1110$	$\nu = 990-1080$	$\nu = 960-990$	$\nu = 1080-1110$
		$p = 10$ mb		
0,157	0,127	0,196	0,038	0,012
0,235	0,161	0,245	0,045	0,021
0,291	0,164	0,265	0,056	0,018
0,424	0,203	0,306	0,049	0,012
0,475	0,215	0,330	0,053	0,023
0,748	0,269	0,401	0,084	0,031
0,966	0,298	0,444	0,096	0,012
1,011	0,311	0,456	0,106	0,043
1,248	0,327	0,474	0,133	0,024
1,273	0,339	0,494	0,125	0,034
1,815	0,372	0,549	0,128	0,069
1,878	0,389	0,567	0,134	0,059
1,947	0,391	0,564	0,166	0,067
2,100	0,402	0,588	0,143	0,098
2,240	0,404	0,587	0,140	0,067
		$p = 20$ mb		
0,018	0,048	0,075	0,008	0,01
0,055	0,097	0,149	0,020	0,011
0,073	0,111	0,168	0,013	0,013
0,086	0,111	0,175	0,021	0,003
0,094	0,108	0,170	0,011	0,017
0,137	0,142	0,225	0,022	0,008
0,161	0,155	—	—	—
0,175	0,158	0,244	0,037	0,015
0,270	0,199			
0,360	0,218	0,338	0,048	0,014
0,438	0,244	0,371	0,045	0,013
0,546	0,261	—	—	—
0,597	0,274	0,415	0,082	0,010
0,654	0,294	0,445	0,081	0,055
0,700	0,301	0,459	0,092	0,015
0,708	0,304	0,457	0,078	0,024
0,819	0,304	—	—	—
0,959	0,329	0,499	0,039	0,119
1,093	0,353	0,534	0,110	0,042
1,154	0,364	0,548	0,100	0,071
1,28	0,376	—	—	—
1,820	0,427	0,629	0,182	0,041
2,533	0,472	0,683	0,202	0,086
2,871	0,490	0,713	0,244	0,047
3,502	0,516	0,740	0,246	0,107
4,053	0,550	0,777	0,285	0,116
4,334	0,560	0,787	0,260	0,144
5,258	0,579	0,806	0,280	0,128
		$p = 40$ mb		
0,216	0,197	0,308	0,032	0,025
0,271	0,219	0,344	0,083	0,020

w, cm	A			
	$\nu = 960-1110$	$\nu = 990-1080$	$\nu = 960-990$	$\nu = 1080-1110$
		$p = 40$ mb		
0,319	0,235	0,373	0,042	0,026
0,334	0,249	0,394	0,055	0,022
0,373	0,255	0,402	0,045	0,029
0,425	0,273	0,425	0,056	0,030
0,679	0,336	0,521	0,092	0,023
1,024	0,396	0,604	0,131	0,028
1,800	0,476	0,690	0,199	0,067
2,187	0,502	0,736	0,210	0,106
2,584	0,519	0,755	0,208	0,107
3,009	0,559	0,794	0,278	0,146
		$p = 50$ mb		
0,023	0,052	—	—	—
0,071	0,118	0,186	0,022	0,004
0,093	0,136	0,217	0,016	0,003
0,137	0,173	0,271	0,033	0,014
0,186	0,203	0,318	0,041	0,018
0,308	0,260	0,408	0,047	0,021
0,389	0,294	0,448	0,070	0,029
0,498	0,315	0,485	0,067	0,027
0,675	0,362	0,544	0,086	0,038
0,857	0,396	0,584	0,126	0,056
1,045	0,416	0,635	0,109	0,075
1,223	0,450	0,671	0,160	0,080
1,427	0,467	0,705	0,146	0,040
		$p = 100$ mb		
0,068	0,129	0,206	0,016	0,005
0,142	0,204	0,323	0,029	0,017
0,205	0,248	0,391	0,039	0,0
0,276	0,284	0,452	0,039	0,010
0,278	0,286	0,453	0,058	0,017
0,342	0,318	0,497	0,051	0,023
0,414	0,349	0,530	0,079	0,041
0,476	0,358	0,546	0,070	0,033
0,581	0,393	0,600	0,102	0,023
0,731	0,413	0,641	0,081	0,043
1,129	0,481	0,725	0,160	0,064
1,196	0,485	—	—	—
		$p = 200$ mb		
0,068	0,131	0,215	0,009	0,003
0,247	0,303	0,478	0,049	0,018
0,278	0,318	0,504	0,051	0,023
0,367	0,357	0,565	0,076	0,031
0,377	0,361	0,570	0,075	0,027
0,416	0,372	0,588	0,072	0,029
0,568	0,428	0,665	0,092	0,046

/118

/119

TABLE 2 (Continued)

w, cm	A			
	$\nu = 960-1110$	$\nu = 990-1080$	$\nu = 960-990$	$\nu = 1080-1110$
		$p = 200$ mb		
0.709	0.453	0.706	0.113	0.044
0.786	0.458	0.707	0.131	0.027
0.866	0.472	0.735	0.132	0.032
1.024	0.495	0.755	0.165	0.034
1.172	0.500	0.769	0.166	0.053
1.144	0.502	0.766	0.159	0.042
1.507	0.539	0.806	0.197	0.072
1.859	0.574	0.839	0.255	0.079
		$p = 300$ mb		
0.017	0.048	0.072	0.016	0.006
0.032	0.075	0.119	0.009	0.002
0.049	0.106	—	—	—
0.062	0.139	0.218	0.022	0.010
0.084	0.160	0.258	0.020	0.007
0.104	0.201	0.313	0.020	0.006
0.129	0.235	—	—	—
0.130	0.229	0.356	0.030	0.014
0.145	0.259	—	—	—
0.195	0.278	0.439	0.045	0.022
0.293	0.353	0.560	0.060	0.030
0.442	0.406	0.635	0.062	0.051
0.479	0.412	0.640	0.104	0.020
0.503	0.433	0.658	0.111	0.051
0.593	0.448	—	—	—
0.604	0.451	0.690	0.129	0.049
0.906	0.497	0.763	0.154	0.05
1.066	0.520	0.789	0.169	0.034
1.263	0.548	0.823	0.187	0.049
		$p \geqslant 400$ mb		
0.028	0.070	0.012	0	0.012
0.036	0.085	0.137	0.013	0.005
0.058	0.147	—	—	—
0.093	0.197	—	—	—
0.112	0.247	—	—	—
0.121	0.238	—	—	—
0.183	0.293	0.467	0.046	0.008
0.184	0.298	0.471	0.039	0.019
0.215	0.325	—	—	—
0.220	0.334	—	—	—
0.248	0.359	—	—	—
0.249	0.354	0.551	0.074	0.008
0.257	0.366	—	—	—
0.264	0.360	0.567	0.054	0.028
0.282	0.382	—	—	—
0.298	0.382	0.599	0.061	0.027
0.312	0.386	—	—	—
0.326	0.405	0.626	0.077	0.043
0.419	0.440	0.681	0.105	0.056

/120

w, cm	A			
	$\nu = 960-1110$	$\nu = 990-1080$	$\nu = 960-990$	$\nu = 1080-1110$
0.450	0.452	—	—	—
0.454	0.451	0.700	0.095	0.036
0.472	0.450	—	—	—
0.488	0.461	0.711	0.111	0.053
0.503	0.470	0.717	0.118	0.022
0.540	0.477	0.738	0.101	0.048
0.559	0.483	0.741	0.129	0.056
0.573	0.476	0.735	0.121	0.042
0.577	0.491	0.754	0.117	0.040
0.693	0.501	—	—	—
0.704	0.512	—	—	—
0.818	0.524	0.801	0.125	0.040
0.888	0.537	0.805	0.175	0.061
0.937	0.543	—	—	—
0.961	0.547	0.822	0.172	0.062
1.084	0.551	—	—	—
1.156	0.563	0.837	0.237	0.083
1.763	0.605	0.886	0.289	0.109
2.350	0.644	0.906	0.340	0.160
3.104	0.668	0.918	0.383	0.194
3.609	0.697	0.934	0.420	0.234
4.210	0.716	0.950	0.442	0.256
4.810	0.732	0.946	0.522	0.256

/121

the order of 400 mb, this dependence does not hold. The change in partial ozone pressure does not affect the amount of absorption, since p_{O_3} does not exceed 1 mb in our study.

It can be seen from Figure 2 that the divergence of the points does not exceed 2%. However, it increases greatly with a decrease in the magnitude of the absorption. Thus, it can be seen from Figure 5, which shows the values of absorption for the branches of the band, that the discrepancy reaches 8-10%. This is due to the fact that, when the ozone content decreases, the error in measuring it increases, and particularly the error in measuring the amount of absorption.

/122

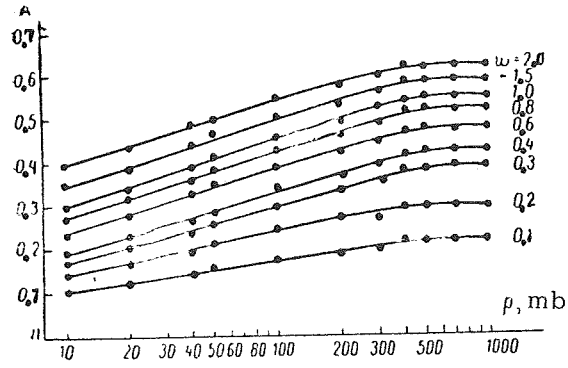

Fig. 4.

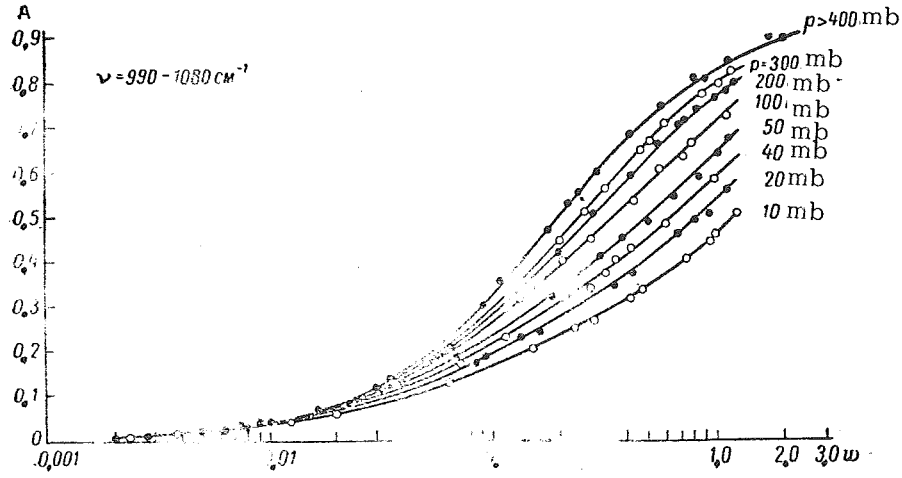

Fig. 5.

4. Representation of Experimental Data in the Form of an Analytical Dependence

The tabular and graphic representation of the value for the absorption as a function of the amount of absorbing gas and pres-

sure is extremely inconvenient in carrying out different types of calculations. Therefore, we attempted to represent the experimental results in the form of an analytical dependence. If the absorption is measured in a rather narrow spectral interval (order of the spectral width of the slit of a standard spectrophotometer), then this dependence is determined with the aid of a certain model of the band (absorption function for the Elsasser model, statistical model, etc.). However, in solving certain problems, there must be /123 an expression which takes account of the absorption for a rather broad frequency interval encompassing the entire band or a substantial part of it. In this case, we must find the empirical or semi-empirical dependence whose fitting parameters are selected in such a way that the computed and experimental results coincide best. Since an analytical expression has a complex form, as a rule, the use of the method of least squares in analyzing the experimental data is complicated, while the term "best coincidence" means that the deviation in experimental and computed data does not exceed the error in the measurements or a preset value.

Having analyzed his results, C. Walshaw established an empirical dependence of the amount of absorption due to the 9.6 μm ozone band on the ozone content and the pressure. According to Walshaw,

$$\int A_\nu d\nu = \Delta\nu \left[1 - 10^{-\mu f(\varphi)}\right]. \qquad (4)$$

Here the integration in the left-hand part is carried out over the entire 9.6 μm band; $\Delta\nu$ is some effective bandwidth (found as a fitting parameter) equal to 138 cm^{-1}; $\mu = w\eta$; $\phi = \frac{w\eta\alpha}{p}$; w is the ozone content, cm; a is an empirical constant; η is some function of w; p is the pressure, expressed in mm Hg. According to the data of Walshaw's measurements, a = 2.11, while the function η (w) is selected thus:

$$\eta(w) = \begin{cases} \frac{1 + 0{,}1025\,w}{1 + 1{,}6\,w}, & w \leqslant 0{,}1, \\ 0{,}984 \cdot 10^{-0{,}53\,w}, & 0{,}1 \leqslant w \leqslant 0{,}4, \\ 0{,}317\,w^{-0{,}74}, & w \geqslant 0{,}4. \end{cases}$$

The function $f(\phi)$ has the form of

$$f(\varphi) = 1{,}185\,(1 + 734\,\varphi)^{-\frac{1}{2}}\,\xi(\varphi).$$

The values of $\xi(\phi)$ are given below:

$\log\varphi$ — 4,0; —3,9; —3,8; —3,7; —3,6; —3,5; —3,4; —3,3; —3,2; —3,1;
$\xi(\varphi)$ 1; 0,998; 0,995; 0,993; 0,989; 0,984; 0,982; 0,980; 0,977; 0,977.
$\log\varphi$ —3,0; —2,9; —2,8; —2,7; —2,6; —2,5; —2,4; —2,3; —2,2; —2,1; —2,0;
$\xi(\varphi)$ 0,977; 0,979; 0,982; 0,989; 1,002; 1,016; 1,030; 1,045; 1,057; 1,069; 1,079.

The average error in calculations by (4) is 2.4%, while the maximum error is equal to 5%. Considering that Walshaw's experimental data were decreased, compared to ours, calculations by this formula actually yield a significantly great error. In order to /124 decrease it, we must determine the fitting parameters again, using our results. This was not done in the study (because (4) is too cumbersome for computations), but another method was used. The entire spectral region occupied by the ozone band was divided into three intervals: 990-1110 cm^{-1} (center of the band), 960-990 cm^{-1} and 1080-1110 cm^{-1} (branches of the band), and the absorption was measured for these intervals. The frequency intervals were selected in this way because the center of the band makes the principal contribution to the absorption, and the effect of the pressure is found mainly in this value for the absorption. It was found that the experimental results can be described with good accuracy by the formula

$$A = 1 - \exp\left[-\frac{2x}{\pi\sqrt{1+\frac{2x}{\beta}}}\arctan\frac{\rho}{\sqrt{1+\frac{2x}{\beta}}}\right], \qquad (5)$$

where A is the absorption determined in the given spectral interval; $x = \frac{S}{d}w$; β and ρ are fitting parameters. This formula was obtained in [14] as a theoretical one; however, its derivation is not correct, and (5) should be considered to be semi-empirical.

Figure 5 shows the results obtained experimentally and calculated according to (5) for the center of the band (990-1080 cm^{-1}). It can be seen from the figure that the discrepancy in the points is within the limits of the measurement error. In this case, the following values were obtained for the parameters in (5), in dependence on the pressure:

$$\beta = 7{,}8\cdot10^{-3}p + 0{,}096,$$
$$\rho = \frac{c}{p} \doteq \frac{2\cdot10^3}{p}, \qquad (6)$$

where p is the total pressure, mb.

The parameter S/d is determined by the relationship obtained from (5) for x << 1:

$$\frac{S}{d} \cdot \frac{2}{\pi} \arctan \rho = 4{,}07 \pm 0{,}008. \tag{7}$$

For high values of the parameter ρ, (5) converts into the well-known Goody formula, while S/d acquires the significance of the ratio between the average intensity and the average distance. It was found that, starting at pressures of p ≤ 100 mb, we can use the Goody formula instead of (5). The parameters ρ and β and, consequently, S/d, are determined from (6) and (7) for all pressures except those greater than 400 mb. In this case, the best coinci- /125 dence in the results is obtained at β = 20, ρ = 0.53 and S/d = 13.12. Assuming that p = 500 mb, we find from (6) and (7) that β = 4, δ = 4 and S/d = 4.82. The maximum error for such parameters reaches 5-6%.

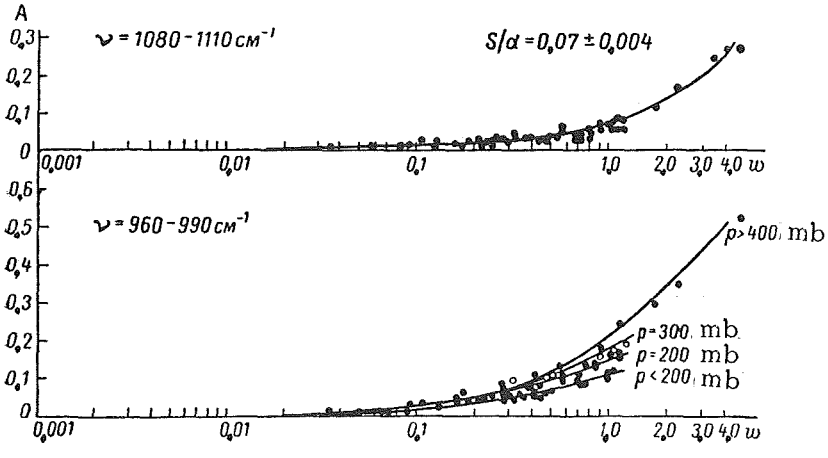

Fig. 6.

The experimental and theoretical results for the branches of the bandaare shown in Figure 6. The data for the spectral interval of 1080-1110 cm^{-1} for all the pressures are plotted on the upper curve. The calculations were carried out by the following formula:

$$A = 1 - \exp\left(-\frac{S}{d} w\right), \tag{8}$$

where S/d = 0.07±0.004.

The fact that all the data obtained for different pressures occur on one curve can be explained by the weak intensity of the spectral lines in the branch and their strong superposition on one another.

The data for the interval of 960-990 cm^{-1} are plotted on the lower part of Figure 6. In this case, we can still distinguish the absorption obtained for pressures of 400, 300 and 200 mb. However, starting with pressures of $p \leq 100$ mb, all the results also occur on one curve within the limits of the measurement error. The calculations were carried out according to (5) with the following values of the parameters:

/126

p, mb	$\frac{S}{d}$	ρ	β
400	0.28	4.3	2.6
300	0.26	10	1.0
200	0.25	15	0.54
100	0.24		0.08

It was found that β depends on the pressure in the following way:

$$\beta = 0{,}46 \cdot 10^{-2} p - 0{,}38.$$

A universal dependence of the following type was suggested in [15] for representing the experimental data:

$$\frac{\Psi_n(P)}{w} = \left\{\frac{2}{\sqrt{\pi}} \frac{\Phi^{-1}(A)}{w}\right\}^n \left\{-\frac{\log P}{w}\right\}^{1-n}, \qquad (9)$$

where Φ^{-1}, (x) is the inverse function of the error function; P = 1-A is the transmission function; n is a fitting parameter. This expression was used in order to describe the experimental results obtained by Summerfield in the spectral interval of 990-1087 cm^{-1}. It was found that, at n = -1.0, they fit rather well on the curve constructed according to (9).

Figure 7 gives the data we obtained for the center of the band (interval of 990-1080 cm^{-1}, which practically coincides with the interval Summerfield selected) and data computed by (9) for n also equal to -1.9. It can be seen from the figure that, in contrast to the data of W. Godson, the discrepancy at the points greatly exceeds the error in the measurements. Unfortunately, the deviation could not be decreased by selecting other values of n, although this possibility is probably not excluded, since the experimental data fit well on the curves for $\log \frac{P}{W}$ and $\frac{\Phi^{-1}(A)}{W}$ (Figures 8 and 9).

The problem of selecting the fitting parameters in the empirical formulas of Howard-Burch-Williams was not raised in this study.

However, it can be seen from Figures 2 and 3 that these formulas can be used in order to describe the absorption in the 9.6 μm band of ozone, and only with limited intervals for the change in ozone content. Thus, the studies we carried out showed that

(a) the data of C. Walshaw must be made more accurate (they were decreased, in comparison to ours, by roughly 5%);

(b) the experimental results can be described with a great deal of accuracy with the aid of (5).

In conclusion, I would like to express my appreciation to Professor K.Ya. Kondrat'yev, under the direction of whom this study was completed.

/127

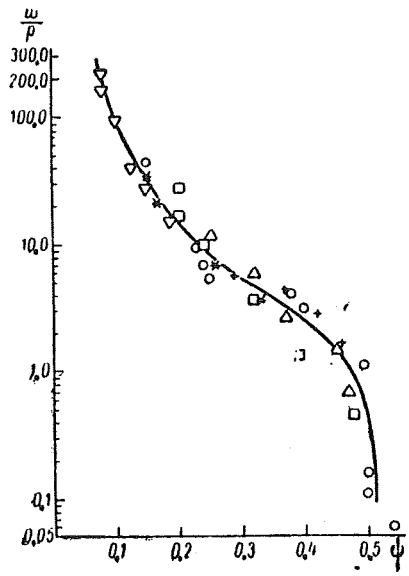

Fig. 7.

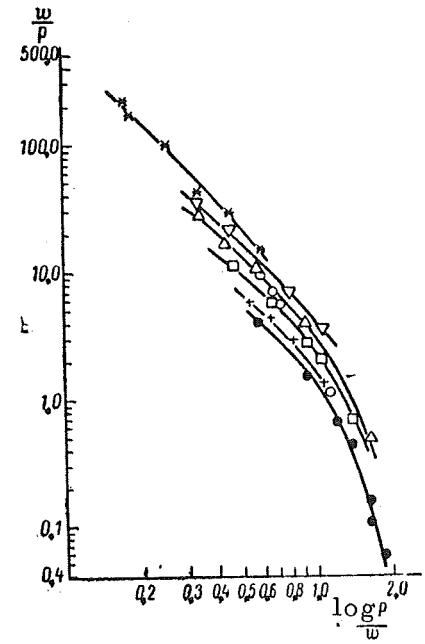

Fig. 8.

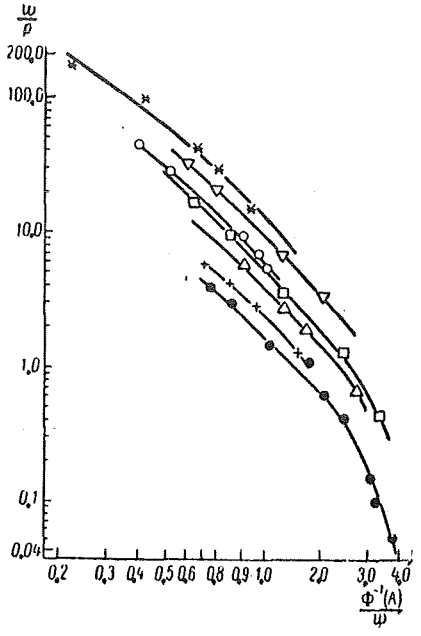

Fig. 9.

REFERENCES

1. Wilson, W.K., R. Badger: A Reinvestigation of the vibration spectrum of ozone. J. Chem. Phys., Vol. 16, 741, 1948.
2. Herzberg, H.: Kolebatel'nyye i vrashchatel'nyye spektry mnogoatomnykh molekul (Vibrational and Rotational Spectra of Multi-Atomic Molecules). Foreign Literature Publishing House, 1948.
3. Yakushevskaya, K.Ye.: Uglovoye i spektral'noye raspredeleniye teplovogo ukhodyashchego izlucheniya (Angular and Spectral Distribution of Outgoing Thermal Radiation). Author's Abstract of Candidate's Dissertation. Leningrad State University Press, 1964.
4. Hitschefld, W., and I. Houghton: Radiative transfer in the lower stratosphere due to the 9.6 micron band of ozone. Quart. J. Roy. Meteorol. Soc., Vol. 87, No. 374, 1961.
5. Raketnaya i sputnikovaya meteorologiya (Rocket and Satellite Meteorology). "Gidrometeoizdat", 1965.
6. Strong, J: A new method of measurement of the average altitude of the atmospheric ozone layer. J. Frankl. Instr., Vol. 232, No. 1, 1941.
7. Walshaw, C.D.: Integrated absorption by the 9.6 micron band of ozone. Quart. J. Roy. Meteorol. Soc., Vol. 83, No. 357, 1957.
8. Walshaw, C.D.: Line widths in the 9.6 micron band of ozone. Proc. Phys. Soc., Vol. 68, No. 426 A, 1955.
9. Walshaw, C.D.: An experimental investigation of the 9.6 micron band of ozone in the solar spectrum. Quart. J. Roy, Meteorol.

Soc., Vol. 82, No. 352, 1956.
10. Thorp, C.: Bibliography of ozone technology. Illinois, 1955.
11. Forbes, G., and L. Heidt: The influence of water upon the photolysis of ozone at 280, 254 and 210 micron. J. Amer. Chem. Soc., Vol. 56, No. 8, 1934.
12. Hearn, A.: The absorption of ozone in the ultra-violet and visible regions of the spectrum. Proc. Phys. Soc., Vol. 78, No. 503, 1961.
13. Ozone Chem. and Technology. Washington D.C., Amer. Chem. Soc., 1959.
14. Gal'tsev, A.P.: Issledovaniye polosy ozone 9,6 mkm v iskusstvennoy atmosfere (Investigation of the 9.6 μm Band of Ozone in the Artificial Atmosphere). Author's Abstract of Candidate's Dissertation. Leningrad State University Press, 1965.

APPLYING STATISTICAL METHODS TO SOME PROBLEMS IN SPECTROSCOPY

A.P. Gal'tsev, V.P. Kozlov and M.M. Rivin

ABSTRACT: Using some statistical methods of spectroscopy, calculation of "threshold scales" yields that the ranges of concentration of matter can be determined (within measurement accuracy), making it possible to improve measurement conditions and predict the applicability of the instrument to specific cases. With maximum accuracy in concentration measurement, the optimal path length of the ray in the absorbing medium can be determined.

Introduction

In addition to the reversible conversion of measurable values, /129 which is characterized by the operative function of the instrument at (t,λ), the spectral instrument distorts the real spectrum $S(\lambda,\alpha)$ irreversibly, because of the internal noises of the instrument $n(t)$. Because of noises, instead of the determined instrumental spectrum

$$m(t, \alpha) = \int a(t, \lambda) S(\lambda, \alpha) d\lambda, \qquad (1)$$

which we would obtain at the output of an undisturbed instrument, the realization $r(t)$ of a random function whose statistical properties are determined by the fluctuations in electrical current of the receiving-recording system arises at the output of the real instrument. (In (1), α is an unknown parameter of the real spectrum $S(\lambda,\alpha)$ which underlies the determination of, for example, the temperature or mass of the emitting gas). Because of the presence of a random component $n(t)$, only the probability characteristics of the real spectrum $S(\lambda,\alpha)$ can be obtained from the realization $r(t) = m(t,\alpha)+n(t)$.

The statistical formulation of the measurement problem involves a description of the instrumental conversion of (1) and the statistics of the noises $n(t)$, and allows that the threshold possibilities of a certain measurement method be evaluated in reality. The quantitative expression for the threshold possibilities of the measurement method depends on the method used for interpreting the experimental data. Two such methods are generally used: (1) direct calculation of the unknown value α according to the realization of $r(t)$ with the least possible root-mean-square error; (2) comparison of the state of the measured object to some scale of possible states and its identification with the closest "division" of this scale. These two methods are closely related.

In particular, the scale of states can be graduated in values of the parameter α. However, the second method is more general and applicable even when the root-mean-square error depends on the unknown real value of the parameter (in this case it is difficult to estimate the computed value of the parameter). We will use the information-metrical approach in order to construct a scale characterizing the threshold possibilities of the measurement method. /130

The quantitative measure of distinguishability of two states of the measured object relative to a fixed spectral instrument proposed before by one of the authors [1-3] will underly our construction of the "threshold scale". The distinguishability of the states characterized by the values of the parameters α_1 and α_2 is expressed quantitatively by the magnitude of the information space, or the length L of the interval $[\alpha_1, \alpha_2]$ in the information metric:

$$L_{(\alpha_1, \alpha_2)} = \int_{\alpha_1}^{\alpha_2} \sqrt{\mu_{\alpha\alpha}(\alpha)}\, d\alpha, \qquad (2)$$

where $\mu_{\alpha\alpha}$ is the Fisher information matrix (of first order) corresponding to one unknown parameter α. Assuming that the noise n(t) is a stationary Guassian random process with a spectrum of capacity $G(\omega)$, the following expression is obtained for $\mu_{\alpha\alpha}$ [3]:

$$\mu_{\alpha\alpha}(\alpha) = \frac{1}{2\pi} \int_{-\infty}^{+\infty} \left| \frac{\partial \tilde{m}(\omega, \alpha)}{\partial \alpha} \right|^2 \frac{d\omega}{G(\omega)}, \qquad (3)$$

where $\tilde{m}(\omega,\alpha)$ is the Fourier transform of the instrumental spectrum $m(t,\alpha)$.

Let us list the principal properties of the information space [1.2].

1. L is a dimensionless value, regardless of the physical dimensions of the measured value α and, moreover, it does not depend at all on the selection of the parameter characterizing the state.

2. The statistical significance of the information space $L(\alpha_1,\alpha_2)$ between the states α_1 and α_2 is determined by its connection with the probability P of a correct discrimination of the signals $m(\omega_1,\alpha_1)$ and $m(\omega,\alpha_2)$ by the selected instrument:

$$P \leqslant \frac{1}{2} + \Phi\left(\frac{L}{2}\right) \qquad (4)$$

where Φ (x) is the proability integral. When L = 1, this probability $P \leq 0.7$, which practically corresponds to the discrimination threshold. The "length" L = 1 is essentially the threshold distance, sine there is a "blind spot" inside the interval $[\alpha_1, \alpha_2]$ with length L = 1, in the sense that only the states α_1 and α_2 at the ends of this interval can be distinguished. Given the reliability of discrimination P, we can determine from (4) that minimum L which should satisfy this reliability. Consequently, for a given pair of states/131 of an object $[\alpha_1, \alpha_2]$ we can plan the experiment according to the reduced reliability (i.e., reduced "length" L) in the sense of selecting $a(t, \lambda)$ and $G(\omega)$ so that the interval $[\alpha_1, \alpha_2]$ corresponds to the requisite L.

3. If the interval of the parameter $[\alpha_1, \alpha_2]$ corresponds to the information space of L > 1, then the number of recognizable states in pairs in this interval is equal to L + 1, for determining the threshold distance. Using only these properties of the information space, we can construct the "threshold scale" of the given measurement method, for which the "characteristic function" is calculated, i.e.,

$$\Phi(\alpha) = \int_{\alpha_1}^{\alpha} \sqrt{\mu_{\alpha\alpha}(\alpha)}\, d\alpha \tag{5}$$

and, taking the whole-number values of n = 1, 2, 3..., on the graph for $\Phi = \Phi(\alpha)$, we obtain the sequence of values of the parameter $\alpha_1, \alpha_2, \ldots, \alpha_n$ which are divided in the construction by intervals with information space of L = 1, i.e., the corresponding states are found at the discrimination threshold, so that no values of α between neighboring points on the scale differs from any other. A more precise scale cannot be constructed for a <u>given</u> measurement method.

Using the information metric, we can also evaluate the power of the selected ,easurement method relative to the given range of states of the object $\alpha_{min} \leq \alpha \leq \alpha_{max}$ as the number of divisions of the "threshold scale" which intersect the given range of states $[\alpha_{min}, \alpha_{max}]$:

$$L_0 = \int_{\alpha_{min}}^{\alpha_{max}} \sqrt{\mu_{\alpha\alpha}(\alpha)}\, d\alpha = \Phi(\alpha_{max}) - \Phi(\alpha_{min}). \tag{6}$$

It can be seen that L_0, an associated characteristic of the measurement method and the measurement problem (range of possible changes of the measured parameter), allows us to determine the suitability of the selected instrument before the experiment, since it shows how many states of the object can be recognized in the best case on the <u>given</u> instrument in the <u>given</u> range of $[\alpha_{min}, \alpha_{max}]$. If the

purpose of the measurements is to study the states of the object in maximum detail, then we have the problem of optimization of the measurement method, as the problem of selecting the instrument with $a(t, \alpha)$ and $G(\omega)$ which guarantees the maximum "length" L for the given rnage of $[\alpha_1, \alpha_2]$, which characterizes the range of real states of the object.

We should mention that the characteristic of the threshold possibilities of the method with a "threshold scale" also determine the limit accuracy of the measurement in the ordinary sense. If the value of $\mu_{\alpha\alpha}(\alpha)$ changes little in the interval $[\alpha_{min}, \alpha_{max}]$, /132 then the information space $L(\alpha_1, \alpha_2)$ is the length of the interval $[\alpha_1, \alpha_2]$ in units of the minimum permissible root-mean-square error in the measurement, i.e., the greater the accuracy in measuring the parameter, the more close values of the parameter can be distinguished, and the greater the total number of recognizable states in the given range.

1. Determination of the Concentration of Matter According to the Integral Absorption

For the sake of simplicity, we will consider that the absorption line for the substance of interest to us does not intersect any other lines, i.e., is isolated.

The signal at the output of the radiation receiver is determined by the expression:

$$F(c) = \begin{cases} \int\limits_{\Delta\lambda} F_0(\lambda)\, e^{-cl k(\lambda)} \tau_0(\lambda)\, \eta(\lambda)\, d\lambda, & 0 \leqslant t \leqslant T, \\ 0 & t > T, \end{cases} \tag{7}$$

where t is the time constant of the system; $F_0(\lambda)$ is the spectral distribution of the emission of the light source; c is the consentration of absorbent in millimeters of the substance deposited under normal conditions per 1 m path (mm/m); $\tau_0(\lambda)$ is the transmittance of the optical system; $\eta(\lambda)$ is the spectral sensitivity of the radiation receiver; T is the total recording time; l is the length of the path of the ray in the medium, m; $k(\lambda)$ is the absorption coefficient.

Let us use the following symbol for the effective flux

$$F(\lambda) = F_0(\lambda)\, \eta_0(\lambda)\, \tau_0(\lambda), \tag{8}$$

where $\eta_0(\lambda) = \frac{\eta(\lambda)}{\eta}$ is the relative spectral sensitivity of the radiation receiver; η is the absolute sensitivity at a fixed wavelength.

Considering the noise to be white [$G(\omega) = G = \text{const}$] and using the Parseval formula on the invariance of the signal capacity in time and frequency, we can obtain the following expression for the degree of accuracy in measuring the concentration from (3) and (7), considering (8):

$$\mu_{cc} = \int_0^T \frac{dt}{G} \left| \int_{\Delta\lambda} lk(\lambda) F(\lambda) e^{-clk(\lambda)} d\lambda \right|^2 = \\ = \frac{T\eta^2}{G} l^2 \left| \int_{\Delta\lambda} F(\lambda) k(\lambda) e^{-clk(\lambda)} d\lambda \right|^2. \tag{9}$$

In addition to the ordinary dependence of the accuracy on T, /133
η and G (the accuracy increases if there is an increase in the measurement time relative to the spectral interval of interest to us and in the sensitivity of the receiver, and a decrease in noises), it can be seen from (9) that it decreases with an increase in the concentration. Moreover, there are optimal lengths of the ray path (μ_{cc} has a maximum over λ), which depends on the measured concentration, as well as the optimal absorption coefficient k for the cases when its dependence on λ can be disregarded, which usually occurs in the ultraviolet region of the spectrum. If the concentration itself is not previously known, and only the range for its change $c_1 \leq c \leq c_2$ is known before the experiment, then the power of the measurement method over the interval $[c_1, c_2]$ (i.e., the number of values for the concentration which can be distinguished in the best case with the given instrument in the given range of $[c_1, c_2]$) is characterized by the following expression:

$$l(c_1, c_2) = \int_{c_1}^{c_2} \sqrt{\mu_{cc}}\, dc = \int_{c_1}^{c_2} \sqrt{\frac{\eta^2}{G} T l^2 \left| \int_{\Delta\lambda} F(\lambda) k(\lambda) e^{-clk(\lambda)} d\lambda \right|^2}\, dc = \\ = \frac{\eta\sqrt{T}}{\sqrt{G}} \int_{c_1}^{c_2} \int_{\Delta\lambda} lk(\lambda) F(\lambda) e^{-clk(\lambda)} d\lambda\, dc = \\ = \frac{\eta\sqrt{T}}{\sqrt{G}} \int_{\Delta\lambda} lk(\lambda) F(\lambda) d\lambda \int_{c_1}^{c_2} e^{-clk(\lambda)} dc = \\ = \frac{\eta\sqrt{T}}{\sqrt{G}} \int_{\Delta\lambda} lk(\lambda) F(\lambda) \left[e^{-c_1 lk(\lambda)} - e^{-c_2 lk(\lambda)}\right] \frac{d\lambda}{k(\lambda) l} = \\ = \frac{\eta\sqrt{T}}{\sqrt{G}} \int_{\Delta\lambda} F(\lambda) \left[e^{-c_1 lk(\lambda)} - e^{-c_2 lk(\lambda)}\right] d\lambda. \tag{10}$$

If the effective spectral flux $F(\lambda)$ in the interval $\Delta\lambda$ changes rather smoothly from λ, then it can be considered to be constant, and then

$$L(c_1, c_2) = \frac{\eta\sqrt{T}}{\sqrt{G}} F[A(c_2, l) - A(c_1, l)], \tag{11}$$

where $A(c, l)$ is the integral absorption:

$$A(c, l) = \int_{\Delta\lambda} (1 - e^{-clk(\lambda)})\, d\lambda. \tag{12}$$

Sometimes we can use the absorption function defined as

$$\overline{A}(c, l) = \frac{\int_{\Delta\lambda} F(\lambda)\,[1 - e^{-clk(\lambda)}]\, d\lambda}{\int_{\Delta\lambda} F(\lambda)\, d\lambda}. \tag{13}$$

If the interval of $[c_1, c_2]$ is unknown, then we can consider that /134
$c_1 = 0$, $c_2 = \infty$, and then

$$L(0, \infty) = \frac{\eta\sqrt{T}}{\sqrt{G}} \int_{\Delta\lambda} F(\lambda)\, d\lambda, \tag{14}$$

i.e., $L(0, \infty)$ characterizes purely photometric qualities of the instrument: actually, (14) is the "signal-to-noise" ratio for the entire light flux. It follows from (13) and (14) that the power of the method can be described in the following way:

$$L(c_1, c_2) = L(0, \infty)\,[\overline{A}(c_2, l) - \overline{A}(c_1, l)]. \tag{15}$$

For the characteristic function of the "threshold scale", we can take the following (considering that $c_1 = 0$):

$$\Phi(c) = L(0, \infty)\,\overline{A}(c, l), \tag{16}$$

This coincides, with accuracy up to the multiplier, with the effective absorption function. In constructing the scales, it was assumed that the accuracy of the purely photometric scheme was 4%, i.e., $L(0, \infty) = 25$.

The results of calculations of l_{opt}, $L(c_1, c_2)$...for different absorption coefficients are presented below.

2. Calculation of Threshold Scales for the Case of an Absorption Line of the Dispersion Contour

Determination of the Threshold Scale for the Parameter $x = \frac{Scl}{2\pi\gamma}$

The absorption coefficient for the line of the dispersion contour is equal to

$$k(\nu) = \frac{S}{\pi} \frac{\gamma}{\nu^2 + \gamma^2}, \tag{17}$$

where S is the intensity of the spectral line; γ is the half-width of the line.

The absorption function in the finite spectral interval $\Delta\nu$ is determined by the following expression [4] for $F(\lambda)$ = const:

$$A(x) = \frac{2\pi\gamma}{\Delta\nu} F(x) + (1 - e^{-az}) - \sqrt{az}\sqrt{k}\Phi(\sqrt{az}), \tag{18}$$

where $F(x) = xe^{-x}[I_0(x) + I_1(x)]$ is the Ladenburg-Reich function tabulated in [5, 6], while $I_0(x)$ and $I_1(x)$ are Bessel functions of purely imaginary argument of zero and first order, respectively;

$$z = \frac{1}{\left(\frac{\Delta\nu}{2\gamma}\right)^2 + 1} \quad \left(\frac{\Delta\nu}{2\gamma} \text{ was taken as equal to three for us}\right)$$

$$a = \frac{Scl}{\pi\gamma} = 2x.$$

The results of the calculations by (16) are given in Table 1 /135
and Figures 1 and 2.

TABLE 1

x	$\Phi(x)$	x	$\Phi(x)$	x	$\Phi(x)$	x	$\Phi(x)$
0	0	0,6	8,3	3,0	19,0	10,0	24,5
0,1	2,0	0,8	10,7	4,0	20,2	20,0	24,7
0,2	3,5	1,0	12,0	5,0	22,0	30,0	25,0
0,3	5,0	1,2	13,3	6,0	22,5	40,0	25,0
0,4	6,5	1,5	14,7	7,0	23,5	50,0	25,0
0,5	7,5	2,0	17,0	8,0	24,0		

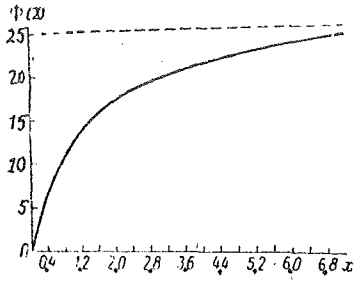

Fig. 1

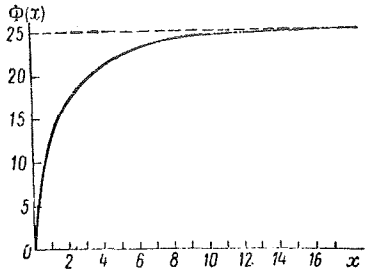

Fig. 2

An examination of the "threshold scale" permits us to draw the following conclusions.

1. This scale is "unequally accurate" - for small values of x, the measurement accuracy is greater than for high values of x. For example, the states of $x_1 = 0.2$ and $x_2 = 0.3$ can be distinguished for small x, since the interval of x = [0.2-0.3] with the "blind spot" equal to 0.1 corresponds to a length of the information space of $L(0.2; 0.3) = \Phi(0.3) - \Phi(0.2) = 1$. For high values of x, only $x_1 = 7$ and $x_2 = 15$ are distinguishable, i.e., the "blind spot" in this interval is equal to 8. The "saturation" of accuracy (increase of the "blind spot") corresponds to the "saturation" of absorption ($A \to 1$).

2. The power of a given instrument can be determined in relation to the measurement of the parameter x, for example, in the range of $[x_1, x_2] = [2, 8]$. The range of x's of interest to us is intersected by 7 divisions of the threshold scale: from 17 to 24. Thus, in the range of x = [2, 8], we can distinguish L + 1 = 7 + 1 = 8 different gradations of x's. If this power of the instrument is insufficient for solving the problem imposed by the experimenter, another instrument must be selected (for example, an instrument with a photometric system which has accuracy of 2%, i.e., L(0,) = 50). Thus, the possibility of planning the experiment arises, since the /136 threshold scale is constructed before the experiment.

3. Given the requisite power of the method L and the range of states of the real object $[x_1, x_2]$ (i.e., given the number of distinguishable states in pairs L + 1 in the given interval for change in x's), we can determine the quality of the instrument F necessary for solving this problem on the basis of (11), or, which is the same, as follows from (8), we can determine F_0, the sensitivity η_0 and the transmittance of the optical system τ_0.

4. We can determine the possibilities of solving the problem (i.e., determine the interval $[x_1, x_2]$) on the given instrument ac-

cording to the specified power of the method L and quality of the instrument F.

Calculation of the Optimal Path of the Ray

Although the optimal path can be obtained from Table 1, it is interesting to illustrate the method with a specific example. We will consider that the concentration changes in the interval [10^{-3} -10^{-4} cm/m]. The optimal length of path of the ray l is determined by calculating the power of the measured system (number of distinguishable gradations of the concentration) in dependence on the base line l on the basis of (15). The data from this calculation are presented in Table 2 and Figures 3 and 4 (semi-logarithmic scales). (For line parameters, we took $\gamma = 0.5$ cm^{-1} and $S = 100$ cm^{-2}).

It can be seen from an investigation of Figure 3 that there is an optimal base line $l_{opt} \approx 80$ m which guarantees the maximum number of different gradations the instrument can distinguish: for precision of the photometric scheme of 4%, this number $L + 1 = 15$, in the range of concentrations of $[c_1, c_2] = [10^{-3}-10^{-4}]$cm/m. It is of interest that l_{opt} corresponds to absorption of $A \approx 0.6$, which, as will be shown below, corresponds roughly to optimal absorption of $A_{opt} = 0.63$. A great decrease in the power of the instrument for small base lines can be explained by the limitation introduced by the finite accuracy of the purely photometric scheme, the noises, and, for large base lines ($l \geq 3000$ m), by the "saturation" of absorption ($A \to 1$). The power of the instrument is not sharply critical to the deviation of the base line from the optimal value. For example, a decrease in the optimal (maximum) number of distinguishable states by one (from $L + 1 = 15$ to $L + 1 = 14$) corresponds to the possiblity of selecting a base line in the range of $l = [60-250]$ m, while the sensitivity of the power of the system is sharply asymmetric in relation to the nature of the deviation of the length of the ray l from l_{opt}: it is sharper to a decrease in the base line than to its increase. For base lines of $l < 2$ and $l > 2000$ m, the instrument does not distinguish the concentrations $c_1 = 10^{-3}$ cm/m and $c_2 = 10^{-4}$ cm/m, since the information space L between them is less than 1 for these base lines. Figure 4 illustrates the physical visualizability of the existence of l_{opt}. This figure also /137
shows the characteristic functions of the threshold scales $\Phi(c_2, l)$ (Position 1) and $\Phi(c_1, l)$ (Position 2) as functions of the length of the ray in the absorbing medium. The optimal base line in this figure is determined as that value of l (in meters) which corresponds to the greatest distance between the characteristic curves. For $l > 2000$ m. The absorption $A \approx 1$ for both concentrations, so that the possibility of distinguishing these concentrations [see (15)] is decreased. On the other hand, for $l < 2$ m, the absorption is so low ($A \approx 0$) that the signal "sinks" in the noises, which also makes a recognition of the concentrations c_1 and c_2 impossible. Thus, it is clear that the l_{opt} at which the reliability in distinguishing c_1 and c_2 (or the number of values for the concentrations which

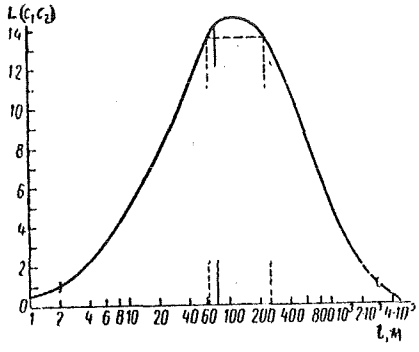

Fig. 3

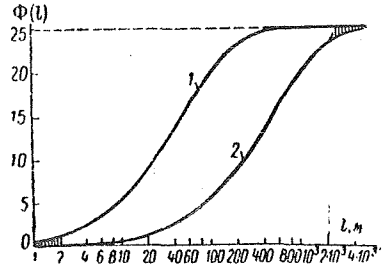

Fig. 4

are distinguishable in paris in the range of $[c_1, c_2]$) is maximum occurs somewhere in the interval of l = [2-2000] m.

3. Calculation of the Threshold Scales for the Case of a Constant Absorption Coefficient

By the fixed concentration we mean such a small neighborhood of $[c_0 - \delta, c_0 + \delta]$ that the length of the information space L corresponding to this neighborhood is less than one.

The calculation of l_{opt} is carried out on the basis of (9) with a consideration of $k(\lambda)$ = const, as a determination of the base line guaranteeing the maximum permissible accuracy in measuring c:

$$\mu_{cc} = \frac{\eta^2}{G} T l^2 (e^{-clk} k)^2 \left[\int_{\Delta\lambda} F(\lambda)\, d\lambda \right]^2 = L(0, \infty)^2 k^2 l^2 e^{-2clk}. \tag{19}$$

Since the constant factor $L(0, \infty)^2 k^2$ in (19) determines only the scale of the absolute value of the accuracy, then it is sufficient to calculate the behavior of the following function to find l_{opt}:

$$l^2 e^{-2clk} \tag{19a}$$

in dependence on l, or to determine the l which corresponds to μ_{cc} = max from the condition /138

$$(\mu_{cc})' = 0;$$

from which

$$l_{opt} = \frac{1}{ck}. \tag{20}$$

Consequently, the optimum length of the ray is continuous function of the concentration of absorbing substance. In using in the

TABLE 2

l	$\Phi(c_1, l)$	$\Phi(c_2, l)$	$L(c_1, c_2)$
1	0,04	0,47	0,50
2	0,11	1,12	1,00
4	0,19	2,48	2,25
6	0,30	3,45	3,25
8	0,37	4,37	4,00
10	0,47	5,50	5,00
20	1,12	9,00	7,75
40	2,48	13,25	11,20
60	3,45	16,50	13,00
80	4,37	18,70	14,30
100	5,50	19,70	14,30
200	9,00	23,00	14,00
400	13,25	24,80	11,30
600	16,50	25,70	8,50
800	18,70	24,00	6,25
1000	19,70	26,00	5,20
2000	23,00	25,00	2,00

TABLE 3

l	μ_{cc}/const	A
0	0	0
2	2,68	0,18
5	9,30	0,39
8	12,80	0,55
10	14,00	0,63
12	13,00	0,70
15	11,20	0,78
17	9,50	0,82
20	7,20	0,86
25	4,20	0,92
30	2,20	0,95
40	0,50	0,97

experiment an l_{opt} which depends continuously on the concentration, we find that the absorption is equal to

$$A = 1 - e^{-ckl_{opt}} = 0{,}63.$$

It can be considered as the optimal absorption $A_{opt} = 0.63$ in the sense that the highest accuracy μ_{cc} in measuring the concentration or absorption coefficient is achieved for this value of the absorption. On the other hand, μ_{cc} characterizes the importance of the measurement result, i.e.,

$$c \pm (\mu_{cc})^{-\frac{1}{2}}. \tag{21}$$

The accuracy μ_{cc} determines the amount of information included in (21), since the smaller the value of μ_{cc}, the greater the indefiniteness of (21). (In the extreme case of $\mu_{cc} = 0$, this is equivalent to a situation where we know nothing of the concentration c.) Table 3 and Figure 5 show the results of a calculation of the course of μ_{cc} according to (19a) in dependence on l for measuring the concentration in a small neighborhood of c = 0.001 cm/m for an absorbent with $k = 10^2$ cm^{-1}. The degree of sensitivity of μ_{cc} to the deviation of l from l_{opt} can be evaluated from the figure. Since the base line l is unambiguously interconnected with the absorption $A = 1-e^{-ckl}$ for fixed c and k, then it is interesting to clarify the range of absorption which is most advantageous (in the sense of providing the greatest accuracy μ_{cc}) for measuring c. This range can be estimated by examining Figure 6: $A_{opt} \approx [0.55-0.75]$. /139

Let us consider the case of measuring concentrations in the range of $[c_1, c_2]$. Based on (10) and considering the independence of the absorption coefficient on the frequency, we can look for

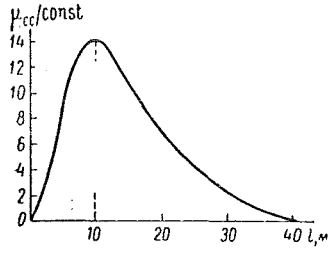

Fig. 5

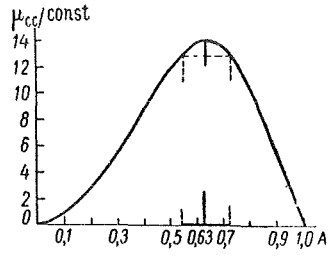

Fig. 6

l_{opt} as for that length of the ray which corresponds to the maximum $L(c_1, c_2)$:

$$\max L(c_1, c_2) = \max L(0, \infty)\,[e^{-c_1 lk} - e^{-c_2 lk}].$$

4. Metrical Approach to the Problem of Discriminating Two Superposed Lines with Dispersion Contours

As was shown in the introduction, the real states of an object, the information space between which is equal to one, can be distinguished by an instrument. The characteristics of the instrument are used for calculating L = 1 with reliability of 0.75. Thus, L = 1 can be considered as the criterion for discriminating two states of an object. In the general case, the state of the object means any physical characteristic of the object (humidity, brightness, percentage of absorbent, etc.). We will be interested in discriminating the states in the sense of regular geometric discrimination of two superposed lines. Expressions for the integral absorption of two overlapping dispersion lines are given in [7,8] as the functions of two parameters: the already mentioned parameter $x = \frac{Scl}{2\pi\gamma}$ and the distance between the centers of the lines in percentages of the half-width of the line $d \equiv \frac{\nu_{01}\ \nu_{02}}{\gamma}$, where ν_{01} and ν_{02} are wave numbers of the centers of the lines. It was shown in [8] that the integral absorption of two overlapping lines is equal to

$$A = A_1 + A_2 - \Delta, \tag{22}$$

where A_1 and A_2 are the absorption of the first and second lines, respectively, while Δ characterizes the effect of the overlap of the lines. It is very difficult to use a precise expression for Δ for the calculations; however, an approximative expression for Δ was presented in [8], which gives an error no greater than 5% in the worst case: /140

$$\Delta = \frac{4\pi\gamma_1\gamma_2 F(x_1)\,F(x_2)}{\left[\frac{\gamma_1 x_1}{F(x_1)}\right] + \left[\frac{\gamma_2 x_2}{F(x_2)}\right]} \cdot \left\{1 + \left[\frac{(\nu_{01} - \nu_{02})}{\frac{\gamma_1 x_1}{F(x_1)} + \frac{\gamma_2 x_2}{F(x_2)}}\right]^2\right\}^{-1}, \tag{23}$$

This can be represented in the following form:

$$\frac{\Delta}{2\pi\gamma_2}=\frac{2nA(x_1)A(x_2)}{\left[\frac{nx_1}{F(x_1)}+\frac{x_2}{F(x_2)}\right]\cdot\left\{1+\left(\frac{\nu_{01}-\nu_{02}}{\gamma_2}\right)^2\frac{1}{\left[\frac{nx_1}{F(x_1)}+\frac{x_2}{F(x_2)}\right]}\right.}. \tag{24}$$

Here n characterizes the ratio between the half-widths of the lines under examination, i.e.,

$$\gamma_1=n\gamma_2. \tag{25}$$

Expression (24) can be greatly simplified if we consider the problem of distinguishing two identical lines ($x_1 = x_2$, $n = 1$):

$$\frac{\Delta}{2\pi\gamma}=\frac{A^3(x)}{x}\frac{1}{1+\left(\frac{\nu_{01}-\nu_{02}}{2\gamma}\right)^2\frac{A^2(x)}{x^2}}. \tag{26}$$

Using (26) and (22), we can calculate the characteristic function of the "threshold scale", i.e.,

$$\Phi(d)=L(0,\ \infty)A(x,\ d) \tag{27}$$

for a discrete series of values of x. The results of the calculation are presented in Table 4 for different values of x, and on Figures 7 and 8. It can be seen from the curves on Figure 7 that the curves of all the characteristic functions are "saturated" at $d > 10$ (for some x's, the saturation occurs at much lower values of d). Two lines which are a distance of $d > 10$ from each other (i.e., more than five half-widths) can be considered as completely non-overlapped, completely distinguishable lines. The situation characterizing the value of $d = 0$ corresponds to two lines completely overlapping at all points. Thus, the "saturation" of the characteristic functions or, which is the same, the "saturation" of the power of the method

$$L(0,\ 10)=\Phi(10)-\Phi(0) \tag{28}$$

for all values of x means that a further increase in the distance between the lines on the scale of the wavelengths does not increase the length of the information space L between them, i.e., does not /141 give additional information.

The power of the method L(0, 10) determined from Figure 7 according to (28) depends continuously on x, and there is an optimal value ($x \approx 2$) at which the "power" is maximum. It was said in the

TABLE 4

d	x					
	0,1	0,5	1,0	2,0	5,0	10,0
0	7,75	27,30	42,45	60,10	81,20	93,25
0,2	—	27,35	42,50	60,14	81,20	—
0,3	—	—	42,56	—	—	—
0,4	—	27,45	—	60,25	—	—
0,5	—	—	42,75	60,32	81,23	—
0,6	7,80	27,60	42,88	—	—	93,27
0,7	—	—	—	60,53	—	—
0,8	—	27,80	43,17	60,65	81,33	—
1,0	7,85	28,00	43,49	60,92	81,40	93,30
1,3	—	28,30	44,00	61,40	—	—
1,5	7,90	28,50	44,35	61,74	81,64	93,36
2,0	7,93	28,90	45,00	62,6	81,95	93,44
2,5	7,95	—	—	—	82,35	93,53
3,0	7,96	29,4	46,0	64,0	82,4	93,64
4,0	8,00	29,6	47,0	65,0	83,4	94,0
5,0	8,00	29,8	47,3	66,0	84,0	—
6,0	8,00	29,8	47,6	66,6	85,0	94,6
7,0	8,00	29,8	47,6	67,0	85,4	95,0
8,0	8,00	29,8	47,6	67,0	85,6	—
10,0	8,00	29,8	47,6	67,4	86,2	95,4
15,0	8,00	30,0	48,0	68,0	86,8	96,0

introduction that the statistical meaning of the information space $L(d_1, d_2)$ consists in its mutually unambiguous correspondence with the probability of distinguishing two states. Thus, L(0, 10) as a function of x can be understood as the reliability in discriminating two lines in dependence on x. The "saturated" power of the method L(0, 10) can be treated differently - as the number of lines L + 1 (for example, in the band) which can be distinguished by the instrument in the interval of d = [0, 10]. The information space between these lines should be equal to 1, while the distance in this "fencing" in the scale of wave numbers is nonuniform (for example, for x = 5 on Figure 7, these lines are designated by a, b, c, d, e, f). The problem of discriminating two lines is illustrated in Figure 8, where graphs of the information spaces L = L(0, d) are constructed for lines of varying "brightness" (different x). The line L(0, d) ≡ 1 corresponding to the threshold of discrimination of two overlapping lines intersects the curves for L[(0, d), x] at /142 points with various abscissa values d = d(x). If the problem is to determine the discrimination acuteness (i.e., the minimum interval of [0, d] which corresponds to L = 1), then the advantage of average values of x (on the order of x = [0.5-2.0]) in the interval of x = [0-10] is obvious from Figure 8. These optimal values of x correspond to absorption A in the range of A = [0.3-0.7]. It is clear that, for values of x for which A ≈ 1 (absorption of the Π-type) or A ≈ 0 (the signal "sinks" in noises), the resolution condition worsens. The determined course of the dependence of the threshold interval [0, d] on x is shown in Figure 9. Figure 10 shows dependences of L[0, d] = f(A) and L(0, 10) = f(A).

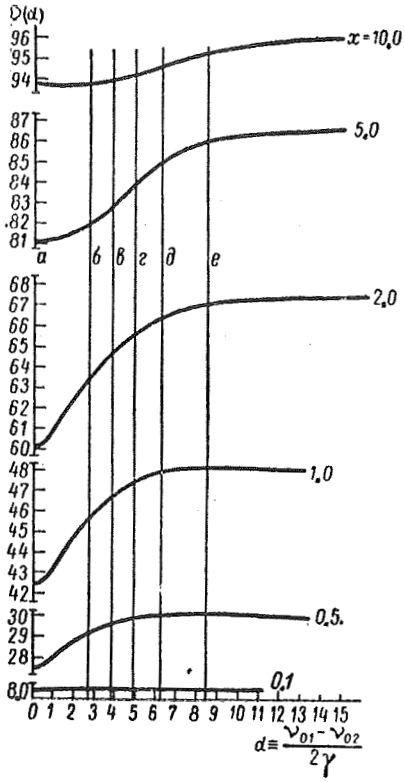

Fig. 7

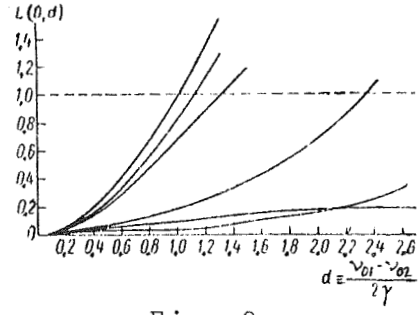

Fig. 8

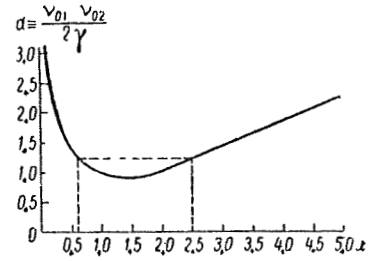

Fig. 9

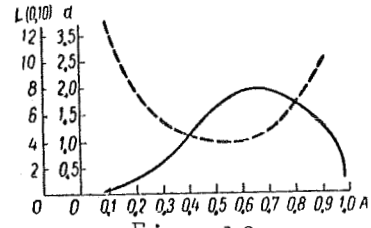

Fig. 10

Conclusion

/143

Let us write out the results obtained briefly.

1. From an examination of the "threshold scales", it was found that the most suitable ranges of the concentration values for the measurements (in the sense of accuracy) can be found, specific recommendations for planning the optimal measurement conditions can be given (determine the characteristics of the filter instrument), and it can be established beforehand whether or not the instrument will distinguish the concentrations c_1 and c_2 of interest to us.

2. We can calculate the optimal length of the ray path in the absorbing medium, which corresponds to maximum accuracy in measuring the concentrations (in the course of solving this problem, the range of absorption most advantageous for measuring the concentrations of the substance is found).

3. We can investigate the problem of discriminating two superposed lines with dispersion contours.

All this shows that the application of the statistical method to spectral problems is extremely helpful.

APPENDIX

Determination of the Most Suitable Spectral Regions for Satellite Measurements of the Ozone Concentration

The course of the optimal absorption coefficient can be calculated according to the standard vertical distribution of the concentration of the substance c = c(h) for some altitude $k_{opt}(h)$, so that the measurement is carried out at all altitudes with maximum accuracy. Since

$$A_{opt} = 0.63 \text{ at } clk = 1, \tag{29}$$

then, knowing the standard concentration distribution c(h) and the length of the ray path $\underline{l}(h)$ in the layer of the substance, we can

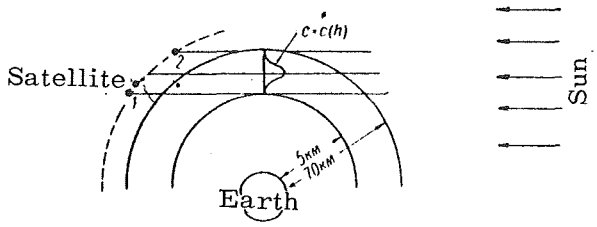

Fig. 11

determine the total percentage of absorbing substance w per ray path. Since the concentration of the substance changes along the ray, the calculations of w(h) are carried out by numerical summation. Based on (29), we can calculate the course of

$$k_{opt}(h) = \frac{1}{w(h)}.$$

In using $k_{opt}(h)$, according to (29), the recording at all altitudes would be for the A_{opt} which corresponds to the permissible accuracy.

It is well known that many substances are characterized by a set of constant absorption coefficients related to different absorption bands. For example, the following set of decimal coefficients [9, 10] occurs for ozone (O_3) in the ultraviolet region: /144

λ, mμ	253.6	289.4	302.1	334.1	576.9	296.7
k, cm^{-1}	133.9	17.2	3.34	0.0498	0.0555	6.969

Thus, if we want to carry out satellite measurements under the most profitable conditions (as close as possible to the optimal value of the absorption coefficient), we must change the wavelength in such a way that the value of the absorption coefficient is closest to the value of k_{opt} at the given altitude. All this relates both to the filtering instrument and to the high-speed scanning instrument, since the part of the spectrum which lends to the telemetry system should change as the position of the satellite changes with altitude in order to decrease the load of the system [9, 10]:

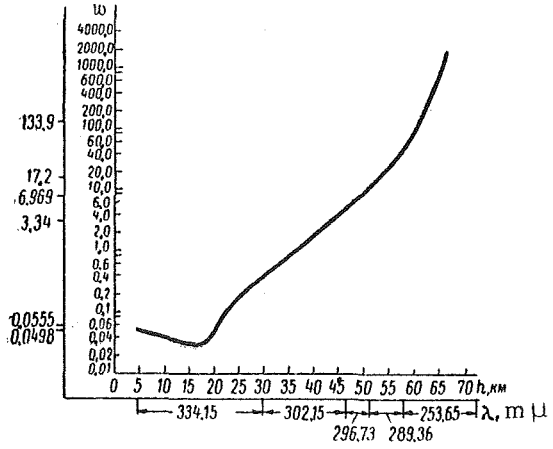

Fig. 12

The calculations for ozone show that, in the motion of a satellite from Postion 1 to Position 2 (see Fig. 11), the value of the optimal absorption coefficient changes within the interval of k_{opt} = [0.005 + 2190]cm^{-1}. The course of the change in $k_{opt} = k(h)$ is shown in Figure 12. The intervals of altitudes in which measurements must be carried out at those wavelengths where the ozone absorption coefficient is close to the optimal value are plotted on the lower scale of this figure.

References

1. Kozlov, V.P.: Power of a Set of Signals in Space and Riemannian Metrics. Doklady Akad. Nauk S.S.S.R., Vol. 166, No. 4, 1966.
2. Kozlov, V.P.: The Problem of Reproducing the Altitudinal Temperature Profile According to the Spectrum of Outgoing Radiation. Izvest, Akad. Nauk S.S.S.R., ser. fisiki atmosfery i okeana, No. 2, 1966.
3. Kozlov, V.P.: The Resolution of Spectral Instruments. Optika i Spektroskopiya, Vol. XVI, No. 3, 1964.
4. Kondrat'yev, K.Ya.: Luchistaya energiya Solntsa (Radiant Solar Energy). "Gidrometeoizdat", 1954.
5. Kaplan, D.: Intensity and Line-width of the 15-Micron CO_2 Band. J. Chem. Phys., Vol. 25, No. 5, 1956.
6. Kondrat'yev, K. Ya.: Perenos dlinnovolnovogo izlucheniya v atmosfere (Transfer of Long-Wave Radiation in the Atmosphere). "Gidrometeoizdat", 1956.
7. Reich, F.: Total Absorption Due to Two Overlapping Spectral Lines. J. Opt. Soc. Amer., Vol. 46, No. 8, 1956.
8. Sakai, H.: Equivalent Width Due to Overlapping Lines. J. Opt. Soc. Amer., Vol. 54, No. 6, 1964.
9. Hearn, A.: The Absorption of Ozone in the Ultraviolet and Visible Regions. Proc. Phys. Soc., Vol. 78, No. 503, 1961.
10. Frit, R.: Determination of the Vertical Ozone Distribution in the Earth's Atmosphere with the Aid of a Satellite. In the Collection: Raketnaya i sputnikovaya meteorologiya (Rocket and Satellite Meteorology). "Gidrometeoizdat", 1964.

SOME RESULTS OF MEASUREMENTS OF THE SPECTRAL TRANSMISSION OF THE ATMOSPHERE UNDER THE CONDITIONS OF UPPER-LEVEL CLOUDS

L.V. Popova and I.Ya. Babinov

ABSTRACT: The article presents some results of determinations of the spectral nature of the transmission of cirrus clouds on the basis of ground measurements of the solar radiation passing through the upper-level clouds over Leningrad, Terskol Peak, and Mineral'nyye Vody. It is shown that the transmission of the upper-level clouds outside the absorption bands in the range of 0.4-0.8 and 4-13 μm is neutral on the average, and equal to 80-90%.

As is well known, the last decade has been characterized by a rapid development of studies of upper-level clouds, as a result of which the spatial structure of these clouds has been clarified to a large extent. The physical condition of these clouds has been described rather fully in the monograph by F.Ya. Klinov [1]. However, the optical characteristics of cirrus clouds have been studied insufficiently, although they are necessary for solving a large number of problems connected with radiation transfer, space research, the use of lasers, etc. /146

In this study, we have attempted to determine the spectral nature of the transmission of cirrus clouds with the aid of ground measurements of the solar radiation passing through upper-level clouds. The measurements were carried out under expeditionary conditions. Data for 12 cloudy days were analyzed.

The spectral apparatus consisted of a combination of two devices - one for studying the visible region of the spectrum (0.4-0.9 μm) [2], and the other for the infrared (3-13 μm) [3].

Knowing the extra-atmospheric values for direct solar radiation $J_{0,\lambda}$ and the values for radiation at a moment with cloudiness of $J_{\lambda_{cle+clo}}$, we can determine the total spectral optical thickness of the atmosphere, i.e.,

$$\tau_{\lambda_{cle+clo}} = \tau_{\lambda_{tot}}$$

according to the ordinary Bouguer formula of

$$J_{\lambda_{cle+clo}} = J_{0,\lambda} e^{-\tau_{\lambda_{tot}} m}$$

On days with upper-level clouds, the optical thickness of the atmosphere $\tau_{\lambda_{tot}}$ undergoes substantial oscillations in correspondence with the change in degree and thickness of the cloud cover. Figure 1(a,b) shows the optical thicknesses of the cloudy atmosphere, beginning with moments of slight cloudiness to moments when the Sun is covered to a maximum extent by clouds (when an image of the solar disk can still be noted and recorded in correspondence with the spectral fluxes of solar radiation), and including all the intermediate variations in this value. /147

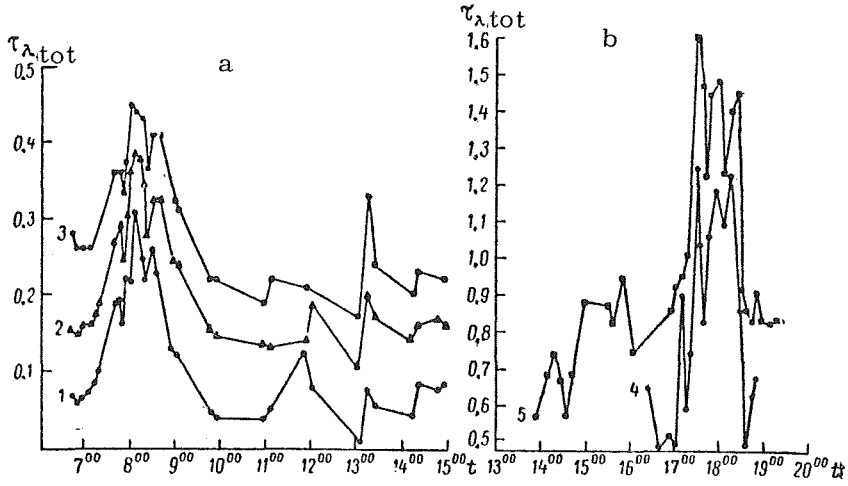

Fig. 1. Change in Time in the Optical Thickness of the Cloudy Atmosphere for Different Wavelengths, Terskol Peak, 9/24/1962(a) and Dependence of $\tau_{\lambda_{tot}}$ on the Time, Leningrad, 5/16/1963(b). (1,4) 780 nm; (2) 465 nm; (3) 421 nm; (5) 465 nm.

TABLE 1

Date, Site	Time	Degree of Cloudiness
9/29/1962, Terskol Peak (the Caucasus, 3060 m above sea level)	7^{40} - 9^{00}	Ci 10/0, Sun in Dense Clouds
	9^{50}	Ci 7/0, Thinner, Transparent Haze
	9^{56}	
	10^{00} - 15^{00}	Ci 2/0, Halo, $\odot^2$
5/16/1963, Leningrad	14^{00}	Ci 3/0, $\odot^2$
	16^{18} - 16^{23}	Ci on the Sun, 4/0
	16 - 16^{40}	Ci 10/0 Sun in Light Veil
	17^{04} - 17^{07}	Ci 10/0, Denser
	17^{11} - 17^{21}	Ci 10/0 Dense
	17^{30} - 18^{20}	Ci 10/0 Dense

As can be seen from Figure 1 and the descriptions of the meteorological situation in Table 1, the total optical thickness of the atmosphere at the moments of maximum attenuation is roughly twice greater than at the beginning of the appearance of the clouds (3/0-4/0 Ci) between the Sun and the observer. Thus, for λ = 465 /148 nm, the ratio $\frac{\tau_{\lambda max}}{\tau_{\lambda av.min}}$ is equal to two over Leningrad on 5/16/1963 and 5/17/1963 and over Terskol Peak on 9/24/1962. During the development and movement of the clouds, there is generally observed a maximum in optical thickness of the atmosphere $\tau_{\lambda_{tot}}$ which is connected with the process of the movement of the front. We should mention that we are speaking in these cases of frontal upper-level clouds, and not of internal ones.

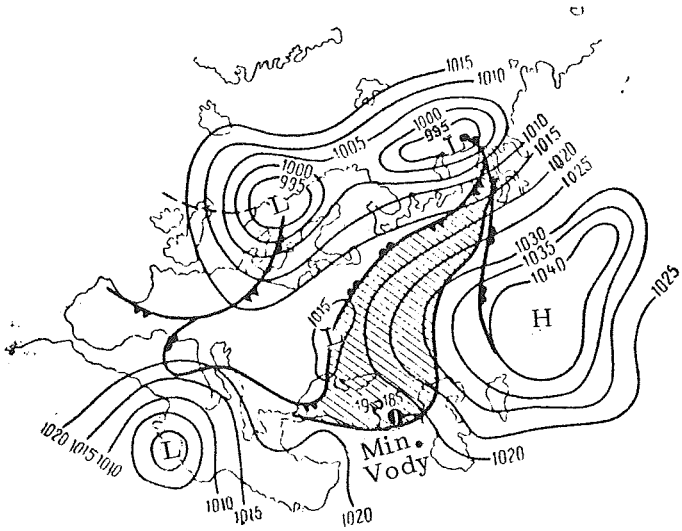

Fig. 2. Typical Synoptic Situation for which the Upper-Level Clouds Under Investigation were Formed, 10/0, Min. Vody, 10/30/1962, 15:00 hrs.

A typical synoptic situation reflecting the twelve cases we examined, when upper-level clouds moved ahead of a warm front, i.e., had average thickness of 2 km [4], is shown in Figure 2. In Leningrad, on May 16 and 17, 1963, Ci clouds went behind the front, carrying lower- and middle-level clouds along. On the evening of May 16, the front passed over, leaving rather dense upper-level clouds, and on the morning of May 17, thinner, transparent clouds were observed behind the same front. The front passed by, and at 1100-1200 on May 17, 1963, the total optical thickness of the atmosphere $\tau_{\lambda_{tot}}$ reached its least value, almost equal to the value of $\tau_{\lambda_{cle}}$ which occurs in Leningrad in clear skies. In the remaining cases, the Ci clouds went ahead of the front. Under the conditions of upper-level clouds, and under the conditions of a clear sky, the monotonous nature of the dependence of the optical thickness /149

of the entire atmosphere $\tau_{\lambda_{tot}}$ on the wavelength is preserved both for large and for small optical thicknesses (Fig. 3).

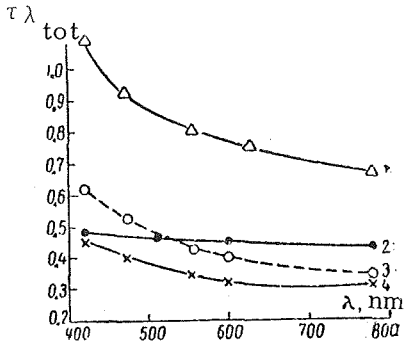

Fig. 3. Dependence of $\tau_{\lambda_{tot}}$ on λ under the Conditions of Upper-Level Ci Clouds 9/0-10/0.
(1) 5/17/1963, Leningrad; (2) 6/10/1962, Terskol Peak; (3) 10/30/1962, Min. Vody; (4) 9/24/1962, Terskol Peak.

We calculated the values for the spectral transmission of the upper-level clouds at the zenith in approximation of the isotropy of the cirrus layer, i.e.,

$$\gamma_\lambda = \frac{J_{\lambda_{cle+clo}}}{J_{\lambda_{cle}}}, \qquad (1)$$

$$\Gamma = \frac{S_{cle+clo}}{S_{cle}}, \qquad (2)$$

where Γ is the integral transmission of the clouds; $S_{cle+clo}$ and S_{cle} are the integral fluxes of direct solar radiation, measured by the actinometer of Yanishevskiy during the spectral measurements and reduced to m = 1. The spectral transmission coefficient of the clouds γ_λ was also reduced to m = 1.

The spectral intensities $J_{\lambda_{cle}}$ and $J_{\lambda_{cle+clo}}$ were related to a unit mass in the following way. The value of $\tau_{\lambda m}$ was first calculated from the relationship

$$J_{\lambda m} = J_{\lambda,0}\, e^{-\tau_{\lambda m} m}$$

by the short Bouguer method from the known values of $J_{\lambda,m}$; $J_{\lambda,0}$; m:

$$\tau_{\lambda m} = \frac{\log J_{\lambda,0} - \log J_{\lambda m}}{m} \cdot 2{,}3. \qquad (3)$$

Then, assuming that m = 1, we found

$$J_{\lambda clo} = J_{\lambda,0}\, e^{-\tau_{\lambda m}}, \qquad (4)$$

where $J_{\lambda\ clo}$ is the intensity calculated for the zenith under the conditions of cloudiness. At the same time, in order to avoid errors in this method of reduction to a unit mass, we selected the

TABLE 2

Date, Site		λ, μm										
		0.42—0.78					3.56—13.05					
9/24/1962, Terskol Peak	$h_{\odot}$	23.1—22.2	30.4—31.2				23.1	30.1	32.2	45.5		
	γ	0.737	0.903				0.682	0.904	0.945	0.881		
5/16/1963, Leningrad	$h_{\odot}$	25.2—25.6	26.7—27.0	29.0 - 29.5	30.1	31.2	11.6—12.2	29.5—30.1	30.8—31.3			
	γ	0.308	0.334	0.624	0.516	0.691	0.905	0.725	0.730			
5/17/1963, Leningrad	$h_{\odot}$	17.2	28.2—31.2	33.0	39.9		23.9—24.4	25.1—28.1	29.5—30.4	31.8—32.6	34.2—34.9	39.2—39.7
	γ	0.969	0.762	0.736	0.918		0.836	0.752	0.742	0.668	0.660	0.885
10/19/1962, Min. Vody	$h_{\odot}$	33.9	35.2	36.2			34.5	36.1				
	γ	0.781	0.882	0.946			0.854	0.876				

cases when

$$h_{\odot clo} \simeq h_{\odot cle}.$$

If the solid angle of the apparatus has finite dimensions, then it follows from the study of V.Ye. Zuyev et al. [5] that, in the case of a rather dense optical medium (uniform and isotropic), we must consider the contribution of light scattered to the sides to the signal from a point source in finding the solid angle of the optical instrument. In our apparatus, the solid angle of the instrument was about 0.05 rad for the visible region of the spectrum, which gives D (factor determining the percentage of scattered parasitic light) on the order of 0.5 for high values of ρ (in upper-level clouds, the dimensions of particles average 0.1-0.5 mm, according to the data of F.Ya. Klinov [1]).

In order to evaluate the portion of scattered light, we used the following relationship from [5]:

$$n = n_0 e^{-\tau}(1 + \tau D). \qquad (5)$$ /151

The evaluation was carried out by the method of successive approximations. We limited ourselves to first approximation and found the real attenuated radiation flux in (1) from the following relationship:

$$J_{\lambda_{cle+clo}} = J_{\lambda_{rl}} = \frac{J_{\lambda_{обл}}}{1 + \tau_{\lambda_{clo}} \cdot 0{,}5}, \quad D = D(\rho, \psi, \theta). \qquad (6)$$

Here ψ is the solid angle of the instrument; θ is the angle of taper of the emitting source; n is the attenuated signal; n_0 is the initial signal.

In our case, $\tau_{\lambda_{clo}}$ was 0.1-0.3; therefore, the percentage of additional parasitic flux of scattered light in the solid angle of the instrument was 5-15%. Table 2 gives the average values for the spectral coefficient of transmission of Ci clouds with a consideration of the correction in the visible spectral region. In order to control the stability of the optical properties of the atmosphere, we determined (Table 3) the turbidity factors of L.G. Makhotkin N (see [2]) and the total content of water vapor in the atmosphere by the spectroscopic method (see [6]) for the same moments of time.

TABLE 3

Site	Date	Γ_{clo}	N_{cle}	N_{clo}	$\frac{W_\infty}{m}$ см clear	$\frac{W_\infty}{m}$ см cloudy
Terskol Peak	9/24/62	53–61	0,3–0,5	1–1,2	0,5	0,63
	9/24/62	80	0,3–0,5	—	—	—
Mineral'nyye Vody	9/30/62	37–41	0,7–0,9	2,5–3,4	1–1,6	2,9–2,4
	10/19/62	90	0,7–0,9	1,1	—	—
	10/17/62	46	0,7–0,9	3,55–4,0	—	—
Leningrad	5/16/63	19–30	1–2,4	$\frac{9}{4}$	1–2	1,7–2,0
	5/17/63	—	1–2,4	2,6–3	1–2	1,5

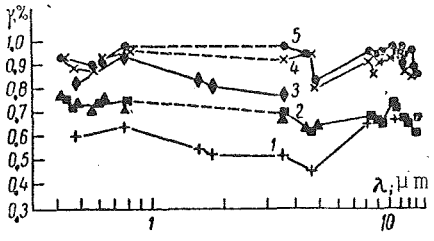

Fig. 4. Spectral Characteristic of Transmission of Direct Solar Radiation by Ci Clouds on 9/24/1962, Terskol Peak. (1 and 3) According to the Data of D. Gates and C. Shaw; (2) at $h_\odot$ = 22-23°; (4) at $h_\odot$ = 30.1°; (5) at $h_\odot$ = 31-32.

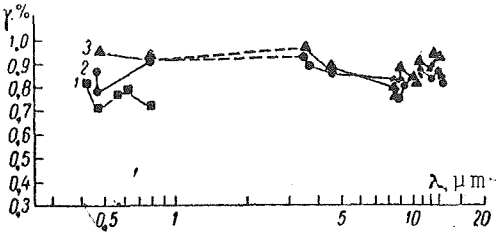

Fig. 5. Spectral Transmission of Radiation by Ci Clouds on October 19 and 30, 1962, Min. Vody. (1) 10/19, $h_\odot$ = 13.7°; (2) 10/19, $h_\odot$ = 34.5°; (3) 10/30, $h_\odot$ = 36/2°. /152

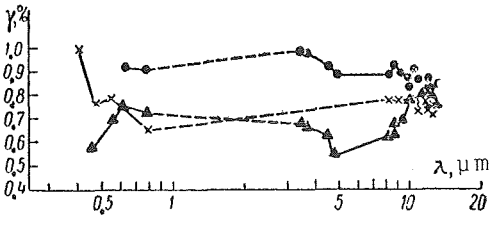

Fig. 6. Spectral Transmission of Radiation by Ci Clouds at Different Levels of the Sun on May 16 and 17, 1963, Leningrad. $h_\odot$ = 25.4-39.9°.

The spectral course of the transmission coefficients of upper-level clouds is depicted in Figures 4, 5 and 6, in percentages, for Terskol Peak, 1962, Min. Vody, 1962 and Leningrad, 1963. Each broken line corresponds to one case of measurements (height of the Sun) for the given site.

It follows from the data of the measurements that the transmission of upper-level clouds outside the absorption bands in the range of 0.4-0.8 and 4-13 μm is neutral on the average, and 80-90%. For the conditions of Leningrad, where, obviously, a large quantity /153 of crystallization nuclei is brought to the upper layers of the troposphere [4], this figure decreases to 50-70%. In order to compare our data with those of other authors, Figure 4 shows the data of D. Gates and C. Shaw [8], who give a small decrease in the transmission in the region of 4-5 μm. These authors carried out their measurements in mixed clouds (Ci + ACu + Cu) with a predominance of Ci.

REFERENCES

1. Klinov, F.Ya.: Voda v atmosfere pri nizkikh temperaturakh (Water in the Atmosphere at Low Temperatures). Akad. Nauk S.S.S.R., 1960.
2. Dayeva, L.V.: The Problem of Determining the Spectral Transmittance Coefficients of the Real Turbid Atmosphere in the Spectral Region of 0.4-1 m. In the Collection: Aktinometriya i optika atmosfery (Actinometry and Optics of the Atmosphere). "Nauka", 1964.
3. Kondrat'yev, K.Ya., I.Ya. Badinov, S.V. Ashcheulov and S.D. Andreyev: Apparatus for Studies of the Infrared Spectrum of Absorption and Thermal Radiation of the Atmosphere. Izvest. Akad. Nauk S.S.S.R., ser. fiziki atmosfery i okeana, Vol. 1, No. 2, 1965.
4. Baranov, A.M.: Frontal'nyye oblaka i usloviya poletov v nikh (Frontal Clouds and the Conditions for Flying in Them). "Gidrometeoizdat", 1964.
5. Zuyev, V.Ye., M.V. Kabanov and A.G. Borovoy: The Weakening of a Light Signal in a Dispersing Medium. Izvestiya VUZov, fizika, No. 6, 1963.
6. Makhotkin, L.G.: Direct Radiation and the Transparency of the Atmosphere. Izvest. Akad. Nauk S.S.S.R., ser. geofiziki, No. 5, 1957.
7. Badinov, I.Ya., A.P. Gal'tsev and G.A. Nikol'skiy: The Problem of the Spectroscopic Method of an Integral Determination of the Water Vapor Content in an Atmospheric Column. In the Collection: Problemy fiziki atmosfery (Problems of Atmospheric Physics), No. 1. Leningrad State University Press, 1963.
8. Gates, D.M. and C. Shaw: Infra-red Transmission of Clouds. J. Opt. Soc. Amer., Vol. 50, No. 9, 1960.

SPECTROPHOTOMETER WITH A NORMAL EMISSION SPECTRUM AT THE OUTPUT OF THE RECORDER

V.V. Mikhaylov and V.P. Voytov

ABSTRACT: The authors describe a spectrophotometer whose operative model was designed in the special research laboratory of atmospheric physics of Leningrad State University. The instrument was designed to avoid two basic difficulties: low speed for recording spectra, and selectiveness of the sensitivity of the device.

A spectrophotometer whose operative model was designed in the special research laboratory of atmospheric optics of Leningrad State University is described in this study. /154

In the designing of this spectrophotometer, which was intended for optical atmospheric studies, we attempted to avoid two basic disadvantages found in the ordinary spectrophotometric apparatus. First of all, we attempted to avoid the low speed of recording the spectra, since the speed regularly used for recording spectra with a spectrophotometric apparatus (10-100 Å/sec) is insufficient for studying many phenomena of atmospheric optics, because of the activity of the latter. Moreover, in the case of a change in transmittance, the presence of variable haze or a change in the albedo of the underlying surface, and the long recording time, can introduce substantial distortions in the defined spectral intensities. Secondly, we tried to avoid selectiveness of the sensitivity of the device in this design, because it is the most significant disadvantage of all spectrophotometers, since the spectrograms obtained on them must be re-calculated with a consideration of the selectiveness of the instrumental sensitivity. In the case of numerous serial measurements, these re-calculations of the spectrograms for the normal spectrum represents very laborious computational labor, requiring the work of many computers.

The high-speed spectrophotometry in this device is achieved by using several output slits in the monochromator, as in the single-beam spectrophotometer described in [1]. The normal spectrum at the output of the device is obtained as a result of the use of a dual-beam optical scheme and the installation of a resolver at the output. The use of the dual-beam scheme with a simultaneous comparison of the analyzed and standard radiation fluxes on the same photographic receiver guarantees independence of the results of the measurements from the sensitivity of the emission receiver and the transmission coefficients of the optical scheme. The installation of a resolver operating by a definite program allows us to eliminate /155

the dependence of the measurement results on the spectral properties of the source of the reference emission.

The spectrophotometer (see block diagram) consists of the following principal elements: a four-beam illuminator with a modulator, the source of the reference emission, a monochromator with three output slits, photographic detectors of the radiation, and an electronic device which amplifies the photocurrents of the detectors and corrects the measurement results for the normal spectrum.

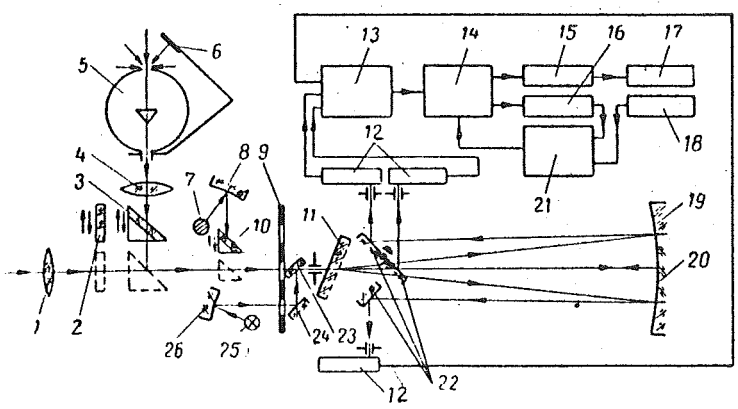

Block Diagram of the Spectrophotometer.

One of the channels of the illuminator, which consists of a quartz-crystal lens, 1*, with focal distance of 430 mm, is used for projecting a small segment of the sky on the output slit of the monochromator for measurements of the spectral sky brightness or the solar disk in measurements of the spectral fluxes of direct solar radiation. In the latter case, a neutral reducing filter, 2, made by depositing aluminum in vacuum on a quartz substrate, is inserted in the channel.

The second channel of the illuminator, which consists of a quartz-crystal lens, 4, and a plane movable mirror, 3, serves for projecting, on the input slit of the monochromator, the output aperture of the Ulbricht sphere, 5, which is used in measuring the fluxes of total and scattered radiation. The inner surface of the sphere and the surface of the protective screen are coated with barium sulfate. The diameter of the sphere is equal to 200 mm, and the diameter of the input aperture is 50 mm. The protective screen is cone-shaped. With this shape of the protective screen, /156 the cosine law for the sphere is fulfilled in the best manner [2]. There is a shade, 6, for protection from direct solar rays of the input aperture of the sphere in measurements of the scattered radiation.

The third channel, which consists of a plane movable mirror 10

*Figures set aside by commas refer to the Block Diagram [translator's note].

and a spherical concave mirror,8, directs the radiation from the standard scale of wavelengths,7,- a mercury-vapor lamp UFO-4 - onto the input slit.

The arrangement of the fourth channel of the illuminator is similar to the third. It consists of a concave elliptical mirror, 26, a plane mirror,24,and a translucent mirror,23. The purpose of this channel is to illuminate the input slit by the reference radiation from the photometric standard. A low-voltage incandescent lamp,25,serves as the photometric standard.

A modulator of the light flux,9, representing a perforated disk with two paths for the apertures, is arranged in the illuminator. The disk is planted on the axis of the electric motor with a centrifugal governor.

The monochromator of the spectrophotometer is constructed according to the vertically-symmetric design. Two concave spherical mirrors,20,and,19,with identical focal distances of f = 480 mm are used as the projecting elements of the monochromator. The radiation is split up by a diffraction grating,11, which has 600 lines per mm. The dimensions of the ruled area are 60 x 50 mm. The first order is effective. The inoperative orders of the spectrum are cut off by light filters.

The light flux is projected onto the output slits by plane mirrors,22, behind which the photomultipliers,12,are fixed. One of them, with an antimony-cesium photocathode (FEU-17), is intended for recording the ultraviolet radiation with wavelength from 280 to 380 nm. The second photomultiplier has a multi-slit photocathode (FEU-51). The radiation with wavelength from 380 to 715 nm is recorded with the latter. The photocathode of the third photomultiplier is an oxygen-cesium one (FEU-62). It is used for recording the radiation from 700 to 1100 nm.

The operational principle of the spectrophotometer is the following. The radiant flux $\Phi_1(\lambda)$ being analyzed, focused at the input slit of the monochromator by the first or second channel of the illuminator, passes through the modulator, where it is modulated by one of the paths with frequency f_1 equal to 1500 Hz. The reference flux $\Phi_2(\lambda)$, which also passes through the modulator, where it is modulated by the other path with frequency f_2 equal to 1000 Hz, is focused on the same slit with the aid of the fourth channel of the illuminator.

The monochromatic beams of the radiation sent by the monochromator go to the photocathodes of the photomultipliers through the output slits. The signals from the photomultipliers are trans- /157
mitted to the commutator,13,through the cathode repeaters which are mounted together with the photomultipliers. The commutator transmits the signal from one of the photomultipliers to the calculating-

resolving device [3] automatically, in dependence on the photometering spectral region. The calculating-resolving device consists of a cascade with regulated coefficient of amplification,14, a selective amplifier of the analyzed signal,15,tuned to the modulation frequency f_1 of the analyzed flux $\Phi_1(\lambda)$, a selective amplifier of the contrast signal,13,tuned to the modulation frequency f_2 of the reference flux $\Phi_2(\lambda)$, a differential amplifier,21,and an oscillator,18.

The voltage at the output of the selective amplifier,15,is equal to

$$U_1 = \Phi_1(\lambda)\,\Delta\lambda\tau(\lambda)\,\gamma(\lambda)\,k_1k_2k_3, \tag{1}$$

while, at the input of the selective amplifier 16, it is equal to

$$U_2 = \Phi_2(\lambda)\,\Delta\lambda\tau(\lambda)\,\gamma(\lambda)\,k_1k_2k_4, \tag{2}$$

where $\Delta\lambda$ is the spectral interval isolated by the monochromator; $\tau(\lambda)$ is the transmission coefficient of the monochromator; $\gamma(\lambda)$ is the sensitivity of the photoreceiver; k_1 is the transfer constant of the cathode repeater; k_2 is the transfer constant of the cascade with regulated amplification coefficient; k_3 is the amplification factor of the selective amplifier of the analyzed signal, 15, k_4 is the amplification factor of the selective amplifier of the contrast signal.

The signal U_1 being analyzed is transmitted to the recorder, 17, while the contrast signal is sent to the differential amplifier,21. The signal U_3 from the oscillator,18,is sent to the same differential amplifier. The signal U_3 changes during the process of spectrum scanning in a way similar to the change of the spectral emissivity of the source of the reference emission:

$$u_3 = k_5\Phi_3(t), \tag{3}$$

where k_5 is the mechanical coefficient of the oscillator; t is the scanning time

$$\Phi_3(t) = \Phi_2(\lambda) \tag{4}$$

for a connection of $\lambda = vt + \lambda_0$. Here v and λ_0 are certain constants: v is the speed of spectrum scanning, λ_0 is the initial

scanning wavelength.

The difference in the signals $\Delta U = U_3 - U_2$ is amplified by the differential amplifier and sent to the cascade with variable amplification coefficient k_2 as the master voltage U_{mas}. The coefficient k_2 varies monotonously with a change in U_{mas} [4]:

$$k_2 = k_2(U_{mas}) = A(U_3 - U_2' k_2), \tag{5}$$

where A is a positive number proportional to the coefficient of amplification of the differential amplifier, but which depends on the value of U_{mas} in the general case; $U_2 = \Phi_2(\lambda)\Delta\lambda k_1 k_4$. /158

It follows from (5) that

$$k_2 = \frac{AU_3}{1 + AU_2'}. \tag{6}$$

For a rather high value of A, (6) is simplified, converting into the following equation:

$$k_2 \approx \frac{U_3}{U_2'} = \frac{k_5 \Phi_3(t)}{\Phi_2(\lambda)\Delta\lambda\tau(\lambda)\gamma(\lambda)k_1 k_4}. \tag{7}$$

Thus, the feedback automatically keeps the value of the amplification factor k_2 close to the value of U_3/U_2'.

The accuracy with which (7) approximates (6) depends on the value for the amplification factor of the differential amplifier and the value of u_2'. These have such values in our design that the product of Au_2' is greater than 100; therefore, the accuracy of (7) is better than 1%.

Substituting an explicit expression for k_2 into (1) with a consideration of (4), we can find the following expression for the signal sent to the input of the recorder:

$$U_1 = \frac{k_3 k_5}{k_4}\Phi_1(\lambda) \equiv k\Phi_1(\lambda), \tag{8}$$

i.e., U_1 does not depend on the selective transmission of the monochromator or the sensitivity of the photoreceivers.

It seems to us that the proposed dual-beam spectrophotometer has definite advantages over the previously-known single-beam spectrophotometers for recording emission spectra in which compensation for the variable spectral sensitivity of the photocathode and

the variable transmittance of the optics of the monochromator occurs directly, and not because of the use of a contrast flux [5,6,7]. The fact is that, in the direct compensation for the change in spectral sensitivity of the spectrophotometer, a rather complex function of the type $\gamma(\lambda)\tau(\lambda)$ must be modeled during the spectrum-scanning process, or the converse function $\frac{1}{\gamma(\lambda)\tau(\lambda)}$; these functions have a large number of extrema. On the other hand, in using the dual-beam design with a contrast source, a more suitable function $\Phi_2(\lambda)$ is modeled, and it is close to the Planck function, with a monotonous nature in the region of interest to us.

REFERENCES

1. Mikhaylov, V.V. and V.P. Voytov: Universal Spectrophotometer for Studying the Field of Short-Wave Radiation in the Atmosphere. In the Collection: Problemy fiziki atmosfery (Problems of Atmospheric Physics), No. 4. Leningrad State University Press, 1966.
2. Niylisk, Kh.: A Simplified Spectrophotometer for Measuring Spectral Fluxes of Scattered Radiation. In the Collection: Issledovaniya po fizike atmosfere (Studies on the Physics of the Atmosphere), No. 3, Institute of Physics and Astronomy of the Academy of Sciences of the Estonian S.S.R., Tartu, 1962.
3. Hasky, G.D. and G.A. Korn: Vychislitel'naya tekhnika (Computer Technology), Vol. 1. Foreign Literature Publishing House, 1955.
4. Korn, G. and T. Korn: Elektronnyye modeliruyushchiye ustroystva na postoyannom toke (Electronic Modeling Devices on Direct Current). Foreign Literature Publishing House, 1955.
5. Shklover, D.A.: Methods of Measuring the Optical Characteristics of the Emission of Luminophors, Luminescent Lamps and Cathode-Ray Tubes. Izvest. Akad. Nauk S.S.S.R., ser. fiziki, Vol. 15, No. 6, 1951.
6. Martin, A.E. and S.N. Roberto: Measuring Color of Cathode-Ray. Screens, Vol. 23, No. 2, 1950.
7. Coch, G., W. Taylor and H. Johnston: A Recording Grating Spectrometer with Linear Wave-Length Scale. J. Opt. Soc. Amer., Vol. 41, No. 2, 1951.

RADIATION BALANCE AND ITS COMPONENTS IN THE TROPOSPHERE AND STRATOSPHERE ACCORDING TO ASCENTS OF AIRSHIPS IN THE AUTUMN IN 1964-1965

K.Ya. Kondrat'yev, N.M. Yevdokimova and G.A. Nikol'skiy

ABSTRACT: The radiation balance and its components in the troposphere and stratosphere are discussed on the basis of data from actinometric airship soundings in the autumn in 1964 and 1965. It is suggested that, particularly in the cases under investigation, a volcanic eruption and an increase in meteors could bring about an anomalous decrease of direct solar radiation.

Introduction

The results of actinometric soundings of the troposphere and stratosphere in the autumn in 1964 and 1965 are presented in this stody. There was one launching in the autumn of 1964 (October 23), and two in 1965 (October 1 and 21). The launching on October 21 was coordinated with the time the comet Ikeya-Seki passed near the Sun. /160

The radiation fluxes were studied with the aid of a standard actinometric system, which was described in [1, 2]. Two parallel instruments were used for the actinometer of Yanishevskiy in the launchings in 1965 for the purpose of refining the corrections for the pressure. One actinometer was enclosed in a pressurized casing, the pressure in which remained unchanged and equal to 1000 mb during the flight. The direct solar radiation penetrated into the casing through a quartz window, and its passage was carefully investigated; particular attention was given to the transmission in the ultraviolet spectral region. It was explained that the transmission of the window was practically constant and equal to 94% in the spectral region from 0.25 to 3 μm. In the range of wavelengths less than 0.23 μm, the transmission decreased slowly, but this should not be reflected on the results of the measurements, since the intensity of the radiation with such wavelengths was negligibly small even at altitudes of 30-33 km [3]. The other actinometer operated without any changes in design. The temperature of the cold junctions of the thermal was measured for both actinometers. A simultaneous measurement of the intensity of direct solar radiation by the two actinometers aided in evaluating the effect of the changing pressure under the real conditions of the ascent of the airship. Thus, in a pressure change from 760 to 30 mm Hg, the correction for the pressure increased from 0 to 2.4%.

Direct Solar Radiation /161

The profiles of direct solar radiation S 1 and 3 (Figure 1) were obtained -- one in 1964, and the other in 1965 -- for identical heights of the Sun of 26.32° and for almost equal distances from the Sun to the Earth. The air mass in the sounding site can be determined according to the form of the profiles. For Profile 1, the initial point is at an altitude of 1.96 km, since there is a layer of solid clouds (Sc_5 10/0) at altitudes of 1.00-1.96 km. Above the cloud layer, there is a layer of air with increased turbidity and humidity (from 2.6 to 5 km), as indicated by the low value of S = 1.21 cal/cm^2·min at an altitude of H = 1.96 km and the large gradient of S in this layer; for example, the gradient is equal to 0.15 cal·cm^{-2}·min^{-1}/km in the lower part of the layer. The formation of a layer with such diminishing properties is connected with the presence of temperature inversions at altitudes of 2 and 5 km, although the depth of these inversions is small (0.5°C). A relatively uniform mass is found above 5 km.

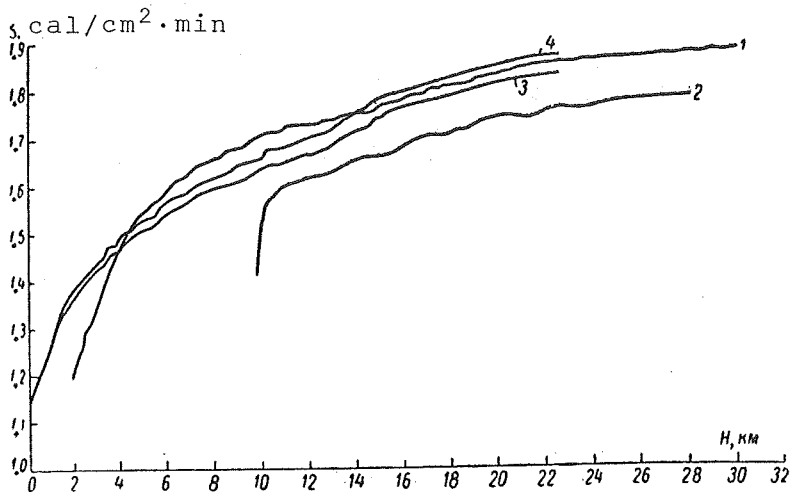

Figure 1. Fluxes of Direct Solar Radiation. (1) 10/23/1964; (2) 10/1/1965; (3) 10/21/1965; (4) 10/21/1965 (without correction for the pressure).

Profile 3 in the troposphere has a form which differs from Profile 1. In this case, the principal decreasing mass is not located in a narrow five-seven kilometer layer, as occurred for Profile 1, but extends up to 16 km and higher. The lower three-kilometer layer in this case is substantially turbid, as is ordinary for the sounding site. The layer of 6-13 km has average reduction factors, and, at the upper boundary of this layer, the value S = 1.67 cal/cm^2·min, which is less than the extreme low value fixed /162

in the previous flights ($S_{13\ km}$ = 1.71 cal/cm^2·min), i.e., this profile indicates that there are overlying attenuating layers. The layer of 13-16 km is less transmittive (0.023 cal·m^{-2}·min^{-1}/km than the layer of 6-13 km, where the gradient is 0.0166 cal·cm^{-2}·min^{-1}/km. However, the value of S remains decreased above the layer of 13-16 km, in comparison with the average value for several flights. From Profile 2, which has a nature similar to that of Profile 3 in the stratosphere, it can be seen that, up to an altitude of 28 km, there is no layer or layers in which a similar decrease in S could occur.

At an altitude of 22.5 km, we find that S_3 = 1.8 for the pressurized actinometer and S_4 = 1.85 for the open one, according to Profiles 3 and 4. Profile 2 gives a value of S = 1.79 for the pressurized actinometer only at an altitude of H = 28 km. According to Profile 1, for an altitude of 28 km we have S = 1.94 cal·cm^{-2}·min^{-1} (open actinometer), while, if we consider the correction for the pressure, S decreases down to 1.89. Thus, the difference in the values of S according to Profiles 1 and 2 for different conditions is 0.10 cal/cm^2·min at an altitude of 28 km, while it is equal to 0.05 cal/cm^2·min for Profiles 1 and 3 at an altitude of 22.5 km. It can be said that the values of S obtained in the flights of October 1 and 21, 1965 indicate that there is a diminishing layer of an aerosol origin on the path of the solar ray above 28 km, since the concentration of other weakening components necessary for such a decrease at altitudes higher than 28 km is doubtful. We should mention that the reduction component can be found, not only in the Earth's atmosphere, but also outside it.

The profile for S obtained on 10/23/1964 (Curve 1) is above the others, except for part of Profiles 3 and 4 in the layer up to 4 km, and part of Profile 4 at altitudes of 15-22.5 km. However, we should note that Profile 4 was presented only in order to illustrate the effect of the pressure on the indixes of the actinometer, whereas the real changes in S during the flight on 10/21/1965 are represented by Profile 3. The decrease of S up to altitudes of 9 km in the two cases presented varies to a large extent. For example, on October 23, in the air layer above the clouds, which had exceptionally high attenuating properties, the values for the direct solar radiation varied at an altitude of 2 km (Profiles 1 and 3) by 0.15 cal/cm^2·min, while they differed by 0.05 cal/cm^2·min at an altitude of 6 km. At an altitude of 9 km, $\Delta S_{1.3}$ = 0.075 cal/cm^2·min. In the layer of 9-13.5 km, this difference was practically constant. On October 21, 1965, the attenuation in the layer of 13.5-15.5 km was 0.03 cal·cm^{-2}·min^{-1}/km, and was clearly of an aerosol origin. $\Delta S_{1.3}$= 0.025 at an altitude of 15.5 km. Above this, the difference increased slowly up to 0.035 at an altitude of 22.5 km.

The flight of October 1 can be separated from all the others because of the low values of S at all altitudes. During this day, there were three-layered clouds extending up to an altitude of 10 km; therefore, the recording of S_2 began only when the apparatus /163 left the dense cloud layer at an altitude of 9.8 km. It is possible that the semitransparent clouds extended up to 10.7 km. At altitudes of 11-13 km, the values of S_2 only by 0.06 cal/cm^2·min. Above 14 km, Profile 2 changed insignificantly, and its graduated form indicated that there were a number of aerosol layers (15-17 km, around 19 km, 21.5-22.5 km, etc.). After passing through these layers, the value for the intensity of direct solar radiation nevertheless remained anomalously low - 1.79 cal/cm^2·min, while $\Delta S_{1.2}$ was 0.1 cal/cm^2·min at 28 km altitude. If we assume that the values of S_1 in the stratosphere are close to the average values for the autumn, then we should mention that, on October 1, the air mass in the stratosphere up to altitudes of 28 km had a relatively small decrease, despite the presence of aerosol layers. Consequently, the anomalous attenuation can be related only to the presence of an aerosol component above 28 km, since the ozone concentration at an altitude of 22 km on October 1 was only 1.5 times less than on October 23 (Profile 1), while the ozone distributions by altitude differed insignificantly in these flights. If we compare Profiles S_2 and S_3, we can see that the reason for the anomalously low values of S_2 also held on October 21 (Profile 3), but the effect of this cause was reduced (anomalous decrease shortened from 6 to 2%). This could be due to the deposit of an aerosol mass, which then collected in the layer of 13-15.5 km.

The profiles for S in the lower stratosphere have a roughly parallel course, broken by aerosol layers, which give the profiles a graduated appearance. The laminar structure of the stratosphere brings about a shift of the profiles, but the parallelism of the course of Profiles S_1 and S_3 is preserved after the passage of this layer. This course indicates that the principal decrease occurs because of the exponentially distributed components of the atmosphere. The change in gradient of Profiles S_1 and S_3 at an altitude of 22 km is probably linked with the passage of a layer of maximum ozone and aerosol concentration [7].

In 1963-1964, an anomalous reduction of S was observed at meteorological stations over Antarctica and the Hawaiian Islands [4,5]. The most probable reason for this phenomenon was considered by the authors of [5] to be the emission of volcanic dust into the atmosphere during the eruption on Bali Island. On the Hawaiian Islands, the anomalous reduction was noted more after the eruption, and was observed for three months. The magnitude of the anomalous reduction changed from 3 to 6%. At the South Pole station, an anomalous reduction was observed from November of 1963 for the course of one year and longer. The greatest value for the anomalous decrease was equal to 22%, and noted in November of 1963. In both cases, the magnitude of the anomalous reduction was evaluated according to the ratio between the intensities of direct solar radiation

at a given moment and the average value for several previous years /164
for a given moment.

A different explanation for the anomalous decrease of S was suggested in [4]. The authors indicated that an increase in the number of meteors was noted in the middle of 1963, which could bring about an increase in the quantity of the aerosol component in the upper layers of the atmosphere. The settling particles of meteor origin can corm layers of increased particle concentration in the mesosphere and the lower stratosphere because of inversions and turbulent vertical motions. The contribution of these layers to the reduction is indisputable, and is realized largely in the form of scattering. Therefore, the values for the scattered radiation in the stratosphere at this time should be much higher than average. The supporters of the volcanic theory for the origin of this phenomenon completely reject the meteor variation, considering the extreme length of the phenomenon of anomalous reduction (more than a year). In our opinion, there was an interaction of both the cited causes here, supplementing each other in time and intensifying the decrease in solar radiation. A comparison of the results of the airship sounding of the atmosphere in 1963 and 1964 shows that, despite the substantial difference in heights of the Sun, the values for the intensity of direct solar radiation at an altitude of 30 km are 1% higher for October of 1964 ($h_{\odot} = 26.5°$) than for July of 1963 ($h_{\odot} = 58°$).

G.V. Rozenberg [6] suggested an explanation for the physical causes of the anomalous decrease, using Young's idea of the mechanism for the formation of an aerosol layer at an altitude of 20-25 km and the results of a test of aerosol samples in this layer (chemical analyses show that 84% of the aerosol consists of sulfuric compounds). It was proposed that the sulfur dioxide ejected into the stratosphere reacts with ozone, as a result of which sulfur compounds of $(NH_4)_2SO_4$ and $(NH_4)_2S_2O_8$ are formed; the latter play the role of the reducing component. Certainly, during eruptions, when the passage of SO_2 to the stratosphere increases sharply, the capacity of the aerosol layer increases at altitudes of 20-25 km. However, we must also mention that, in the eruption of a volcano, a substantial amount of fine dust particles and ashes pass into the stratosphere. Thus, in the eruption of the Taal volcano on Luzon Island on September 28-30, 1965, the ejection of matter into the atmosphere amounted to 30-40 million tons, according to preliminary evaluations [7]. Eyewitnesses said that a cloud, consisting of dust and ashes, vapor and volcanic gases, climbed to an altitude of 15-20 km and then moved to the west. It is completely probable that some of the matter ejected into the stratosphere could be carried to significant distances by stratospheric jet streams, the velocities of which were 100 km/hour and higher during the autumn at altitudes of about 30 km. When there was a jet stream with such velocities moving northwest, turbidity of the stratosphere in the middle band of the European territory of the Soviet Union /165
could occur even on October 1. The matter ejected by the eruption-

explosion which was not settled on the first days was gradually spaced over the entire globe by stratospheric air currents.

An increase in the aerosol component can be noted at those ground stations where the local conditions do not create a substantial turbidity in the troposphere, or in radiation sounding of the atmosphere, when the solar radiation is measured continuously. There is no doubt that the anomalous decreased observed during the flights on October 1 and 21, 1965 was connected with the eruption of the Taal volcano. Therefore, we can say that the products of the eruption or their derivatives could propagate at velocities higher than 100 km/hour, and that the removal of the reducing component of volcanic origin from the stratosphere could take 1-1.5 months.

Thus, we can conclude that the ash-dust component of the aerosol layer at altitudes of 17-30 km is variable, and that particles with dimensions less than 1 μm can be kept at these altitudes for a long time.

Reflected Total and Scattered Radiation

The profiles for the reflected radiation R for the three autumnal flights were obtained under completely different meteorological situations (Fig. 2): with one-layered clouds at an altitude of 1-2 km (Curve 1); with three-layered clouds from the altitude of the upper boundary of 10.5-10.7 km (Curve 2); in slightly-cloudy weather (Curve 3). The highest values of R = 0.695 were obtained in the flight on 10/1/1965 over upper-level clouds (upper boundary of 10.7 km), and these values remained unchanged in the layer over the clouds with thickness of 2.3 km. The decrease in R above 13 km was connected with the decrease in the number of clouds below the airship, and also with the shielding effect of the aerosol layers when they remained below. A similar phenomenon, but at lower altitudes, occured in the flight of 10/23/1964 for a lower-level cloud layer. The profile of reflected radiation 3 relates to slightly cloudy weather. The changes in R from 0.11 to 0.2 cal/$cm^2 \cdot min$ are average for the autumn.

The total radiation Q is represented in Figure 2 only by two profiles, 4 and 5. The fluxes of total radiation were related to a height of the Sun of 26.32°. The greatest difference, on the order of 0.4 cal/$cm^2 \cdot min$, at altitudes up to 2 km was connected with the difference in cloud conditions on these days. These differences are concealed above this altitude, and Profiles 4 and 5 come in contact at the 9 km altitude, although the profiles for S differ substantially at this altitude. The complex relationship between the values of $S' = S \sin h_\odot$ and the fluxes of scattered radiation D_1 and D_2 (Fig. 2) changing at this altitude resulted in a situation where the course of the profiles was similar and the values of Q were close for these flights. Only above the tropopause

did the fluxes Q_4 and Q_5 begin to diverge. The reason for this is /166 found in the phenomenon of anomalous decrease of S in the stratosphere. An aerosol layer at altitudes of 13-15 km is clearly noticeable in the course of Q_5. The profile of Q_4 lies below Profile Q_5. This Q-ratio can be explained by the increased values of the scattered radiation in the flight of 10/21/1965 (Profile D_2), which were obtained under the conditions of an anomalous reduction of S. The value of D_2 at an altitude of 22 km is equal to 0.05 cal/cm^2·min, although the values of D at these altitudes in other flights are within the limits of measurement errors. The values for the scattered radiation represented by Profile D_1 are typical for air masses with good transmittance.

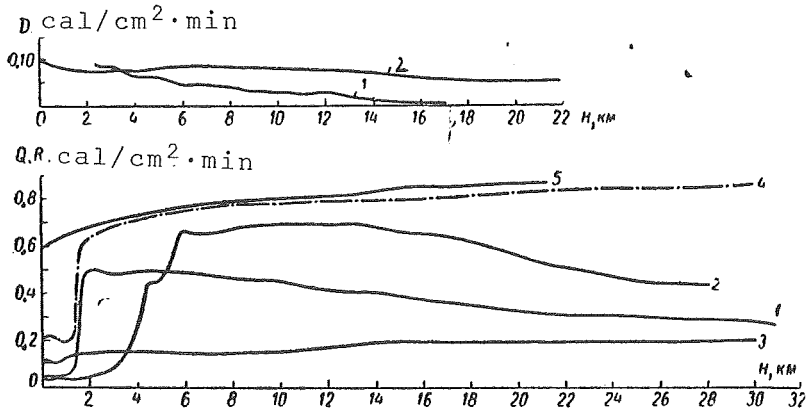

Fig. 2. Vertical Profiles of Total, Reflected and Scattered Radiation. Reflected Radiation R: (1) 10/23/1964; (2) 10/1/1965; (3) 10/21/1965; Total Radiation Q: (4) 10/23/1964; (5) 10/21/1965; Scattered Radiation D: (1) 10/23/1964; (2) 10/21/1965.

Radiation Balance and Its Long-Wave Components

The autumnal profiles for the net radiation balance are also represented by three curves (Fig. 3a). It is of interest that Profiles 1 and 2 coincide almost completely from the level of the ground to an altitude of 18 km. There was a cloud cover in both cases, the only difference being that its thickness was 1 km and it propagated at altitudes of 1-2 km for Profile 2, while the cloud cover for Profile 2 extended upwards up to 10.7 km. The deviation of the profiles above 18 km was connected with the increased turbidity in the stratosphere due to the presence of an aerosol component. Profile 3 was obtained under the conditions of slightly /167 cloudy weather, and its course corresponds largely to the typical profile for the autumn. Thus, an increase in the balance is observed in the stratosphere for cloudy weather, and a small decrease is observed for cloudless weather.

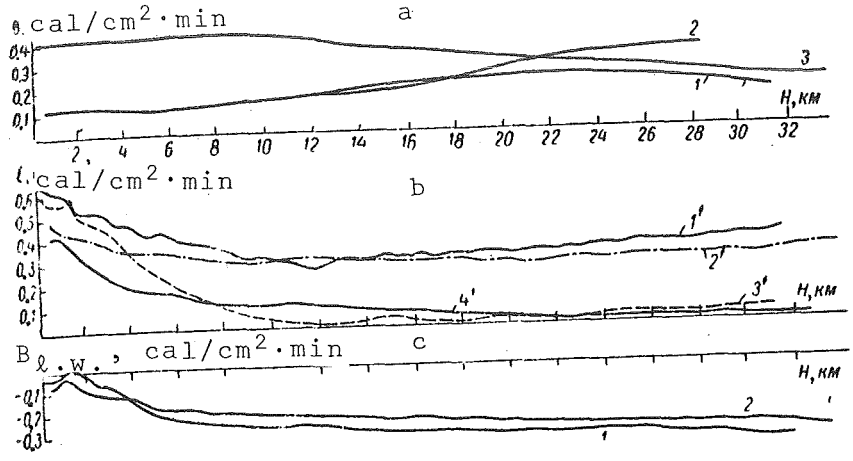

Fig. 3. Profiles of the Net and Long-Wave Radiation Balance and Long-Wave Components.
(a) Profiles of the Net Radiation Balance: (1) 10/23/1964; (2) 10/1/1965; (3) 10/21/1965. (b) Ascending Long-Wave Fluxes: (1) 10/23/1964; (2) 10/21/1965. Descending Fluxes: (3) 10/23/1964; (4) 10/21/1965. (c) Long-Wave Radiation Balance: (1) 10/23/1964; (2) 10/21/1965.

The profiles for the long-wave ascending and descending fluxes and long-wave balances are represented for two flights (Fig. 3b,c). In the first flight, the profiles of $E_1^{\uparrow}$ and $E_3^{\downarrow}$ change almost only in the troposphere, for the presence of clouds and a pure stratosphere. Near the underlying surface, the ascending and descending fluxes are close (0.62 and 0.59 cal/cm^2·min), while they are equal in the middle of the cloud layer. The ascending flux $E_1^{\uparrow}$ has a minimum below the tropopause, and then there is a slow increase up to a value of 0.37 cal/cm^2·min at the 31 km altitude. The descending flux in the stratosphere is close to zero, but begins to increase gradually as the temperature of the air increases.

The course of the profiles obtained on 10/21/1965 has a somewhat different form. This can be explained by the absence of clouds and the increased aerosol concentration. The ground values were such: $E_2^{\uparrow}$ = 0.506 cal/cm^2·min, $E_4^{\downarrow}$ = 0.435 cal/cm^2·min. The change in fluxes during the ascent was much less, and there were no abrupt variations in the tropopause. A particularly smooth increase was observed for $E_2^{\uparrow}$, which was probably linked with the scattering of long-wave radiation on aerosol particles. The value of $E_2^{\uparrow}$ at an altitude of 31 km was equal to 0.29 cal/cm^2·min. Above /168
30 km, a small increase in $E_2^{\uparrow}$ was noted.

The long-wave balance was constructed according to the net and short-wave balances obtained (Fig. 3c, Curve 2). Figure 3 also

shows one profile of the long-wave balance (Curve 1) for the flight of 10/23/1964. There are many general features in these two profiles which had been obtained other years. A warm-up of the air in the lower 1-15 km layer due to absorption of the radiation of the underlying surface was observed in both profiles. For Profile 1, the transition from the warm-up to cooling occurs in the middle of the cloud layer, while, for Profile 2, it occurs at an altitude of 1 km. Above this, there is a layer of air (up to 2-2.5 km) where there is intensive cooling. Then there follows a layer where transformation of long-wave energy practically does not occur. In one case, its thickness was 0.5, and, in the other case, it was 1 km. An intensive cooling up to an altitude of 5 km then occurs again for both profiles. Above 5 km and up to the upper sounding point for both profiles, there is cooling, but its speed is much less than in the lower layers. The course of the long-wave balance is, in general outline, opposite to that of the short-wave balance.

REFERENCES

1. Kondrat'yev, K.Ya., G.N. Gayevskaya and G.A. Nikol'skiy: Experimental Investigations of the Radiation Banance in the Free Atmosphere. In the Collection: Problemy fiziki atmosfery (Problems of Atmospheric Physics), No. 1. Leningrad State University Press, 1963.
2. Kondrat'yev, K.Ya., G.N. Gayevskaya and G.A. Nikol'skiy: Airship Studies of the Radiation Balance of the Earth's Surface-Atmosphere System. Kosmicheskiye Issledovaniya, Vol. 1, No. 3, 1964.
3. Kondrat'yev, K.Ya.: Aktinometriya (Actinometry). "Gidrometeoizdat", 1965.
4. Ellyett, C.D., and C.S.L. Keay: Meteors:An Unexpected Increase in 1963. Science, Vol. 146, No. 3650, 1964.
5. Flowers, E.C., and H. J. Viebrock: Solar Radiation: An Anomalous Decrease of Direct Solar Radiation. Sciences, Vol. 148, No. 3669, 1965.
6. Rozenber, G.V.: Discovery of Cosmic Sunrises and Sunsets. Priroda, No. 3, 1966.
7. Moore, J.G., K. Nakamure and A. Alcaraz: The 1965 Eruption of Taal Volcano. Science, Vol. 151, No. 3713, 1966.

SOME PROBLEMS IN THE METHOD OF ANALYZING THE RESULTS OF OBSERVATIONS OF RADIATION BALANCE COMPONENTS

G.A. Nikol'skiy and S.G. Shugayeva

ABSTRACT: The errors in measurements of the radiation balance which are connected with a deviation of sensitive areas of pyranometers from a horizontal position are discussed in relation to 19 airship flights carried out from 1961 to 1965. The effects of the temperature and pressure, the envelope of the airship, spectral and angular corrections, and calibration are considered.

From 1961 to 1965, actinometric apparatus were launced on 19 /169
airships. Standard pyranometers of Yanishevskiy were used to measure the total raidation in all the flights. Naturally, the use of pyranometers in the airship flights required a special method for analyzing the data of these instruments.

The most important factor which complicates an analysis of the measurement results is a deviation from horizontal position of the sensitive areas of the pyranometers. The temperature and pressure have a substantial effect on the sensitivity of a pyranometer. Moreover, the temperature affects the amount of resistance of the measuring circuit. In low-impedance circuits, a change in the resistance affects readings much more greatly than does a change in sensitivity. Substantial errors can appear in airship measurements if the spectral and angular corrections and the effect of the envelope of the airship are disregarded.

Elimination of Errors Connected with a Deviation of the Sensitive Area from a Horizontal Position

Since a flux of radiation incident on a lower pyranometer can be considered, in first approximation, to be isotropic, a deviation of the sensitive area from a horizontal position should not cause noticeable distortions in the indices of the instrument. A turn of the sensitive area of an upper pyranometer from its horizontal position has a substantial effect on its indices, since direct solar radiation, which is the principal part of the total radiation in a clear sky, is incident on this sensitive area. Important studies on a method for pyranometric aircraft measurements were carried out by V.G. Kastrov [1,2]. Kastrov showed that the errors connected
with a non-horizontal position of the sensitive area of the upper /170
pyranometer are increased for high zenith distances of the Sun (>60°) and when the results of the measurements are not averaged

over the azimuth. That is why there are always repeated readings of the pyranometer for the same altitude and for two opposite courses of the aircraft ("Sun on the left" and "Sun on the right") in pyranometric aircraft measurements. The use of such a measurement method is impossible in airship flights. In this case, the fact that an airship turns around the vertical axis simplifies the situation.

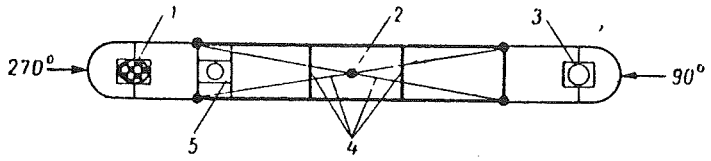

Fig. 1. Arrangement of Actinometric Instruments on Frame-Wiring. (1) Pyranometer; (2) Suspension Patch; (3) Balance-Meter; (4) Cables; (5) Celestial-Guidance Block.

The apparatus is suspended on the airship on a control cable with length up to 70 m. Since the frame-wiring is somewhat asymmetric aerodynamically relative to the suspension patch, then the arisal of torque on the cable is possible. Moreover, one reason for the fact that a rotation of the frame-wiring is observed at certain levels could be the difference in velocity and direction of the wind in neighboring layers of air. The orientation instrument which makes it possible to follow this rotation and determine the position of the instrument relative to the Sun at every moment of time is the celestial-navigation block. In analyzing the data of the celestial-navigation block, the control tie-in of readings of the solar azimuth by the graticule is based on the position of the instruments on the frame-wiring. For example, if the azimuth is equal to 270°, then there is a peak on the record of the data from the balance-meter due to the shade from the cable when the balance-meter is located in the same position on the wiring as shown in Figure 1. This disturbance on the indices of the pyranometer is observed for an azimuth of 90°. The data of the celestial-navigation block are marked on the tape of the oscillograph.

Let us consider the behavior of wirings with the instruments during Flights No. 15, 18 and 19. Segments of rapid rotation alternate with slow rotation (Fig. 2). The number of revolutions to one side can reach 10 and, in addition to the cited reasons for the revolution, there is also the speed of ascent. Rolling then takes place, but the number of revolutions decreases. As the airship ascends, the rotation diminishes, and ceases completely upon entry into the equilibrium zone, and only slight oscillations in the range of 90° remain. The angular velocity during the climb changes continuously. A maximum value of the angular velocity of /171
1-1.5 rev/min is fixed.

The rotation changes the azimuth of the Sun relative to the longitudinal axis of the frame-wiring. Since the radiation receiver has a certain non-horizontal position and an azimuthal dependence, then a wavy curve whose period is variable will be fixed on the recorder tape. It is easy to find which azimuth corresponds to the increased index of the instrument and the converse, and, consequently, to which side the instrument is inclined. An analysis of the results of flights No. 11, 15, 18 and 19 showed that the maximal indices of the pyranometers are observed in the intervals of 140-200° (for flight 11), 200-260° (for flight 15), 240-260° (for flight 18), 300-340° (for flight 19), while the minimal values correspond to intervals of 340-020°, 0-60°, 60-100° and 140-180°, respectively. This substantial angle spread (40-60°) indicates that the pyranometer in the Cardan joint nevertheless has a variable inclination. We must also keep in mind that, in addition to the vibrational motions, the wiring with the instruments is subjected to swinging oscillations during the climb. The swinging oscillations also disturb the horizontal position of the sensitive areas. These errors can reach values of 10-20%, depending on the vertical gradients of the wind velocity. They can be decreased to 2-4% by averaging the sinusoidal curve which the instrumental indices give during swinging oscillations. Obviously, inaccuracy in this averaging makes a substantial contribution to the angle straggling over the azimuth. After this preliminary analysis, we will turn directly to means of eliminating the errors due to the non-horizontal position of sensitive areas.

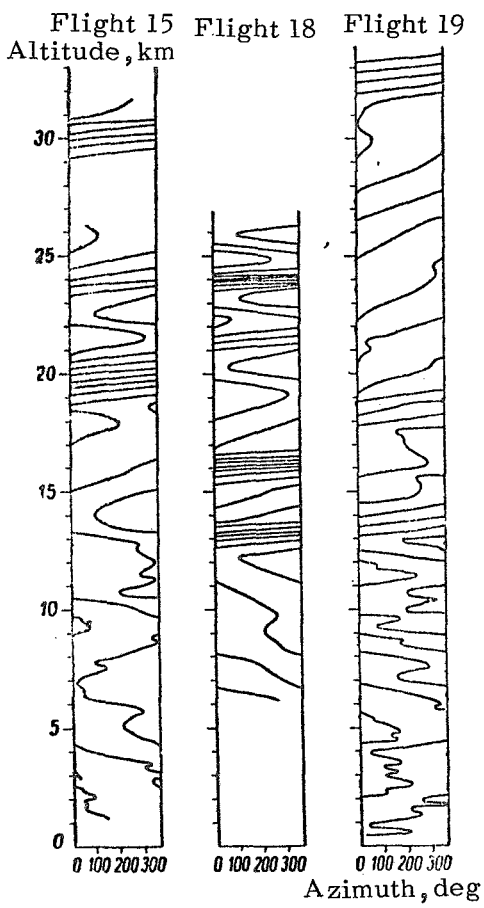

Fig. 2. Behavior of the Frame-Wiring with Instruments during Flights No. 15, 18, 19.

Let us first examine the ranges of rapid rotation of the frame-wiring (Fig. 3). The indices of the pyranometer are recorded in these segments in the form of a wave-like curve whose period acquires a minimal value. The maximal readings by this curve correspond to the maximal inclination of the instrument toward the Sun, while the minimal values correspond to minimal inclination from the Sun. Using the data presented in [3], we can find the magnitude of the angle of inclination of the sensitive area from the

from the horizontal position according to the ratio between the /172

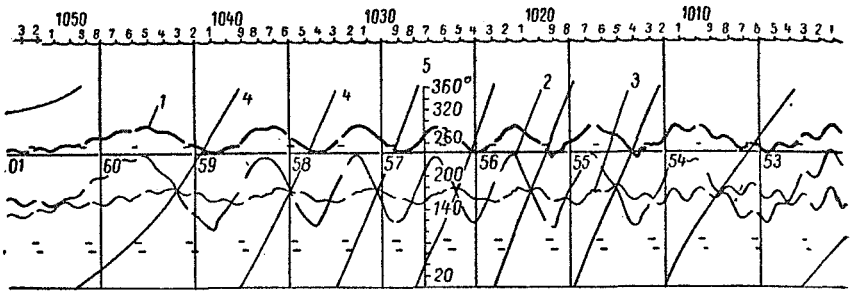

Fig. 3. Part of the Record of Indices of Actinometric Instruments on Oscillograph Tape (Flight No. 11).
(1) Curve of the Balance-Meter Indices; (2) Same, of the Upper Pyranometer, without Cardan Joint; (3) Same, of the Upper Pyranometer in a Cardan Joint; (4) Curve for the Rotation of the Frame-Wiring with the Instruments; (5) Angles of Rotation Relative to the Sun.

the averaged maximal reading and the averaged minimal one $(\frac{\overline{n}+}{\overline{n}-})$, i.e., we can find $\Delta h = h_H - h_\odot$, where h_H is the height of the Sun over the inclined sensitive area of the pyranometer; $h_\odot$ is the height of the Sun over the horizon. The angle Δh is determined by linear interpolation with accuracy up to 0.1° from Table 1.

TABLE 1. DEPENDENCE OF THE RATIO $\frac{\overline{n}+}{\overline{n}-}$ ON THE ANGLE OF INCLINATION OF THE PYRANOMETER Δh AND THE HEIGHT OF THE SUN $h_\odot$

Δh, deg.	$h_\odot$				
	20°	30°	40°	50°	60°
1	1.11	1.06	1.04	1.03	1.01
2	1.22	1.12	1.08	1.05	1.03
3	1.33	1.19	1.11	1.08	1.05
4	1.45	1.25	1.15	1.11	1.06

An analysis of the measurement results showed that the angle /173
of inclination of the pyranometers was equal to 2° on the average. We must then determine the reduction coefficients for the angles of inclination found. These coefficients were obtained by Y.e.A. Lopukhin [4] experimentally for heights of the Sun from 10 to 70° (Table 2). Having multiplied the maximal and minimal readings by the corresponding coefficients, we can find the average index of the pyranometer corrected for the non-horizontal position. As calculations show, this value differs from the mean arithmetic

value for a given segment of the record by 2-4%. Consequently, the errors connected with an inclination of the pyranometer toward the Sun are 2-4% less than the errors connected with an inclination of the pyranometer away from the Sun.

TABLE 2. CORRECTION COEFFICIENTS FOR REDUCING THE INDICES OF THE PYRANOMETER INCLINED BY AN ANGLE Δh FROM A HORIZONTAL POSITION TO THE INDICES OF THE PYRANOMETER FIXED HORIZONTALLY FOR DIFFERENT HEIGHTS OF THE SUN $h_{\odot}$ OVER THE HORIZON

Δh*, deg.	$h_{\odot}$						
	10°	20°	30°	40°	50°	60°	70°
+10	0,581	0,718	0,834	0,870	0,905	0,937	0,966
+ 9	0,608	0,718	0,834	0,880	0,913	0,948	0,969
+ 8	0,632	0,740	0,850	0,890	0,921	0,948	0,972
+ 7	0,668	0,766	0,863	0,902	0,930	0,955	0,975
+ 6	0,700	0,795	0,878	0,913	0,938	0,961	0,979
+ 5	0,733	0,824	0,893	0,924	0,945	0,967	0,982
+ 4	0,780	0,852	0,911	0,936	0,954	0,974	0,986
+ 3	0,829	0,885	0,929	0,948	0,965	0,981	0,990
+ 2	0,885	0,920	0,951	0,964	0,975	0,987	0,993
+ 1	0,942	0,958	0,972	0,982	0,986	0,994	0,996
0	1,000	1,000	1,000	1,000	1,000	1,000	1,000
− 1	1,104	1,060	1,030	1,018	1,013	1,009	1,004
− 2	1,205	1,119	1,064	1,038	1,025	1,018	1,009
− 3	1,320	1,179	1,100	1,056	1,040	1,026	1,015
− 4	1,440	1,237	1,132	1,077	1,054	1,035	1,019
− 5	1,573	1,293	1,168	1,096	1,066	1,044	1,027
− 6	1,733	1,353	1,207	1,118	1,080	1,054	1,035
− 7	1,947	1,424	1,245	1,142	1,096	1,066	1,042
− 8	2,190	1,518	1,288	1,168	1,110	1,077	1,051
− 9	2,489	1,609	1,328	1,193	1,126	1,090	1,060
−10	2,842	1,700	1,380	1,222	1,142	1,102	1,071

* The "+" sign designates inclination of the pyranometer toward the Sun, and the "-" sign designates the same away from the Sun.

The segments of rapid rotation alternate with segments where the wiring revolves very slowly, often without completing a full revolution around the axis. Therefore, we must find the average correction for a non-horizontal position $\overline{\Delta n}$ for all the segments /174 of rapid rotation, for each azimuth less then 20°. These corrections are used for reducing the readings in segments with slow rotation.

During flight 19, a similar study was carried out with a balance-meter. The angle of inclination of the balance-meter from a horizontal position varied from 1.5 to 2°, and the angle spread over the azimuth was equal to 20°. The average line obtained as a result of the analysis, for which the error in the non-horizontal position was eliminated, was 5-6% higher than the preset mean arithmetic value. Obviously, we are not entirely justified in analyzing the

data of the balance-meter to use the Saviskovskiy ratio and the reduction coefficients of Lopukhin obtained for a pyranometer. Therefore, the accuracy in the analysis decreases.

Naturally, in order to simplify the elimination of errors in a non-horizontal position of the instruments, the frame-wiring must be ascribed a constant rotation around the vertical axis at a velocity of 0.5 rev/min.

Consideration of the Effect of the Temperature and Pressure

The corrections for the temperature and pressure are conveniently included in the indices of the instrument by the method which V.G. Kastrov proposed [1]. The effect of the temperature on the sensitivity and resistance of all the elements of the measuring circuit can be evaluated according to the following formula.

$$\delta_t n = n/100\ [a(t_{lp.cal.} - t_{lp.msr.}) + b(t_{pyr.cal.} - t_{pyr.msr.})],$$

where n is the uncorrected reading on the tape of a loop oscillograph; a is the coefficient which takes account of the temperature dependence of the parameters of the loop; b is the coefficient which takes account of the temperature dependence of the parameters of the pyranometer; $t_{lp.cal.}$ and $t_{lp.msr.}$ are the loop temperatures in calibration and in measurement; $t_{pyr.cal.}$ and $t_{pyr.msr.}$ are the temperatures of the pyranometer in calibration and in measurement. The average values of the coefficients for the instruments used are such: a = -0.009%/deg, b = -0.13%/deg. The correction for the pressure is determined according to the following formula:

$$\delta_p n = -0{,}058\left[1 - \left(\frac{p}{p_0}\right)^{0{,}5}\right] n,$$

where p is the pressure on the level at which the measurements are conducted; p_0 is the pressure at ground level.

The coefficient which takes account of the effect of the pressure was obtained by Kastrov. The corrections are included in the reading by the formula

$$n_{corr.} = n + \delta_p n + \delta_t n.$$

Calculations showed that the correction for the pressure is 0.2-4%, and that for the temperature is 1-12%.

Spectral and Angular Corrections

/175

Since the pyranometer has a selectively absorbing receiving area and the spectral composition of the emission during the calibration af the pyranometer can differ from that of the radiation incident on the sensitive area of the instrument during the study, spectral corrections must be made for the conversion factors of the pyranometers. Two spectral corrections must be made for the total radiation Q: for the scattered radiation D and for the direct solar radiation S′. A consideration of the spectral and angular corrections in the ascent of pyranometers is made in the following way: according to the data of the actinometer, we find

$$S' = S \cdot \sin h_{\odot},$$

and then we determine

$$S'_{\text{uncor.}} = \frac{S'}{F_h \cdot Z_S^H},$$

where F_h is the angular correction for the pyranometer; Z_S^H is the spectral correction for the pyranometer, for direct solar radiation S′, in dependence on the altitude H. An example of the altitudinal dependence of Z_S is presented in the graph (Fig. 4), which was constructed according to the data of Yu. Ross and O. Avaste [5,6]. As can be seen from Figure 4, this correction reaches 6-7% at the upper boundary of the atmosphere.

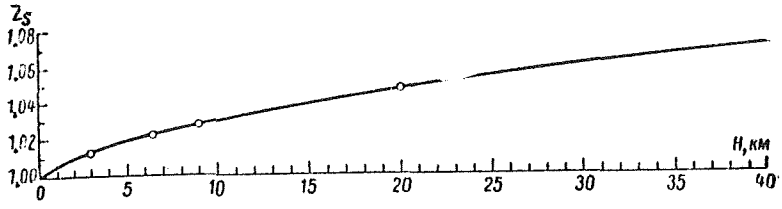

Fig. 4. Vertical Profile of the Spectral Correction for the Pyranometer According to the Data of Yu. Ross and O. Avaste.

Further,

$$Q_{\text{uncor.}} - S'_{\text{uncor.}} = D_{\text{uncor.}},$$

$$D_{\text{uncor.}} \cdot F_D \cdot Z_D = D_{\text{corr.}}$$

Here F_D is the angular correction for scattered radiation; Z_D if the spectral correction for D, which is taken as constant for all levels. Above 10-15 km, the corrections for D can be eliminated, since the scattered radiation itself is low in the majority of

cases. The flux of total radiation is obtained according to the following formula:

$$S' + D_{corr.} = Q_{corr.}$$

Consideration of the Effect of the Envelope of the Airship /176

The scattered radiation reaches a maximal value in the presence of upper-level semitransparent clouds (D = 1 cal/cm^2·min). For this case, we can consider that the sky is uniformly clear, and then scattered radiation of $D_{30°}$ = 0.074 cal/cm^2·min enters from a zone at 30° with center at the zenith. We can assume that this value is equivalent to the radiation reflected and scattered by the envelope at the solid angle of 30°, since the brightness of the envelope of the airship illuminated by the Sun is comparable to the brightness of upper-level semitransparent clouds, and, near the upper sounding point, the shell has angular dimensions of 30°. Thus, it is found that an additional flux approximately equal to 0.07-0.08 cal/cm^2·min falls on the actinometric instruments receiving the radiation from the upper hemisphere at altitudes of 28 km. For lower altitudes, the correction decreases because of the reduction of the horizontal thickness of the envelope and the increase in scattered radiation of the sky. Actually, the contribution of the envelope is equal to the radiation flux reflected and scattered by the envelope at a definite solid angle, minus the scattered sky radiation at the given altitude at the same solid angle. In the layer near the ground, for a cloudless sky and flux of scattered radiation of D = 0.1 cal/cm^2·min, the correction is equal to 0.001 cal/cm^2·min. The dependence of the correction for the effect of the airship envelope on the pressure is expressed by an exponential curve (Fig. 5).

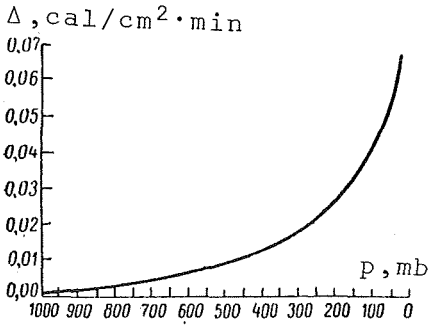

Fig. 5. Dependence of the Correction for the Effect of the Envelope of the Airship on the Sounding Level.

Calibration

The calibration of actinometric instruments used in an airship complex should be given a great deal of attention, since the results of single calibrations can vary because of a difference in meteorological conditions. The temperatures of the actinometric and recording instruments, the optical properties of the atmosphere, the state of the cloud cover, and the velocity and direction of the

wind always vary; therefore, the results of calibrations also have deviations. The method used for calibration has its own specific characteristic; therefore, we should discuss it in more detail.

The conversion factors for solar radiation were tested before the flight and, when possible, after the flight, in order to find their change during the flight. The calibration was carried out by the "Sun-shadow" method with the aid of an actinometric tube /177 whose design differed somewhat from that recommended by Yu.D. Yanishevskiy [7]. The change in design was connected with the fact

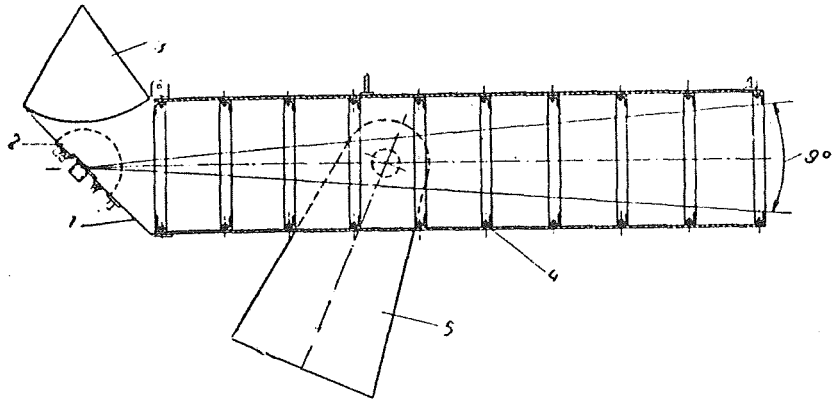

Fig. 6. Design of Actinometric Tube with Adapter for the Inclined Arrangement of the Pyranometers. (1) Adapter for Pyranometers; (2) Pyranometer; (3) Cone; (4) Diaphragm; (5) Strut.

that single pyranometers were used in each flight for measuring the total and reflected radiation, and the radiation fluxes on the upper and lower pyranometers could differ for middle latitudes by a factor of 8. Therefore, in order to increase the measurement accuracy, loops of the corresponding sensitivity were selected for the upper and lower pyranometers, which aided in working under conditions of great inclinations of the loop (using the entire scale of the oscillograph). However, this selection of the sensitivity of the loops complicates calibration of the lower pyranometer by the Sun, since, in the normal incidence of solar radiation on the sensitive area, the inclinations of the loop can be higher than the permissible values. Actually, reliable calibration can be carried out with good transmissivity of the air around noon, but under such conditions the magnitude of direct solar raidation is great (1.2 - 1.4 cal/cm^2·min). This complication can be overcome if we change the angle of incidence of solar radiation of the pyranometer, for which the latter is established at an angle of h = 45° to the axis of the calibration tube, and the light reflected from the pyranometer is incident in a black body, which has the shape of a cone, where it is mainly absorbed (Fig. 6). The indices of the pyranometer decrease roughly by a factor of 0.7 in this case. Moreover, the angle of incidence of 45° was selected in connection

with the fact that the measurements by the pyranometers were carried out most frequently for heights of the Sun of 25-60°; therefore, the angle of 45° is close to the average one for these limit changes. In calibration with an inclined pyranometer, the conversion factor can be obtained by a consideration of the correction for the angle of incidence:

$$a_{h=45^\circ} = \frac{S \cdot \sin 45^\circ}{N_\odot - N_T}, \qquad /178$$

where S is the flux of direct solar radiation measured by the actinometer; $N_\odot - N_T$ is the difference between the readings of the pyranometers with open and closed covers. The normal conversion factor is calculated according to the following formula:

$$a_n = \frac{S}{F_{h=45^\circ}} \cdot \frac{0.707}{N_\odot - N_T},$$

where F_h is the correction factor for the angle of incidence of the radiation. This calibration does not eliminate the need to introduce a correction factor of F_h for heights of the Sun which differ from 45°, but it aids in controlling the constancy of the sensitivity of the pyranometer and its angular correction.

For good pyranometers, the correction factor for the angle of incidence is close to unity up to heights of the Sun of 30°. The pyranometers made in Tbilisi most often have a correction factor which differs from unity even at small angles of incidence. For one set of pyranometers (23 units), $F_{h = 45}$ varies from 0.9 to 1.01 while the average value of $F_{h = 45} = 0.965$. One of the reasons for this behavior of F_h is the presence of schlieren in the upper part of the cap.

A consideration of F_h is an important step in an analysis of the indices of pyranometers; therefore, frequent control of the constancy of angular corrections is necessary. The calibration method used allows us to check the dependence of the angular correction on the solar azimuth. By revolving the pyranometer around the axis of the tube, we can change the azimuth of solar rays for a constant angle of incidence.

The corrections for a pyranometer which have been examined usually have a negative sign, and only the spectral correction and the correction for the non-horizontal position are positive. Almost all the corrections increase with the altitude, and the negative corrections are always greater than the positive ones in sum. The total correction can reach 10%. All the cited dependences must be considered in airship sounding in order to increase the accuracy of measurements.

REFERENCES

1. Kastrov, V.G.: A Measurement of the Absorption of Solar Radiation in the Free Atmosphere up to 3-5 km. Trudy Tsentr. Aerol. Observ., No. 8, 1952.
2. Kastrov, V.G.: An Investigation of Some Errors in Determining the Absorption of Solar Radiation in the Atmosphere with the Aid of Pyranometers. Trudy Tsentr. Aerol. Observ., No. 32, 1959.
3. Savikovskiy, I.A.: Observations on the Solar Radiation in the Free Atmosphere. Trudy Tsentr. Aerol. Observ., No. 23, 1957.
4. Lopukhin, Ye.A.: A Study of the Radiation Field in the Lower Part of the Troposphere for Cloudless Days over Tashkent. Trudy Instit. Matematiki i Mekhaniki, No. 14, Izdat. Akad. Nauk Usbek. S.S.R., 1955.
5. Ross, Yu.K.: Izvest. Akad. Nauk Est. S.S.R., ser. tekhn. i. fiz. -matem. Nauk, Part 1, Vol. 6, No. 1, 1957; Part 2, Vol. 6, No. 2, 1957.
6. Shifrin, K.S. and O.A. Avaste: In the Collection: Issledovaniya po fizike atmosfery (Studies on the Physics of the Atmosphere). Izdat. Instit. Fiz. Atmosfery Akad. Nauk Est. S.S.R., No. 2, 1960.
7. Yanishevskiy, Yu.D.: Aktinometricheskiye pribory i metody nablyudeniy (Actinometric Instruments and Observation Methods). "Gidrometeoizdat", 1957.

EFFECT OF CLOUDS ON RADIATION FLUXES AND RADIATIVE HEAT TRANSFER IN THE FREE ATMOSPHERE

G.N. Gayevskaya

ABSTRACT: The author reviews the data obtained experimentally by different authors for the amount of radiative heat transfer and the magnitude of radiative temperature changes in the free atmosphere when there are different types of clouds. The data obtained by the actinometric soundings on airships which were directed by scientists at Leningrad University in 1961-1963 under conditions of variable cloudiness, with solid clouds, are discussed in detail.

Aircraft and airship actinometric soundings of the free atmosphere which give information on the vertical profiles of radiation fluxes also give data on the values for the absorbed radiation and radiative heat flux up to high altitudes. It is of substantial interest to find these values when there are clouds, which distort the vertical distribution of radiation fluxes to the greatest extent. /179

Actinometric measurements carried out on aircraft allow us to immediately determine the values for transmission, absorption and reflection of solar radiation by clouds. Unfortunately, at present there is still an insufficient amount of experimental data, which could give total clarity to the problem under investigation.

Rather complete measurements of the transmission and absorption of short-wave radiation by stratus clouds were carried out by M. Neiburger [1] in 1948 and N.I. Chel'tsov [2] in 1952. Having measured the ascending and descending fluxes of short-wave radiation, Neiburger found that the magnitude of absorbed radiation changes from 5 to 9% for clouds of the St type with thickness of about 450 m. The circumstantial measurements of Chel'tsoc, which were carried out for different forms of stratus clouds in the autumn and spring with Yanishevskiy pyranometers, showed that the value for transmission of solar radiation is closely connected with the value for the albedo of clouds and depends on the width and shape of the clouds, equal to 43% for Ac with thickness of 200 m, and to 59% for Sc of the same width. When the thickness of Sc increases to 500 m, the value for the transmission decreases down to 24%.

The values for the absorption of radiation obtained by Chel'tsov in separate flights had even a negative value, which was connected with the high measurement errors. The average value for absorption out of 26 flights carried out at Arkhangel'sk was 3.5%, and that for 16 flights carried out at Moscow was 7.2%. This difference in /180 values was due to an increase in the thickness in the clouds over

Moscow. The average rate of radiative heating corresponding to the absorption values obtained were: 0.23 for Arkhangel'sk, and 0.31 deg/hour for Moscow.

During three aircraft flights over complex systems of frontal clouds with upper boundary at a level of 7-8 km, S. Fritz and T. MacDonald [3] obtained an average value for the absorbed radiation of about 20%.

In one of the flights in the summer of 1952, V.L. Gayevskiy [4] found that a Cu Cong cloud with lower boundary at an altitude of 1.3 km and upper boundary at about 2.7 km absorbs up to 21% short-wave radiation. After analyzing aircraft measurements, G. Robinson [5] obtained a value roughly of the same order, equal to 22%.

The calculations carried out in [6] indicate that the absorption of short-wave radiation over the peaks of clouds is greater than that at the same altitudes in a cloudless sky. In all probability, this is connected with the increase in humidity in the first case. The absorption decreases below the lower boundary of the clouds, and it is much greater inside the clouds than at the same level under cloudless conditions.

Having estimated the rate of radiative heating for the cloudy sky under the conditions of Antartica, V.F. Belov [7] noted that the value for the rate of radiative warm-up above the clouds remains roughly of the same order as in the absence of clouds, while the radiative warm-up below the clouds decreases by a factor of 1.5-2 in comparison with the cloudless sky.

Clouds which absorb a substantial amount of incoming short-wave radiation also transform the field of thermal radiation to a great extent.

As the aircraft measurements of Ye. A. Lapukhin [8, 9] for different types of clouds showed, the radiation balance inside the cloud cover is close to zero. The increase in radiation balance occurs almost twice more rapidly for a clear sky than for a cloudy sky. The large vertical gradients of long-wave radiation fluxes near the upper and lower cloud boundaries bring about more significant radiation changes in the temperature than in the case of the cloudless sky. The magnitude of radiative heating or cooling depends on the thickness and shape of the clouds. For example, the cooling below the lower boundary of thick Ns clouds was 0.22, and over the upper boundary it was 0.16 deg/hour, while, for thin Ns, these values were much lower, equal to 0.02 and 0.03 deg/hour, respectively. Lapukhin noted that, if there were only stratus clouds, then a radiative warm-up averaging about 0.06 deg/hour was observed below their lower boundary, while cooling equal to 0.28 deg/hour occurred over the upper boundary. If there were clouds /181 of other types in addition to the St, then cooling which could reach 0.06 deg/hour occurred below the lower cloud boundary, while

the radiative heating and cooling observed above the clouds were varied.

The aircraft measurements carried out by V.L. Gaevskiy [4, 10] during the day and the night for St, Sc, Cu, Cb, Nb, As and Ac clouds confirm Lapukhin's conclustion on the low radiation balance inside clouds. The radiation balance inside clouds is practically equal to zero, but the degree of radiative heating of the lower cloud boundary, according to Gayevskiy's data, depends substantially on the water content of the cloud and the size of the drops. For clouds of the Ac and As type at an altitude of about 3 km, the rate of radiative heating can reach 4 deg/day, while for lower clouds (to 1 km), the radiative heating is insignificant. During the day and the night, the cloud peaks are subjected to substantial cooling, which is -9.3 deg/day on the average for 12 night flights, and -7.5 deg/day for 7 day flights. In the summer, the clouds increase the radiative cooling of the atmosphere, compared to the cloudless sky, by 20-25%.

The vacuum bolometer designed by A. Brewer and J. Houghton [11] for aircraft measurements made it possible to obtain information on the radiative cooling of the atmosphere in the presence of stratus and cirrus clouds was 2.5 deg/day and, below the cloud layer, there was radiative cooling equal to 0.6 deg/day.

The calculations of P. Clapp, F. Winninghoff and G. Fisher [6] showed that, in the case of multilayer clouds, inside and below cumulus clouds and middle-level clouds, the cooling diminishes rapidly, reaching 1 deg/day. In most cases, there is a radiative warm-up below the base of the clouds. For upper-level clouds, the cooling reaches 5 deg/day, which greatly exceeds the values for the cloudless sky.

The use of actinometric radiosondes opens up wide prospects for the study of radiation fields up to high altitudes. Measurements of the heat fluxes with actinometric radiosondes up to altitudes of 20-30 km [12-17] aid in evaluating the effect of the clouds on the radiative heat transfer in the free atmosphere.

P. M. Kuhn, V.E. Suomi and G.L. Darkov [15] found from winter soundings that, for a lower Sc boundary at a level of 870 mb, there is radiative heating, while the upper cloud boundary is cooled at /182
a rate of 8.5 deg/day.

Simultaneous launchings of several actinometric radiosondes at different sites [18, 19] aided in constructing cross-sections of the field of effective radiation and the field of the radiative heat transfer. With such vertical cross-sections, we can speak of the change in the field of the radiative heat transfer in dependence on the synoptic situation. Under the conditions of the passage of fronts and in the presence of internal clouds, the vertical sections of the field of long-wave radiation and radiative heat transfer

represent a complex picture, from which it is clearly seen that regions with radiative cooling are replaced by regions with radiative warm-up.

It can be seen from the survey above that the values for the radiative heating and cooling of the atmosphere and clouds change within a rather broad range. The values for the absorbed radiation and radiative heat transfer depend substantially on the thickness, shape, water content and altitude of the clouds, the precise values of which are far from always known.

After this brief review, let us turn to an investigation of the data obtained by airship actinometric soundings in 1962-1963. Of 13 flights carried out by colleagues at Leningrad University in 1961-1963 [20, 21, 22], three took place under conditions of variable cloudiness, with solid clouds.

Figures 1 and 2 give the data for two flights carried out on June 22 and July 4, 1962. The first flight took place under the conditions of intense variable altocumulous and cirrus clouds of 8/7, with a lower boundary at an altitude of about 3 km. The second flight was also carried out for variable cloudiness, but with cumulus clouds, with a lower boundary at an altitude of 1 km.

The variable cloudiness distorted the vertical profiles of radiation fluxes to such an extent that it was rather difficult to find any regularities common to both flights in measurements of the components of the radiation balance.

In the flight of June 22, 1962, the direct solar radiation decreased abruptly from 0.78 to 0.03 cal/cm$^{2}\cdot$min during the entry of the airship into the cloud, and then it increased slightly and, finally, after the passage of the lower, rather dense cloud layer, it increased abruptly up to 0.88 cal/cm$^{2}\cdot$min. The rapid increase in the flux of direct solar radiation above the level of 250 mb was connected with the passage of the apparatus through a layer of cirrus clouds. The total and net radiation balances in the clouds underwent the same intensive changes as did the direct solar radiation. As for the reflected short-wave radiation, it did not undergo such substantial variations, although it increased rather significantly after the passage of the cloud layer.

Unfortunately, in the data for the flight carried out on July /183
4, 1962, there was no information on the reflected short-wave radiation over the entire sounding layer, and a record of the data appeared only at a level of 450 mb, where the flux of reflected short-wave radiation was 0.195 cal/cm$^{2}\cdot$min, which corresponded to the ground value. Just as in the preceding case, the radiation fluxes varied greatly both below the clouds and in the cloud layers. In both cases, synchronous changes in the direct solar and total radiation, as well as the net radiation, indicated that there were not random changes connected with oscillations of the frame-wiring on

which the measuring apparatus was fixed, but changes caused by the effect of the clouds. In this case, the data on direct solar radiation, which was measured by a thermoelectric actinometer arranged on the tracking system, served as a good control [23].

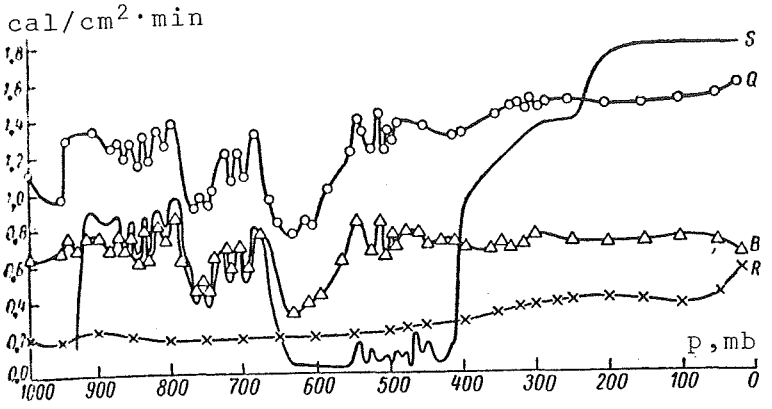

Fig. 1. Vertical Profiles of the Radiation Balance and Its Constituents in the Case of Variable Cloudiness (6/22/1962). S -- Direct Solar Radiation; Q -- Total Radiation; R -- Reflected Short-Wave Radiation; B -- Radiation Balance.

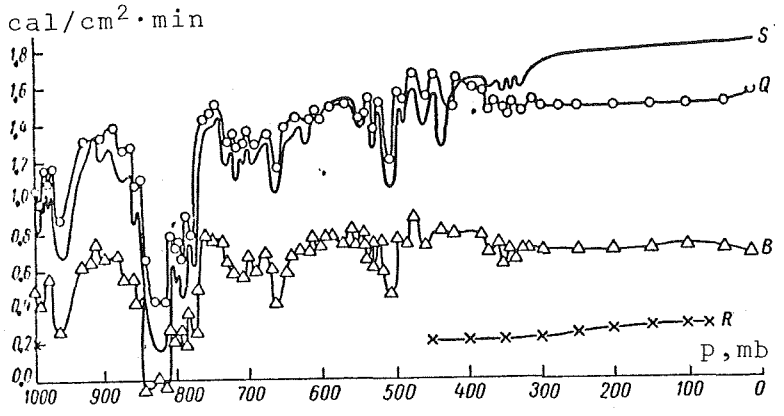

Fig. 2. Vertical Profiles of the Radiation Balance and Its Constituents in the Case of Variable Cloudiness (7/4/1962). Symbols the Same as in Figure 1.

An intensive change in the vertical profiles of the radiation /184
fluxes in the layer below the clouds, in variable cloudiness, complicates a precise evaluation of the lower cloud boundary, and it must be determined visually, by the time when the apparatus enters the clouds. It is much easier to estimate the lower boundary of clouds when there is a solid cloud cover (Figure 3). In this case, the abrupt break in the profiles for the radiation fluxes gives

clear cloud boundaries.

During the flight of July 6, 1963 (Figure 3), the As and St clouds were 10/10 on the scale. In this flight, the direct solar radiation could be recorded only after the passage of the cloud layer, which served as a good indicator of the upper boundary of the cloud layer. After the apparatus left the clouds, the direct solar radiation gradually increased up to 1.83 cal/cm^2·min. The recording of total and reflected short-wave radiation was cut off at an altitude of about 420 mb for technical reasons.

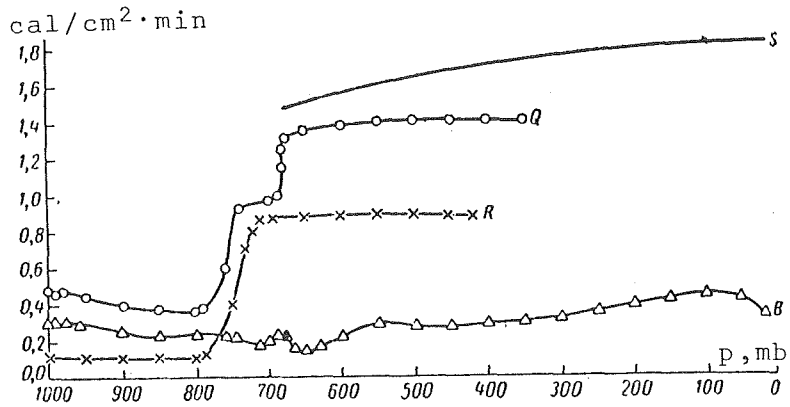

Fig. 3. Vertical Profiles of the Radiation Balance and Its Constituents in the Case of Solid Clouds (7/6/1963). Symbols the Same as in Figure 1.

The abrupt increase in reflected short-wave radiation during the passage through the cloud layer decreased the value of the net radiation balance, which reached a maximum at an altitude of 100 mb, and then diminished to 0.34 cal/cm^2·min. This change was due to the horizontal nonuniformity of the underlying surface and, primarily, /185 to the atmosphere itself.

A substantial change in the radiation fluxes in the troposphere when there are clouds complicates an evaluation of the magnitude of radiative heat transfer.

As calculations show [24], even in the case of a cloudless sky the vertical profiles for the radiative heat transfer and radiative changes in temperature up to an altitude of 15 mb represent a complex picture: rather high values for the radiative heat transfer in one layer can be replaced by very low values in neighboring layers. This great variability in the vertical profiles for the radiative heat transfer is connected with the fact that, having carried out calculations for 50-millibar layers, we obtain detailed vertical profiles relating to an absorbing mass decreasing with an increase in the altitude. The second reason is the substantial effect of the horizontal nonuniformity of the underlying surface and the atmosphere itself. When there are clouds, the vertical profiles for

the radiative heat transfer and radiative temperature changes become even more complex (Figure 4, 5). In this case, there is a sequence of single zones where the radiative heat transfer changes greatly, not only in magnitude, but also in sign. This can be clearly seen from the data for the flight conducted on July 6, 1963 (Figure 4).

The greatest change is seen in the value for the absorbed short-wave radiation, which can be determined by examining the vertical profiles for the fluxes of short-wave radiation (see Figure 3). The appearance of a negative value for the absorbed short-wave radiation has no physical meaning, and it proves that the measurement and calculation methods are imperfect (i.e., we have not an instantaneous vertical but a spatial-temporal profile of the radiation fluxes). The values for the radiative heat transfer do not undergo such substantial oscillations, which is connected with the lesser variability of the radiation balance itself both over the entire sounding layer and in passage through the clouds, where its value averages about 0.2 cal/cm^2·min.

The radiative temperature changes $\left(\frac{dT}{dt}\right)$ undergo even greater oscillations than the value for the radiative heat transfer. This is clearly seen in an investigation of Figure 5. As would be expected, the greatest changes in the vertical profile $\left(\frac{dT}{dt}\right)$ occur in the lower atmospheric layer up to a level of 500 mb. Here the value of $\left(\frac{dT}{dt}\right)_{\Delta B}$ varies from -0.23 to +0.40 deg/hour. In the layer of the atmosphere from 450 to 150 mb, there is a radiative warm-up due to the total radiative heat transfer, and strong radiative cooling is observed above this.

/186

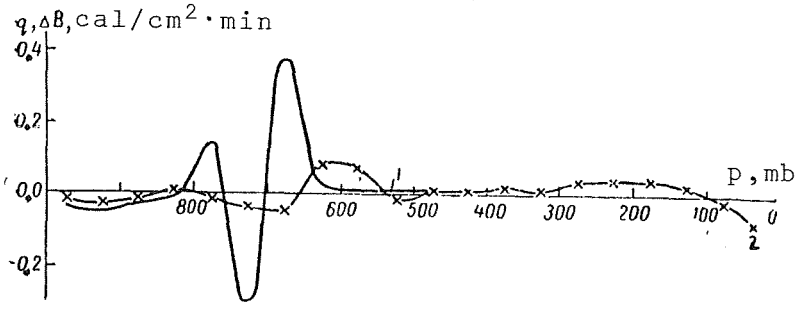

Fig. 4. Absorbed Short-Wave Radiation (Curve 1) and Radiative Heat Transfer According to the Data of Measurements of the Net Radiation Balance (Curve 2) in the 50-millibar Layers for the Flight Data of July 6, 1963.

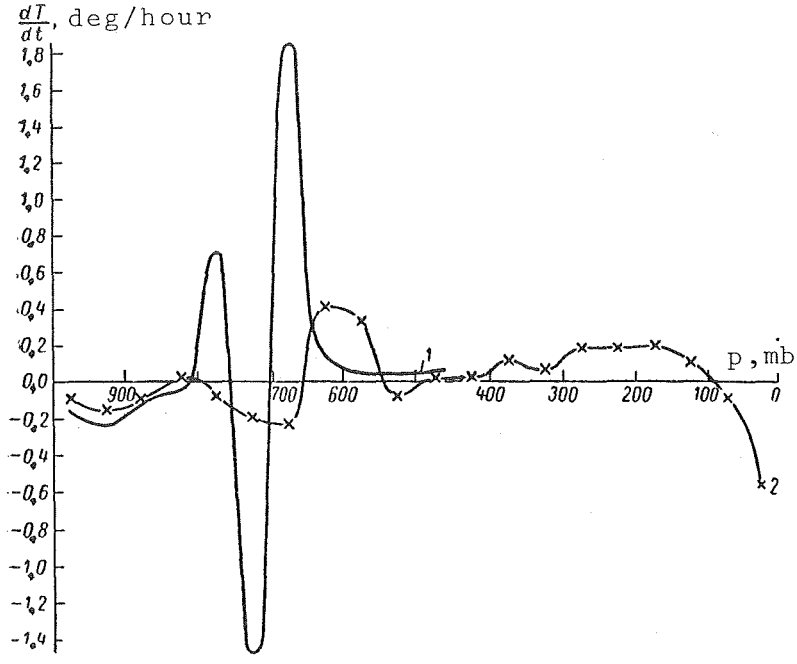

Fig. 5. Radiative Temperature Changes in the 50-millibar Layers According to the Flight Data for July 6, 1963. (1) Due to the Absorption of Short-Wave Radiation; (2) According to the Data of Measurements of the Net Radiation Balance.

ABSORBED SHORT-WAVE RADIATION q, RADIATIVE HEAT TRANSFER ΔB IN THE LAYERS AROUND THE LOWER AND UPPER CLOUD BOUNDARIES AND OVER THE ENTIRE SOUNDING LAYER, AND RADIATIVE TEMPERATURE CHANGES AT THE UPPER BOUNDARIES OF THE LAYERS. /187

Date of Flight	Altitudes of Lower and Upper Cloud Boundaries, Maximum Sounding Point	q	$\left(\frac{dT}{dt}\right)_q$	ΔB	$\left(\frac{dT}{dt}\right)_{\Delta B}$
6/22/62	680	0,209	0,160	0,122	0,093
	150	0,188	0,054	0,067	0,019
	17	0,114	0,028	−0,016	−0,004
7/4/62	900	0,225	0,461	0,136	0,277
	250	0,339	0,108	0,163	0,052
	13			0,146	0,036
7/6/63	790	−0,101	−0,119	−0,064	−0,076
	670	0,086	0,064	−0,122	−0,091
	15			0,039	0,010

As can be seen from the table, there is a radiative warm-up of the upper and lower cloud boundaries due to the absorption of short-wave radiation in the first two flights carried out under the conditions of variable cloudiness. The total radiative heat transfer also brings about radiative heating both in the first and in the second case, although the values for the radiative warm-up are almost twice less. The effect of long-wave radiation, which decreases the value of the total radiative heat flux, shows up very clearly here. In the case of solid clouds (July 6, 1963), the upper and lower cloud boundaries are cooled. The lower cloud boundary is cooled at a rate of -0.076 deg/hour, while the upper one is cooled at an even greater rate, and radiative heating occurs at the sounding ceiling.

We should mention that the values for the radiative heat transfer and radiative temperature changes presented here are only rough estimates. The most complete and reliable values can be obtained only on the basis of a rather large amount of experimental data.

References

1. Neiburger, M.: Reflection, Absorption and Transmission of Insolation by Stratus Clouds. J. Meteorol., Vol. 6, No. 2, 1959.
2. Chel'tsov, N.I.: An Investigation of the Reflection, Transmission and Absorption of Solar Radiation by Clouds of Several Types. Trudy Tsent. Aerol. Observ., No. 8, 1952.
3. Fritz, S. and T.H. MacDonald: Measurements of Absorption of Solar Radiation by Clouds. Bull. Amer. Meteorol. Soc., Vol. 32, No. 6, 1951.
4. Gayevskiy, V.L.: Measurement of the Radiation Fluxes in Clouds. Trudy Glavnoy Geofizicheskoy Observ., No. 46(108), 1955.
5. Robinson, G.D.: Some Observations from Aircraft of Surface Albedo and the Albedo and Absorption of Cloud. Archiv Meteor., Geophys. and Biokl., Bd. 9, No. 1, 1958.
6. Clapp, P.F., F.J. Winninghoff, and G.E. Fisher: Vertical Distribution of Atmospheric Heating and Cooling at Washington, D.C., June-July 1961. Technical Memorandum, No. 21. Numerical Weather Prediction Group National Meteorol. Center U.S. Weather Bureau.
7. Belov, V.F.: Absorption of Solar Radiation in the Free Atmosphere Over Davis Sea and the Antarctic Decline. Trudy Tsent. Aerol. Observ., No. 45, 1962.
8. Lopukhin, Ye.A.: Radiation Fluxes in the Atmosphere over Tashkent Under a Cloudy Sky. Trudy Tashkent. Geofiz. Observ., No. 13, 1957.
9. Lopukhin, Ye.A.: Radiative Warming or Cooling of the Air Near the Surfaces of Clouds. Trudy SANIGMI, No. 2(17), 1959.
10. Gayevskiy, V.L.: Profile of the Long-Wave Radiation Fluxes in Clouds. In the Collection: Issledovaniya oblakov, osadkov i grozovogo elektrichestva (Research in Clouds, Precipitation and Thunderstorm Electricity). Izdat. Akad. Nauk S.S.S.R., 1961.

11. Brewer, A.W. and J.T. Houghton: Some Measurements of the Flux of Infra-red Radiation in the Atmosphere. Proc. Roy. Soc. Amer., Vol. 236, No. 1205, 1956.
12. Pohl, W.: Measurement of Infra-red Radiation Fluxes in the Free Atmosphere. Berichte des deutsches Wetterdienstes, Vol. 4, No. 2, 1956.
13. Staley, D.O. and P.M. Kuhn: Measurements of Radiative Cooling Through Two Intense Baroclinic Zones in the Middle Troposphere. J. Meteorol., Vol. 18, No. 2, 1961.
14. Businger, J.A. and P.M. Kuhn: On the Observation of Total and Net Atmospheric Radiation. J. Meteorol., Vol. 17, No. 4, 1960.
15. Kuhn, P.M., V.E. Suomi and G.L. Darkov: Soundings of Terrestrial Radition Flux. Monthly Weather Rev., Vol. 87, No. 4, 1959.
16. Mantis, H.T.: Observations of infra-red Cooling of a Tropical Air Mass. J. Geophys. Res., Vol. 66, No. 2, 1961.
17. Mani, A., C.R. Sreedharan and V. Srinivasan: Measurements of Infra-red Radiative Fluxes Over India. J. Geophys. Res., Vol. 70, No. 18, 1965.
18. Kuhn P.M. and V.E. Suomi: Infra-red Radiometer Soundings on a Synoptic Scale. J. Geophys. Res., Vol. 65, No. 11, 1960.
19. Kostyanoy, G.N.: Aktinometricheskoye radiozondirovaniye atmosfery (Actinometric Radiosonde of the Atmosphere). Author's Abstract of Candidate's Dissertation. "GUGMS", 1965.
20. Kondrat'yev, K. Ya., G.N. Gayevskaya and G.A. Nikol'skiy: Vertical Profile of the Radiation Balance and Its Constituents in the Free Atmosphere During the Day. Iskustvennyy Sputnik Zemli, No. 14, 1962.
21. Kondrat'yev, K.Ya., G.N. Gayevskaya and G.A. Nikol'skiy: Experimental Studies of the Radiation Balance in the Free Atmosphere. In the Collection: Problemy fiziki atmosfery (Problems of Atmospheric Physics), No. 3. Leningrad State University Press, 1963.
22. Kondrat'yev, K.Ya., G.N. Gayevskaya and G.A. Nikol'skiy: Airship Studies of the Radiation Balance of the Earth's Surface Atmosphere System. In the Collection: Kosmicheskiye issledovaniya (Space Research), Vol. 1, No. 3. Izdat. Akad, Nauk S.S.S.R., 1963.
23. Badinov, I. Ya.: Three-Stage Photoelectric Tracking System on Transistors. Iskustvennyy Sputnik Zemli, No. 14, 1962.
24. Kondrat'yev, K.Ya. and G.N. Gayevskaya: Radiative Changes in the Temperature in the Free Atmosphere. In the Collection: Problemy fiziki atmosfery (Problems of Atmospheric Physics), No. 3. Leningrad State University Press, 1965.

AN OZONE SONDE FOR MEASURING THE VERTICAL DISTRIBUTION OF ATMOSPHERIC OZONE

L.G. Bol'shakova

ABSTRACT: The author describes the apparatus used for measuring the vertical distribution of atmospheric ozone, as well as the measurement method. An analysis showed that, with this method, the scattered light of the sky incident on the measuring instrument has a great effect on the change in the signal of the ozone sonde with altitude in the lower layers of the atmosphere.

In July-August, 1965, measurements of the vertical distribution of ozone were carried out in the city of Ryl'sk of the Kursk region, at the base of the Central Aerological Observatory (TsAO) of GUGMS (Main Administration of the Hydrometeorological Service), by launching the apparatus on the cables of ballons. The measurements were carried out with the aid of photomultipliers by recording the solar light scattered from a gypsum deflector in two spectral regions (3100 and 3310 Å). The spectral regions were separated by interference light filters. The signals were transmitted to the ground with the telementric system of the TsAO. /189

The apparatus, measurement methods, and methods of analyzing the data are described in this article. The results of one of the flights are presented.

1. Apparatus. A two-channeled ozone sonde with a deflecting screen somewhat different from that described in [1] was used. End-window photomultipliers with a quartz window and antimony-cesium cathode (FEU) were used as the radiation detectors. The rejection of photocells with subsequent amplification was due to the high interference in the direct-current amplifier during the operation of the transmitter. The sensitivity of the photomultipliers was sufficient for operation without further amplification. The total weight of the launched apparatus was about 10 kg.

For the sake of simplicity, one FEU (photomultiplier) is shown on the basic block diagram of the ozone sonde used in this study (Fig. 1). The output signal of the photomultiplier (I_{out}) passes through resistors forming the potentiometer, on which a constant negative bias is supplied. The signals are taken at three points (1, 2, 3 on Fig. 1), and are sent in order to the input of the transmitter, through the commutator. The signals are recorded by photographing the screen of the oscillograph of the receiving device on a revolving photofil width of the film of 35 mm. The bias supplied

to the output potentiometer is calculated in such a way that the signal of only one of the three photographed points is sent to the screen of the cathode oscillograph (200 mV), depending on the I_{out} of the FEU. Thus, for 0 μa < I_{out} < 2 μa, a signal is recorded only from point 1 (see Fig. 1); for 2 μa << I_{out} < 4 μa, only from point 2; for 4 μa < I_{out} < 6 μa, from point 3. In this case, the scale of the oscillograph is used three times. /190

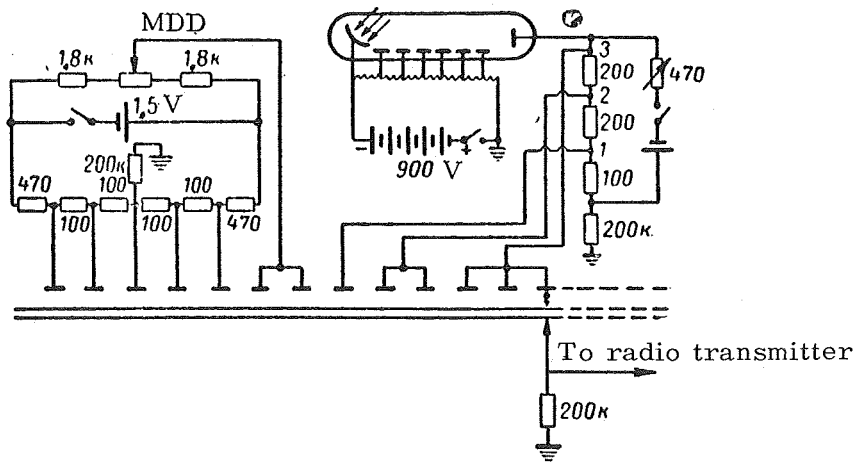

Fig. 1. Basic Block Diagram of the Ozone Sonde. On the Left - Circuit for sending the calibration signals and for the pressure pick-up (MDD) on the commutator bars; On the Right - Circuit for sending the signals of the FEU; On the Bottom - Segment of the commutator bars.

The signals coming from these points were called the signals of the first, second and third ranges, respectively. This recording design allowed us to maintain a rather high sensitivity in the recording for a rather broad range of signal changes. For the sake of convenience in computations, each of the three points of the potentiometer was connected with the corresponding number of commutator bars.

In addition to the signals from the photomultipliers, calibration signals from a standard supply source and the signal of the pressure pickup (MDD, see Fig. 1) were sent to the commutator. The commutator contains 60 bars and revolves at a rate of 4 rev/min. During one revolution, both photomultipliers are "searched" 4 times. Thus, each photomultiplier is questioned 16 times a minute.

The time marking is transmitted by light signals every five minutes by flashing a bulb focused on the center of the oscillograph scale. The photomultipliers and the supply batteries are placed inside the body of the instrument, in the photomultiplier Section 3 (Fig. 2). The light is sent to the photomultipliers through tubes 2 blackened inside, which guarantee the requisite solid angle within the boundaries of the screen 1 (Fig. 3). The round gypsum screen (diameter = 24 cm) is put a distance of 30 cm from the lower base /191 of the body, which guarantees independence from the position of the shadow all the way to a height of the Sun of 60° for a pyramid design. The photomultipliers are inclined somewhat toward the center in order to provide coincidence of the energy fields.

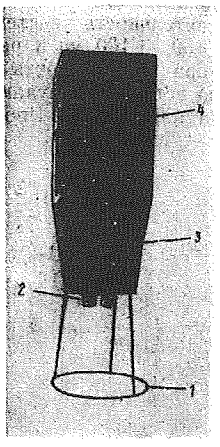

Fig. 2. General Appearance of the Ozone Sonde. (1) Screen; (2) Limiting Tubes; (3) Section of Photomultipliers; (4) Section of Radio Transmitter and Commutator.

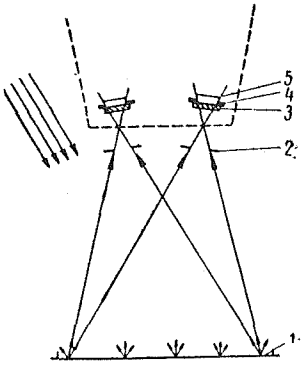

Fig. 3. Optical Scheme of the Ozone Sonde. (1) Screen; (2) Limiting Tubes; (3) Light Filter; (4) Iris Diaphragm; (5) Cathode of Photomultiplier.

2. Supply of Photomultipliers. In order to supply the photomultipliers, we used small high-voltage batteries of the type 400-PMTsG-0.01. To increase the capacity, two sets of batteries were put in parallel connection. To avoid possible breakdown during the climb into the atmosphere, the supplying potentiometer of the photomultipliers and the battery units were lined with paraffin. Pressure-chamber tests did not show any voltage leaks all the way to 5 mm Hg for effective voltages of the photomultipliers of 900 V.

3. Light Characteristics of the Photomultipliers. Special measurements were carried out to determine the linearity regime of the photomultipliers. It was established that the output signal in

the photomultipliers used was proportional to the incident light flux within a range up to 5.5 μa.

4. Light Filters. In order to separate the necessary spectral intervals in the ultraviolet, we used interference light filters with the following parameters:

1. λ_{max} = 3100 Å, $\Delta\lambda$ = 40 Å, τ_{max} = 4.5% /192
2. λ_{max} = 3310 Å, $\Delta\lambda$ = 30 Å, τ_{max} = 10.5%,

where $\Delta\lambda$ is the half-width of the filter; τ_{max} and λ_{max} are the transmission and wavelength at the maximum, respectively.

5. Graduation of the Ozone Sonde. Before the flight, the instrument is graduated by current. The graduation is carried out by transmitting carefully-measured control signals from 0 to 6 μa every 0.5 μa to the output potentiometer, and comparing them in each region to the signals of the calibration scale. The calibration scale, characterizing the sensitivity of the system, contains five signals: -100; -50; 0; +50; +100 mV. This is recorded in each revolution of the commutator (stability of the calibration is guaranteed by the high capacity of the feeding source). Moreover, a signal of 0 mV is recorded each time after recording the signals from the photomultipliers (see Fig. 4).

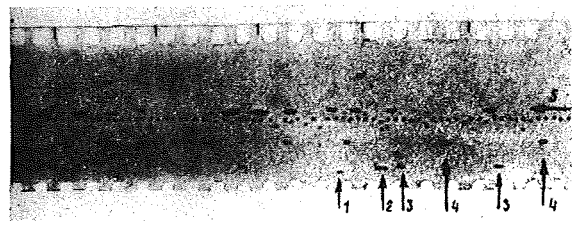

Fig. 4. View of a Record of Signals of the Ozone Sonde on the Film. (1) Calibration Scale (five signals from bottom to top); (2) pressure pickup; (3) Signals from the FEU-1; (4) Signals from the FEU-2; (5) Reference Signals for Calibration (0 mV).

Random changes in the sensitivity of the system bring about a change in the distances between the calibration signals on the photofilm. The graduation is carried out for each of the channels and is used in processing the entire film, in order to reduce signals of different ranges to one scale, with a consideration of the possible changes in sensitivity of the system.

6. Analysis of the Data. The data analysis consists in a measurement of the deviations of the signals of the photomultipliers on the film from the calibration zero, as from the reference point. Moreover, the deviation from zero of other calibration signals is determined for each measurement cycle. Analyses show that the sensitivity of the system varies somewhat during flight.

An effective graph is constructed for a series of measurements with identical sensitivity on the basis of a graduation of the calibration scale by current for each range. One such graph, from 0 to/193 2 μa (Range 1) is shown in Figure 5. The distances d of the calibration signals from the zero are plotted along the ordinate, and the corresponding values of the current, in microamperes, are plotted along the ordinate, and the corresponding values of the current, in microamperes, are plotted along the abscissa. Having measured the distance of the FEU signal from the calibration zero, and using the graph in Figure 5, let us determine I_{out}, μa.

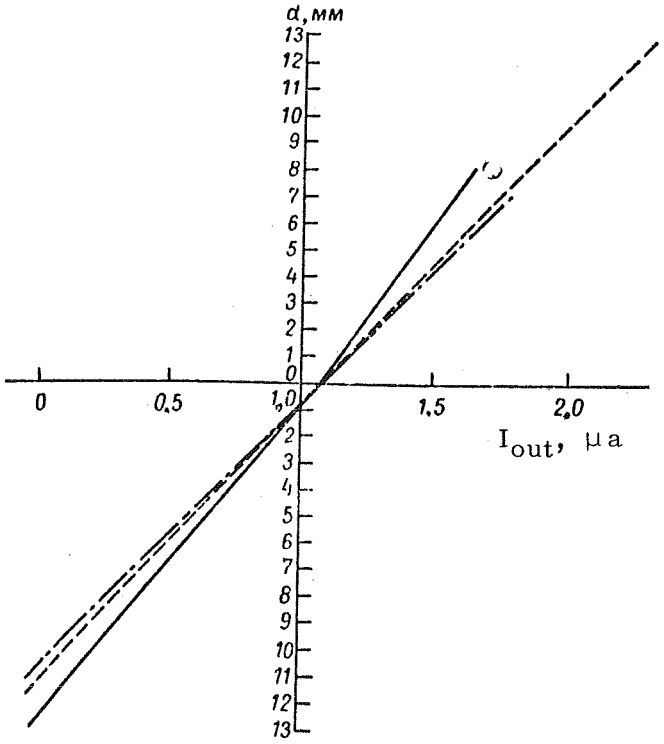

Fig. 5. System of Graduated Lines for Range 1.

The characteristic "fan" of the graduated lines on Figure 5 illustrates the limits to the change in sensitivity of the system during one flight (however, the linearity is not disturbed in this case). The methods used for recording and analyzing the data eliminate this effect completely.

7. Adjustment of the Initial Signals of the Photomultipliers before launching. It was mentioned above that the photomultipliers used were linear up to 5.5 μa. Consequently, the maximum signal at the output of the photomultiplier should not exceed this value during the climb (the recording system was therefore calculated up to 6 μa).

In order to fulfill this condition, it was necessary to estab- /194
lish the initial signals correctly before the climb into the atmosphere. In our instrument, the exposure of the FEU photocathdoes was regulated by an iris diaphragm (see Fig. 3).

The order of magnitude of the initial signal for a given λ can be calculated according to the Bouguer law:

$$I_\lambda = I_{0\lambda} 10^{-(\alpha_\lambda x + \beta_\lambda + \delta_\lambda)^{\sec z}} \qquad (1)$$

where I_λ is the intensity of direct solar radiation, proportional to the signal of the ozone sonde at the surface of the Earth; $I_{0\lambda}$ is the intensity of direct solar radiation, proportional to the signal of the ozone sonde beyond the limits of the atmosphere; α_λ is the ozone absorption coefficient; β_λ is the coefficient of Rayleigh scattering; δ_λ is the attenuation coefficient in aerosols; $\underline{z}$ is the zenith angle of the Sun; $\underline{x}$ is the total percentage of ozone in the atmosphere.

If we assume that, over the level of the maximum flight altitude, $\underline{x} = 0$, $\beta_\lambda = 0$ and $\delta_\lambda = 0$, i.e., that, in conditional units, $I_{0\lambda} = I_{max} = 5.5$ μa (where I_{max} is the signal of the ozone sonde at the maximum flight altitude), then, taking the logarithm of (1), we find the following:

$$\log I_\lambda = \log 5.5 - (\alpha_\lambda x + \beta_\lambda + \delta_\lambda) \sec z \qquad (2)$$

For given $\underline{x}$, β_λ and δ_λ, the value of I_λ depends only on sec z, the value of which corresponds to the moment of establishing I_λ. However, the difficulty is that the aerosol extinction coefficient is still an indefinite value. Moreover, in usnng the deflecting screen at the same time as the direct solar light, the light scattered from the entire firmament is transmitted to the instrument. Therefore, the initial signal must be fixed with a consideration of this supplementary component, which is not found in (1). As experiments showed, this component greatly exceeds the requisite signal from the

line of the Sun calculated for this time during the hours before the launching, when the height of the Sun does not exceed 20°. Therefore, we fixed the initial signal regardless of the appointed take-off time, beforehand, around noon-time for clear days (z = 30°). At this time, the supplementary component of the scattered light is small, and it can be considered partially by shading the screen from direct solar rays.' The effect of the aerosol component during this time can also be considered minimal. Consequently, the value of the initial signal in microamperes for noon is determined rather well from (2) without a consideration of δ_λ. The conditions selected for a specific moment for exposure of the photocathode which satisfy (2) will satisfy it at any moment of time for direct solar light at the ground at least within the limits of the requirements /195 for our study.

8. Results of the Flight. Figure 6 shows the curves for the change with altitude of the output current of the photomultipliers, in microamperes, for two channels during the flight over Ryl'sk on July 23, 1965. The film was processed on a standard measurer IZA-2. The cross sections show the magnitude of the deviation of the data obtained. As can be seen from the figure, this deviation is rather great. However, due to the large amount of information obtained, we have a rather reliable average.

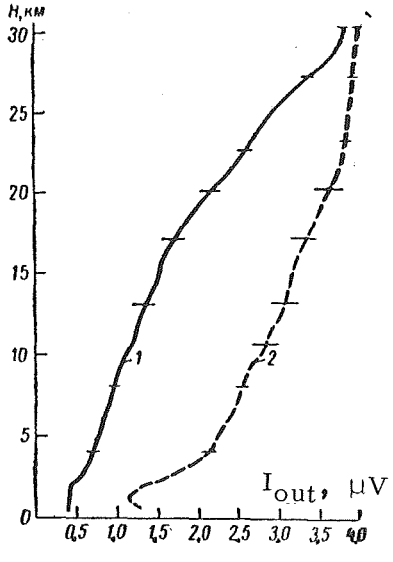

Fig. 6. Change with Altitude in the Output Current of the Photomultiplier. (1) First Channel, 3100 Å (FEU-1); (2) Second Channel, 3310 Å (FEU-2).

9. Calculation of the Curves for x(h). The change with altitude of the value for the total ozone content x in the overlying layer was calculated according to the data of Figure 6. The integral curves obtained were then used for calculating the vertical distribution of ozone.

In order to evaluate to some extent the effect of aerosol attenuation and the scattered light of the sky incident on the instrument, let us represent the output signal in the form of the sum of tow components:

$$I_{c\lambda} = I_\lambda + I_{s\lambda}. \qquad (3)$$

Here $I_{c\lambda}$ is the output signal of the ozone sonde at a given altitude; I_λ is the part of the signal which is proportional to the direct solar radiation; $I_{s\lambda}$ is the part of the signal which is

proportional to the scattered light of the sky incident on the instrument. Let us substitute the value of I_λ according to (1) into this equation, take its logarithm and, solving for x, find that

$$x = \frac{\log I_{0\lambda} - \log I_{c\lambda}}{\alpha_\lambda \sec z} - \frac{\beta_\lambda}{\alpha_\lambda} - \frac{\delta_\lambda}{\alpha_\lambda} - \frac{1}{\alpha_\lambda \sec z} \log \frac{I_{c\lambda} - I_{s\lambda}}{I_{c\lambda}} . \tag{4}$$

It is easy to see that the last term of this equation is a negative value if $I_{s\lambda} \neq 0$, and consequently, (4) can be represented in the following way in this case:

$$x = \frac{\log I_{0\lambda} - \log I_{c\lambda}}{\alpha_\lambda \sec z} - \frac{\beta_\lambda}{\alpha_\lambda} - \frac{\delta_\lambda}{\alpha_\lambda} + \frac{1}{\alpha_\lambda \sec z} \left| \log \frac{I_{c\lambda} - I_{s\lambda}}{I_{c\lambda}} \right| \tag{5}$$

For the case of two wavelengths, we find that /196

$$x = \frac{L_0 - L}{\Delta\alpha \sec z} - \frac{\Delta\beta}{\Delta\alpha} - \frac{\Delta\delta}{\Delta\alpha} + \frac{1}{\Delta\alpha \sec z} \left(\log \frac{I_{c2} - I_{s2}}{I_{c2}} - \log \frac{I_{c1} - I_{s1}}{I_{c1}} \right). \tag{6}$$

Here the subscripts 1 and 2 correspond to the wavelengths λ_1 and λ_2 ($\lambda_1 = 3100, \lambda_2 = 3310$ Å); $L_0 = \log \frac{I_{01}}{I_{02}}$; $L = \log \frac{I_{c1}}{I_{c2}}$; $\Delta\beta = \beta_1 - \beta_2$; $\Delta\alpha = \alpha_1 - \alpha_2$; $\Delta\delta = \delta_1 - \delta_2$.

Such equations can be constructed for each given altitude. For the sake of convenience in further analysis, we will call the sum of the first two terms in the right-hand parts of these equations γ, and we will introduce the index h to designate the altitude, i.e., let

$$\left[\frac{\log I_{0\lambda} - \log I_{c\lambda}}{\alpha_\lambda \sec z} - \frac{\beta_\lambda}{\alpha_\lambda} \right]_h = \gamma'_h, \tag{7}$$

$$\left[\frac{L_0 - L}{\Delta\alpha \sec z} - \frac{\Delta\beta}{\Delta\alpha} \right]_h = \gamma''_h. \tag{8}$$

Then, expressing (5) and (6) relative to γ, and considering the altitude, we find the following:

$$\gamma'_h = x_h + \left[\frac{\delta_\lambda}{\alpha_\lambda} - \frac{1}{\alpha_\lambda \sec z} \left| \log \frac{I_{c\lambda} - I_{s\lambda}}{I_{c\lambda}} \right| \right]_h, \tag{9}$$

$$\gamma''_h = x_h + \left[\frac{\Delta\delta}{\Delta\alpha} - \frac{1}{\Delta\alpha \sec z} \left(\log \frac{I_{c2} - I_{s2}}{I_{c2}} - \log \frac{I_{c1} - I_{s1}}{I_{c1}} \right) \right]_h. \tag{10}$$

Since we do not know the values of δ_λ and $I_{s\lambda}$, then, using the data of the sounding, we carried out our calculations according to (7) and (8) and then, comparing the behaviors of the curves obtained for $\gamma(h)$, we conducted a qualitative analysis of the effect of the factors which we did not consider according to (9) and (10) and found the altitude at which we could assume practically that $\gamma_h = x_h$.

The extra-atmospheric values for the intensities in the requisite units were also determined from (7) and (8), which were constructed for a certain altitude h by substituting in them the value for the total percentage of ozone ($x_{h=0}$), the latter was determined independently by the ground ozone-meter for the entire thickness of the atmosphere. It was assumed that the conditions of $x_{h=} \approx x_h = \gamma_h$ are fulfilled at this altitude. After a preliminary analysis, we selected an altitude of h = 10 km for this purpose. The value of γ_h was calculated according to (7) and (8) every 1 km over the entire sounding height. In this case, the mean arithmetical value of nine values obtained in a kilometer layer was taken as the final result for the given altitude. In this regard, the relative error, calculated according to the mean square root of the arithmetical mean, never exceeded 2% (Fig. 7). The existence of a positive course of γ_h', beginning at three kilometers, shows the predominant role of the scattered light decreasing with altitude $I_{s\lambda}$ in the change of this value, since the aerosol attenuation, which also decreases with the altitude in this layer, results in the converse /197 effect [see (9)]. The curve for γ_h'' also has a similar behavior; however, the effect of the scattered light is less in this case. The increase in values of γ_h'' ceases at an altitude of 6 km, while it is maintained up to an altitude of 15 km for γ_h'. The fact that both curves converge with subsequent divergence can indicate the presence of non-selective or slightly-selective aerosols in the wavelength interval used at altitudes from 13 to 18 km. In the very lowest layer, up to 3 km, both curves differ in their course and reflect, obviously, the strong effect of both the aerosols and the scattered light. Thus, an analysis of the curves in Figure 7 shows that, with our measurement method, the scattered light of the sky incident in the instrument has a great effect on the change in the signal of the ozone sonde with altitude in the lower layer of the atmosphere. Even for calculations by two close wavelengths, they apparently can be disregarded only at altitudes of 10 km and higher. If the lower layer of the atmosphere is the object of the study, then the effect of the scattered light, as well as the aerosol extinction, should be considered carefully. Obviously, the accuracy of the measurements themselves should be very high in this case. This conclusion should also be valid for ozone sondes with other types of scattering radiation detectors. Therefore, it is best of all to use chemical sounding [2, 3], chemiluminscent methods [4], or optical methods with direct focusing on the Sun [1] in the lower layers of the atmosphere.

10. Calculation of the Vertical Distribution of Ozone. The vertical distribution of ozone, calculated according to the curve for γ''_h (Fig. 7), is shown in Figure 8. In this case, we assumed th t the condition $\gamma''_h = x_h$ is fulfilled at an altitude of 10 km. The calculations were carried out over layers with thickness of 2.5 km. The ozone concentration (Δx) in the layer was determined as the difference between x_h and $x_{h+2.5}$. The relative error of this difference, for the accuracy in determining γ_h mentioned above, was about 30%, while it reached 100% in layers with very low concentrations. Nevertheless, the course of the curve represented in Figure 8 goes a good deal beyond the limits of the errors.

The ozone concentration [cm/km] was determined for each layer according to the formula $\varepsilon = \Delta x : 2.5$. Unfortunately, the error cited above did not allow us to take a smaller range for this calculation. The general course of the curve in Figure 8 coincides with the well-known data on the vertical distribution of ozone. We cannot say that the structure of the curve obtained shows some stratification of the O_3 layer; however, the latter assumption is not excluded. The complex path of the curve can be connected, not only with the variations in ozone, but also with the possible effect of aerosol layers over Ryl'sk, since it is not completely /198 excluded in the calculations.

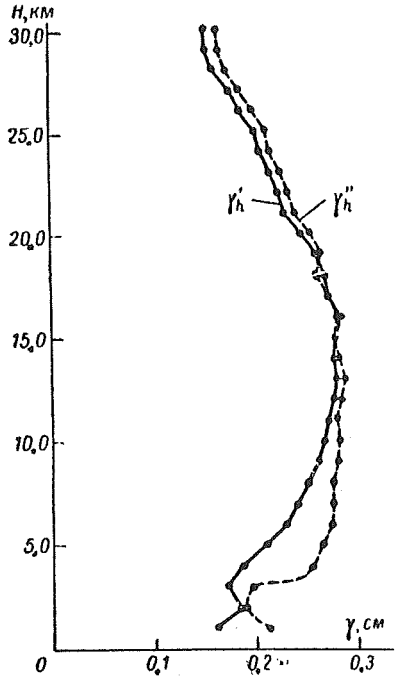

Fig. 7. Change With Altitude of the Function γ_h.

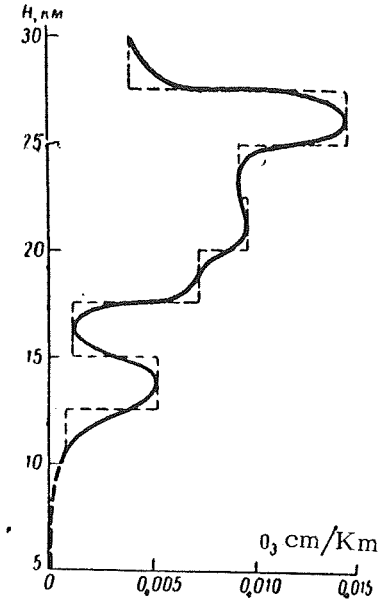

Fig. 8. Vertical Distribution of Ozone over Ryl'sk on July 23, 1965 (the Launch was at z = 64°).

The results presented in Figures 7 and 8 should be considered as preliminary. They are published only for the sake of showing some characteristics of the method.

In conclusion, I would like to express my sincere gratitude to the direction of the Central Aerological Observatory of GUGMS, which granted permission for carrying out this study, and also to Professor S.F. Rodinov, for his valuable advice and counsel.

References

1. Bol'shakova, L.G., A.L. Osherovich, S.F. Rodionov, A.K. Suslov and N.S. Shpakov: Photoelectric Ozone-Meters for Investigating the Vertical Ozone Distribution. Pribory i Tekhnika Eksperimenta, No. 4, 1965.
2. Brewer, A.W. and J.R. Milford: The Oxford-Kew Ozone Sonde. Proc. Roy. Soc., Ser. A, Vol. 256, 1960.
3. Britayev, A.S.: The Problem of Determining the Ozone Content by the Chemical Method. In the Collection: Atmosfernyy ozon (Atmospheric Ozone), 1961.
4. Regener, V. H.: Measurement of Atmospheric Ozone with the Chemiluminescent Method. J. Geophys. Res., Vol. 69, No. 18, 1964.

HYDROGEN COMPOUNDS IN THE MESOSPHERE

V. N. Konashenok

ABSTRACT: The author discusses different reasons for studying the hydrogen compounds in the mesosphere, and he describes a relatively simple method of measuring the H_2O and OH emission profiles there.

The study of hydrogen compounds in the mesosphere is of interest for the following basic reasons: (a) these compounds have a direct effect on the thermal regime of the mesosphere, which consists in its cooling due to the intensive infrared emission of hydroxyl, and an indirect effect, which consists in some contrast in the vertical distributions of the most important oxygen components for the thermal regime in the pure oxygen and oxygen-hydrogen atmospheres; (b) there is no complete understanding of such phenomena as noctilucent clouds and OH emission; (c) these compounds can serve as an indicator of a large number of micro-and macroprocesses. /199

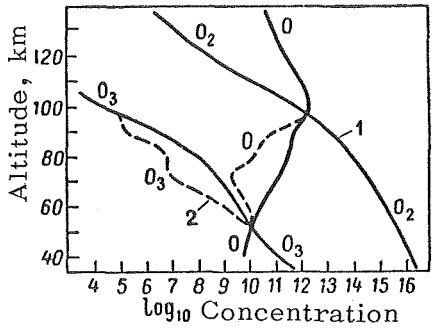

Fig. 1. Diurnal Equilibrium Concentrations of Oxygen (according to Hesstvedt). (1) in a Pure Oxygen Atmosphere; (2) in an Oxygen-Hydrogen Atmosphere.

The first calculations of the oxygen-hydrogen atmosphere found in photochemical equilibrium were carried out in 1950 by Bates and Nicolet [1]. It follows from their results that the water vapor is the principal hydrogen-containing component all the way up to 68 km. Above this level, the water vapor content decreases very rapidly because of photodissociation. In the altitude range of 68-73 km, H_2 becomes the principal component. Above 73 km, most of the hydrogen is an atomic state. Hesstvedt [2] recently carried out more precise photochemical calculations of the vertical distribution of gaseoud components in the oxygen-hydrogen atmosphere. These /200 calculations are represented in Figures 1 and 2. It can be seen from the figures that the qualitative behavior of the curves for the distribution is roughly the same as for Bates and Nicolet. Hesstvedt also calculated the characteristic times for restoration of photochemical equilibrium for various components (Fig. 3).

The low characteristic times for the components OH, HO_2, and O_3 confirm the assumption that they have photochemical equilibrium.

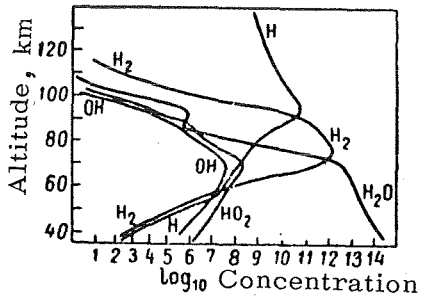

Fig. 2

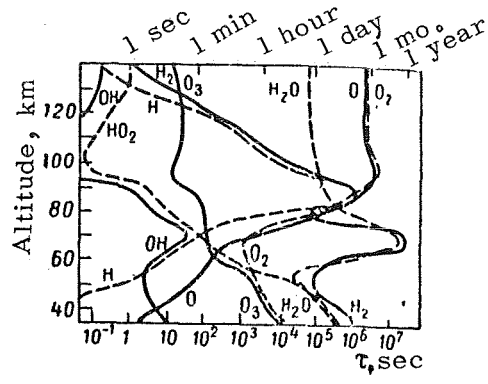

Fig. 3

Fig. 2. Diurnal Equilibrium Concentration of H_2O, H_2, H, OH and HO_2 in the Oxygen-Hydrogen Atmosphere (according to Hesstvedt).

Fig. 3. Characteristic Times in the Diurnal Atmosphere (according to Hesstvedt).

The characteristic times of H, H_2, H_2O, O, and O_2 in the region of the mesopause are relatively high; therefore, their photochemical equilibrium is not as obvious. In order to solve the problem of the possibility of photochemical equilibrium for some gaseous components, we must know the characteristic times of the non-photochemical processes which affect the vertical distribution of this component. Diffusion, vertical motions, and general circulation could serve as such processes. In this study, we will examine only the diffusion, and, since the velocity of the diffusion is proportional to the concentration gradient, while the greatest gradient for water vapor is found in the region of the mesopause, we will limit ourselves to an investigation of the H_2O diffusion.

Characteristic Times for Turbulent Transport of Water Vapor in the Region of the Mesopause

The mesosphere is a region with intensively developed turbulence. The coefficient of turbulent exchange can reach values of 10^6 - 10^7 cm^2/sec there [3,4,5]. The level of gravity separation of gases is at altitudes of about 105 km, i.e., above the mesopause, and the coefficient of molecular diffusion has an order of magnitude of 10^6 cm^2/sec at these altitudes. Therefore, it is natural to expect that the velocities of molecular diffusion in the mesosphere are much less than those of eddy diffusion, and, because of /201 this, we can disregard the molecular transport in comparison with the turbulent one.

Let us define the characteristic time for turbulent transport of water vapor to some level as the times during which the initial mass concentration of H_2O at this level changes by a factor of 2 because of eddy diffusion. A rough estimate of this time can be

obtained according to the formula $\tau = \frac{(z-z_0)^2}{2k}$, which gives a value of τ equal to $5 \cdot 10^5$ sec at $K = 10^6$ cm^2/sec and $(z-z_0) = 10$ km. This estimate is good for an instantaneous point source, while it can be completely disadvantageous for the real distribution of water vapor. Therefore, we will look for the characteristic time from a solution to the semi-empirical equation of diffusion, for a case close to the real one.

Let us consider a model in which a photochemically equilibrious distribution of water vapor is found at the initial moment of time t_0. We will find how the mass concentration of H_2O at different levels changes for this initial distribution by the single effect of eddy diffusion. In the one-dimensional case, the equation for the eddy diffusion has the form of

$$\frac{\partial r}{\partial t} = \frac{\partial}{\partial z}\left[K(z)\rho(z)\frac{\partial r}{\partial z}\right], \tag{1}$$

where z is the vertical coordinate; t is the time; $\rho(z)$ is the density of the air; K(z) is the coefficient of eddy diffusion; $r = \frac{\rho_{H_2O}}{\rho_{air}}$ is the mass concentration of water vapor. For an exponential atmosphere with $\rho = \rho_0 \exp(-\frac{z}{H})$, where H is the altitude of the uniform atmosphere, and for a K(z) which does not depend on the altitude, (1) is rewritten in the following form:

$$\frac{\partial r}{\partial t} = K\left(\frac{\partial^2 r}{\partial z^2} - \frac{1}{H}\frac{\partial r}{\partial z}\right). \tag{2}$$

Since the mass concentration of H_2O remains constant up to an altitude of 70 km, we will take the level of 70 km as the zero. The initial condition can then be represented by the following function:

$$r(0, z) = a\exp\left(-\frac{z}{\beta}\right), \tag{3}$$

which is close to that calculated by Hesstvedt [2]. The boundary conditions for (2) can be written in the following way:

$$\begin{aligned} r(t, 0) &= a, \\ r(t, \infty) &= 0. \end{aligned} \tag{4}$$

By substituting $r = \exp\left(\frac{z}{2H} - \frac{Kt}{4H^2}\right) \cdot u$ into (2), this equation is reduced to the following: /202

$$\frac{\partial u}{\partial t} = K\frac{\partial^2 u}{\partial z^2} \tag{5}$$

with the initial condition of

$$u(0,\ z) = ae^{-\left(\frac{1}{2H}+\frac{1}{\beta}\right)z} = ae^{-\mu z} \tag{6}$$

and boundary conditions of

$$\begin{gathered} u(t,\ 0) = ae^{\frac{K}{4H^2}t} = ae^{\lambda t}, \\ \lim_{z\to\infty} e^{\left(\frac{z}{2H}-\frac{K}{4H^2}t\right)}\cdot u(z,\ t) \to 0. \end{gathered} \tag{7}$$

The general solution to (5) which considers the conditions of (6) and (7) has the following form:

$$\begin{aligned} u = \frac{1}{2\sqrt{\pi Kt}}\int_0^\infty \left[\exp\left(-\frac{(z-\xi)^2}{4Kt}\right) - \exp\left(-\frac{(z+\xi)^2}{4Kt}\right)\right]\cdot ae^{-\mu\xi}d\xi + \\ + \frac{z}{2\sqrt{K\pi}}\int_0^t \frac{1}{(t-\tau)^{3/2}}\exp\left[-\frac{z^2}{4K(t-\tau)}\right]\cdot ae^{\nu\tau}d\tau. \end{aligned} \tag{8}$$

The first integral in (8) is easily converted into a tabular one, and taken precisely, while the second one is approximate, found from the expansion of $e^{\nu\tau} \approx 1 + \nu\tau + \frac{(\nu\tau)^2}{2}$, which is valid for $|\nu\tau| << 1$.

Converting from the function of u to r, we can immediately write out the solution to (2) with the conditions of (3) and (4):

$$\begin{aligned} r = \frac{a}{2}e^{\frac{Kt}{\beta}\left(\frac{1}{H}+\frac{1}{\beta}\right)}\cdot\left\{e^{-\frac{z}{\beta}}\cdot\Phi\left(\frac{2kt\mu - z}{2\sqrt{kt}}\right) - e^{z\left(\frac{1}{H}+\frac{1}{\beta}\right)}\times\right. \\ \left.\times\Phi\left(\frac{2kt\mu + z}{2\sqrt{Kt}}\right)\right\} + ae^{\frac{z}{2H}}\cdot\left\{\Phi\left(\frac{z}{\sqrt{4kt}}\right)\cdot\left(1+\frac{z^2}{8H^2}-\frac{3z^4}{16^2H^4}\right)+\right. \\ \left.+\frac{e^{-\frac{z^2}{4Kt}}}{\sqrt{\pi}}\left(\frac{3z^3\sqrt{4Kt}}{64H^4}-\frac{3z(Kt)^{3/2}}{16H^4}\cdot\frac{z\sqrt{Kt}}{4H^2}\right)\right\}, \end{aligned} \tag{9}$$

where $\Phi(x) = 1 - \int_0^x e^{-\alpha^2}d\alpha$ is the probability integral.

For calculations according to (9), we must know the parameters H and β. We assigned the following values: H = 6 km, β = 1 km. The parameter K does not have to be given, since it is included here only in the form of the product Kt. Calculations were carried /203 out for levels of 80, 85, and 90 km, i.e., equal to 10, 15 and 20 km, respectively, in (9). The results of the calculations are given in Figure 4. It can be seen from this figure that, at the moment of time numerically equal to 1/K, where K is expressed in km^2/sec, the mass concentration of water vapor at all the levels is several times higher than the initial concentration. In an interval of time which is 100 times higher, there is almost complete balancing of the concentration in the range of 70-90 km. However, the latter conclusion is not completely precise, since at Kt = 100, $\nu t = \frac{Kt}{4H^2} = 0.7$, and the representation of the exponent in the form of the trinomial $1 + \nu t + \frac{(\nu t)^2}{2}$ is insufficient.

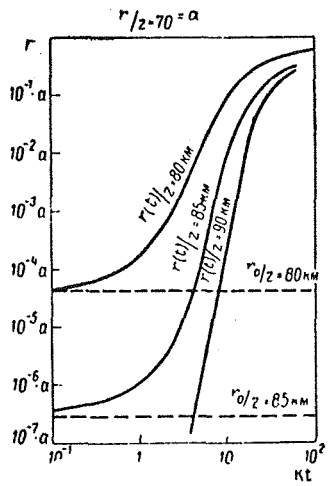

Thus, for coefficients of eddy diffusion of 10^{-4} - 10^{-3} km^2/sec (10^6-10^7 cm^2sec), the characteristic time for turbulent transport of water vapor in the upper mesosphere has values of 10^4 - 10^3 sec. The time for restoration of photochemical equilibrium, as seen in Figure 3, is greater than 10^5 sec. A comparison of the photochemical and turbulent times shows that the water vapor is not in photochemical equilibrium.

Fig. 4. Dependence of the Mass Concentrations of H_2O on the Time for the Levels of 80, 85, and 90 km. K-Coefficient of Diffusion, Expressed in km^2/sec; t-Time; r-Mass Concentration of Water Vapor.

Minimum Amount of Water Vapor in the Upper Mesosphere

As was shown above, photochemical processes and eddy diffusion affect the vertical distribution of water vapor. The diffusion tends to make the mass concentration constant at different altitudes, while the photodissociation decreases it with the altitude. Since photodissociation occurs only in the day-time, while diffusion occurs during the entire 24-hour period, and, moreover, since the time for diffusion is less, it is obvious that the amount of water vapor at any altitude can be much greater than the photochemically equilibrious concentration.

For a more accurate estimate of the H_2O content, we must examine the diffusion equation with a consideration of the reactions. The values for the photochemical and diffusion times allow us to assume that there are no substantial daily variations, so that we

can examine the stationary case. We can then write out the equation for the volume concentration: /204

$$\frac{d}{dz}\left(KN\frac{dn}{dz}\right) = L - P, \tag{11}$$

Where N is the concentration of air particles; $n = \frac{N_{H_2O}}{N_{air}}$ is the volume concentration of H_2O; L and P are the rate of losses and production of H_2O due to the chemical reactions. The losses in water vapor at each level occur at a velocity of J(z)n(z)N(z). The coefficient of photodissociation J(z) increases with an increase in the altitude, and has a maximum value at the upper boundary of the atmosphere. If we consider J(z) to be a constant equal to the value for the coefficient of dissociation for zero optical thickness, then the velocity of photodissociation is somewhat increased. Moreover, if we disregard the production of H_2O by chemical reactions in (11), then the computed concentration is much more decreased. Thus, in order to determine the minimum amount of water vapor, (11) can be written in the form of

$$\frac{d}{dz}\left(KN\frac{dn}{dz}\right) = JNn. \tag{12}$$

The boundary conditions for (12) will be represented thus:

$$\begin{aligned} n|_{z=0=70\ \text{км}} &= b, \\ n|_{z=\infty} &= 0. \end{aligned} \tag{13}$$

For the exponential atmosphere with $N = N_0 \exp(-\frac{z}{H})$ and for a constant coefficient of diffusion, equation (12) with the conditions of (13) has the following solution:

$$n = b\exp\left(\frac{\frac{1}{H} - \sqrt{\frac{1}{H^2} + \frac{4J}{K}}}{2} z\right). \tag{14}$$

Using the value for the coefficient of water vapor dissociation at the upper boundary of the atmosphere as equal to 10^{-5} sec^{-1} [6], we find the following selected values of H = 6 km and K = 10^{-4} km^2/sec:

$$n = b\exp(-0{,}24z). \tag{15}$$

It follows from (14) and (15) that, if the diffusion factor is no less than 10^{-4} km^2/sec, then the volume percentage of water vapor in the upper mesosphere depends slightly on the altitude.

Obviously, (14) can also be used for evaluating the water vapor content above the turbopause, since the molecular diffusion is described by the same equation and it also moves the water vapor upwards.

Possibilities of Experimental Proof

The basic hindrance to the development of the theory of the oxygen-hydrogen atmosphere consists in the almost complete absence of experimental data on the concentrations of hydrogen-containing compounds in the mesosphere. Direct rocket measurements of such small concentrations are extremely complex, and it is difficult to imagine how they could be carried out in the near future; therefore, we should turn our attention to indirect methods. The basic indirect source of information on the hydrogen in the mesosphere is the hydroxyl emission. If we consider the ozone-hydrogen reaction to be the principal mechanism for excitation of this emission, then it is possible to formulate an experiment by which the vertical distribution of atomic hydrogen can be obtained. It can be seen from the equation for transfer of radiation in the OH line (when there is no self-absorption), i.e., /205

$$\frac{dI}{dz} = k\,[O_3]\,[H] \qquad (16)$$

(here I is the intensity; $[O_3]$ and [H] are the ozone and atomic hydrogen concentrations; K is the velocity constent of the reaction $O_3 + H \rightarrow OH + O_2$) that, in order to determine the vertical profile of [H] we must measure I(z) in arbitrary units, the vertical distribution of ozone and the total emission of the infinite column, expressed as the number of photons. The difficulty in this experiment is the need for simultaneous measurements of the ozone and OH emission.

To obtain the H_2O and OH profiles, we can use the method developed for satellite measurements of ozone; however, the measurements themselves and their interpretation are obviously much more complex.

REFERENCES

1. Bates, D and M. Nicolet: The Photochemistry of Atmospheric Water Vapor. J. Geophys. Res., Vol. 55, 1950.
2. Hesstvedt, E.: Some Characteristics of the Oxygen-Hydrogen Atmosphere. Geophys. Publikasjoner Geophys. Norvegica, Vol. XXVI, No. 1, 1965.
3. Lettau, H.: Diffusion in the Upper Atmosphere. Compend. of Meteorol, Boston, 1951.
4. Zimmerman, S.R. and K.S.W.Champion: Transport Processes in the Upper Atmosphere. J. Geophys. Res., Vol. 68, No. 10, 1963.
5. Colegrove, F.D., W.B.Hauson, and F.S.Johnson: Eddy Diffusion and Oxygen Transport in the Lower Thermosphere. J. Geophys. Res., Vol. 70, No. 19, 1965.
6. Nicolet,M.: Aeronomiya (Aeronomy). "Mir, 1964.

ON THE VERTICAL AEROSOL DISTRIBUTION AND AEROSOL LAYERS IN THE ATMOSPHERE

A.M. Bunakova and L.S. Ivlev

ABSTRACT: The authors review and appraise data obtained by different authors for the vertical distribution of aerosols in the atmosphere by altitude. It is shown that laser methods and spacecraft measurements have become very useful in these studies.

The radiation regime of the atmosphere is determined mainly /206 by the presence of aerosols and water vapor in the atmosphere, their interaction, and the variability in concentrations of these components. As is well known, aerosols are the most active, optically speaking, and the least studied constituent of the atmosphere, and are found in it at practically all altitudes, whereas the computed concentration and spectrum of aerosol particles change with the altitude. Numerous studies on the vertical distribution of aerosols, carried out both with an indirect intake of aerosol specimens on filters, inertial catchers and condensation-nucleus counters [1-5], as well as by optical methods, allow us to conclude that aerosols are the principal factor determining the conditions for light scattering up to altitudes of 80-90 km, or up to higher altitudes, according to the data of A.Ye. Mikirov [9]. The optical methods include: an investigation of the atmosphere by the method of a projected beam (a laser beam, recently), a study of twilight phenomena, photometry of the Earth's shadow in lunar eclipses, measurement of the brightness of the sky, the attenuation of direct solar light, and the polarization of the light in the atmosphere [6-18]. A study of the optical characteristics of the atmosphere gives only a qualitative idea of the vertical distribution of aerosols in the atmosphere.

The contribution of aerosols to the decrease in solar radiation can be determined by using a model of the standard atmosphere and experimental data on the decrease of direct solar light. Careful calculations of this type allow us to construct the curve for the distribution of aerosol attenuation up to 80 km for the standard pure atmosphere. These curves, constructed by various authors, show clearly-pronounced aerosol layers in the region of the tropopause at altitudes from 16 to 23 and from 80 to 90 km. Direct investigations of the aerosol concentration also confirm that there are constantly-existing layers of aerosol particles with radii /207 greater than 0.1 μm.

The curves for the vertical distribution of large aerosol particles up to an altitude of 30 km which were obtained by L. Elterman

[14] and C. Junge [1] were constructed mainly according to the same experimental data. We should mention that Elterman disregarded the break in the exponential curve for the vertical distribution of tropospheric aerosols at an altitude of about 5 km, and considered that the concentration of particles with $r > 0.1$ μm was equal to 0 above 30 km. However, the experimental data of G. Newkirk [6] show that this model is too approximative. Newkirk found thin thirty-meter aerosol layers separated by three-hundred-meter layers of relatively pure air. Simultaneous airship measurements of the solar aureole and ion concentration at different altitudes correlate well, which can serve as a confirmation of this conclusion.

Lasers [10,11] have recently been used for long-range observations in the atmosphere; in particular, laser measurements have been carried out for the atmospheric constituents [12,13]. The measurements obtained with lasers [10,14,15] show that the aerosol scattering all the way to altitudes on the order to 80 km is of the same order as the gaseous diffusion (it is just as intense), while the scattering power of aerosols in the short-wave part of the visible region is no lower than that of the gaseous component of the atmosphere, and exceeds the latter in the long-wave region.

The great variability of aerosol scattering both in time and in altitude is a characteristic aspect. For example, aerosol layers which have an assumed cloud structure [16] are clearly distinguishable. These layers are most often concentrated in the region of the tropopause (9-12 km in our latitudes) and in the region around 25 km (nacreous clouds) [19,20]. Aerosol layers have also been observed at other altitudes (25-35 and 40-45 km, see [7]). These layers are most often formed in the region of temperature inversions [16], to which the tropopause and the level of about 80 km, in particular, belong.

Unfortunately, there is almost nothing certain known of the nature, concentration or size of particles in aerosol layers, although interest in the optical properties of aerosols has increased greatly during recent years.

Investigations of the aerosol component in the troposphere [1,2,8] confirm that aerosol layers exist there; however, these layers depend greatly on the local meteorological conditions: temperature stratification, season, time of the day, incoming air masses and underlying surface. Nevertheless, there are some regularities in the vertical distribution of tropospheric aerosols for the pure atmosphere. We can consider that the distribuiion of particles by size which was found experimentally and theoretically bu C. Junge - with an abrupt decrease in the computed aerosol concentration at $r \leq 10^{-2}$ μm - is reliable for it, i.e., /208

$$\frac{dn}{dr} = -\frac{C}{r^{\alpha+1}},$$

where $\alpha = 3$. However, the exponent can decrease down to 2 when the humidity of the atmosphere increases. In the layer around the ground up to an altitude of about 2 km, the computed aerosol concentration is determined by the underlying surface, the presence of point sources of aerosols, and changes in the widest limits from 10^6 to 10^0 particles/cm^3 for particles with diameters greater than 0.1 μm. Above 1 km, the computed concentration decreases with the altitude according to an exponential curve whose exponent changes at an altitude of about 5 km.

The results of the measurements G. Newkirk carried out with airships are interesting [6,15]. He found thin layers with increased scattering power, whose thickness was roughly 30 m. Weak temperature inversions corresponded to these layers.

Some of the disagreements in the results of studies of the vertical aerosol distribution in the atmosphere by different optical methods might be explained by the meteorological factors (airship measurements are usually carried out in an anticyclone during the morning hours), as well as by a disregard of the role of multiple scattering and the albedo. Integral and spectral optical measurements of the transmissivity of the atmosphere can give different information on the thickness or presence of an aerosol layer. As is well known, the aerosol extinction is composed of three components: absorption, which can be substantial for a very high computed concentration of aerosol particles; scattering on large aerosol particles whose dimensions are comparable with the wavelengths of the solar radiation; scattering on Rayleigh aerosol particles (Aitken nuclei). The last factor is not usually considered. However, if we recall that the maximum of the distribution particles by size occurs in the range of Rayleigh scattering, where Rayleigh aerosol particles are 2-3 times greater than molecules of the air, then it becomes clear that the finely-divided aerosols (so-called condensa-nuclei) can make a substantial contribution to the radiation regime of the atmosphere.

In the measurements by C. Junge, the condensation-nucleus counter did not detect any aerosol layers consisting of Aitken nuclei (see Fig. 1). This smooths out the layers of aerosol attenuation somewhat in integral measurements. At the same time C. Junge reported that the condensation-nucleus counter possibly gave decreased data on the Aitken nuclei [6].

It is essential to note that the methods of studying aerosols with sample specimens also have their disadvantages, in relation to the difficulty of converting from the data on the sampler to the real distribution of particles in the atmosphere. Moreover, under the real conditions of airship measurements, there are two /209
factors which are usually not considered: (1) air bubbles which move for some time with the airship are constantly produced above it; (2) the effectiveness of a capture for wet consolidated particles is higher than for the nuclei which remain after evaporation;

therefore, a re-calculation for the distribution of particles in the atmosphere gives a decreased number of fine aerosol particles.

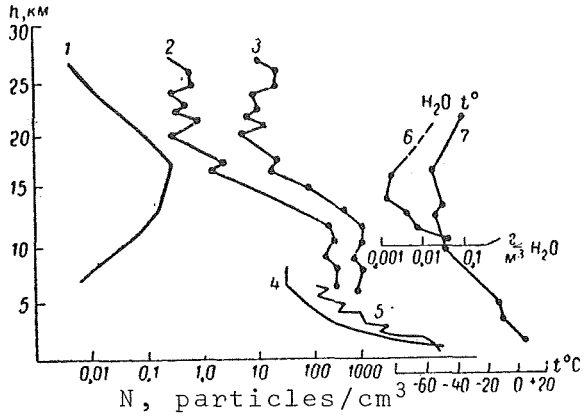

Fig. 1. Vertical Aerosol Distribution. (1) Vertical Distribution of Aerosol Particles with r > 0.1 μm (according to C. Junge); (2) Vertical Distribution of Condensation Nuclei (According to C. Junge); (3) Vertical Distribution of Condensation Nuclei (Reduced to Standard Pressure and Temperature); (4) Aerosol Distribution (according to Wiggand); (5) Aerosol Distribution (According to Wakeman); (6) Percentage of Water Vapor in the Atmosphere; (7) Temperature Profile of the Atmosphere.

The principal problem in a study of the vertical aerosol distribution in the atmosphere is to find what the aerosol layers are composed of - dust particles or small ice crystals and water drops condensed in solid aerosol particles - and what their particle concentration is. This problem is closely related to those of the origin of aerosol particles and their chemical composition. Examining the problems of the origin of aerosols and the distribution of particles by size, G.M. Idlis [21] concluded that the distribution of particles by size should obey the law proposed by C. Junge, and he also confirmed that the aerosol distribution in the atmosphere should have a layered nature.

Obviously, only dust layers can exist at altitudes from 30 to 70 km. At an altitude above 70 and below 30 km, either a very strong supersaturation of water vapor, which can be caused by powerful convective flows, or relatively low supersaturation and the presence of hygroscopic /210 condensation nuclei is necessary for the formation of ice crystals or water drops. Numerous investigations of the dependence of aerosol attenuation on the relative humidity in the layers of the atmosphere around the Earth show a good correlation: the attenuation of radiation is increased when the relative humidity increases. Some researchers have observed an anomalous increase in the transmission at 70% relative humidity. A correlation between the total water vapor content and the aerosol extinction has not been detected [22], which shows the need for considering convective flows. During the morning and the evening, when the convective flows are weak, there is a direct relationship between the absolute humidity and the water vapor content in the vertical atmospheric column [23]. Under such conditions, a correlation should probably be observed between the humidity and the aerosol extinction. There is a sufficient amount of hygroscopic par-

ticles in the troposphere. The aerosol layers in the region of the tropopause probably also consist of drops condensed in hygroscopic nuclei, and represent ordinary tropospheric clouds. Obviously, as a result of the condensation of water vapor in aerosol particles, nacreous clouds are also formed, appearing from time to time at an altitude of about 25 km. They consist of particles with average radius of 0.75 μm and computed concentration on the order of several particles per cubic centimeter (this corresponds to condensation of 10^{-12} g/cm^3 of water). An analysis of the optical data confirm that nacreous clouds consist of supercooled water drops.

The direct measurements of the aerosol distribution at altitudes from 10 to 30 km which have been carried out by sampling from airships and aircraft have shown the existence of a relatively stable (in time) aerosol layer which changes little in dependence on the geographic coordinates, which is located at altitudes between 16 and 24 km, and which consists of 94% hygroscopic sufur-containing ammonium compounds with dimensions of 0.1-1 μm (the distribution of aerosol particles by size in the stratosphere layer was studied in [24]). These aerosol particles are proba ly of a photochemical origin. Their computer concentration N has a maximum in order of magnitude close to N = 1 cm^{-3}, while the volume concentration V is on the order of 10^{-14} cm^3/cm^3. The altitudinal profiles N(h) are close in nature to those obtained by V.V. Nikolayeva-Tereshkova and G.V. Rozenberg [24].

The spacecraft experiments have certainly found new prospects for the study of the vertical optical structure of the atmosphere. The authors of [24] used observations of the twilight aureole of the Earth form a spacecraft in order to find the structure of stratospheric layers (these layers are imperceptible to the ground observer because of the small vertical optical thickness).

Assuming that the aerosol component of the atmosphere is uniform in the horizontal direction, we can approximate the real altitudinal distribution of aerosols by a system of spherical uniform layers of a definite thickness. Using this method, we can determine the absolute values and change of the scattering factor with the altitude for atmospheric aerosols which are distributed irregularly with altitude, i.e., the altitudinal optical structure of aerosol layers in the stratosphere.[1] The results are given in Figure 2. /211

As can be seen from this figure, a relatively thin and weakly-

[1] The quantitative characteristics of the stratospheric aerosol layer obtained by V.V. Nikolayeva-Tereshkova and G.V. Rozenberg are provisional. In particular, the problem of the degree of horizontal uniformity of the aerosol layer remains open.

pronounced aerosol layer at altitudes of 11.5 ± 1 km and a much larger layer at an altitude of 19.5 ± 1 km appear clearly. According to the calculations of the authors, the half-thickness of the upper layer is about 5 km and $\sigma_{max} = 5 \times 10^{-3}$ km^{-1}, which agrees roughly with Opik's estimate [1].

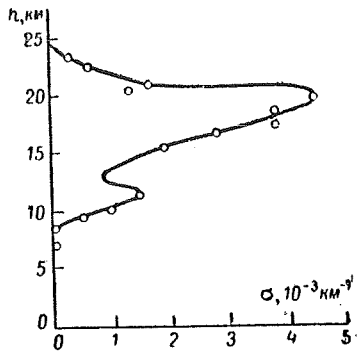

Fig. 2. Altitudinal Change in the Scattering Factor σ.

The existence of an aerosol layer at altitudes of about 20 km which greatly weakens the light rays at this altitude had already been suggested long ago [16, 17]. However, this purely qualitative assumption had been scarcely convincing, since it had not been proven by corresponding quantitative evaluations. More precise results in this direction were obtained in [17] on the basis of a quantitative analysis of the phenomena of purple light.

Some information was also obtained from data of long-range sounding of the stratosphere in [7]. It was found that the degree of polarization of scattered light in the range of altitudes of 12-20 km doubtlessly exceeds the value expected for molecular scattering. Consequently, the scattering occurs on isotropic particles whose dimensions are close to the length of the light wave. Measurements of the scattering factors at altitudes of 8-17.5 km showed [13] that, beginning at 13 km, the extent of the factor increases with an increase in the altitude, which also indicates that the role of the aerosols in the scattering of light increases.

The value of N obtained in [17] practically coincides with that found in [1,3-5] (in both cases, this value is determined with accuracy up to the order of magnitude). As for the volume concentration V, it is one order higher according to the measurements of Rozenberg and Nikolayeva-Tereshkova than according to [1,3-5]. The /212 reason for this discrepancy could be the fact that hygroscopic aerosol particles in the stratosphere are "clothed in a jacket of water or ice", while, after the sampling of particles in traps, only their dry core, which naturally has less volume, is subjected to analysis (For the "drying" of aerosol particles, see, for example, [1] by C. Junge.)

A comparison of the values of τ, r (effective radius of particles and N obtained by different methods in different experiments shows that a high-altitude aerosol layer delivers condensation nuclei for the formation of nacreous clouds, and that the latter arise as a result of the condensation of water vapor in adiabatic cooling of an air mass moving from altitudes of 16-20 km to 21-25 km. The existence of a dust layer around the Earth at an altitude

of roughly 19 km is once more confirmed by the data obtained by astronauts during the flights of the "Vostok" and Voskhod" spacecraft. A series of optical observations carried out on these craft confirmed that there is a layer at an altitude of 19 km, as well as certain other aerosol layers (their number varies - from one to three) which are relatively stable and extensive; these studies also showed that these layers are observed not only during twilight but also during the day. It is interesting that they are sometimes not seen at all on photographs, which probably depends on the photographing conditions [28].

There is no single point of view relative to the nature of noctilucent clouds. Some researchers maintain that they consist of ice crystals, and others hold that they are formed by an accumulation of dust particles, mainly of a meteoric origin.

Noctilucent clouds coincide with the lower boundary of the planetary aerosol layer observed by different scientists with optical methods (see [9,16,17,25]). The upper boundary of this layer has been defined up to altitudes of 150 km [25]. In analyzing twilight data, F. Volz and R. Goody [17] concluded that there is no aerosol layer above 100 km. This agrees with the fact that the density of the air at such altitudes is so low that the particles, regardless of their size, cannot be in suspension. The flow of meteoric dust begins to slow down in the region of the inversion at a level of about 80-90 km, where frozen particles also accumulate.

According to the data of A.Ye. Mikirov [9], who studied the brightness of the sky, the density of aerosol matter at the maximum of the aerosol layer reaches 10^{-16} g/cm^3, which gives a computed concentration on the order of 10^{-4} particles/cm^3. The rocket data on the computed concentration of aerosol particles in noctilucent clouds obtained by C. Hemenway, R. Soberman and G. Witt [27] show that the amount of particles in the clouds reaches 10^{-2} particles/cm^3 (i.e., exceeds the concentration of particles when there are /213
no clouds by a factor of two). Particles with dimensions from 0.1 to 0.5 μm predominate. An analysis of specimens showed that they are particles of a meteoric origin in an ice shell [27].

The calculations of S. Chapman and P. Kendall [26] show that the percentage of water vapor in the mesopause is sufficient for noctilucent clouds to appear under favorable conditions. For example, there must be a high concentration of aerosol particles, which can be in the form of condensation nuclei, and there must not be rigid radiation, by the effect of which water dissociates. The experimental data presently known on the vertical aerosol distribution and the aerosol layers in the atmosphere still do not permit us to construct a clear representation of the stratification of the atmosphere. The results of different experiments do not always coincide, and occasionally differ greatly in the quantitative aspect, in relation with which the need for re-examining some data

arises. It is impossible to make even a cursory review of the reasons for the existing contradictions in a very short survey. Nevertheless, we have attempted to touch on some of them.

REFERENCES

1. Junge, C.E.: Air Chemistry and Radioactivity. N.Y., Pergamon Press, 1963.
2. Laktionov, A.G.: Distribution of the Concentration of Aerosol Particles by Altitude. Izvest. Akad. Nauk S.S.S.R., ser. geofiziki, No. 9, 1960.
3. Rosen, J.M.: Vertical Distribution of Aerosols. J. Geophys. Res., Vol. 69, No. 21, 1964.
4. Bigg, E.K., C.T. Miles and K.J. Hefferman: Stratospheric Ice Nuclei. J. Meteorol., Vol. 18, No. 6, 1961.
5. Friend, J.P., R.D. Sherwood and B.E. Sobels: NASP Stratospheric Particle Studies. Bull. Amer. Meteorol. Soc. No. 1, 1964.
6. Newkirk, G.A., and J.L. Kroening: Aerosols in the Stratosphere. J. Atmosph. Sci., Vol. 22, p. 5, 1965.
7. Collection: Prozhektornyy luch v atmosfere (Searchlight in the Atmosphere), Ed. G.V. Rozenberg. Izdat. Akad. Nauk S.S.S.R., 1960.
8. Penndorf, R.: The Vertical Distribution of Mie Particles in the Troposphere. Geophys. Res. Papers USAF, Vol. 25, p. 1, 1954.
9. Mikirov, A.Ye.: Aerosol Layer in the Upper Atmosphere. Doklady Akad. Nauk S.S.S.R., Vol. 142, No. 3-4, 1962.
10. Fiocco, G., and L. Smullin: Detection of Scattering Layers in the Upper Atmosphere (60-140 km) by Optical Radar. Nature, Vol. 199, p. 1275, 1963.
11. Collis, R., and M. Ligda: Laser Radar Echoes from the Clear Atmosphere. Nature, Vol. 203, p. 508, 1964.
12. Hirono, M.: On the Observation of the Upper Atmospheric Constituents by Laser Beams. J. Radio Res. Lab., Vol. 11, No. 56251, 1964.
13. Harris, E. and oth.: AFCRL-65-177. Air Force. Cambridge Research Laboratories. Office of Aerospace Research. United States Air Force. Bedford (Mass.), 1965.
14. Elterman, L., and A.K. Campbell: Observations of the Atmospheric Aerosols. J. Atmosph. Sci., Vol 21, p. 456, 1964.
15. Newkirk, G., and J.A. Eddy: Light Scattering by Particles in the Upper Atmosphere. J. Atmosph. Sci., Vol. 21 (1), 1964.
16. Rozenberg, G.V.: Sumerki (Twilight). "Fizmatgiz", 1963.
17. Volz, F.E. and R.M. Goody: The Intensity of the Twilight and Upper Atmosphere Dust. J. Atmosph. Sci., Vol. 19, p. 385, 1962. /214
18. Sandomirskiy, A.B., N.T. Al'tovskaya and G.I. Trifonova: Studies of the Brightness of the Daytime Sky at Altitudes of 8.0-17.5 km. In the Collection: Aktinometriya i optika atmosfery (Actinometry and Optics of the Atmosphere). "Nauka", 1965.
19. Ludlam, F.H.: Noctilucent Clouds. Tellus, Vol. 9, p. 341, 1957.
20. Opik, E.J.: Interplanetary Dust and Terrestrial Accretion of Meteoritie Matter. Irish Astron. J., Vol. 4, p. 84, 1956.

21. Idlis, G.M.: The Origin and Distribution by Size of Different Dust Particles. Izvest. Akad. Nauk Kaz. S.S.R., ser. astrofiziki, Vol. 12, 1961.
22. Compendium of Meteorology. Ed. by T. Malone. Boston, Amer. Meteorol. Soc., 1951.
23. Green, H.L. and W.R. Lane: Particulate Clouds, N.Y. 1964.
24. Rozenberg, G.V. and V.V. Nikolayeva-Tereshkova: Stratospheric Aerosols According to Spacecraft Measurements. Izvest. Akad. Nauk S.S.S.R., ser. fiziki atmosfery i okeana, Vol. 1, No. 4, 1965.
25. Memoires de la Societe Royale des Sciences de Liege, Vol. 15, p. 55, 1955.
26. Chapman, S. and P.S. Kendall: Noctilucent Clouds. Quart. J. Meteorol. Soc., Vol. 91, p. 388, 1965.
27. Hemenway, C.L., R.K. Soberman and G. Witt: Sampling of the Particles in the Noctilucent Clouds. Tellus, Vol. 16, No. 1, 1964.
28. Feoktistov, K.P., G.V. Rozenberg, A.B. Sandomirskiy, V.N. Sergeyevich and D.M. Sonechkin: Some Results of Optical Observations on the "Voskhod". Transactions of an All-Union Conference on Space Physics, Moscow, 1965.

THE EFFECT OF THE VERTICAL AEROSOL DISTRIBUTION ON THE RADIATION REGIME OF THE ATMOSPHERE

K. Ya. Kondrat'yev and A. M. Bunakova

ABSTRACT: Experimentally-determined profiles characterizing the extinction of direct solar radiation by the aerosol components of the atmosphere are discussed in this article. The nature of the changes which the aerosol layers make in the vertical profile of the thermal radiation is examined.

In [1], we attempted to examine as systematically as possible the experimental data presently known on the vertical aerosol distribution and the aerosol layers in the atmosphere. This was necessary in connection with the airship studies of the radiation regime of the troposphere and stratosphere being carried out by the Department of Atmospheric Physics. /215

This study is a continuation of [1] to an extent. It is of substantial interest to study and compare occasionally contradictory results of measurements and to find the reasons for these contradictions. This study consists of two parts. The first part contains a discussion of experimentally-determined profiles characterizing the extinction of direct solar radiation by aerosol components. In the second part, we will examine the nature of the changes which the aerosol layers make in the vertical profile of thermal radiation.

The fole of aerosols in the radiation regime of the atmosphere, particularly its upper layers, has been studied relatively little. It is true that methods of studying the atmosphere from satellites and other space vehicles have recently become more developed. It is enough to mention the infrared satellite measurements from "Tiros".

It is mainly the extinction of solar radiation (absorption + scattering) which has been studied. The reflected and scattered radiation are essential components of the atmospheric radiation balance and play an important role in the thermal balance of the Earth. The direct solar radiation which reaches the ground observer represents only part of the solar radiation transformed by the atmosphere; the other part is absorbed and scattered in the atmosphere. Some of this scattered radiation goes back into outer space, while the remaining part reaches the Earth's surface in the form of the scattered radiation of the sky.

The data on the vertical distribution of direct solar radiation permit us to determine the distribution of various components which weaken the direct solar radiation S in the atmosphere. /216

During a number of airship flights in 1964, a group of colleagues at Leningrad State University [2] found the altitudinal distribution of total energy S weakened by aerosols above a given level all the way to altitudes on the order of 25-30 km, as well as vertical profiles for the decrease of S by layers (1.0 km) (Fig. 1).

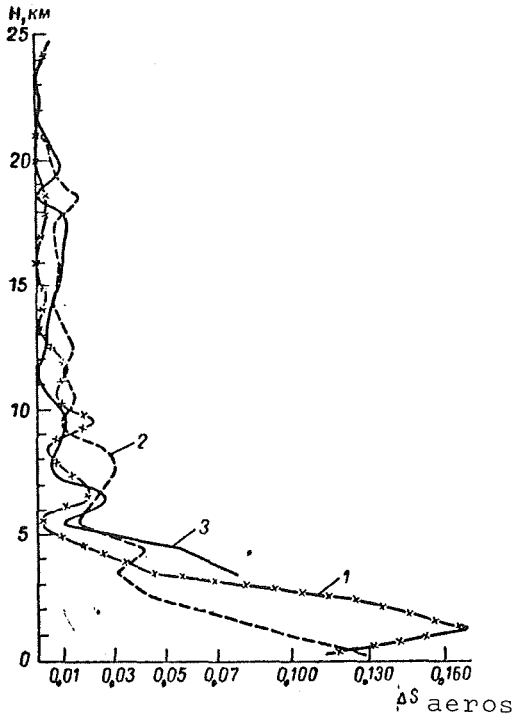

Fig. 1. Vertical Distribution of the Decrease of S by Layers by the Aerosol Components, $cal \cdot cm^{-2} \cdot min^{-1}/km^{-1}$. 1,2,3,- Experimental Curves For Flights in 1964.

Having analyzed these data, we can find some general rules connected with the vertical structures of aerosol layers in the atmosphere. We should mention that the vertical profiles obtained during the cited flights differ somewhat from those found by G.V. Rozenberg and V.V. Nikolayeva-Tereshkova [3]. It is true that we can also find aerosol layers at altitudes on the order of 9.5 and 18.5 km here; however, they are not as clearly pronounced, and the layers themselves are somewhat lower. The upper layer given in [3] is much more strongly pronounced and thicker, while the lower layer, on the other hand, is more weakly pronounced. The common feature is the notable stability of the upper layer in time.

Naturally, it is difficult to draw any final conclusions on these data, which are far from complete, but they show again that there is an aerosol layer in the interval of altitudes from 16 to 24 km which consists of hygroscopic nuclei [4-7] and which is relatively stable in time and changes insignificantly in depen dence on the observation site.

A rather intense layer is also observed near the 6 km level. /217
In contrast to the results obtained in [4-7], an increase in the aerosol concentration was noted in almost all the flights above 24 km. This discrepancy can be explained by the different experimental conditions. Naturally, additional investigations are needed for more precise quantitative conclusions.

As is well known, the interaction between the matter and the radiation can be attenuation (extinction) or radiation (emission). These processes differ only by the sign for the intensity as a result of the interaction.

A study of the effect of aerosols on the thermal radiation of the atmosphere is of particular interest. The long-wave radiation of high-altitude aerosol layers was studied in detail by F. Möller and W. Zdunkowski [8,9]. These authors referred to the measurements by G. Rönicke [10] of the radiation balance in the free atmosphere over central America which, in contrast to all the theoretical and experimental data known until then, showed that there is a strong radiative warm-up, roughly of 5°C/day and more, in the upper troposphere and the lower layers of the stratosphere. Since atmospheric gases almost always bring about cooling due to radiative heat exchange, the measured strong heating can be explained only by assuming that there is an additional absorbent.

Thus, we can give the measurement results an indirect interpretation by considering that the atmosphere contains a complementary gray emitter in addition to a selective one. Möller suggested a graphic method for calculating the density of the radiation flux in such an atmosphere. W. Zdunkowski developed it into a numerical method, the application of which for a number of experimental models agrees well with the measured profiles for the warm-up $(\frac{dT}{dt})_{rad}$ (T-temperature, t-time). Nevertheless, the densities of the radiation fluxes are roughly 20% decreased in this case.

It is interesting to find which chagnes the aerosol layers cause in the vertical profile for the thermal radiation.

The heating or cooling of the atmosphere is proportional to the divergence of the density of the effective radiation flux, the magnitude and sign of which are determined by the distribution of the temperature by altitude and a number of other factors (concentration of absorbing gas, etc.). The divergence itself is obtained with the aid of a radiation nomogram. It is held that cooling usually takes place in the cloudless atmosphere, in which the temperature and quantity of absorbents decrease with the altitude. However, different bends in the curve for the temperature with the altitude, as well as the curve for the distribution of humidity by altitude, can result in anomalous cooling or heating. Möller explained a similar, seemingly incomprehensible anomaly in the tropopause by assuming that there was a layer of a gray radiator. It is well known that anomalous cooling or heating due to discontinuities in the temperature and humidity occur only in thin layers /218 of a few hundreds of meters.

Some characteristic features appear because of the atmospheric distribution of ozone. The ozone content is minimum at the ground level and increases with the altitude. The maximum concentration is observed roughly at an altitude of 25 km. At altitudes of 5-20 km as well as in the lower part of the ozone layer, even in the atmospheric water vapor window, there is a slight warm-up of the atmosphere (several tenths of a degree). There are no such characteristics for the vertical distribution of the concentration of

carbon dioxide or water vapor. Because of the constant concentration of carbon dioxide in the tropopause (except for the level of the temperature inversion), there is slight cooling due to the CO_2.

For water vapor, an increase in the realitive humidity with the altitude generally does not cause a warm-up, since the elasticity of saturation decreases greatly with a decrease in the temperature. That is why the results of the measurements which G. Rönicke [10] carried out over Central America for the balance of long-wave radiation, which give a strong warm-up in the layers of several--kilometer thickness, are surprising.

An analogous anomalous effect (although weaker--on the order of 1° C/day) was detected by V. Suomi and P. Kuhn [11], as well as by other researchers (see [12], for example). This anomalous effect was that the balance of long-wave radiation decreased unexpectedly, whereas (if we consider only the emitting gases in the atmosphere) it should be practically constant. As researchers show, the ascending flux of effective terrestrial radiation at tropical latitudes does not increase monotonously with the altitude as usual during the night; in the layer roughly 6 km below the tropopause (and sometimes above it), the flux decreases substantially.

How can this heating effect be explained? It cannot be due to the effect of the ozone layer, since it is well known that there are substantial ozone concentrations only above 18 km at tropical latitudes. G. Plass [13], in particular, showed that ozone cannot be the reason for such a strong heating effect (5°C/day and more).

Since no clouds which could explain the warm-up have been observed, it is natural to assume that there is another, complementary, radiator, because this strong heating can be explained only by the presence of such a radiator. Obviously, we are speaking of alayer of haze, which is often observed during aircraft experiments, even if the ground observations show a clear sky. The existence of such a layer has been confirmed by measurements [14]. /219

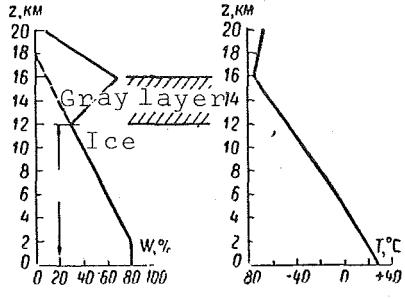

Fig. 2. Distribution of Temperature (on the Right) and Humidity (on the Left) With the Altitude.

D. Deirmendjian [15] showed that the attenuation factor (absorption coefficient plus scattering factor) of atmospheric haze, which is assumed to consist of water drops, changes for a given distribution in a spectral interval of 3-15 μm (in rough approximation) by a factor of 10, while the coefficient of attenuation of water vapor in the same interval changes by a factor of 10^4. Thus, compared to water vapor, the haze can be considered as a gray absorbent.

As was already mentioned, F. Möller was the first to develop a method for calculating the radiation of a gas + aerosol system. Müller and Zdunkowski treat the results of Rönicke's measurements precisely as the effect of haze (aerosol effect), i.e., they attribute this anomaly to the presence of a layer of haze at a high altitude. Since, on the one hand, an apparent increase in the ozone content is observed during the night at tropical latitudes, and, on the other hand, the tropospheric heating effect is characteristic of these latitudes, it could be considered that it is not the ozone content but the aerosol scattering which increases roughly by a factor of 7 during the night, 30-50% being of a Rayleigh nature. However, the difficulty is that there is no definite information on the composition or origin of this layer of haze. It is possible that we are speaking of optically thin cirrus clouds in this case. These clouds obscure the ascending flux, which could also explain the above-mentioned anomaly. Pilots almost always notice abrupt boundaries of aerosol haze in the tropopause; however, there is no more precise information on its nature. Considering the data on the distribution of the concentration with the altitude [16], it seems hardly probable (although we cannot exclude such a possibility completely) that this haze consists of dust particles.

At present, a method has been developed for studying the effect of such thin cloud layers, which are not visible from the ground, on the outgoing long-wave radiation, particularly in the range of 6.0 - 6.5 and 9 - 12 μm [16].

A curve for the distribution of temperature with altitude, illustrating the existence of a "layer of gray absorbent" at a level from 12 to 16 km, is shown in Figure 2.

In his calculations, Zdunkowski used four selected distributions of the absorbtion coefficients of the "gray layer" (Fig. 3a). /220 The optical thicknesses of the layer were considered to be roughly identical (0.45 - 0.55). The change in the absorption coefficient with the altitude is expressed clearly in the curves for $\frac{dT}{dt}$ characterizing the heating, which were calculated for 4 points (see Fig. 3b). Figure 3c gives the corresponding curves for the effective radiation.

Having compared the results for the heating curves $\frac{dT}{dt}$ obtained by using the radiation patterns of Möller and Jamamoto, it can be seen that these curves repeat each other, the only difference being that Möller's curves give somewhat lower values.

In summary, it can be said that, despite the difference in the change of absorption coefficients with altitude for a roughly identically great optical thickness, the maximum heating is almost identically great. In this case, the computed data do not disagree to a great extent with the results of measurements.

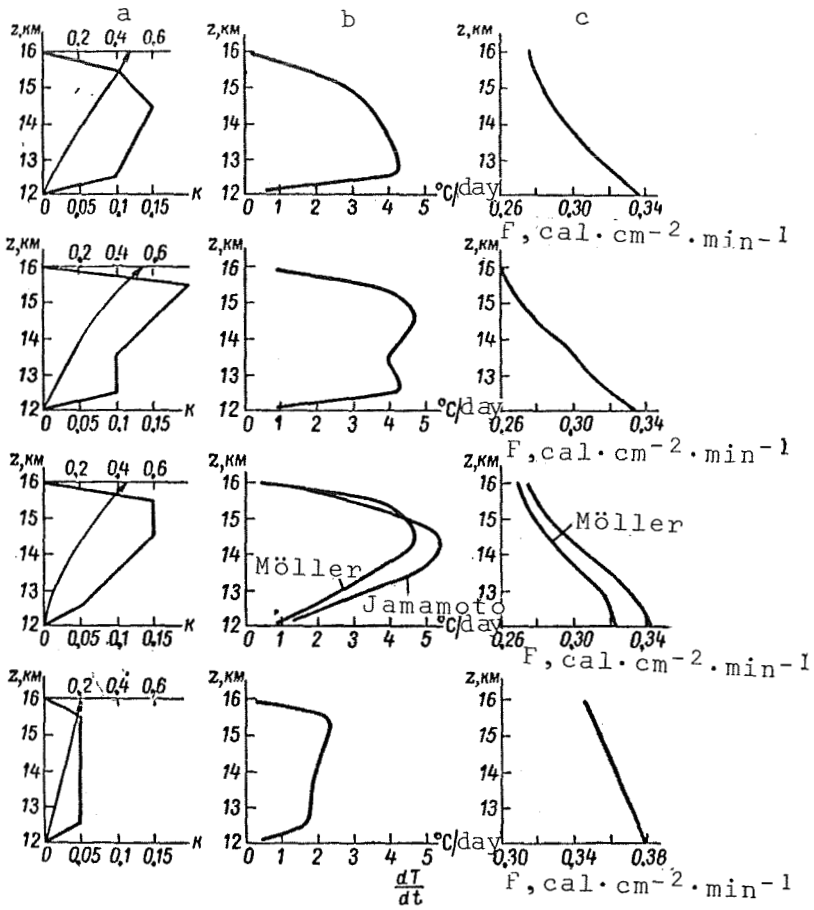

Fig. 3. Change in Absorption Coefficient (a) of the Heating Curves (b) and the Effective Radiation With the Altitude (c).

It is interesting to compare these results to those obtained /221
during airship flights [2]. Using the data of these flights, we calculated the velocities of radiative heating due to the absorption of direct solar radiation by aerosols (if we assume that roughly 20% of the decrease by aerosols is caused by absorption) and water vapor (Fig. 4). The maximum values of $\left|\frac{dT}{dt}\right|_{aeros}$ and $\left|\frac{dT}{dt}\right|_{H_2O}$ are roughly of one order. A minimum is noted in the vertical variation in these values below the tropopause, and a certain increase is noted in the stratosphere. This is qualitatively similar to the picture obtained by Zdunkowski for the vertical profiles of thermal radiation. However, note the striking quantitative disagreements in the magnitudes of the warm-up (up to 5° C/day and more according to Rönicke [10], and maximum of 1° C/day according to the

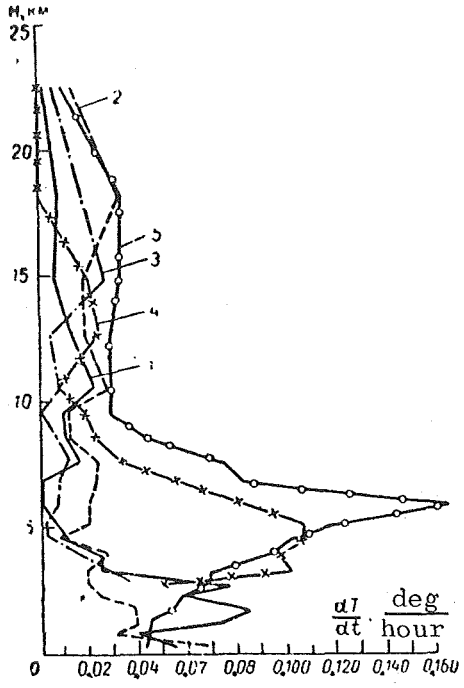

Fig. 4. Velocities of Radiative Heating of the Atmosphere Due to Absorption of Direct Solar Radiation by Aerosols (1, 2, 3), Water Vapor and Atmospheric Gases (4,5), Calculated for Layers of 50 mb. 1,2,3 --$\frac{dT}{dt}_{aeros}$ in the flights in 1964; 4--$\frac{dT}{dt}$ due to the Absorption of CO_2, O_2 by Water Vapor in Flight No. 1; 5--$\frac{dT}{dt}$ due to the Water Vapor in Flight No. 3.

data of [2]). Even considering that we are speaking of direct solar radiation in this case, it is difficult to explain this great discrepancy. Naturally, Rönicke's experiment must be tested carefully, since this great heating is nevertheless doubtful.

It is of interest to examine the problem of the effect of atmospheric layers on single radiation components. It has been found that the complementary "gray radiation" at altitudes from 12 to 16 km greatly exceeds the radiation due to the gaseous H_2O component. The difference between these densities of radiation fluxes going toward the Earth might be found in this penetration of the gray radiator in the so-called "atmospheric window". /222

In the case of carbon dioxide, the same effect as that for water vapor is observed, but to a much lesser degree (because of the high intensity of the CO_2 absorption band). Even at an altitude of 8 km, no difference has been noted between the curves, since the gray radiation is replaced here by CO_2 emission.

The heating in the aerosol layer can be reduced mainly to the radiation of the Earth in the "atmospheric windows", i.e., to the region of the water vapor spectrum, which is almost transparent for the radiation of the Earth, and in which the curves for the Planck radiation at ground temperature has a maximum. The "gray layer" shields the "window", and covers it to an extent, regardless of the altitude. Consequently, the aerosol layer is heated at least at the lower boundary.

Thus, the measured heating can be explained by the aerosol layer in the upper troposphere. A mathematical analysis of this problem still cannot give definite conclusions on the structure of the aerosol layer. It is necessary that there be simultaneous aerosol measurements and measurements of the radiation balance similar to those of Rönicke.

REFERENCES

1. Bunakova, A.M. and L.S. Ivlev: The Vertical Aerosol Distribution and Aerosol Layers in the Atmosphere, This Collection, p. 207.
2. Kondrat'yev, K. Ya., G. A. Nikol'skiy and Ye. N. Yesipova: Airship Studies of Radiation Fluxes in the Free Atmosphere. Izvest. Akad. Nauk S.S.S.R., ser. fiziki atmosfery i okeana, No. 4, 1966.
3. Rozenberg, G.V. and V. Nikolayeva-Tereshkova: Stratospheric Aerosols according to Spacecraft Measurements. Izvest. Akad. Nauk S.S.S.R., ser. fiziki atmosfery i okeana, Vol. 1, No. 4, 1965.
4. Junge, C.E.: Sulfur in the Atmosphere. J. Geophys. Res., Vol. 65, No. 1, 1960.
5. Junge, C.E., C. W. Chagnon, and Y. E. Manson: Stratospheric Aerosols. J. Meteorol. Vol. 18, 1961.
6. Chagnon, C. W. and C. E. Junge: The Vertical Distribution of Submicron Particles in the Stratosphere. J. Meteorol. Vol. 18, No. 6, 1961.
7. Junge, C.E. and Y. E. Manson: Stratospheric Aerosols Studies. J. Geophys. Res., Vol. 66, No. 7, 1961.
8. Möller, F. and W. Zdunkovski: Computational Methods of Long Wave Atmospheric Radiation. Technical Reports, 1962.
9. Zdunkowski, W.: Dissertation at the Department of Natural Sciences of Munich University, 1963.
10. Rönicke, G.: On Measurements of the Change in Balance of Thermal Radiation in the Free Atmosphere in San Salvador. C.A.Z. Meteorol., Vol. 15, No. 8, 1961.
11. Suomi, V.E. and P. M. Kuhn: Airborne Radiometer Measurements of Effect of Particulates on Terrestrial Flux. J. Appl. Meteorol., Vol. 4, No. 2, 1965.
12. Riehl, H.: Radiation Measurements over the Caribbean. J. Geophys. Res., Vol. 67, 3935, 1962.
13. Plass, G.N.: The Influence of the 9.6 micron Band on the Atmospheric Infrared Cooling Rate. Quart. J. Roy. Meteorol. Soc., Vol. 82, No. 30, 1956.
14. Appleman, H.S.: Occurrence and Forecasting...World Meteorol. Organization 47, Techn. Note, No. 40, 1964.
15. Deirmendjian, D.: Atmospheric Extinction of Infrared Radiation. Quart. J. Roy. Meteorol. Soc., Vol. 86, No. 371, 1960.
16. Zdunkowski, W., D. Henderson and J. Hales: The Influence of Haze on Infrared Radiation Measurements Detected by Space Vehicles. Tellus, Vol. 17, No. 147, 1965.

THE SELECTIVITY OF AEROSOL ATTENUATION IN OZONOMETRIC OBSERVATIONS OVER ZAILIYSKIY ALA TAU

A.L. Osherovich and A.K. Suslov

ABSTRACT: This article is an attempt at solving the problem of considering aerosol extinction in ozonometric observations. After a discussion of such measurements at three geographic sites around Alma Ata at different sea levels, it is shown that narrow light filters and instruments of the same type should be used to compare the data obtained.

In order to compare different methods of considering the aerosol attenuation and for the sake of their further improvement, a series of parallel electrophotometric observations of atmospheric ozone was undertaken at three geographic sites around Alma Ata at different sea levels (see Figure 1 and Table 1). /224

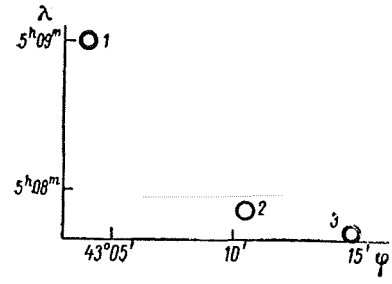

Fig. 1. Relative Position of Observation Sites of the Expedition of the Photometry Laboratory of Leningrad State University over Zailiyskiy Ala Tau. The Geographic Latitude and Longitude are Plotted Along the Axes of the Coordinates. (1) Observatory of the Shternberg State Astronomical Institute, "Djaylyau"; (2) Institute of Astrophysics of the Academy of Sciences of the Kazakh S.S.R., on the Kamenskoye Plateau; (3) Alma Ata, "Astrobotany Sector".

The electrophotometric method of determining the total ozone content X is still the only sufficiently reliable method which also permits us to determine X_H, or the ozone content in strata of the atmosphere above the observation site H, i.e., its vertical distribution X (H). The photographic method of determining X (H), which was first proposed by E. and V. Regener [1], is less precise, complex in analysis, requires more cumbersome apparatus, and does not have prospects of automation.

TABLE 1

Sites	ϕ	λ	H, m
Alma Ata.....	43°14'47"	$05^h07^m42^s$	850
Kamenskoye Plateau.....	43 10 30	05 07 51	1500
Ojaylyau.....	43 04	05 09	3000

The principle of any optical method, particularly the method /225 we used for determining X, is the Bouguer-Lambert law [2]:

$$I_\lambda = I_{0\lambda} 10^{-\alpha_\lambda X\mu - \beta_\lambda m - \delta_\lambda M}, \quad (1)$$

where $I_{0\lambda}$ is the value for the intensity of solar radiation outside the atmosphere; α_λ is the ozone extinction coefficient; μ is the ozone mass; β_λ is the decimal coefficient of Rayleigh scattering; m is the atmospheric mass; δ_λ is the extinction coefficient for aerosols; M is the aerosol mass.

Equation (1) is fulfilled more precisely when there is an increase in the degree of monochromatization of the ultraviolet radiation of the Sun I_λ measured in the region of the Hartley band. However, an overnarrowing of the spectral interval $\Delta\lambda$ results in an increase in the complexity and weight of the apparatus, which is not necessary for extra-atmospheric studies, and to a decrease in the flux of measured radiation. The minimum measurable flux is limited by the sensitivity threshold of the photocathode, and is about 10^{-14} W/cm^2.

According to the data presented by F. Johnson [3], at λ_1 = 3100 Å there is radiation which produces irradiance of E = 0.076 W/cm$^2\cdot\mu$ at the boundary of the Earth's atmosphere on a plane perpendicular to the direction toward the Sun. According to the data of other authors and references [4-7], this value varies within the range of 0.053 - 0.074 W/cm$^2\cdot\mu$. The capacity of radiant fluxes which must be measured in the ozonometric region of the spectrum can be determined according to the data presented below (without considering the aerosol attenuation):

$Z_\odot$	E, W/см^2	$Z_\odot$	E, W/см^2
65°	$6.41\cdot10^{-6}$	80°	$1.03\cdot10^{-8}$
70°	$1.04\cdot10^{-6}$	85°	$6.74\cdot10^{-12}$
		89°	$1.51\cdot10^{-25}$

The calculations were carried out for sea level at a wavelength of λ_1 = 3100 Å, spectral interval of $\Delta\lambda$ = 25 Å and total thickness of the ozone layer of X = 0.3 cm (average temperature of the ozone layer of T = 44° C). The Rayleigh scattering co-

efficient for a uniform atmosphere with thickness of 7.99 km is $\beta_1 = 0.46$ [8], and the ozone absorption coefficients $\alpha_1 = 1.08$ cm^{-1} [9]. Thus, the radiation at $\lambda_1 = 3100$ Å and $Z_\odot$ 85° - 89° cannot be measured by the electrophotometric method without high-transmission optics and storage. The data of G.P. Gushchin (see Table 45 in [7]) cannot be considered, since he uses a finite spectral interval of λ2900-3100 Å in the calculations, and introduces an average of $\lambda_{av} = 3000$ Å, while, in the real atmosphere in this spectral interval, the maximum irradiance is actually produced near the boundary of the interval $\lambda_1 = 3100$ Å. Moreover, /226
our calculations were carried out for a plane perpendicular to the direction of the propagation of a flux of radiant energy, while Gushchin's calculations related to a horizontal surface.

The inaccuracy in using an average of $\lambda_{av} = 3000$ Å is illustrated by the following formulas. According to the well-known theory on the average

$$\int_{\lambda_1}^{\lambda_2} I_\lambda d\lambda = I_{\lambda_{av}}(\lambda_2 - \lambda_1), \tag{2}$$

but

$$E = \int_{\lambda_1}^{\lambda_2} I_\lambda d\lambda = \int_{\lambda_1}^{\lambda_2} I_{0\lambda} 10^{-\alpha_\lambda X\mu - \beta_\lambda m - \delta_\lambda M} d\lambda, \tag{3}$$

where

$$\int_{\lambda_1}^{\lambda_2} 10^{-\alpha_\lambda X\mu} d\lambda \neq 10^{-\bar{\alpha}_{\lambda_{av}} X\mu} (\lambda_2 - \lambda_1), \tag{4}$$

so that

$$\bar{\alpha}_{\lambda_{av}} = \frac{\alpha_{\lambda_1} + \alpha_{\lambda_2}}{2}; \quad \lambda_{av} \neq \frac{\lambda_1 + \lambda_2}{2}. \tag{5}$$

Having calculated the quantity of incoming radiation at λ = 2900, 3000 and 3100 Å, we can see that, even for a position of the Sun at the zenith at $\lambda_1 = 3100$ Å, radiant energy 7 times greater than at $\lambda_{av} = 3000$ Å passes through the atmosphere.

Our calculations show that, for low Z for ozonometric studies using the radiant energy reflected from the Moon, artificial Earth satellites, or other bright luminaries, we must use high-transmission optics and very sensitive electrophotometric instruments (for example, a photon counter).

For some special studies of the structure of the absorption

bands of atmospheric ozone, for example, for determining the temperature in the layer of its maximum concentration, the spectral interval must be narrowed (to 0.5 - 1 Å), which also leads to the need for measuring very low radiant fluxes in the Hartley band. Therefore, the Sun can be observed in such cases only for low $Z_{\odot}$, using high-transmission optics and photomultipliers with a photocathode of small area.

The determination of X in network measurements is usually carried out at $Z_{\odot} < 80°$; therefore, the sensitivity of the photometers with the photoelectric radiation pickup is completely sufficient. Our observations confirmed that the use of the interval $\Delta\lambda$ = 20-30 Å does not bring about any noticeable deviations from the Bouguer-Lambert law [1] all the way to $Z_{\odot} = 80°$. The dielectric interference light filters we used over a spectral transmission width of $\Delta\lambda$ in the ultraviolet spectral region of ozone can be compared to spectral instruments of average dispersion [10]. Since, in addition to a maximum at λ_1 = 3100 or λ_2 = 3300 Å, these light /227 filters also have secondary maxima at $\lambda' = k\lambda$, they were complemented by stained glass of UFS-2 and ZhS-3 of the corresponding thickness. The interference light filters with dielectric coating do not change properties during a change in T°, while the glass light filters do not have thermal stability. However, the thermal instability of the latter does not greatly affect the position or half-width of the principal maximum, but affects mainly the ratio between the transmissions at the principal and secondary maxima, which has been proven in a thermal pressure chamber [11].

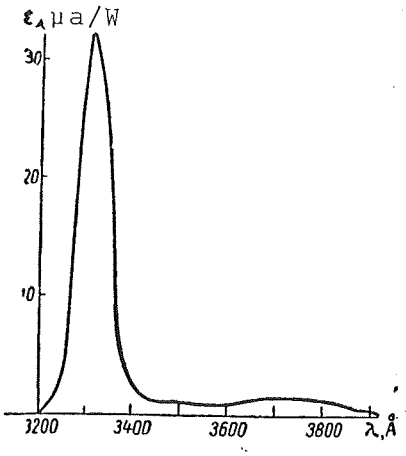

Fig. 2. Spectral Curves for the Transmission of the Principal Maximum of the Long-Wave Light Filter of the Ozonometric Couple.

The light filters were studied spectrographically and on an SFD-2 (diffraction spectrophotometer). Since the precision of the SFD-2 did not permit us to measure transmission of $\tau \leq 1\%$ reliably, then, in order to find the secondary maxima with a consideration of the curve for the spectral sensitivity ε_λ of the photocathode, we measured the ε of the ozonometer on the whole with the aid of a dual monochromator DMR-4 and a stabilized source of emission. Figures 2, 3 and 4 show the curves for transmission of one group of light filters. For a more precise determination of the maximum τ_m, the transmission band of the light filter was photographed parallel with the photographing of the mercury spectrum on the same plate (Figure 5).

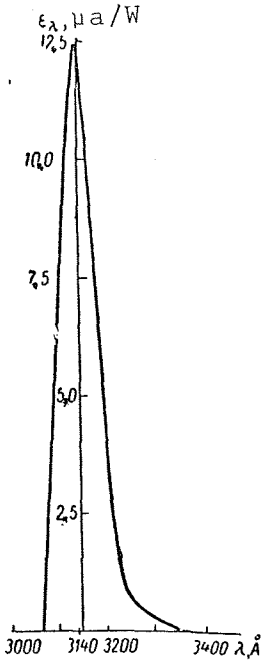

Fig. 3. Spectral Curve of the Transmission of the Principal Maximum of one of the Ozonometric Light Filters.

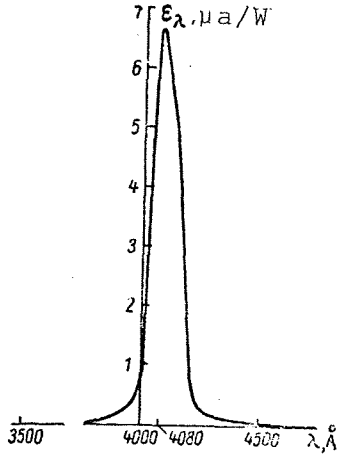

Fig. 4. Spectral Curve for the Transmission of the Principal Maximum of one of the Control Light Filters.

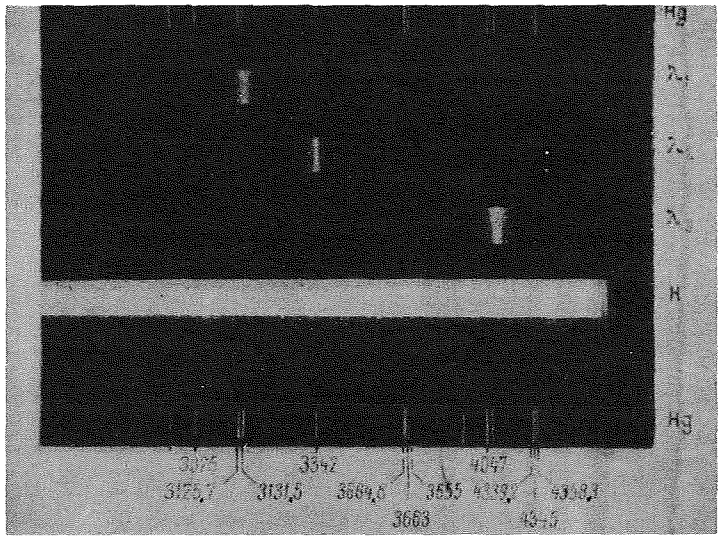

Fig. 5. Contact Print of the Negative of Spectrograms of the Transmission of the Ozonometric Light Filters of the Ozonometer No. 2. The Mercury Hg Spectra are Placed Above and Below for the Sake of Comparison. H is the Spectrum of a Hydrogen-Filled Tube. The λ of the Bright Mercury Lines are Shown. /228

If the receiving device of the ozonometer has a large solid angle, then, in addition to the direct solar radiation on the photocathode, there is also radiation scattered by the region of the sky around the Sun, and a deviation from (1) is possible, all the more so as $Z_{\odot}$ increases, so that we must use the following formula in the calculations: /229

$$I_{\lambda} = I_{0\lambda} 10^{-\alpha_{\lambda} X\mu - \beta_{\lambda} m - \iota_{\lambda} M} (1 + R_{\lambda}\omega). \qquad (6)$$

Since the correction for scattering R_{λ} cannot be determined with the necessary accuracy, the ozonometers were equipped with a spectral collimation adapter, which limited the solid angle of the instrument ω to dimensions of a cone with radius of $R_{\omega} \approx 2° - 3°$ (Figure 6). The collimation adapters represent cylinders with parallel metal tubes placed inside them, blackened on the inside, which allowed us to irradiate the entire effective area of the photocathode simultaneously, practically at the same solid angle. The solid angles of the tubular collimators were measured in a parallel monochronomatic flux, and the data of the measurements are depicted in Figure 6. The general appearance of the ozonometer with the collimators can be seen in Figure 7. The collimation of the measured flux of radiant energy improves the monochronamatization of the "source-light filter-photocathode" system. Moreover, the use of small solid angles with diameter of the cone of 3° aids in carrying out observations at $10° < H_{\odot} < 30°$ without substantial errors due to the scattered light.

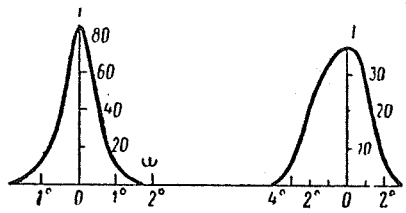

Fig. 6. Photometric Curve for the Distribution of Intensity Inside the Solid Angle of the Tubular Collimator.

When using the electrophotometric method under the conditions of a dry and pure Rayleigh atmosphere, X is usually calculated according to (1) from observations of the Sun at different $H_{\odot}$, assuming that $\delta\lambda_1 \approx 0$, which is usually not observed in practice, but which brings about an increase in the estimate of X, since the aerosols weaken the ultraviolet radiation in the same spectral region as does ozone. It is well known that the ultraviolet aerosol extinction is connected mainly with scattering, and not with pure absorption. As will be shown below, this permits us to determine δ after measuring the characteristic curve for scattering on aerosols.

Ozone has pure absorption, and its effect on the characteristic curve for scattering in the atmosphere is relatively small. One of the methods of considering the aerosol extinction is that /230

of G. Dobson [12], which underlies the position of the non-selectivity of scattering on aerosols. If we use (1) for λ_1 λ_2, then the average ozone content per day is determined by the following formula:

$$X = -\frac{d\eta}{d\mu} \cdot \frac{1}{\alpha_1 - \alpha_2} - \frac{\beta_1 - \beta_2}{\alpha_1 - \alpha_2} \cdot \frac{dm}{d\mu}. \qquad (7)$$

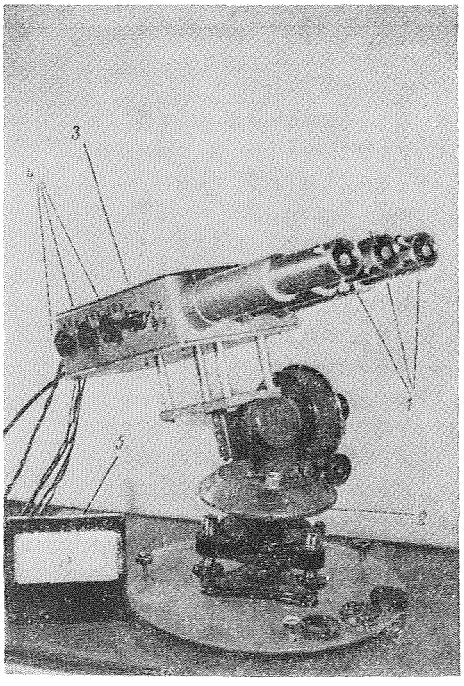

Fig. 7. Threefold Ozonometer No. 2. (1) Tubular Collimators; (2) Pilot-Balloon Theodolite; (3) Photocathode Regime Selector; (4) Sensitivity Selectors; (5) Microammeter M-24.

In Dobson's method, the principal condition is the assumption that

$$\delta_{\lambda_1} \approx \delta_{\lambda_2}. \qquad (8)$$

It is obvious that (1) permits us to determine X when $0 < \delta_1 << \delta_2$. If $\delta_1 \geq \delta_2$, then (7) and (8) give a more precise result.

A linear analysis according to the formula

$$X = -\frac{1}{\alpha}\left(\frac{d \lg I}{d\mu} + \beta\right) \qquad (9)$$

immediately permits us to determine both the quality of the ozonometer and the state of the atmosphere. If the linear dependence is not observed during the course of one day, then the data obtained are not suitable for determining X. If the Bouguer line has an inclination less than required by the Rayleigh law, then this also indicates that the data are unsuitable. Since

$$\tan\psi = -(\alpha x + \beta + \delta) = \log p, \qquad (10)$$

the presence of aerosols results in a decrease in the transmission coefficient P, the angle $|\psi|$ is increased, the Bouguer line becomes shorter, and X is decreased by a value of

$$\Delta X = \frac{\delta m}{\alpha\mu}. \qquad (11)$$

It was mentioned above that the precision of the optical method of determining X depends on a consideration of the aerosol components of extinction of radiant energy. At $m = \mu = \sec Z_{\odot}$ (in first approximation), (1) leads to the following expression:

$$X = -\frac{\tan\psi + \beta}{\alpha}. \tag{12}$$

For the condition of (8), we can calculate X according to Dobson's formula, i.e.,

$$X = \frac{\eta_0 - \eta - m(\beta_1 - \beta_2)}{(\alpha_1 - \alpha_2)\mu}. \tag{13}$$

For the case of three λ, on the condition that $\delta_1 = \delta_2 = \delta_3$, and with the coefficient K as

$$K = \frac{(n_1^2 - 1)^2 \lambda_1^{-4} - (n_2^2 - 1)^2 \lambda_2^{-4}}{(n_3^2 - 1)^2 \lambda_3^{-4} - (n_2^2 - 1)^2 \lambda_2^{-4}} \tag{14}$$

the total ozone content is calculated by the following formula:

$$X = \frac{S_0 - S - K(\eta_0 - \eta)}{[\alpha_1 - \alpha_2(1 + K)]\mu}. \tag{15}$$

We should mention that the difference $\delta_1 - \delta_2$ does not depend on the absolute value of the optical thickness of the aerosols δ; however, in practice, the use of the ratio

$$\frac{I_1}{I_2} = \eta_0 10^{-(\alpha_1 - \alpha_2) x\mu - (\beta_1 - \beta_2) m - (\delta_1 - \delta_2) M}$$

for substantial and discontinuous extinction of radiation in the atmosphere results in a larger error than for $\delta_1 = \delta_2 = 0$.

The role of aerosol extinction in ozonometric observations was examined by Sh.A. Bezverkhniy, A.L. Osherovich and S.F. Rodinonov [13]. Using the results of a number of studies [14-18], these authors concluded that a quantitative consideration of the aerosol component of atmospheric extinction is necessary in ozonometric observations. A number of attempts were made [20-22] at /232 considering this component more precisely (both as a constant and as a variable). However, there are still no final recommendations for a practical use of these methods in ozonometry.

G.Sh. Livshits and V.Ye. Pavlov [23] recently proposed the

following method for considering the aerosol extinction in determining X. (This method is strictly founded theoretically and practically feasible at the present, and we will discuss its essence briefly.)

If the aerosol attenuation is rather great in the Hartley band and, moreover, it changes to a large extent over the spectrum, then a determination of X is marred by serious difficulties, because of the need for separating the components of the optical thicknesses τ_{Boug} observed by the Bouguer method. Let us use the following formula:

$$\tau_{Boug} = \tau_{Rayl} + \tau_s \frac{\Gamma-1}{\Gamma+1} + \tau_{ab}, \tag{16}$$

Where τ_{Rayl} is the Rayleigh optical thickness, τ_{ab} is the optical thickness for total absorption.

$$\tau_s = \frac{2\pi}{Em_\odot} \int_0^\pi B_s(\varphi) \sin\varphi d\varphi, \tag{17}$$

$$\Gamma = \frac{\int_0^{\frac{\pi}{2}} B_s(\varphi) \sin\varphi d\varphi}{\int_{\frac{\pi}{2}}^{\pi} B_s(\varphi) \sin\varphi d\varphi}, \tag{18}$$

$B_s(\phi)$ is the brightness of the cloudness sky at the almucantar of the Sun; ϕ is the angle of scatter; E is the irradiance of the perpendicular area at the observation site; $m_\odot$ is the atmospheric mass in the direction of the Sun. Formula (16) is most precise in the ultraviolet region; therefore, we can find the unknown optical thickness for pure absorption by the difference between the observed and computed values of τ_{Boug}. The aerosol scattering can be calculated according to the following formula:

$$\tau_a = \tau_s \frac{\Gamma-1}{\Gamma+1}. \tag{19}$$

Using the results of [23], we can conclude that the role of pure absorption by aerosols is small in the near ultraviolet region outside the Hartley band, and we can single out the component of the aerosol optical thickness caused only by scattering for observations for determining X at a rural mountain region around Alma Ata. This is a substantial simplification, since (16) allows us to solve the ozonometric problem with a consideration of the /233 aerosol extinction. Thus, the solution becomes relatively simple, if, in determining the transmissivity by the Bouguer method, we also carry out measurements of the brightness of the sky at the

almucantar of the Sun.

Simultaneous ozonometric observations at close sites with different altitudes are a rather simple method of avoiding the effect of aerosol extinction on the value of X. However, since the sites are some distance from each other and the difference in altitudes is not too great, our results depend somewhat on the local conditions.

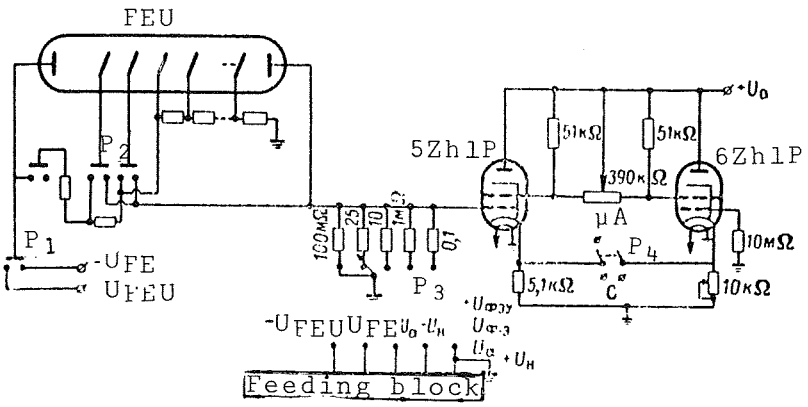

Fig. 8. Schematic Diagram of the Amplifier of one of the Channels of the Ozonometer.

In order to measure the direct solar radiation in three spectral regions, we used three-channeled ozonometers (Figures 7 and 8) designed at Leningrad State University with photomultipliers [24]. A comparison of the four ozonometers was conducted at Kamenskoye on 7/30-8/1 and 9/5-9/7, 1965, during an expedition of the photometry laboratory of Leningrad State University. The ozonometric observations were carried out at the Kamenskoye Plateau from July 30 to September 7, 1965, on every clear day from sunrise to sunset. At Dzhaylyau, the observations were held from August 5 to September 3, and at Alma Ata from August 29 to September 3, 1965. Table 2 shows the characteristics of the light filters.

For the light filters which had a principal maximum in the region of 3100 - 3200 Å, there were very small complementary maxima in the region of λ' 3600 - 3800 Å with transmission on the order of 1%, and in the region of 7100 - 7300 with transmission no greater than 0.3%. In the analysis of the observations, there was a special evaluation of the effect of these complementary maxima on the inclination of the Bouguer line. During the observations, we obtained values for the photocurrents from the irradiation of the corresponding channels of the ozonometers of the direct solar radiation at fixed moments of time. Using the diagrams of M.Ye. Nabokov, we /234
determined $Z_{\odot}$ and the air masses. The Bouguer lines were constructed for λ_1, λ_2 and λ_3 (Figure 9).

TABLE 2

Principal Maximum λ, Å	Transmission τ_{max}, %	Half-Width Δλ, Å
Ozonometer No.1, Kamenskoye Plateau		
3140	6.3	20
3315	9.6	50
4080	1.1	45
Ozonometer No.2, Dzhaylyau		
3115	8.17	30
3335	7.43	20
4100	1.82	24
Ozonometer No.3, Kamenskoye Plateau		
3195		
3350		40
4120		
Ozonometer No.4, Alma Ata		
3150	1.9	35
3290	1.6	30
3335	0.4	100
4125	3.5	40
3135	2.9	40

The observations at $3300 \leq \lambda \leq 4100$ Å, where the ozone absorption αX can be disregarded, allowed us to determine the optical thickness of the aerosols, and it was found that the spectral properties of the aerosols observed changed from day to day. Figure 10 shows a vector diagram of the spectrophotometric gradients of the aerosols in the region of 3300 - 4100 Å. An extrapolation of the approximate linear dependence of $\tau(\lambda)$ on the ozone spectral region obtained in this range brought about satisfactory results in those cases when τ decreased with an increase in λ. At $\frac{d\tau}{d\lambda} < 0$, this extrapolation did not bring about good results, and we used the method of two λ. Thus, our observations substantiated the opinion that, at $\lambda_1 = 3100$ Å, the spectral properties of aerosols differ little from those at λ3300 - 4100 Å. However, we should mention that the results obtained are of practical significance mainly under the local conditions of the region of Alma Ata, in the foothills of Zailiyskiy Ala Tau, during the summer. For an example, let us present an analysis of the observations on September 3, 1965 at Alma Ata (Figure 11). The time is plotted on the graph along the axis of the abscissae, and the difference in optical thicknesses $\Delta\tau = \tau_{\lambda_1} - \tau_{\lambda_2}$ is plotted along the axis of the ordinates. Curve 1 was constructed according to the data for λ_2 /235
and λ_3. The points obtained for the difference $\Delta\tau = \tau_{3290} - \tau_{4125}$ fit well on this curve. The horizontal line 3 corresponds to the difference in optical thicknesses of the Rayleigh atmosphere $\beta_{3335} - \beta_{4125}$. Line 2 illustrates the component of the optical thickness caused by absorption in the ozone layer X = 0.5 cm at $\lambda_2 = 3335$ Å.

It is obvious that all the oscillations in optical thickness during the course of one day which exceed the interval between lines 2 and 3 in scale cannot be caused by measurements in the ozone layer, even when the concentration of the latter is maximum.

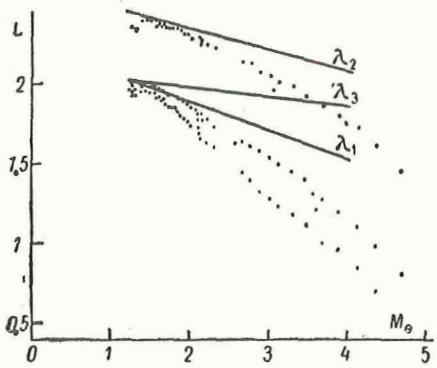

Fig. 9

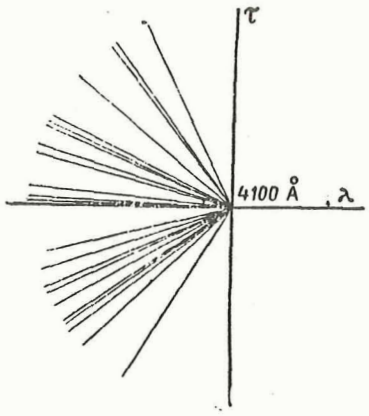

Fig. 10

Fig. 9. Bouguer Lines Obtained on 9/7/1965 on the Kamenskoye Plateau With Ozonometer No. 2. The Air Mass $M_\odot$ is plotted along the abscissa in Bemporads, and L = log I is plotted along the ordinate.

Fig. 10. Vector Diagram Illustrating the Spectral Change in Aerosol Extinction From 3300 to 4100 Å. The optical thickness of the Aerosols is plotted Along the Ordinate.

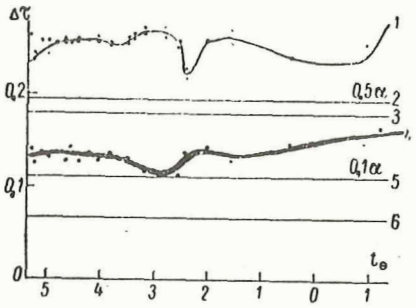

Fig. 11. Change in Optical Thickness of Aerosols and Total Ozone Content During 24 Hours. The Horizontal Lines for $\beta_{3335}-\beta_{4125}$ Signify the Difference in Rayleigh Thicknesses in the Spectral Regions Under Comparison. The Hourly Angle of the Sun is Plotted Along the Abscissa in Hours, Reading on Both Sides From Noon.

The fact that, in comparing λ_3 = 4125 Å to λ_2 = 3290 and 3335 Å no substantial differences are observed, indicate that there are changes in the optical thickness of aerosols during 24 hours, since at λ_3 = 4125 Å there is practically no ozone absorption, while its low absorption at λ_2 equal to 3290 and 3335 Å cannot bring about the observed changes in $\Delta\tau$. Curve 4 was constructed according to the differences of $\Delta\tau = \tau_{3150} - \tau_{3290}$ and its path varies from that for Curve 1. The horizontal lines 5 and 6 correspond to the differences in optical thicknesses of the Rayleigh atmosphere and the ozonosphere at X = 0.1 cm. The scale of the changes on Curve 4 /236

fits completely within the limits to the optical thickness of ozone αX, while the disagreement in time of these changes with the changes in the aerosol layer on Curve 1 indicate that they are connected more with the ozone content than with the aerosols.

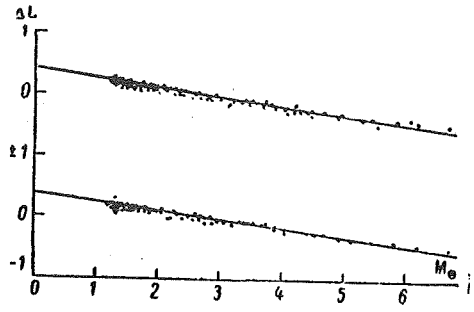

Fig. 12. Bouguer Lines Constructed According to the Data of Observations at Alma Ata With Ozonometer No. 4 With Two Pairs $\lambda_1\lambda_2$. The Spectral Factor $\Delta L = \eta = \log \frac{I_1}{I_2}$ is Plotted Along The Axis of the Ordinates.

Thus, the curves for the daily change in X presented by different authors do not always correspond to the real changes in ozone content, but can be a reflection of the changes in the layer of aerosols. For a clarification, we must carry out control measurements at several λ similar to the measurements discussed above. The result of a comparison of the data obtained on the Kamenskoye Plateau and at Alma Ata with ozonometer No. 4 show the best inner convergence. Averaged Bouguer lines were constructed for all the days for both geographic sites (Fig. 12) with an altitude difference of about 0.65 km, by using two pairs of λ, which gave the following:

Pair 1...$X_{\text{Alma Ata}} - X_{\text{Kamenskaye Plateau}} = 0.004$ cm,
Pair 2...$X_{\text{Alma Ata}} - X_{\text{Kamenskaye Plateau}} = 0.041$ cm.

The systematic difference in X obtained during observations at Alma Ata and Kamenskaye Plateau is identical for both pairs and can be explained by the presence of a layer of aerosols with thickness of 0.65 km.

The measurements with ozonometer No. 2 with a light filter of $\lambda_1 = 3115$ Å, which has a half-width of 30 Å and very broad wings, are of certain interest. An analysis of the measurements by integration over the entire filter showed that, for high $Z_{\odot}$, the long-wave wing of this filter affects the value of X because of the Forbes effect (Fig. 13, 14).

A comparison of different methods for analyzing the results of observation on filtered ozonometers showed that it is best to use three λ on the assumption that

$$\frac{d\delta_1}{d\lambda} = \frac{d\delta_2}{d\lambda} \neq 0 \qquad (20)$$

or

$$\delta(\lambda_1) - \delta(\lambda_2) = (\lambda_1 - \lambda_2) \cdot \text{const.} \tag{21}$$

/237

The total ozone content is then

$$X = \frac{\tan\psi_2 - \tan\psi_1}{A(\lambda_2 - \lambda_1)} - \frac{\tan\psi_3 - \tan\psi_2}{A(\lambda_3 - \lambda_2)} + \frac{B}{A} \tag{22}$$

where

$$\tan\psi = \frac{d \lg I}{d\mu};$$

$$A = -\left(\frac{\alpha_2 - \alpha_1}{\lambda_2 - \lambda_1} + \frac{\alpha_2}{\lambda_3 - \lambda_2}\right);$$

$$B = \frac{\beta_2 - \beta_1}{\lambda_2 - \lambda_1} - \frac{\beta_3 - \beta_2}{\lambda_3 - \lambda_2}.$$

The error caused by the assumption in (20) and (21) is determined by the following:

$$\Delta X = \frac{D}{A}, \tag{23}$$

where

$$D = \frac{\delta_2 - \delta_1}{\lambda_2 - \lambda_1} - \frac{\delta_3 - \delta_2}{\lambda_3 - \lambda_2}.$$

For ozonometer No. 1, (22) acquires the following form:

$$X = 1.785(\tan\psi_2 - \tan\psi_1) - 0.407(\tan\psi_3 - \tan\psi_2) - 0.0648. \tag{24}$$

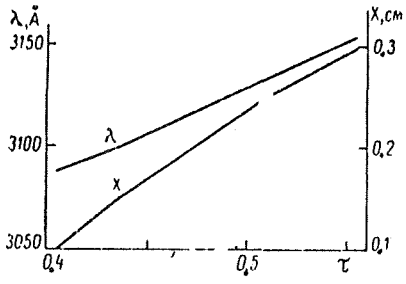

Fig. 13

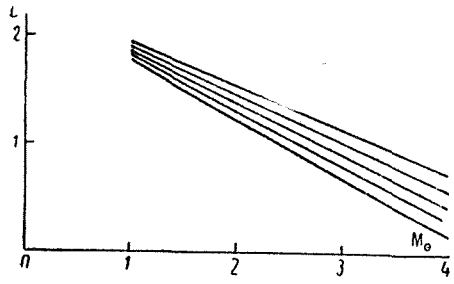

Fig. 14

Fig. 13. Dependence of the Effective Wavelength of the Broad-band Light Filter (Upper Curve) and Observed Uncorrected Value of X (Lower Curve) on the Optical Thickness $\tau = -\log P = \tan \Psi$.

Fig. 14. Calibrated Graph for Determining the Total Ozone Content According to Observations With Ozonometer No. 2 With a Broad-band Light Filter for Values of X = 0.1, 0.2, 0.3, 0.4, 0.5 cm.

We calculated X (in cm) according to (24) for a number of days, and compared its values to the data of the ozonometric station of the Kazakh Scientific Research Hydrometeorological Institute (Table 3) [25]. Based on the results of this study, we can draw the following preliminary conclusions.

1. The methods we used for considering the aerosol correction permits us to obtain more precise values for the total ozone content X under the conditions of the given locality.

2. Simultaneous observations at different altitudes carried out in flight are necessary for a further investigation of the aerosol correction.

3. A comparison of the data for different altitudes should be carried out with narrow light filters and instruments of the same type, since in the opposite case the Forbes effect greatly decreases the accuracy. /238

TABLE 3

Date	Ozonometer No.1 (Leningrad State University)	Ozonometer of the Main Geophysical Observatory (Alma Ata)
Aug. 6, 1965	0.291	0.298
7,	0.264	0.267
17,	0.291	0.301
19,	0.273	0.297
22,	0.271	0.272
24,	0.308	0.296
26,	0.281	0.275

This report is only an attempt at solving the problem of considering aerosol extinction, which is very important for ozonometry and other atmospheric-optic studies. Investigations in this direction will be continued.

In conclusion, we consider it our privilege to express our gratitude to the observers Ya. F. Verclaynen, N. I. Kolyzhev and V. I. Dubenskiy, and also to the mechanic I. F. Voshchilo and Professor S. F. Rodionav for their aid in this study.

REFERENCES

1. Regener, E. and V.H. Regener: Recording of the Ultraviolet Solar Spectrum in the Stratosphere and Vertical Ozone Distribution. Phys. Zs., Vol. 35, No. 19, 1934.
2. Gyatts, P.: Atmospheric Ozone. In the Collection: Uspekhi geofiziki (Advances in Geophysics). GTTI, 1934.
3. Johnson, F.S.: The Solar Constant. J. Meteorol., Vol. 11, No. 6, 1954.
4. Allen, K. W.: Astrofizicheskiye velichiny (Astrophysical Values). Foreign Literature Publishing House, 1960.
5. Smithsonian Meteorological Tables. Washington, No. 416, Table 131, 1951.
6. Kondrat'yev, K.Ya: Aktinometriya.Prilozheniye 4 (Actinometry . Appendix 4). "Gidrometeoizdat", 1965.
7. Gushchin, G.P.: Issledovaniye atmosfernogo ozona (Study of Atmospheric Ozone). "Gidrometeoizdat", 1963.
8. Penndorf, R.B.: Tables of Refractive Index for Standard Air and the Rayleigh Scattering Coefficient for the Spectral Region Between 0.2 and 20 μ and Their Application to Atmospheric Optics. J. Opt. Soc. Amer., Vol. 47 (2), 1957.
9. Vigroux, E.: Contribution to the Experimental Study of Ozone Absorption. Ann. Phys., Vol. 8, 1953.
10. Bol'shakova, L.G., A.L. Osherovich and I.V. Peysakhson: Systematic Errors in Filter Ozonometry. In the Collection: Atmosfernyy ozon (Atmospheric Ozone). Moscow State University Press, 1961.
11. Bol'shakova, L.G., A.L. Osherovich, S.F. Rodionov, A.K. Suslov and N.S. Shpakov: Photoelectric Ozonometers for an Investigation of the Vertical Ozone Distribution. Pribory i Tekhnika Eksperimenta, No. 4, 1965.
12. Dobson, G.M.B. and D. N. Harrison: Measurements of the Amount of Ozone in the Earth's Atmosphere and Its Relation to Other Geophysical Conditions. Proc. Roy. Soc., Ser. A, Vol. 110, No. A756, 1926.
13. Bezverkhniy, Sh. A., A.L. Osherovich and S.F. Rodionov: Photoelectric Ozonometers. In the Collection: Mezhdunarodnyy geofizicheskiy god (International Geophysics Year). Leningrad State University Press, 1960.
14. Rodionov, S.F.: Transmission of the Atmosphere in the Ultraviolet Region of the Spectrum. Izvest. Akad. Nauk S.S.S.R., ser. geografii i geofiziki, No. 4, 1950. /239
15. Bezverkhniy, Sh.A.: Electrophotometric Studies of the Dynamics of Atmospheric Ozone. Author's Abstract of Candidate's Dissertation. Kazakh State University, Alma Ata, 1957.
16. Rodionov, S.F., Ye. N. Pavlova and N.N. Stupnikova: A New Anomalous Effect in the Short-Wave End of the Solar Spectrum 1. Doklady Akad. Nauk S.S.S.R., Vol. XIX, No. 1-2, 1938.
17. Rodionov, S.F., Ye. N. Pavlova, Ye. V. Rdultovskaya and N.M. Reynov: Spectral Transmission of Atmospheric Aerosols. Izvest. Akad. Nauk S.S.S.R., ser. geografii i geofiziki, No. 4, 1942.

18. Karankikar, R.V.: Studies in Atmospheric Ozone. Proc. Indian Acad. Sci., Vol. XXVIII, Ser. A, No. 2, 1948.
19. Gowan, E.H. and R. E. Leppard: Meteorological Variations in the Quantity of Atmospheric Ozone Over Edmonton (Lat. 54°34' N. Long. 113°31'W) Canad. J. Phys., Vol. 31, No. 5, 1953.
20. Ramanathan, K. and R. Karandikar: Effect of Dust and Haze on Measurements of Atmospheric Ozone Made with Dobson's Spectrophotometer. Quart. J. Roy. Meteorol. Soc., Vol. 75, No. 35, 1949.
21. Rodionov, S.F.: Transmissivity of the Atmosphere in the Ultraviolet Region of the Spectrum. Author's Abstract of Candidate's Dissertation. Physics Institute of the Academy of Sciences of the U.S.S.R., Kazan', 1942.
22. Gushchin, G.P.: The Problem of Measuring the Total Content of Atmospheric Ozone and its Vertical Distribution. Meteorologiya i Gidrologiya, No. 6, 1957.
23. Livshits, G.Sh. and V.Ye. Pavlov: The Transmissivity of the Atmosphere and the Interconnection between Certain Optical Parameters. Materials of the Plenary Council of the Commission on Optical Instability of the Earth's Atmosphere on 9/30-10/2, 1965 (unpublished).
24. Verolaynen, Ya. F., A. L. Osherovich, A.K. Suslov and N.S. Shpakov: Observations of the Ozone Content During the Total Solar Eclipse on July 20, 1963. Geomagnetizm i Aeronomiya, Vol. 5, No. 1, 1965.
25. Ozone Data for the World, July-August, 1965, Vol. 6, No. 4, p. 136. Toronto, Ontario.

THE PROBLEM OF THE ROLE OF THE MECHANISMS FOR THE DISTRIBUTION AND SOURCES OF ATMOSPHERIC AEROSOLS

L.S. Ivlev

ABSTRACT: In order to construct an approximating schematic diagram of the aerosol distribution in the atmosphere, the atmosphere is divided into zones where different distribution mechanisms and sources are effective, and simplifying assumptions, such as the idea that there is no interaction between cosmic matter and the remaining aerosols, are made.

The experimental and theoretical data from studies on the vertical distribution of aerosols which have recently been accumulated allow us to construct approximate schematic diagrams of the distribution of aerosols in the Earth's atmosphere [1, 2, 3]. In constructing diagrams of such a type, we must analyze the role of various mechanisms for the aerosol distribution and the contribution of various aerosol sources to the overall distribution. In this study, I will attempt to evaluate the role of various mechanisms of the aerosol distribution for different altitudes, and to show the possibility of constructing a theoretical model of the vertical distribution of atmospheric aerosols. /240

It is clear from physical concepts and approximating calculations that, above 25 km, the transport of aerosol particles by convective currents and the mechanism of eddy diffusion with the underlying layers is complicated, due to which the concentration of atmospheric aerosols of terrestrial origin should decrease abruptly down to zero at 30-35 km altitude, and we can consider that the aerosols of higher layers are either of cosmic or of photochemical origin. The lower denumerable aerosol concentration and its rather rapid subsidence at altitudes higher than 35 km permit us to disregard the coagulation effect (see the figure).

If we consider that aerosol particles with dimensions of $r \leq 0.2$ μm are of a cosmic origin, and that the aerosols are distributed uniformly in the horizontal direction, then we can write the following for a fixed stationary current with

$$K\frac{\partial m_r}{\partial h} - v_{sr}\cdot m_r = \Phi(r). \qquad (1)$$

Here h is the altitude; m_r is the aerosol mass of cosmic origin with a defined amount r of aerosol particles per cm^3 of air; $\Phi(r)$ is the flux of aerosol particles: K is the coefficient of eddy diffusion according to Booker [4], which is equal to /241

$$K(h) = K_{10} + K_1 h; \tag{2}$$

K_{10} = 0.18 cm^2/sec at an altitude of 10 km; K_1 = 10^2 cm^2/sec [(2) is valid for h < 80 km]; v_{sr} is the speed of sedimentation of aerosol particles of a certain size from the molecular-kinetic theory for the case of r << λ (mean free path of molecules) which is equal to

$$v_{sr} = \frac{2\pi\rho_r g r}{3\alpha n_b}\left(\frac{\pi}{2m_b kT}\right)^{1/2}; \tag{3}$$

ρr is the density of the aerosol particles; r is the radius of the particle, μm: α is the coefficient characterizing the mechanism of reflection of air molecules from the surface of the particles; n_b is the concentration of air molecules, which is equal to

$$n_b = n_0 e^{-\frac{m_b g h}{kT(h)}}; \tag{4}$$

k is the Boltzmann constant; T(h) is the absolute temperature of the gas; m_b is the mass of the gas molecules.

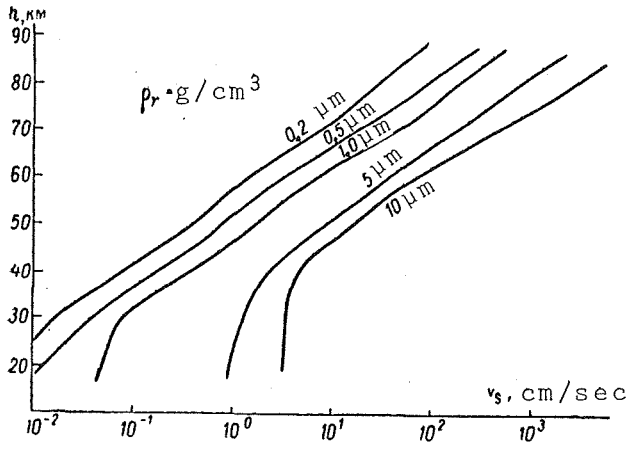

Fig. Speed of Gravitational Precipitation of Aerosol Particles.

It can be considered that particles of cosmic dust and micrometeorites pass from outer space with distribution by size of

$$\frac{dn(r)}{dr} = \frac{C_1}{r^\beta}, \tag{5}$$

where $C_1 \simeq 10^{-20}$ $cm^{-1 \cdot 2}$ while $\beta \simeq 2.8$, if we consider that the principal source of the extra-terrestrial matter in the atmosphere is a zodiacal dust cloud [2]. The inflow of cosmic matter from here is roughly a thousand times greater than that from meteorites of all sizes. The dimensions of the particles in the zodiacal cloud change from several tenths of a micron to 300 μm. According to the data of G.M. Idlis [5], the exponent $\beta \simeq 4$, which is characteristic of the fractionation processes, while the distribution of particles of a cosmic origin is bounded on the side of small particles, since the light pressure of the Sun ejects particles with $r \leq r_{min}$ from the solar system, i.e., /242

$$r_{min} \simeq \frac{3L_{\odot}}{16\pi c G M_{\odot} \rho_r} \simeq (1-3) \cdot 10^{-5} \text{ см}, \qquad (6)$$

if $\rho_r \simeq (2\text{-}6)$ g/cm^3 ($L_{\odot}$ is the luminosity of the Sun, $M_{\odot}$ is the mass of the Sun, G is the gravitation constant, c is the speed of light). Because of the varying rate of incidence of the particles, their distribution by size should change. It can be considered that, up to an altitude of 150 km, aerosol particles of a cosmic origin move at a speed which does not depend on the dimensions of the particles, and $\overline{V}_{150} \simeq 3 \cdot 10^6$ cm/sec. Considering that, above 80 km, only the sedimentation mechanism has effect, we find from the condition of the steady state of the flux that, at altitudes between 150 and 80 km, the percentage of the finely-divided fraction of cosmic dust increases, and the computed aerosol concentration decreases exponentially with the altitude.

The heating and evaporation of the meteorites results in an increase in the finely-divided fraction, but it is probable that this contribution is not very great. If we consider that the yearly influx of cosmic matter to the Earth is $4 \cdot 10^5$ m, then the flux of cosmic dust every cm^2 is roughly equal to $\Phi \simeq 2 \cdot 4 \cdot 10^{-5}$ g/cm$^2 \cdot$sec.

The concentration of cosmic aerosols at an altitude of about 80 km is equal to $n \sim 10^{-15}$ g/cm^3. We can solve (1) for altitudes of 30-80 km by dividing the atmosphere into several layers according to their thermodynamic characteristics. However, there are a number of instances when the solution of this problem becomes complicated: with high rarefaction of the atmosphere, turbulent pulsations of the medium do not completely entrain aerosol particles, which decreases the role of eddy diffusion; vertical convective currents in the atmosphere can change the vertical distribution of aerosols, and make it laminar; radiation (light pressure and photophoresis) can have a substantial effect on the movement of aerosol particles in the atmosphere [7]. These factors should increase the period of aerosol particles in the upper atmosphere and reduce temporal (seasonal, daily) variations in the vertical aerosol distribution.

Calculations of the time for precipitation of particles of cosmic origin to the tropopause give values from 30 days to 3 years

(the second value for particles with r ~ 0.5 μm). The time during which half of the aerosols of the lower atratosphere fall to the Earth is also on the order of 3 years, according to measurements of the concentration of radioactive aerosols. Therefore, we can /243 assume that there are several times more aerosols of cosmic origin in the entire stratosphere than the average yearly inflow from outer space, while the majority is contained in the lower stratosphere. Transport of the aerosols from the stratosphere to the troposphere can occur because of the high gradient in the computed concentrations and the effect of the force of gracity. In the lower stratosphere, when the computed aerosol concentration is rather high and the particles stay for a rather long time, the coagulation mechanism of increase in particles can play an important role in the distribution of aerosol particles by size. The formation of water aerosols during the condensation of water vapor is possible only at altitudes of about 80 km and below 30 km, and is of a sporadic nature. However, for some hygroscopic particles (for example, H_2SO_4), there can be condensation of water vapor at a vapor pressure below saturation.

Many researchers assume that the aerosols of the lower stratosphere are mainly of a photochemical origin. The photochemical processes with the formation of aerosol particles are possible during reactions with SO_2, NH_3, CN_4 and CO. The most important reactions of sulfur dioxide are the following:

$$SO_2 + h\vartheta \rightarrow SO_3, \quad SO_2 + O_2 \rightarrow SO_4, \quad SO_3 + H_2O \rightarrow H_2SO_4, \quad SO_2 + O_3 \rightarrow SO_3 + O_2.$$

The industrial activity of humans, the vegetation of the Earth and volcanos can be sources of sulfur dioxide, sulfur and its compounds. The contribution of vegetation is hardly significant, where the sulfur is 0.1% of the dry matter. It is well known that the yearly extraction of sulfur dioxide SO_2 by industry is roughly $1.2 \cdot 10^8$ tons, which is almost 3 orders greater than the yearly influx of all cosmic matter. However, the lifetime of sulfur dioxide in the atmosphere is short ($\sim$ 5 days) because of its active bonding in the troposphere, so that the total mass of sulfur dioxide of industrial origin in the atmosphere is roughly equal to $\sim 2 \cdot 10^6$ tons. The total amount of yearly precipitation of sulfur in rainfall (in the scale of SO_4^{-2}) is $\sim 4 \cdot 10^8$ tons, and possibly more. Thus, it is probable that volcanos make a substantial contribution to the precipitation of sulfur into the atmosphere. During the eruption of volcanos, from 10^8 to 10^{11} tons and more of matter is ejected into the atmosphere. A great part of it enters the stratosphere, so that its lifetime in the atmosphere is very long. The after-effects of strong volcanic eruptions (Katmai, Krakatau) have been felt for several years. Therefore, the equation which describes the aerosol distribution in the lower stratosphere should include a term which considers the ejection of aerosols by volcanos. The distribution of aerosols of a volcanic origin should also obey the law

$$\frac{\partial N}{\partial r} \simeq -\frac{C}{r^4},$$

However, the volcanic matter takes an active part in the photochemical reactions in the lower stratosphere mainly because of the rich content of sulfur in solid and gaseous components of the volcanic matter. /244

The problem of the vertical aerosol distribution in the troposphere was examined in detail in [8], but only for finely-divided aerosol fractions - Aitken nuclei.

The coagulation, wash-out of aerosols, conductive currents, and photochemical reactions (near the Earth, not far from industrial areas) should be considered as the principal mechanism for the distribution of aerosols in the troposphere. If we must consider point sources up to an altitude of 2 km, and extended sources up to an altitude of 5 km, then we can assume that, above 5 km, the aerosol distribution is of a global nature with a clearly pronounced latitudinal dependence, and a seasonal and daily variation. Disregarding the term characterizing the sedimentation of particles, the equation describing the aerosol distribution at these altitudes can be written approximately thus:

$$\frac{\partial}{\partial z}\left(D\frac{\partial n}{\partial z}\right) - a(z)\cdot n + b(z)\cdot n^2 = 0. \qquad (7)$$

Here $a(z)\cdot n$ corresponds to the withdrawal of the aerosols due to wash-out and depends on the relative humidity of the atmosphere and the ascending convective currents, $b(z)\cdot n^2$ corresponds to the change in aerosol concentration due to the coagulation mechanism. In the turbulent atmosphere,

$$b \simeq \frac{4kT}{3\eta} + \frac{r^3}{6}\left|\frac{\partial u}{\partial z}\right|.$$

Thus, it is possible to construct an approximating schematic diagram of the aerosol distribution in the atmosphere, dividing the atmosphere into zones where different mechanisms and sources are effective, with simplifying assumptions (no interaction between cosmic matter and the remaining aerosols, simplification of the temperature dependence on the altitude, etc.).

REFERENCES

1. Elterman, L.: Atmospheric Attenuation Model 1964. Environmental Res. Pap., No. 46, 1964.
2. Junge, C.E.: Air Chemistry and Radioactivity. Acad. Press. N.Y. London, 1963.
3. Bigg, E.K.: Atmospheric Stratification Revealed by Twilight Scattering. Tellus, Vol. 16, No. 1, 1964.
4. Booker, H.G.: Turbulence in Ionosphere. J. Geophys. Res., Vol. 61, No. 4, 1956.
5. Idlis, G.M.: Origin and Distribution by Size of Different Dust Particles in Different Layers of the Earth's Atmosphere. Izvest. Astrofiz. Instit., Vol. 12, 1961.
6. Mikirov, A.Ye.: The Aerosol Layer in the Upper Atmosphere. Doklady Akad. Nauk S.S.S.R., Vol. 142, No. 3-4, 1962.
7. Orr, C. and E.Y. Keng: Photophoretic Effects in the Stratosphere. J. Atmosph. Sci., Vol. 21, No. 5, 1964.
8. Selezneva, Ye.S.: Atmosfernyye aerozoli (Atmospheric Aerosols). "Gidrometeoizdat", 1966.

THE EFFECTIVENESS OF DEPOSITING AEROSOL PARTICLES ON A PLANE BACKING

L.S. Ivlev

ABSTRACT: The author planned an experiment to evaluate the effectiveness of depositing aerosol particles on different kinds of plane backings. It is shown that collectors of the impactor type must be standardized in order to obtain representative measurements.

In studying the effectiveness of aerosol collectors of the inertial type, the problem amounts to finding: /245

(1) The effectiveness of taking a sample into the input aperture of the instrument;

(2) The effectiveness of depositing the particles on the walls of the instrument;

(3) The effectiveness of depositing the aerosol particles on a plane backing.

It can be considered in first approximation that the gas in non-viscous in relation to the walls of the instrument but viscous for the particles, and that the flow is laminar (this is valid for aerosol collectors with Re on the order of several thousands). Obviously, the assumptions that the flow is stationary and the particles do not disturb the velocity field of the air current are valid for most aerosol traps.

The number of particles deposited on the backing is

$$n = n_0 \Psi_1 \Psi_2 \Psi_3, \tag{1}$$

Where Ψ_1 is the effectiveness of drawing the aerosol particles into the instrument; Ψ_2 is the percentage of particles passing along the instrument to the output of the nozzle; Ψ_3 is the effectiveness of depositing the particles on a backing.

Uncomplicated calculations according to Fuks [1 and 2] show that, for particles in the range of 0.1 μm < r < 2 μm, the first two factors are insignificant and are considered approximatively. Consequently, in designing aerosol collectors of the inertial type for finely-divided aerosols, there must first be an examination of the problem of depositing aerosol particles from an air current onto a backing. It can be considered in approximation that $n \approx n_0 \Psi_3$, where Ψ_3 (effectiveness of deposition) consists of two parts:

$$\Psi_3 = \Psi_l \cdot \Psi_v. \qquad (2)$$

Here Ψ_l is the effectiveness of the particles reaching the backing, while Ψ_v is the percentage of particles which are not blown off the backing. The second term in (2) depends on the interaction between /246 the particle and the backing and is determined by the adhesion properties of the backing and the force which blows the particle from the backing, which obviously is proportional to the particle size and the current velocity. The empirical formula for the dry backing is

$$v_{max} \simeq \frac{100}{d} (\text{m/sec}), \qquad (3)$$

Where d is the particle size, μm.

The investigations of A.D. Zimon and T.S. Volkova [3] show that, for micro-roughnesses of the backing which are commensurate with the particle sizes, the particles are practically not blown off. Thus, Ψ_v lends poorly to mathematical calculations; therefore, it is desirable to work with those current velocities at which it can be considered that the particles of the size range under investigation are not blown off.

The effectiveness of the particles reaching the backing is a function of two dimensionless values:

Reynolds number

$$\mathrm{Re} = \frac{v_0 l \rho}{\eta} \qquad (4)$$

and Stokes number

$$\mathrm{Stk} = \frac{2 v_0 r^2 \rho_a}{9 \eta l}, \qquad (5)$$

Where v_0 is the current velocity at the output of the nozzle; ρ is the density of the air; $\underline{l}$ is the characteristic size of the obstacle; η is the viscosity of the air; ρ_a is the density of the aerosol particles; r is the radius of the particle. When the current flows around the backing, the Re number has an order of one thousand and the motion of the air can be considered as potential.

The simplest equation of motion of the aerosol particle is the following, when there are no external forces:

$$m \frac{d\vec{v}}{dt} = 6\pi\eta r \left(\vec{u} - \vec{v}\right). \qquad (6)$$

Since Re is great, the following equation is more valid:

$$\frac{m}{6\pi\eta r} \cdot \frac{d\vec{v}}{dt} = \left[\vec{u} - \vec{v}\right] \left\{1 + 0{,}17\,\mathrm{Re}^{2/3} \left(\vec{u} - \vec{v}\right)^{2/3}\right\}, \qquad (7)$$

where $\vec{u}$ is the field of current velocities; $\vec{v}$ is the velocity vector of the particle (see [4]).

The solutions for (6) and (7) are simple for the case of $\vec{u} = 0$. This is the case when a particle with initial velocity of v_0 is stopped in a motionless medium. The length of the inertial path from the first equation is equal to

$$l_l = 2v_0 \frac{\rho_a r^2}{9\eta}. \tag{8}$$

/247

The second equation can be solved by the substitution $\Omega = v^{-2/3}$, under the initial conditions of $t = 0$, $v = v$. [For the sake of simplicity, we will consider that $a = \frac{9}{2}\frac{n}{\rho r^2}$ and $b = 0.17\, a\left(\frac{2r\rho_b}{n}\right)^{2/3}$]. Equation (7) then acquires the form of

$$\frac{dv}{dt} + av + bv^{5/3} = 0, \tag{7a}$$

and its solution is

$$\Omega = e^{2/3\, at}\left[c_1 - \frac{b}{a} e^{-\frac{2}{3} at}\right] \tag{9}$$

or

$$v = e^{-at}\left[v_0^{-\frac{2}{3}} + \frac{b}{a} - \frac{b}{a} e^{-\frac{2}{3} at}\right]^{-\frac{3}{2}} \tag{9a}$$

Having integrated this equation, we can find the expression for the inertial path of the particle (we will first make the substitution $\zeta = e^{2/3}\, at$)

$$y = \int v dt = \frac{3}{2a}\int \frac{d\zeta}{\zeta\sqrt{\left(c_1\rho - \frac{b}{a}\right)^3}} =$$

$$= -\frac{3}{b}\left[\frac{1}{\left(c_1\zeta - \frac{b}{a}\right)^{1/2}} + \sqrt{\frac{a}{b}}\arctan\left(\frac{c_1 a}{b}\zeta - 1\right)^{1/2}\right] + c_2; \tag{10}$$

We will then find c_2 from the condition of $t = 0$, $x = 0$, $\zeta = 1$:

$$c_2 = \frac{3}{b}\left[\left(c_1 - \frac{b}{a}\right)^{1/2} + \left(\frac{a}{b}\right)^{1/2}\arctan\left(\frac{c_1 a}{b} - 1\right)^{1/2}\right]. \tag{11}$$

The length of the entire inertial path of the particle is determined from the following expression for $t = \infty$:

$$y_\infty = l_i = 2{,}47 \frac{\rho_n r^2}{\eta} \left(\frac{\eta}{r\rho_b}\right)^{2/3} \times$$
$$\times \left\{ u_0^{1/3} + 1{,}92 \left(\frac{\eta}{r\rho_b}\right)^{1/3} \arctan 1{,}92 \left(\frac{\eta}{r\rho_b}\right)^{1/3} - 0{,}96\pi \left(\frac{\eta}{r\rho_b}\right)^{1/3} \right\}. \quad (12)$$

In analyzing the specimen taken by the impactor, we usually consider the particles in a bounded region with radius of $R \approx 0.5$-10 mm. For a velocity of $v \sim 100$ m/sec, the particles pass through this distance in $t \geq 10^{-5}$ sec, so that $y \approx l_i$ for particles with $r \leq 1$ μm. It can be considered in approximation that the particles precipitate on a plate if the distance from which they began to move is less than the length of the inertial path. For a slit of

$$\Psi_i \simeq \frac{l_i}{h}, \quad (13)$$

for a round aperture, this value is somewhat higher.

The solution can be obtained more correctly by determining the current line of the aerosol flux, as was done in [4,5], and then by solving (6) or (7). However, the bulk of the expressions /248 obtained, with the low accuracy of calculations according to them, make this work unnecessary. The aerosol flux can be modeled only for roughly-divided aerosols or for determining the current lines of the air. Equations (6) and (7) are not valid for particles with dimensions comparable to the mean free path of the molecules. The mean free path for particles of different sizes can be calculated according to (8) and (12), as well as according to the formulas with Kenningham's correction:

$$l_i = 2v_0 \frac{\rho r^2}{9\eta} \left(1 + A\frac{\lambda}{r}\right), \quad (8a)$$

$$l_i = 2v_0 \frac{\rho r^2}{9\eta} \left(1 + A\frac{\lambda}{r} + Q\frac{\lambda}{r} e^{-\frac{br}{\lambda}}\right) \quad (8b)$$

And from the molecular-kinetic theory:

$$m\frac{d\vec{v}}{dt} = -\frac{4}{3}\pi d\rho_b \cdot \bar{c} r^2 \vec{v} \quad (14)$$

(see the table)

INERTIAL PATH OF AEROSOL PARTICLES l_i (cm)
(at ρ = 2 g/cm^3, u_0 = 100 m/cm)

d, μm	By (8a)	By (8b)	By (14)	By Stokes	By (7)
0,05	$1,76\cdot10^{-3}$	$2,1\cdot10^{-3}$	$2,2\cdot10^{-3}$	$1,56\cdot10^{-4}$	—
0,1	$4,1\cdot10^{-3}$	$4,7\cdot10^{-3}$	$4,7\cdot10^{-3}$	$6,2\cdot10^{-4}$	—
0,2	$9,1\cdot10^{-3}$	$9,9\cdot10^{-3}$	$9,6\cdot10^{-3}$	$2,4\cdot10^{-3}$	$7\cdot10^{-3}$
0,5	$3,16\cdot10^{-2}$	$3,22\cdot10^{-2}$	$2,44\cdot10^{-2}$	$1,56\cdot10^{-2}$	$1,7\cdot10^{-2}$
1,0	$9,68\cdot10^{-2}$	$9,69\cdot10^{-2}$	$4,7\cdot10^{-2}$	$6,2\cdot10^{-2}$	0,23
2,0	0,31	0,31	$9,5\cdot10^{-2}$	0,24	0,56
5,0	1,72	1,72	—	1,57	2,5
10,0	6,4	6,4	—	6,2	7,7

The effectiveness of depositing aerosol particles on cascade and simple impactors for a pure glass plate and a plate coated with silicone was investigated experimentally. The nozzles had Roeber's configuration [8], which is described by the following equation:

$$r_1^* = \frac{1}{\sqrt{0,99l^{*2} + 0,01}}, \qquad (15)$$

where $l^* = \frac{l}{l_l}$ is the relative distance from the input to the nozzle; l_l is the length of the nozzle; $r_1 = \frac{r_1}{r_l}$ is the relative radius of the nozzle; r_l is the radius of the output.

A comparison of simultaneous measurements on two cascade impactors for pure plates and plates coated with silicone is shown in Figure 1. In the first and last cascades, the effectiveness of the deposition is rather close for both impactors. The effectiveness is greatly decreased for the pure plate in the second cascade (the current velocities at the output of the nozzles were v_1 = (4 ± 0.5) m/sec, v_2 = (20 ± 3) m/sec, v_3 = (200 ± 30) m/sec, respectively). /249

A study of the distribution of particles over the backing showed interesting characteristics in the deposition in the third cascade: the distribution over the backing was strictly symmetrical with the sharply-pronounced maximum at the center and the secondary weak maximum (see Figure 2). For the second cascade, this effect was less pronounced, while in the first cascade there were no regularities observed in the distribution of the deposited particles.

A small inclination of the plate in relation to the flow causes an abrupt change in the distribution of particles over the backing and worsens the effectiveness of depositing the aerosol particles

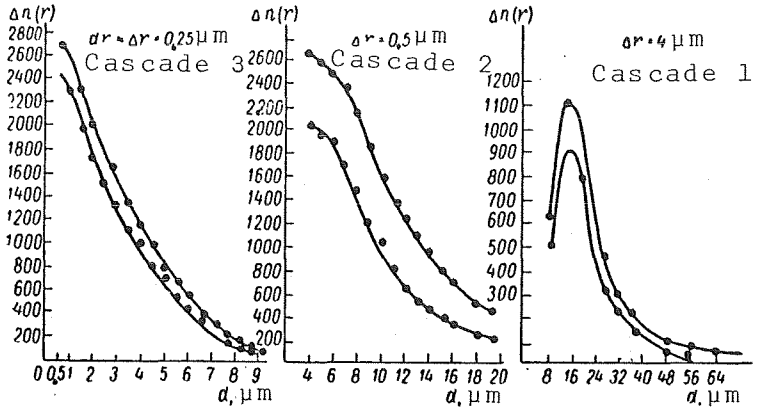

Fig. 1. Effect of the Properties of the Backing on the Effectiveness of Depositing the Particles.

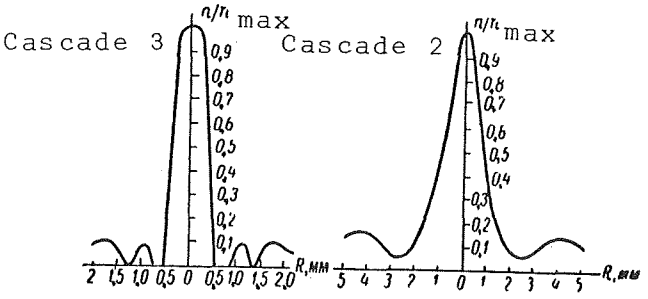

Fig. 2. Distribution of Particles Over the Backing in Deposition on a Backing Perpendicular to the Direction of the Air Current.

(Figure 3). The study of the distribution of particles of different sizes over the backing indicates that there is a regular change in the nature of deposition for different particles; for the largest particles (4-6 μm), the maximum diposition is shifted and, possibly, there is partial blow-off; for average particles (2-3 μm), there are two sharply-pronounced maxima, and the central maximum increases with a decrease in the sizes of the particles; the maximum at the edge begins to spread out here, which indicates there is incomplete deposition of particles (0.3 - 1.6 μm) on the plate (see Fig. 4,5 and 6). Possibly, this could be a partial explanation for the different pictures of the distribution of particles over the backing obtained by Roeber, as well as an indication that the distribution of particles by size with the aid of deposition of the aerosol particles on a backing placed at an angle greater than 90° to the current is hardly effective. The existence of secondary maxima also disproves the explanation of their formation by eddying motions for this case. We carried out a graduation of the effectiveness E of the deposition for all the cascades of the impactor by a Thermal precipitator and with the aid of a sample collector with filters FPP-18 (Fig. 7). All the measurements were carried out for relative humidity less than 60%. The data on the effectiveness of the precipitation agree rather well with [6,7,8], but are somewhat increased.

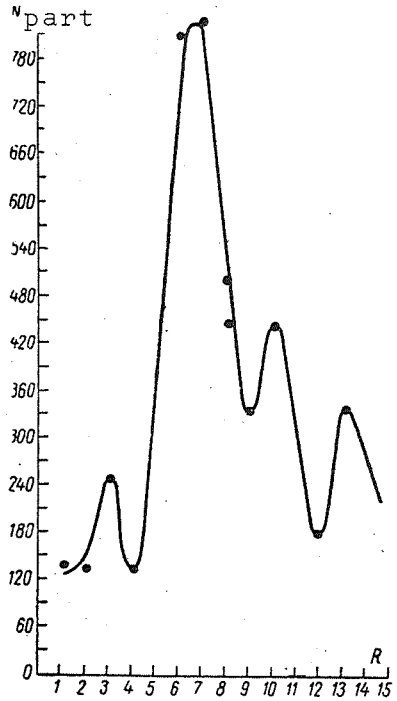

Fig. 3

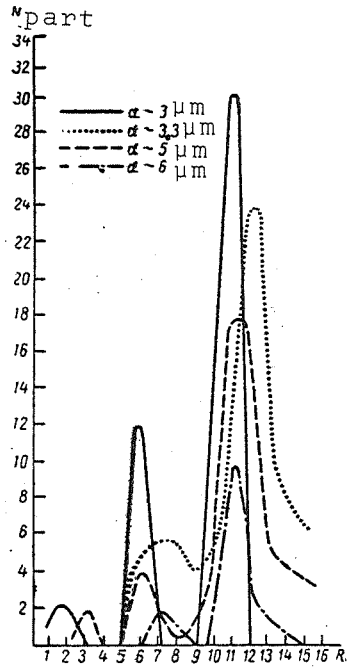

Fig. 4

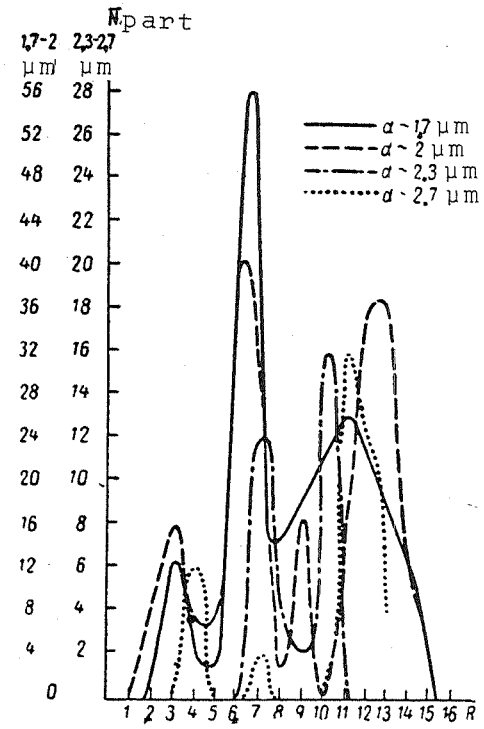

Fig. 5

Fig. 3. Distribution of Deposited Particles on the Backing for an Angle Between the Plate and the Current Greater Than 90°.

Fig. 4. Distribution of Particles on the Backing for d Equal to 3, 3.3, 5 and 6 μm.

Fig. 5. Distribution of Particles on the Backing for d Equal to 1.7, 2, 2.3 and 2.7 μm.

/250

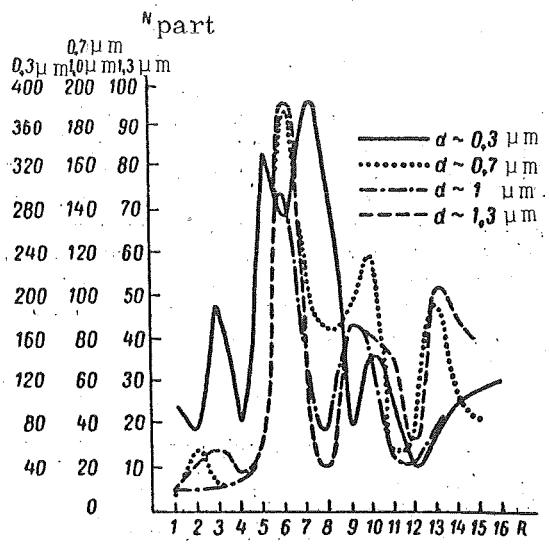

Fig. 6

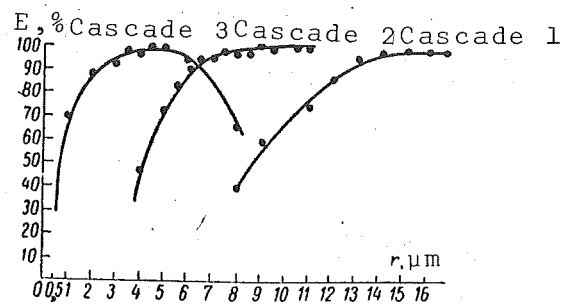

Fig. 7

Fig. 6. Distribution of Particles on the Backing for d Equal to 0.3, 0.7, 1 and 1.3 μm. /251

Fig. 7. Effectiveness of the Cascade Impactor.

In the general case, the solution to the problem for a compressible viscous fluid and a round aperture is practically impossible for particles with $r \approx \lambda$, but each factor can be studied separately. /252

Experimental investigations have shown that it is a complex task to model the deposition of particles of such dimensions, and representative measurements can be obtained only when traps of the impactor type are standardized.

REFERENCES

1. Fuks, N.A.: Mekhanika aerozoley (Mechanics of Aerosols). Izdat. Akad. Nauk S.S.S.R., 1955.
2. Fuks, N.A.: Uspekhi mekhaniki aerozoley (Advances in the Mechanics of Aerosols). Izdat. Akad. Nauk S.S.S.R., 1961.
3. Zimon, A.D. and T.S. Volkova: The Effect of Surface Roughness on the Adhesion of Dust. Kolloidnyy Zhurnal, Vol. 27, No. 3, 1965.
4. Levin, L.M.: Issledovaniya po fizike grubodispersnykh aerozoley (Studies in the Physics of Coarsely-Divided Aerosols). Izdat. Akad. Nauk S.S.S.R., 1961.
5. Davies, C.N. and M. Ailyward: The Trajectories of Heavy, Solid Particles. Proc. Phys. Soc., Ser. B, Vol. 64, No. 382, 1951.

6. Ranz, W. and J. Wong: Impaction of Dust and Smoke Particles. Indust. and Eng. Chem., Vol. 44, No. 1371, 1952.
7. May, K.R.: Cascade Impactor. J. Sci. Instrum., Vol. 22, No. 187, 1945.
8. Roeber, R.: Investigations on Konimetric Dust Measurements. Staub., Vol. 48, 49, 50, 1957.

THE EFFECT OF SOME SUBSTANCES ON THE COEFFICIENT OF CONDENSATION OF WATER DROPS

B. M. Shinyayev

ABSTRACT: The coefficient of condensation of water drops is examined in relation to three substances; sodium alurate, sodium palminate and isoamyl alcohol. It is assumed that the nature of the effect of molecules of soluble surface-active solutions on the evaporation differs basically from the characteristics of surface films of non-soluble SAS's.

In [1], we already examined the conditions and methods for studying the coefficient of condensation - a value characterizing the kinetics for evaporation of drops containing an adsorption layer of a surface-active substance (SAS). At present, there is a significant number of studies in which the problem of retarding the rate of evaporation of SAS solutions has been studied [2,3]. However, the investigation of the coefficient of evaporation of an aquaeous solution of an SAS nevertheless remains a complicated problem. One of the principal difficulties in this problem is the complexity of the experiment. Even the theoretical recommendations which have appeared recently for new methods of determining the coefficient of condensation [3] do not solve this problem in full. /253

The evaporation coefficients of drops of aquaeous solutions of three substances are determined in this study on a more perfected instrument, compared to the preceding one in [1]: sodium laurate, sodium palminate and isoamyl alcohol, with weight concentrations was determined by the conditions of the effect of the concentration on the coefficient of condensation found in [1].

The first experimental investigations of the evaporation coefficient α, which represents the percentage of condensed molecules out of the number hitting the surface, were carried out by T. Alty for several years, beginning with 1931 [4]. The more precise experiments which were carried out recently by T. Alty and C. Mackay [6] gave a value for the coefficient of evaporation of water of 0.036. Alty's experiments show that the rate of evaporation of water under vacuum is only some part of the value

$$n = \frac{P}{\sqrt{2\pi mkT}}, \tag{1}$$

where P is the vapor pressure at the temperature T; m is the mass of the molecules; k is the Boltzmann constant; T is the temperature of a drop.

The value of n was obtained in [7,8] from kinetic concepts on the amount of molecules colliding on an area of 1 cm^2/sec. /254
M. Knudsen and I. Langmuir [7,9] studied the evaporation processes in more detail; therefore, (1) is sometimes called the Knudsen formula. It allows us to calculate the absolute rate of evaporation of a substance under vacuum on the condition that the evaporated molecules are not extracted slowly from the system. However, for a large number of substances, the experimental rate of evaporation is much less than the theoretical one determined by (1); therefore, in order to satisfy the experimental data, we can introduce a certain factor (coefficient of evaporation) which characterizes the probability of a molecule condensing on the surface and is often defined as the condensation coefficient, although its value is obtained by measurements of the rate of evaporation.[1]

Experimental determinations of the coefficients of evaporation give a groad interval of values from the 0.04 obtained for water to 1 for some substances (dibutyl phthalate, long-chain hydrocarbons). According to Alty, each substance should have its own characteristic coefficient of evaporation or energy barrier for condensation, which depends to an extent on its molecular structure.

Method of Measuring the Coefficient of Evaporation

We determined the coefficient of evaporation of surface-active substances by the method Alty developed in order to measure the coefficient of evaporation of distilled water. This method is based on the fact that the evaporation of a drop takes place under a pressure close to the saturated vapor pressure corresponding to the temperature of the surface of the liquid. The scheme is shown in the figure.

The liquid under investigation is put in a vessel 1, and, passing through a capillary with definite radius, is formed in the form of drops, which go into one of the beakers with oil [3]. The air from the cylinder 4 is continuously pumped by a preevacuation pump, due to which a definite pressure P is maintained. There is also dropwise evaporation of the liquid under investigation in this vessel. The amount of evaporated liquid is determined according to the weight differential of the drop before and after evaporation. The first value is determined according to the decrease in the level in vessel 1 with the aid of a cathetometer, which determines the change in level with accuracy up to 0.003 mm. The second value is determined by suspending the beaker on an analytical balance with accuracy up to 0.001 g. The pressure in the cylinder

---

[1]It is necessary to distinguish the coefficient of evaporation, otherwise called the coefficient of condensation, from the coefficient of accomodation, which was defined by Knudsen [7] as the value characterizing the exchange of energy between the gas and the surface of a liquid or solid.

4 is measured by the mercury manometer with accuracy up to 0.05 mb.

The simplest method of increasing the evaporation is to increase the temperature of the water forming in drops, since the saturated vapor pressure P_s increases in this case. For this, the lower part of the vessel 1 is put in a constant-temperature shell 2, the constantsy of the temperature in which is maintained by the thermostat with accuracy up to 0.1°C. /255

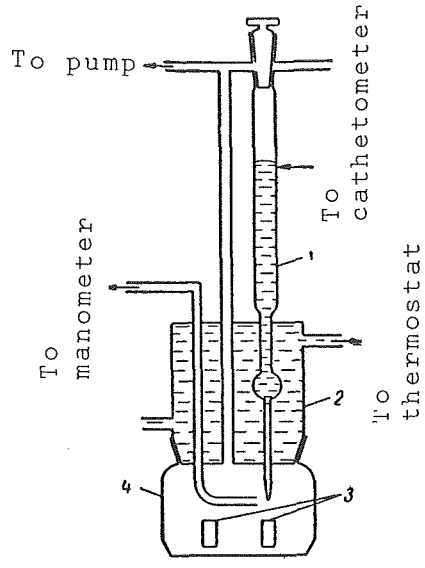

Setup for Determining the Coefficient of Evaporation

At the beginning of the experiment, the coefficient of surface tension σ is calculated according to the following formula from the weight of the drop falling under atmospheric pressure in the given instrument:

$$\Delta P_m = \frac{2\sigma}{r},$$

where P_m is the weight of a drop; r is the radius of the capillary. Knowing σ, it is easy to determine the temperature of the falling drop T_s and then to find the equilibrium vapor tension P_s according to it. Having engaged the pump and having brought the pressure in the vessel to the requisite value, we must insert one of the beakers 3 in which the falling drops accumulate. The latter are usually formed at a rate of 2-3 drops per minute, and the problem consists in collecting the greatest quantity of drops, since this increases the accuracy of the experiment. Thus, we succeeded in collecting 40-50 drops during 1 experiment. We could not collect a greater amount because the temperature of the oil in the beaker gradually rose and became higher than the temperature at which the saturated vapor pressure of the oil was equal to the pressure in the vessel 4. When this occured, the water-oil mixture /256 suddenly boiled over and the experiment was spoiled. The calculations were carried out according to the following formula:

$$\alpha = \frac{M\sqrt{T_s}}{0{,}1834\,(P_s - P)}. \qquad (2)$$

Here M is the mass of the molecules evaporated per 1 cm^2 area per sec; $(p_s - p)$ is the difference between the saturated vapor pressure at temperature T and the residual pressure in the vessel 4: T_s is the temperature of the drop.

Formula (2) is obtained from (1) after substitution of the corresponding constants.

We should mention that the difference in temperatures of the thermostat and evaporating surface changes with a change in the residual pressure T. This graphic dependence, which was first obtained by Alty, was presented in [1]; therefore, we will not repeat it here.

Experimental Results

The experiments were carried out for a temperature of the thermostat of 40°C and residual pressure of 42.0 mb. We first determined the coefficients of evaporation of distilled water. Five experiments in all were carried out. The average value of $\alpha = 0.0365$ we obtained coincided well with Alty's result ($\alpha = 0.037$). We then measured the coefficient of evaporation of drops of aqueous solutions of the SAS's. We completed 5-7 experiments for each substance, and the results are given in the table. The values of T_s for equilibrious vapor tension over the drops of the SAS solution were determined by the dynamic method. The values obtained for the coefficients of condensation α for the solutions of surface-active substances shown in the table indicate that they decrease in comparison to those of the condensation coefficients for pure distilled water.

TABLE

Substance	Chemical Formula	Concentration %	α
Sodium Laurate	$C_{11}H_{23}COO$	0.001	0.025
		0.01	0.021
		0.1	0.013
Sodium Palminate	$C_{16}H_{31}COO$	0.001	0.021
		0.01	0.016
		0.1	0.024
Isoamyl Alcohol	C_5H_4OH	0.001	0.034
		0.01	0.029
		0.1	0.024

If we compare the rate of evaporation of the drops of SAS solutions measured by the method described in [2] to the rate obtained by the decrease in the coefficient of evaporation, then the latter value is several percentages of the former. /257

The data obtained give us reason to assume that the nature of the effect of molecules of soluble SAS's on evaporation differs

basically from the characteristics of surface films of non-soluble SAS's, for which the value of the coefficient of evaporation is equal to 10^{-5}-10^{-4} [10, 11].

In conclusion, I would like to express my sincere appreciation to V.G. Morachevskiy and A.V. Guzhva for their aid and valuable advise in this study.

REFERENCES

1. Morachevskiy, V.G. and B.M. Shinyayev: Experimental Studies of the Value of the Coefficient of Evaporation of Aqueous Solutions of Surface-Active Substances. In the Collection: Problemy fiziki atmosfery (Problems of Atmospheric Physics), No. 2. Leningrad State University Press, 1964.
2. Kiryukhin, B.V., V.G. Morachevskiy and M.N. Orlova: Study of the Rates of Evaporation of Drops of Solutions of Surface-Active Substances. In the Collection: Problemy fiziki atmosfery (Problems of Atmospheric Physics), No. 2. Leningrad State University Press, 1964.
3. Kurgin, Yu.S.: Study of the Kinetics of Evaporation and the Effect on its Surface State (Coefficient of Condensation). Author's Abstract of Candidate's Dissertation. Leningrad State University Press, 1965.
4. Alty, T.: Application of Knudsen's Law to the Evaporation of Water. Nature, July 30, 1932.
5. Alty, T.: The Maximum Rate of Evaporation of Water. Phil. Mag. Vol. 15, No. 83, 1933.
6. Alty, T. and C. Mackay: The Accommodation Coefficient and the Evaporation Coefficient of Water. Proc. Roy. Soc., Vol. 149, No. 104, 1935.
7. Knusden, M.: The Maximum Rate of Evaporation of Mercury. Ann. Physik., Vol. 47, 1915.
8. Knake, O. and I. Stranskiy: The Evaporation Mechanism). Uspekhi Fiz. Nauk, Vol. 68, No. 2, 1959.
9. Langmuir, I.: The Vapour Pressure of Metallic Tungsten. Phys. Rev., Vol. 2, 1913.
10. Baranayev, M.K.: The Effect of Surface Films of Non-Soluble Substances on the Rate of Evaporation of Water. Zhur. Fiz. Khim., Vol. 9, No. 49, 1937.
11. Mason, B.J.: Fizika Oblakov (The Physics of Clouds). "Gidrometeoizdat", 1961.

THE POSSIBILITY OF INTERPRETING THE DATA OF A SEDIMENTATION ANALYSIS

M.M. Kokhanovich and V.G. Morachevskiy

ABSTRACT: The authors present the results of a parallel study of the distribution of drops by size of a modeled nebula obtained by a sedimentation analysis and by the microphotographic method in order to illustrate the advantages of the former method. It is shown that the sedimentation method of analyzing the degree of dispersion of a modeled nebula gives a completely clear and precise representation of the distribution of the drops in it by size.

Recently, of all the different methods used in studying micro- /258
physical characteristics of natural and modeled clouds and nebulae, the sedimentation analysis is becoming more and more important, since it aids in determining the degree of dispersion of aerosols for particles from 1 to 100 μm. On the other hand, the well-known and widely-used meteorological methods of collecting and analyzing specimens of particles in clouds and nebulae are rather cumbersome and are not devoid of disadvantages.

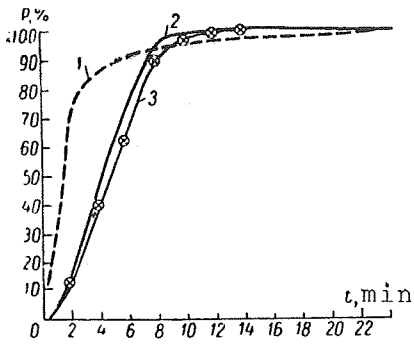

Fig. 1. Sedimentation Curves for the Precipitation of Particles of a Nebula. (1) Analytical; (2) Experimental; (3) Obtained According to Microphotographs.

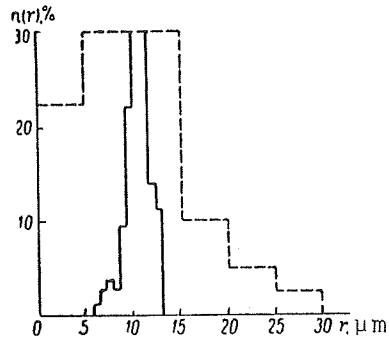

Fig. 2. Histrograms of the Distribution of Drops in a Nebula.
_____ ____ Sedimentation;
_ _ _ _ Microphotographic

Although some authors also show that the sedimentation method has disadvantages [1], it seems to us to be more simple and precise than the microphotography method. In order to show this, we will give the results of a parallel study of the distribution of drops by size of a modeled nebula by the sedimentation and microphotographic methods.

The behavior of the nebula was studied in a sedimentation chamber. A description of this chamber was given by B.M. Shinyayev [2], who took part in tis designing and in adjusting the apparatus. /259

Figure 1 shows the overall curve for a natural deposit of a nebula (sedimentation curve). The spectrum of the particles, which was constructed according to the data of this curve by the method of tangents (see [3], for example) and which is shown in Figure 2, gives a model radius equal to 10 μm.

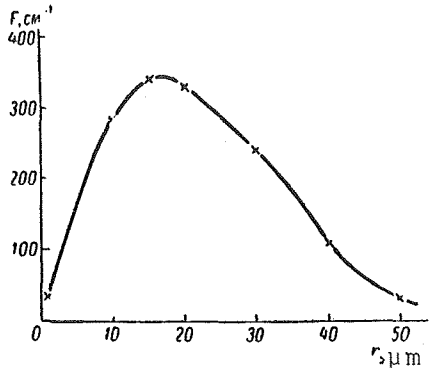

Fig. 3. Analytical Curve for the Distribution of a Nebula by Dimensions.

In using the method of tangents in order to determine the degree of dispersion of the particles, we assumed that the particles did not interact with each other, that their movement was linear and obeys the Stokes law.

The differential equation for the curve of the distribution of the mass of particles of the nebula by size allows us to obtain an analytical expression for their spectrum. For an approximating expression, we studied that given by P. Rozin and Ye. Ramler [4] (Inserting the results of our experiment):

$$F = ndr^{n-1}e^{-\alpha r^n}$$

or, for our conditions,

$$F = 2\alpha r e^{-\alpha r^2}. \qquad (1)$$

The differential curve for the distribution of drops in the nebula which was constructed according to (1) shows (Figure 3) that the modal radius of the drops was equal to 16 μm. Moreover, we studied the analytical expressions for the sedimentation curve proposed by A.A. Bagrov [5]:

$$Q = 100\left(1 - e^{-\frac{1}{\mu t}}\right)\mu t, \qquad (2)$$

where Q is the relative quantity of the substance which has precipitated by the moment t.

The parameters μ and α are connected by the following expression:

$$\alpha\mu = \frac{C}{H},$$

where C is the Stokes constant, H is the height of the deposit. In order to find the parameter μ, we took the values of t and Q according to the data of three measurements corresponding to the regions of the experimental sedimentation curve with greatest curvature. We used a specially constructed table in the calculations. It can be /260 seen from Figure 1 that the analytical curve differs rather greatly from the experimental one. Apparently, this difference is caused by errors in the experiment in relation to the selection of the height of deposition of the particles, as well as the rather imperfect method of the reading on the analytical balance, which was used continuously during the experiment. Moreover, a substantial error was also involved in the recording of the balance itself, since it was subjected to the effect of air currents from the chamber.

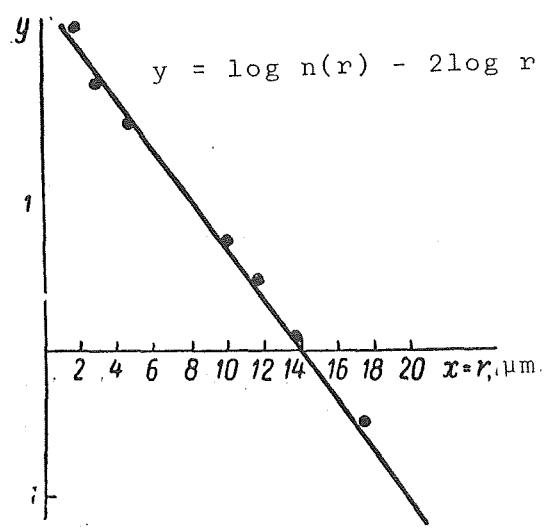

Fig. 4. Distribution of Drops by Size as Obtained by Microphotographs.

At the same time as the sedimentation analysis, we carried out a microphotographic analysis. A correction for the Stokes rate of precipitation of particles of different sizes (for this see [6], for example) was introduced in the calculations. As the calculations showed, the spectra for distribution of drops by size as obtained by the microphotographs (this spectrum is depicted by the dotted line on Figure 2) obey the empirical Hrgian-Mazin law, i.e.,

$$f_r = ar^2e^{-br}.$$

This is clearly seen in Figure 4 (the points fit on the line with small deviations).

The data of the microphotographs allow us to convert to the overall sedimentation curve for the distribution of particles by size presented in Figure 1 (points--circles with crosses), and show good coincidence with the experimental curve for sedimentation. Both methods - microphotography and sedimentation - give coinciding /261 average and modal radii within the limits of the error (r_{mod} = 10 μm, $\bar{r}_{av}$ = 12.6 μm).

Thus, we can conclude that the sedimentation method of analyzing the degree of dispersion of a modeled nebula gives a completely clear and precise representation of the distribution of drops by size in it and thereby allows us to reject the rather cumbersome method of a microphotographic analysis.

REFERENCES

1. Tsyurupa, N.I.: Obtaining the Curves for the Distribution of Powder by Particle Size. Chimicheskaya Promyshlennost', No. 3, 1961.
2. Morachevskiy, V.G. and B.M. Shinyayev: Study of the Properties of Nebulae in a Sedimentation Chamber. In the Collection: Problemy fiziki atmosfery (Problems of Atmospheric Physics), No. 3. Leningrad State University Press, 1965.
3. Figurovskiy, N.A.: Sedimentatsionnyy analiz (Sedimentation Analysis). Izdat. Akad. Nauk S.S.S.R., 1948.
4. Rozin, P. and Ye. Ramler. The Use of a Sedimentation Analysis for an Analysis of Suspensions. Kolloidnyy Zhurnal, Vol. 67, No. 16, 1934.
5. Bagrov, A.A.: A Comparison of the Analytical and Graphical Methods of Analyzing Experimental Data of a Sedimentation Analysis of Precipitated Systems. Kolloidnyy Zhurnal, Vol. 26, No. 5, 1964.
6. Gaydan, E.N., M.M. Kokhanovich, V.G. Morachevskiy and N.S. Shapovalova: A Study of the Dispersion and Rearrangement of Microphysical Characteristics of Nebulae Modeled in Chambers. In the Collection: Problemy fiziki atmosfery (Problems of Atmospheric Physics), No. 2. Leningrad State University Press, 1964.

Translated for the National Aeronautics and Space Administration by:
Aztec School of Languages, Inc.,
Research Translation Division (334)
Maynard, Massachusetts and McLean, Virginia
NASw-1692.

NASA-Langley, 1970 —— 13 F-857

NATIONAL AERONAUTICS AND SPACE ADMINISTRATION
WASHINGTON, D. C. 20546

OFFICIAL BUSINESS

FIRST CLASS MAIL

POSTAGE AND FEES PAID
NATIONAL AERONAUTICS AND
SPACE ADMINISTRATION

POSTMASTER: If Undeliverable (Section 158 Postal Manual) Do Not Return

"The aeronautical and space activities of the United States shall be conducted so as to contribute . . . to the expansion of human knowledge of phenomena in the atmosphere and space. The Administration shall provide for the widest practicable and appropriate dissemination of information concerning its activities and the results thereof."

— NATIONAL AERONAUTICS AND SPACE ACT OF 1958

NASA SCIENTIFIC AND TECHNICAL PUBLICATIONS

TECHNICAL REPORTS: Scientific and technical information considered important, complete, and a lasting contribution to existing knowledge.

TECHNICAL NOTES: Information less broad in scope but nevertheless of importance as a contribution to existing knowledge.

TECHNICAL MEMORANDUMS: Information receiving limited distribution because of preliminary data, security classification, or other reasons.

CONTRACTOR REPORTS: Scientific and technical information generated under a NASA contract or grant and considered an important contribution to existing knowledge.

TECHNICAL TRANSLATIONS: Information published in a foreign language considered to merit NASA distribution in English.

SPECIAL PUBLICATIONS: Information derived from or of value to NASA activities. Publications include conference proceedings, monographs, data compilations, handbooks, sourcebooks, and special bibliographies.

TECHNOLOGY UTILIZATION PUBLICATIONS: Information on technology used by NASA that may be of particular interest in commercial and other non-aerospace applications. Publications include Tech Briefs, Technology Utilization Reports and Technology Surveys.

Details on the availability of these publications may be obtained from:

SCIENTIFIC AND TECHNICAL INFORMATION DIVISION

NATIONAL AERONAUTICS AND SPACE ADMINISTRATION

Washington, D.C. 20546